Table of contents

List of Figures

List of tables

List of abbreviations

µm	micrometres
AMD	age-related macular degeneration
AsODN	antisense oligodeoxynucleotides
BRB	blood-retinal barrier
BSA	bovine serum albumin
CNS	central nervous system
CNV	choroidal neovascularisation
Cx	connexin
ERG	electroretinogram
F-actin	filamentous actin
FITC	fluorescein isothiocyanate
GA	geographic atrophy
GCL	ganglion cell layer
GFAP	glial fibrillary acidic protein
GS	glutamine synthetase
Iba-1	ionized calcium-binding adapter molecule-1
INL	inner nuclear layer
IPL	inner plexiform layer
IS/OS	inner and outer segment of photoreceptors
LD	light damage
MP	mimetic peptide
NFL	nerve fibre layer
NO	nitric oxide
NT	nitrotyrosine
ONL	outer nuclear layer
OPL	outer plexiform layer
PBS	phosphate buffer saline
PED	pigment epithelium detachment
PFA	paraformaldehyde
PVDF	polyvinylidene difluoride
RNS	reactive nitrogen species
ROS	reactive oxygen species
RPE	retinal pigment epithelium
SD rats	Sprague-Dawley rats
SOD-1	superoxide dismutase-1
TBS-T	tris-buffered saline-tween
TUNEL	TdT-mediated dUTP nick end labelling

Chapter 1: Regulation of intercellular communication – seeking a novel therapeutic target for age-related macular degeneration

Age-related macular degeneration (AMD) is the major cause of blindness in people aged 75 years or older in developed countries, and the third leading cause of blindness in the world, following cataract and glaucoma (Klaver *et al.*, 1998b; Biarnés *et al.*, 2011). A recent study reports that the prevalence of late AMD increases exponentially in aged people, reaching 20% in people in their 90s (Rudnicka *et al.*, 2012). In addition to age, studies have shown that many other risk factors also contribute to triggering AMD. Genetic influences on AMD are well recognised. A similar incidence of AMD in monozygotic twins has been reported, suggesting a close association between heredity and AMD (Meyers & Zachary, 1988; Klein *et al.*, 1994; de Jong, 2006). Some genes involved in macrophage activation and complement cascade pathways have been shown to contribute to the onset of AMD (Klaver *et al.*, 1998a; Edwards *et al.*, 2005; Haines *et al.*, 2005; Klein *et al.*, 2005; de Jong, 2006; Gold *et al.*, 2006). Environmental factors such as smoking also pose a significant risk factor for AMD (Thornton *et al.*, 2005; Biarnés *et al.*, 2011). One study has shown a significantly higher risk of developing AMD in heavy smokers compared to that for non-smokers (Khan *et al.*, 2006). Additionally, increased lifetime exposure to sunlight may be another risk factor. The Blue Mountains Eye Study has reported an association between blue iris colour and late AMD, including neovascular AMD and geographic atrophy (Mitchell *et al.*, 1998). The ten-year longitudinal study also suggests a link between skin sensitivity to sunburn and late AMD (Pham *et al.*, 2009). This is further supported by a recent review of the epidemiological literature that has concluded that increased sunlight exposure may lead to a higher risk of development of AMD (Sui *et al.*, 2012).

Many studies have suggested that AMD arises due to accumulative oxidative stress generated by reactive oxygen species produced as a result of normal metabolism in the retina, retinal pigmented epithelium and in the choriocapillaris (Dorey *et al.*, 1989; Beatty *et al.*, 2000; Gray & Woulfe, 2005). In humans, AMD is also recognised as a vascular disease, and blood vessel changes are highly associated with the pathogenesis and progression of the disease (Coorey *et al.*, 2012). Increased connexin43 protein and/or transcript located in the vasculature and astrocytes have been found in many human central nervous system injuries and diseases, including stroke, epilepsy and Huntington's disease (Elisevich *et al.*, 1997; Vis *et al.*, 1998; Nakase *et al.*, 2006). Connexin43 is the most ubiquitously expressed connexin protein in mammalian embryos and adults, and is expressed in endothelial cells and

epithelial cells. By forming junctional channels, connexin43 contributes to intercellular communication that allows the rapid exchange of nutrients, metabolites, secondary messengers, and small molecules. Therefore, it is important for maintaining the normal cellular function under physiological conditions. However, the association between connexin43 and AMD remains unclear.

So far, there is no treatment to cure AMD (Bird, 2010). The current primary therapy is to manage choroidal neovascularisation breakage through to the neuronal retina in late AMD by direct injection of anti-angiogenic agents into the vitreous (Jager *et al.*, 2008). However, there is gathering interest in the role of intercellular communication in tissue injuries. Alterations in intercellular communication have been found in many human health conditions, such as Huntington's disease, Parkinson's disease, stroke and epilepsy (Elisevich *et al.*, 1997; Rufer *et al.*, 1998; Vis *et al.*, 1998; Nakase *et al.*, 2006). This suggests that modulation of intercellular communication may provide a new therapeutic target for AMD.

In this chapter, the fundamental principles of retinal structure and function are introduced, followed by a description of intercellular communication pathways in normal tissue and after tissue injury that could be targeted for intervention. Next, recent investigations with a specific focus on connexin43-formed junctional communication are reviewed. The pathogenesis of AMD is then presented. And finally, the animal model of AMD and the justification for using this particular model in this thesis are discussed.

1.1   Anatomy and physiology of the retina

The retina, together with the vitreous, posterior sclera and choroid comprise the posterior segment, which forms the back two thirds of the eye. The retina is a very thin (about 200µm), transparent neural tissue lying between the vitreous body and Bruch's membrane of the choroid. The central area of the retina is the fovea. The fovea is an avascular zone that measures about 1.5mm in diameter with the foveola in the middle. The foveola itself

measures 0.35mm in diameter and 0.15mm in thickness. The centre of the foveola is called the umbo, a structure which provides for the highest visual acuity. Densely packed cones are involved in the fovea which has high metabolic demands. Vascular arcades surround the fovea. The parafovea is a ring region 0.5mm in width enveloping the fovea. The perifovea is a 1.5 mm region surrounding the parafovea. The umbo, foveola, fovea, parafovea and perifovea together constitute the macula (Figure 1-1), which is responsible for detailed vision such as when reading and recognising faces (Bron *et al.*, 1997; Wässle, 2004; Lens *et al.*, 2008).

This image is blocked due to copyright issues. Please refer to the hard copy of the thesis for the details of the image.

Figure 1-1. A fundus image showing the central retina and the macula. This image shows a fundus view of the central retina from a normal eye. The macula is the area within the white circle. Adapted from (Jager *et al.*, 2008).

1.1.1 Layers in the retina

The retina consists of eight layers, based on light microscopy findings. They are 1) the retinal pigment epithelium, 2) the outer segments of photoreceptors, 3) the outer nuclear layer, 4) the outer plexiform layer, 5) the inner nuclear layer, 6) the inner plexiform layer, 7) the ganglion cell layer, and 8) the nerve fibre layer (Figure 1-2).
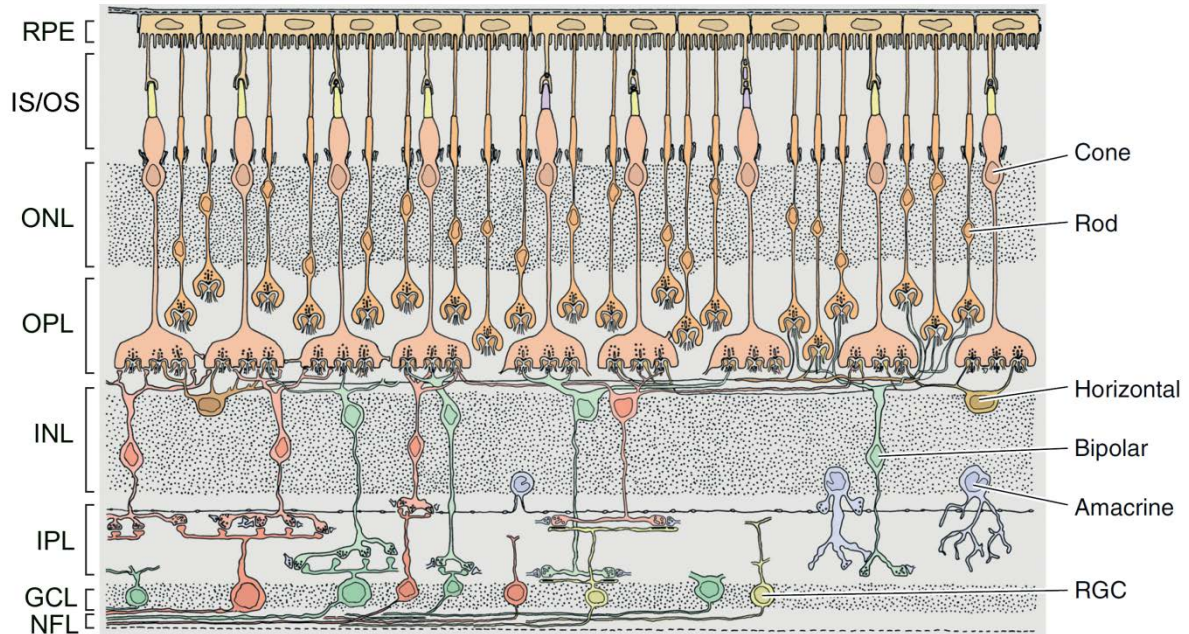
Figure 1-2. A cartoon picture shows the layers and cell types of the retina. The retina consists of six main types of neurons: rod photoreceptors, cone photoreceptors, horizontal cells, bipolar cells, amacrine cells and ganglion cells. The nuclei of the photoreceptors are located in the ONL. The OPL comprises synapses between photoreceptors and post-photoreceptoral neurons. The somata of horizontal cells, bipolar cells, amacrine cells and Müller cells are located in the INL. The IPL comprises synapses between bipolar cells, amacrine cells and ganglion cells. The GCL mainly contains ganglion cells; astrocytes are also located in this layer. Abbreviations: **NFL**, nerve fibre layer; **GCL**, ganglion cell layer; **IPL**, inner plexiform layer; **INL**, inner nuclear layer; **OPL**, outer plexiform layer; **ONL**, outer nuclear layer; **IS/OS**, inner/outer segment of photoreceptors; **RPE**, retinal pigment epithelium. Modified from (Field & Chichilnisky, 2007). *Copyright License Number: 3261711450757.*

1.1.2   Cells in the retina

The retina consists of sensory nerve cells and supporting cells. The nerve cells include photoreceptors, bipolar cells, ganglion cells, horizontal cells and amacrine cells. The supporting cell in the retina includes the Müller cell, the astrocyte and the microglia. Histological morphology and the main functions for each cell type are described in detail below, and the immune cells, including astrocytes and microglia, are described in Section 1.1.7 "The response of retinal immune system to stress and aging".

Photoreceptors   There are two types of photoreceptors, the rods and the cones. The rods are responsible for vision in dim light because of their low threshold to light detection. The cones are responsible for processing fine detailed information and colour vision. The density of the rods and cones varies in different parts of the retina. In humans, the fovea comprises cones only and the number of rods increases rapidly toward the periphery but decreases gently at the extreme edge of the retina (Curcio *et al.*, 1990; Lens *et al.*, 2008). In healthy people, the total number of cones is consistent throughout life from age groups 20s to 90s, while the density of rods starts to drop by 30% from midlife until the 90s (Cuenca *et al.*, 1993).

Photoreceptors are long, slim cells located in the most outer layer of the retina. The cell is divided into three parts, the outer segments, the connecting stalks and the inner segments. The cone outer segment has a conical shape and the rod has a rounded tip. The base is wider in the cone compared to the rod.   The outer segment in rods contains 600 to 1000 transversely arranged membrane discs.   The discs are formed at the base of the outer segment and are progressively pushed towards the end of the outer segments where they are constantly shed. The shed disc membrane from the rod is cleared by the pigment epithelium through phagocytosis. The disc membrane in the cone is continuous with the extracellular space, and is not phagocytosed by the pigment epithelium (Snell & Lemp, 1998). Both rods and cones have photosensitive pigments in their outer segments, which are located in the membrane of the discs. In the rod, the photosensitive pigment is rhodopsin. In the cone, the photosensitive pigment is iodopsin (Tortora & Grabowski, 2000).

6

Bipolar cells   The bipolar cells are located between the photoreceptors and ganglion cells, in the inner nuclear layer of the retina. Based on the morphology shown by Golgi staining, eleven bipolar cell types have been identified in the primate retina (Boycott & Wässle, 1991). They have one or several dendrites forming synapses with photoreceptor terminals. The single axon of most bipolar cell synapses with ganglion cells. Based on their dendrite and axon terminals, bipolar cells are divided into three classes: rod bipolar cells, which connect several rod cells with up to four ganglion cells through contacting AII amacrine cells (Hua *et al.*, 2003); flat or diffuse bipolar cells, which connect several cone cells to several ganglion cells; midget bipolar cells, which connect a single cone cell to a single midget ganglion cell (Tortora & Grabowski, 2000; Levin *et al.*, 2011).

Horizontal cells   The horizontal cells are located in the inner nuclear layer, and their processes lie parallel with the retinal surface. They have several short processes which synapse locally with rods and cones and one long process which contacts with rods and cones some distance away (Snell & Lemp, 1998). There are two types of horizontal cells in most mammalian retina, A-type and B-type, and all the horizontal cells are connected by gap junctions (Kolb, 1974). B-type horizontal cells have a smaller dendritic tree compared to the A-type. The dendrites of both A-type and B-type horizontal cells terminate in cone pedicles while the axon terminals of the B-type end in rod spherules (Kolb, 1974). In the human retina, however, there are three types of horizontal cells identified, HI, HII and HIII (Kolb *et al.*, 1992; Kolb *et al.*, 1994). Horizontal cells have the highest density at the fovea but their density decreases towards the peripheral retina. The horizontal cells serve to modulate and transform visual signals received by the photoreceptors. In contrast to the bipolar cells, which modulate the inputs vertically, the horizontal cells modulate the inputs of the photoreceptor cells horizontally (Bron *et al.*, 1997).

Amacrine cells   The somata of amacrine cells are located in the inner nuclear layer. The cell body is flask-shaped with a diameter of up to 12μm. Each cell has both axons and dendrites, and their processes may extend throughout the inner plexiform layer. Twenty-four different types of amacrine cells have been identified in the human retina based on their morphology impregnated by Golgi procedures (Kolb *et al.*, 1992). The amacrine cells produce various neurotransmitters, including both neuro-active substances (such as

acetylcholine, GABA, dopamine etc.) and neuro-peptides (such as cholecystokinin, glucagon, neurotensin, etc.). Of all the amacrine cells, the AII cell type is the best studied. AII amacrine cells are glycinergic cells (Crooks & Kolb, 1992) and show immunoreactivity for calcium binding proteins parvalbumin, calbindin and calretinin in mouse and human retinas (Wässle, 2004; Thrimawithana *et al.*, 2011). AII amacrine cells are connected to each other by gap junctions (Hartveit & Lin Veruki, 2012). Their functions are mainly involved in transmitting rod-driven signals and modulating visual signals in the cone system (Klump *et al.*, 2009).

Ganglion cells   The ganglion cell bodies are large and round or small and oval in shape and they lie in the most inner cell layer of the retina. They are the last retinal connection for the nerve impulse. The smaller ganglion cells are prominent in the macular area. The axons from the ganglion cells run parallel to the surface of the inner retina to form the nerve fibre layer and finally form the optic nerve. The ganglion cell layer and the nerve fibre layer are thickest around the optic disk and the thickness decreases to a single layer towards the periphery of the retina. Over 18 different types of ganglion cells have been identified (Kolb *et al.*, 1992); the two major types are designated M (or parasol) and P cells. P cells are further subdivided into two subclasses, namely P1 (or midget) and P2 (or small bistratified) cells (Bron *et al.*, 1997).

Müller cells   The Müller cells are the major glial cells in the retina. They are long and narrow cells. Their cell bodies occupy most of the intermediate part of the inner nuclear layer of the retina. The processes from the Müller cells extend through the whole thickness of the retina (Snell & Lemp, 1998). Müller cells are one of the cell types producing endogenous vascular endothelial growth factor (VEGF), which is essential for photoreceptor survival and function (Amin *et al.*, 1997; Saint-Geniez *et al.*, 2008). The Müller cell is considered to be the centre for metabolic activity and neurochemical recycling in the retina (Snell & Lemp, 1998).

1.1.3   The function of the retinal pigment epithelium

The retinal pigment epithelium (RPE) is a single layer of cells located between photoreceptors and the choroid. Horizontal sections parallel to the retina show the cells to be hexagonal. In vertical cross section, the cells are narrow and tall around the optic nerve region and flattened near the peripheral region of the retina. The basolateral side of the RPE rests on the basement membrane, which forms part of Bruch's membrane of the choroid. The apical side of the cells is comprised of multiple microvilli which provide an interface for interaction with the photoreceptor outer segments. The nuclei are located at the basal part of the cytoplasm and the pigment granules extend into the microvilli. These cells have a highly developed endoplasmic reticulum and a prominent Golgi apparatus. These morphological characteristics of the RPE are indicative of its multitude of tasks contributing to visual function. Failure of any of the functions of the RPE leads to retinal degeneration (Snell & Lemp, 1998; Levin *et al.*, 2011).

Absorption of light   The melanin granules of the RPE absorb light that has been focused by the cornea and the lens, which has a high density of energy. This prevents the return of the light back into the photoreceptor layer of the retina. The process of light absorption by the RPE leads to an increase in the temperature of the RPE-choroid complex. The heat generated from light absorption is taken away by the bloodstream in the highly vascularised choroid (Levin *et al.*, 2011). A large amount of reactive oxygen species generated in the RPE is a by-product of light absorption. The RPE is protected by various defence mechanisms, including antioxidant enzymes such as superoxide dismutase (SOD), catalase, and peroxidase. Antioxidant nutrients including vitamin E, beta-carotene, and ascorbic acid may also play a critical role in protection of the RPE from oxidative stress (Algvere & Seregard, 2002).

Phagocytosis of photoreceptor outer segments   The shed rod photoreceptor outer segments are normally phagocytosed by the RPE. The processes of shedding and phagocytosis are tightly coordinated in order to maintain the proper length of photoreceptor outer segments (Levin *et al.*, 2011). Intense light increases the formation of reactive oxygen species by photo-oxidation in the photoreceptors, which may lead to the production of highly

9

peroxidised lipid from shedding photoreceptor outer segments. This may associate with the formation of lipofuscin and drusen in age-related macular degeneration (Curcio & Millican, 1999).

Transport of molecules, ions and water   The RPE is a part of the blood-retina barrier. This barrier means that the exchange of molecules, ions and water is completely reliant on trans-epithelial transport through the RPE. Nutrients such as glucose, omega-3 fatty acids and vitamin A are the main molecules transported from the choriocapillary-side to the photoreceptor side. The transport pathways of the nutrients may be concentration-dependent general diffusion pathway, common to fatty acids, such as omega-3 fatty acids, or by transporters such as glucose transporters, or via a receptor-mediated process such as vitamin A. Transport from the photoreceptor side to the choriocapillary-side mainly includes the transport of metabolic waste such as lactic acid and water generated by the neural retina (Levin *et al.*, 2011).

Secretion   The RPE maintains the structural integrity of photoreceptors, the endothelium of the choriocapillaris and activates the immune system by secreting a large variety of growth factors, cytokines and immune modulators (Snell & Lemp, 1998; Levin *et al.*, 2011). The vascular endothelial growth factor (VEGF) secreted from the RPE has been found to be essential for choriocapillaris development (Marneros *et al.*, 2005). A transgenic mouse model with selective inhibition of VEGF expression in the RPE shows the absence of choriocapillaris (Marneros *et al.*, 2005). Increased expression of VEGF may be associated with pathogenesis and/or development of wet AMD (Kliffen *et al.*, 1997).

1.1.4   Retinal signalling

Light stimulates hyperpolarisation of photoreceptors. The photoreceptor-generated signal is then processed by secondary neurons in the retina before being transmitted to the visual cortex. Horizontal cells and bipolar cells are second order neurons that are responsible for receiving input signals from photoreceptors located in the outer retina and vertically

transmitting the signal to amacrine and ganglion cells in the inner retina. Bipolar cells are divided into two major types, the ON-centre (or depolarising bipolar cells) and the OFF-centre (or hyperpolarising bipolar cells). The network between neurons in the retina is complex and highly organised. Gap junctions have been detected linking adjacent photoreceptors and bipolar cells (Cuenca *et al.*, 1993; Deans *et al.*, 2002; O'Brien *et al.*, 2004), providing channels for electrical coupling between interconnected cells. In addition to electrical coupling, chemical coupling via neurotransmitters, ephaptic coupling, is another form of synaptic interaction between interconnected neurons (Poznanski & Umino, 1997; Levin *et al.*, 2011).

The cone pathway   Cones are responsible for photopic vision with the perception of fine temporal and spatial detail via the integration of information in the cone pathway. Cones also contribute to colour vision. Cone responses to light do not saturate even to the physiologically brightest illumination (Bloomfield & Dacheux, 2001). In humans and primates, there are three types of cones which are sensitive to photons in different regions of the visible spectrum. L- or red cones are sensitive to long wavelength; M- or green cones are sensitive to middle wavelength; S- or blue are sensitive to short wavelength. Two cone-specific circuitries are responsible for colour coding, the red-green opponency and the blue-yellow opponency pathway (Dacey & Packer, 2003). The L- and M- cones are morphologically similar and cannot be distinguished from each other. Signals from both L- and M- cones are combined and transmitted through the red-green opponency pathway. In the central retina, a single L- or M- cone connects through a midget bipolar cell and exclusively to a single midget ganglion cell, which establishes a private pathway to the brain (Kolb & Dekorver, 1991). In the peripheral retina, a single cone connects a midget bipolar cell and several of these connections converge onto an expanded dendritic trees of midget ganglion cells (Dacey & Packer, 2003). Signals from S-cones, which make up only 5-10% of the cones, are transmitted to small bistratified ganglion cells via the blue-ON-yellow-OFF opponent pathway (Dacey & Lee, 1994). Apart from the primates, other mammals have only two types of cones, L- and S-cones (Wässle, 2004).

The rod pathway   Rods are highly sensitive to light and are, therefore, responsible for vision under dim illumination. However, their responses saturate quickly under the dim light

even after being exposed to a few photons (Bloomfield & Dacheux, 2001). There are several pathways that have been revealed for transmission of rod signals to the ganglion cells (Figure 1-3). The first is the rod ON bipolar and AII amacrine pathway (ON1 pathway in Figure 1-3). One rod synaptic terminal interacts with two or more rod ON bipolar cell dendrites. In the dark, the rod synaptic terminals keep releasing glutamate, which works on L-(+)-2-amino-4-phosphonobutyric acid (APB)-sensitive, metabotropic glutamate receptor, mGluR6 located on the postsynaptic membrane of rod bipolar cells and maintains the rod bipolar cell in a hyperpolarised state. Light stimulates the rod photoreceptor decreasing glutamate release and causing a depolarising ON-response of the rod bipolar cells (Nawy & Jahr, 1990). The rod ON-bipolar cell contacts with AII amacrine cells through a sign-conserving glutamatergic synapse. Then, signals from the AII amacrine cells excite ON/depolarising cone bipolar cells through sign-conserving electrical gap junctions and inhibit OFF/hyperpolarising cone bipolar cells through glycinergic synapses (Sharpe & Stockman, 1999). ON cone bipolar cells pass the signals to ON ganglion cells and OFF bipolar cells pass the signals to OFF ganglion cells.

The second rod pathway (OFF2 pathway in Figure 1-3) is via rod-cone gap junctions to cone bipolar cells for stimulations at higher light levels. Rod signals excite ON and OFF cone bipolar cells through gap junctions between neighbouring rod spherules and cone pedicles, which are then passed onto ON and OFF ganglion cells (Nelson, 1977; Sharpe & Stockman, 1999).

The third rod pathway (OFF3 pathway in Figure 1-3), direct rod to OFF bipolar connection has been suggested by a study using transgenic mice that lack cones (Soucy *et al.*, 1998). Certain OFF ganglion cells show an APB-resistant response to rod signals. The APB-resistant response excludes the signals passing through the rod bipolar and AII amacrine pathway. The rod-cone gap junction pathway should not happen as there is no gap junction between rod and cone in the coneless transgenic mouse retina. This study indicates that rod signals can reach ganglion cells bypassing rod bipolar cells and cone photoreceptors. The rods may connect directly to OFF bipolar cells. A recent finding supports this idea. The study suggests that a subpopulation of cone bipolar cells receives substantial input directly from rods by analysing light-evoked cation currents from morphologically identified

depolarizing bipolar cells in the wild-type and three pathway-specific knockout mice (Pang *et al.*, 2010).
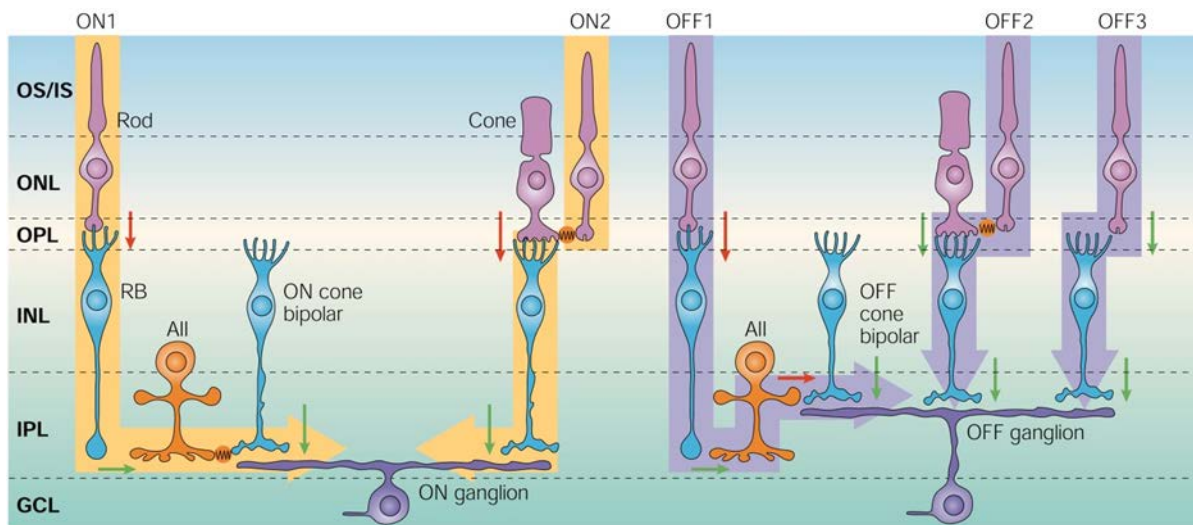
Figure 1-3. The rod pathways. In the ON1 pathway, light causes rod hyperpolarisation and decreases in glutamate release, which leads to rod bipolar cell depolarisation (red arrow). The signal is then transferred from the bipolar cell onto AII amacrine cells through a sign-conserving glutamatergic synapse. AII amacrine cells make gap junctions (electrical synapses) with the ON cone bipolar cells, which pass the signal onto the ON ganglion cells (green arrow). In the OFF2 pathway, light stimulates the rod. The rod signal is passed onto the cone bipolar cells through gap junctions between neighbouring rod spherules and cone pedicles, and thence passed to ON and OFF ganglion cells. In the OFF3 pathway, the signal is transferred directly from the base of rod spherules to the OFF cone bipolar cells and onto the OFF ganglion cells. Abbreviations: **GCL**, ganglion cell layer; **IPL**, inner plexiform layer; **INL**, inner nuclear layer; **OPL**, outer plexiform layer; **ONL**, outer nuclear layer; **OS/IS**, outer and inner segment of photoreceptors; **RB**, rod bipolar cells. This image is adopted from (Wässle, 2004). *Copyright License Number: 3241090969779.*

The lateral pathway The vertical photoreceptor signals are modulated by the "lateral pathway" across the retina to build spatial information and to form complex receptive fields. The lateral pathway consists of horizontal cells and amacrine cells. Horizontal cells branch in the outer plexiform layer and insert lateral elements to the cones through their dendrites and contact with the rods through their axon terminals (Wässle, 2004). The traditional proposal for an inhibitory feedback loop between horizontal cells and the photoreceptors via release of inhibitory neurotransmitter GABA (γ-aminobutyric acid) has been challenged by many studies, including a lack of classical synapses from horizontal cells, lack of GABA receptors on cones, and lack of GABA uptake into horizontal cells (Redburn-Johnson, 1998;

Tatsukawa *et al.*, 2005; Schubert *et al.*, 2010; Deniz *et al.*, 2011). Some investigations suggest that horizontal cells regulate the release of glutamate from cones and rods by modulating Ca^{2+} channels on the photoreceptor cellular membrane. This modulation may be achieved through gap junction hemichannels located on the horizontal cell membrane. Blocking the hemichannels eliminated all the feedback responses (Kamermans *et al.*, 2001). Another mechanism for feedback modulation from horizontal cells is through a pH change in the synaptic clefts which leads to a calcium current in cones (Hirasawa & Kaneko, 2003).

Amacrine cells branch in the inner plexiform layer. The types of amacrine cells are dramatically diverse. There have been about 30 types of GABA-containing amacrine cells and 15 types of glycinergic amacrine cells identified in mammalian retina (Vaney, 2002; Wässle, 2004). AII is the most common type, although it covers only 11% of the amacrine cells in the rabbit retina (Vaney, 1991; Strettoi & Masland, 1996). The function of each type of amacrine cells is still unclear. AII amacrine cells transfer their signal to the axons of ON cone bipolar cells through gap junctions (Vaney, 1991). GABAergic amacrine cells send inhibitory input to bipolar cells, which leads to prolonged glutamate release from bipolar cells and a transient ganglion cell response (Lukasiewicz *et al.*, 1994; Dong & Werblin, 1998; Lukasiewicz, 2005). Cholinergic amacrine cells play a critical role in the direction-selective circuitry. They provide either excitatory input at the preferred side or inhibitory input at the null side of the direction-selective ganglion cells (Euler *et al.*, 2002; Taylor & Vaney, 2002).

1.1.5   Blood-retinal barrier

Retinal blood supply is provided by the central retinal artery and the choriocapillaris. The choroidal blood vessels supply approximately 85% of the blood flow to the outer retina (Bill, 1975). The central retinal artery forms branches into three different capillary layers of the vascular network to supply the inner retina. The first capillary layer runs along the nerve fibre layer; the second capillary layer is located in the ganglion cell layer; and the third capillary layer goes from the inner plexiform layer to the outer plexiform layers through the

14

inner nuclear layer (Leeson, 1979; Cuthbertson & Mandel, 1986). Primates have an avascular region in the retina, the macula. A study on post-mortem human donors by using perfusion and staining techniques has shown that the size of this avascular region varies between individuals (Paula *et al.*, 2010). It also demonstrated that the parafovea region was densely supplied by nine closely arranged pairs of arterioles and venules (Paula *et al.*, 2010).

Similar to the central nervous system, the neural retina is protected by two barriers, the inner blood-retinal barrier (BRB) and the outer BRB. The inner BRB comprises retinal capillary endothelial cells and their surrounding pericytes and astrocyte end-feet (Choi & Kim, 2008). The outer BRB comprises the retinal pigment epithelium (RPE) (Levin *et al.*, 2011). The RPE cells are connected with each other by tight junctions, forming a belt that completely encircles the cells. In cross-sections, tight junctions were observed at the apical end of the paracellular space in the RPE (Rizzolo *et al.*, 2011). Traditionally, it has been recognised that the strict control of permeation across the BRB is achieved through tight junctions (Steuer *et al.*, 2005; Erickson *et al.*, 2007; Xu & Liversidge, 2011). In addition to tight junctions, gap junctions also contribute to the BRB structural integrity and physiological functions. Many recent studies have shown that a gap junction protein connexin43 is expressed on RPE in a range of species, including rabbits, rats, turtles, fish and humans (Janssen-Bienhold *et al.*, 1998; Kerr *et al.*, 2010; Pocrnich *et al.*, 2012). The BRB protects the retina from an over flow of ions, a diffusion of large toxic molecules and attacks by pathogens. Its characteristics of transport and permeation are critical for drug delivery.

1.1.6 The choroid and the sclera

The choroid is an extremely vascularised thin layer between the sclera and the retina (Figure 1-4). It nourishes the outer layer of the retina. In darkness, over 90% of the oxygen consumed by photoreceptors is delivered by the choroidal circulation (Linsenmeier & Braun, 1992). This high oxygen requirement in the retina relies on the high blood flow in the choroid, which is the highest per unit tissue weight compared to any other tissues in the body and about ten times higher than in the brain (Alm & Bill, 1973; Nickla & Wallman, 2010).

The primary blood supply for the choroid is from the long and short ciliary arteries and with some contribution from the anterior ciliary arteries. Blood flow in the choroid is drained through the vortex veins that ultimately merge with the ophthalmic vein (Ruskell, 1997). Unlike the retina, the circulation of the choroid is regulated by extrinsic autonomic innervations (Bill & Sperber, 1990; Nickla & Wallman, 2010). A decrease in the choroidal blood flow is mediated through noradrenaline, which is released by sympathetic efferent nerves from preganglionic cervical sympathetic nerve and works on smooth muscle cells (Kawarai & Koss, 1998; Kur *et al.*, 2012). An increase in the choroidal blood flow is mediated via increased levels of nitric oxide, which is controlled by parasympathetic efferent nerves branched from the facial nerve (Nilsson, 1996; Kur *et al.*, 2012).
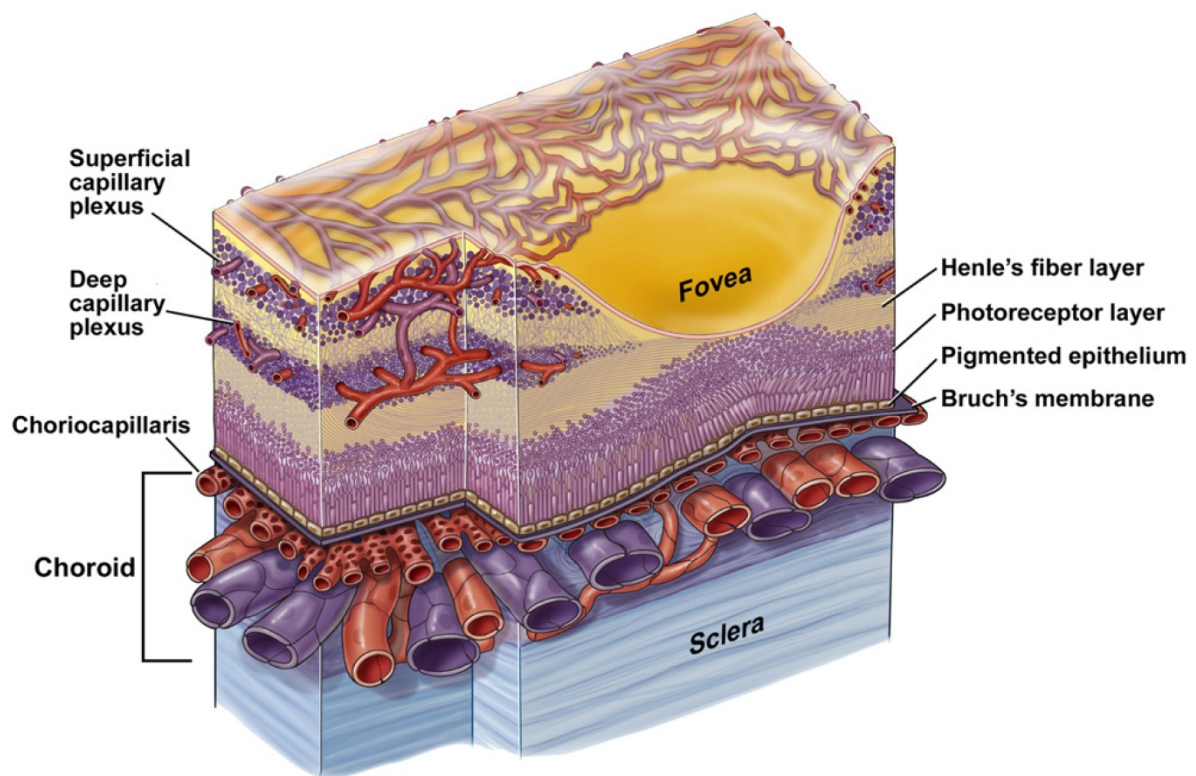
Figure 1-4. A cartoon picture showing the vasculature of the choroid. The choriocapillaris is adjacent to the retinal pigment epithelium and lying in the inner layer of the choroid. The medium and large-sized blood vessels are located in the outer layer of the choroid. This image is adopted from (Kur *et al.*, 2012). *Copyright License Number: 3241091332117.*

The choroid can be divided into three layers from the outmost: 1) the vessel layer that consists of large and medium-sized arteries and veins; 2) the capillary layer that contains fine capillaries; and 3) Bruch's membrane, also known as the "basement membrane", which

16

is a trilaminar structure consisting of the basement membrane of the retinal pigment epithelium of the retina, an intervening elasto-collagen layer, and an outer layer derived from the basement membrane of the endothelium of the capillaries in the capillary layer. The role of Bruch's membrane is to regulate the bilateral diffusion of bio-molecules, fluid and nutrients between the choroid and RPE (Snell & Lemp, 1998; Bhutto & Lutty, 2012).

The sclera is the external coating of the eye and is composed of dense collagen fibres derived from dura mater of the central nervous system. It provides firm protection for the intraocular contents. The sclera is a relatively avascular structure. However, its outmost layer, called episclera, has a rich blood supply from the anterior ciliary arteries (Levin *et al.*, 2011).

1.1.7   The response of the retinal immune system to stress and aging

Oxidative stress is the damage caused by reactive oxygen species (ROS) or reactive nitrogen species (RNS) in cells or tissues. ROS is generated from many sources under physiological conditions, including NADPH-dependent membrane-bound enzymes, mitochondrial metabolism of oxygen during normal cellular activities, and other intracellular oxidases (Finkel, 2011). Cells also possess several antioxidant enzymes to remove ROS, such as superoxide dismutase that reduces O^{2-} to H_2O_2, catalase, and glutathione peroxidase that reduces H_2O_2 to H_2O (Finkel, 2011). The retina has a high consumption of oxygen and is therefore particularly susceptible to oxidative stress (Handa, 2012). Under physiological light conditions, rod outer segments are shed and regenerated (Levin *et al.*, 2011). Focused or prolonged light exposure results in excess ROS and free radicals generated from phagocytosis of the photoreceptor outer segment by the RPE, which can lead to retinal damage (Beatty *et al.*, 2000). Aging contributes to the excess oxidative stress generated and accumulated in the RPE. Age-related inefficiency in phagocytosis, protein degradation and metabolism causes intracellular deposits of lipofuscin in the RPE (Beatty *et al.*, 2000; Kinnunen *et al.*, 2011).

Phagocytes are involved in the loop of amplification of oxidative stress. Many oxidant generating enzymes are activated under stress, such as NADPH oxidase, superoxide dismutase, nitric oxide synthase (NOS), and myeloperoxidase (Babior, 2000). The subunits of NADPH oxidase are located in the resting phagocytes (Leto *et al.*, 1990; Knaus *et al.*, 1991) and the active form of oxidase is assembled on the membrane when the phagocytes are activated (Heyworth *et al.*, 1991). An inducible and highly-active form of NOS is manufactured by activated murine macrophages (Hevel *et al.*, 1991) and increased NOS is released from lipopolysaccharide (LPS) and/or interferon-gamma (IFN-gamma)-activated human macrophages (Weinberg *et al.*, 1995). The activation of phagocytes is not fully clear. A theory, the so-called "lipid whisker model", explains how the oxidised phospholipids of the membrane are recognised by the phagocytes (Greenberg *et al.*, 2008). This model suggests that when the phospholipids of the plasma membrane undergo peroxidation, they will move from the interior of the lipid bilayer to the aqueous exterior, which looks like "whisker growth" on the cellular membrane. This change enables physical contact between these oxidatively modified phospholipids on the stressed cell and the molecular ligands on the phagocytes (Greenberg *et al.*, 2008; Hazen, 2008). When the phagocytes are activated, further reactive oxidants are generated through the process of phagocytosis (Babior, 2000), forming a vicious circle and a loop of amplification of oxidative stress. The retina has residential phagocytes, and they may be activated and involved in the oxidative stress generated from photo-oxidation and aging.

In the developing retina, the presence of subretinal macrophages has been demonstrated to be a feature in a range of mammalian species by using electron microscopy and immunohistochemical methods (McMenamin, 1999). Although the adult retina is regarded as an immune-privileged tissue, it has residential glial cells that provide support and protection of the retinal neurons by supplying nutrients, removing neural waste products and phagocytosis of neuronal debris (Coorey *et al.*, 2012). There are three types of glial cells in the retina: Müller cells, astrocytes and microglia (Coorey *et al.*, 2012). The review on retinal glial cells below is mainly focused on astrocytes and microglia (Figure 1-5).

Retinal astrocytes originate from the optic nerve and migrate to the nerve fibre layer during development (Yuge *et al.*, 1995). They are associated with vasculature in the retina. In the

avascular area, there are no astrocytes (Yuge *et al.*, 1995). The end-feet of astrocytes are said to contribute to the blood-retinal barrier (Choi & Kim, 2008). Degeneration of astrocytes may result in leakage of the blood-retinal barrier (Pérez-Álvarez *et al.*, 2008). In the aged rat retina, astrocytes show gliosis-like morphology and the density and total number of astrocytes are decreased compared to young animals (Trivino *et al.*, 1996). These changes may affect the ability of astrocytes to maintain homeostasis and support neurons during aging (Trivino *et al.*, 1996; Kur *et al.*, 2012). Glial fibrillary acidic protein (GFAP) is a specific marker of astrocytes (Trivino *et al.*, 1996) and reactive astrocytes are usually associated with an increased expression of GFAP (Kaur *et al.*, 2008). In the aged human retina, GFAP-immunoreactivity is higher than that in the young (Ramírez *et al.*, 2001).
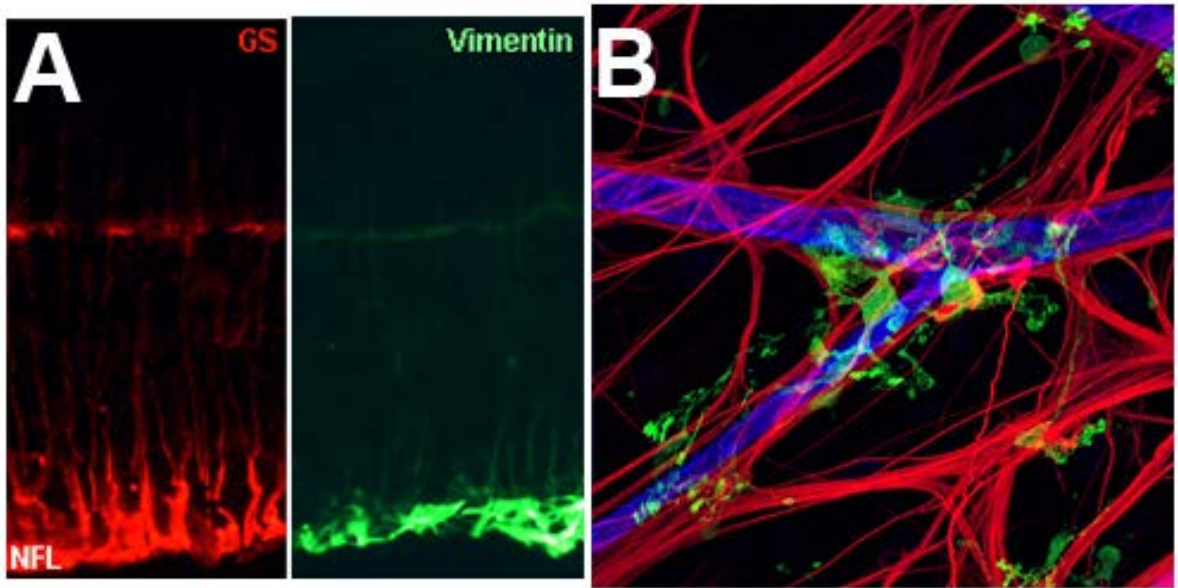
Figure 1-5. Retinal astrocytes and microglia. **A:** Confocal images showing astrocytes, immuno-labelled with GS (red) and vimentin (green) on a cross section of rat retina. Adopted from (Hernandez *et al.*, 2009). *Copyright: Creative Commons Attribution License.* **B**: Confocal image of a flat-mount retina showing astrocytes (red), microglia (green) and blood vessels (blue). Adopted from the webvision website. http://webvision.med.utah.edu/2012/12/human-retina-with-astrocytes-and-microglia/#respond. *Copyright is obtained from the Webvision website.* **C:** Immuno-labelling of microglia on a human retina cross section with anti-HLA-DR (major histocompatibility complex class II antigen) antibody (Zeng *et al.*, 2008). ***This image is blocked due to copyright issues. Please refer to the hard copy of the thesis for the details of the image.***

Microglia are the residential immune cells in the central nervous system (Hanisch & Kettenmann, 2007). In normal adult human retina, microglia are small, stellate cells limited to the inner retinal layers and when activated function as circulating macrophages (Provis *et al.*, 1995; Buschini *et al.*, 2011). It is generally recognised that microglia are of mesenchymal origin and macrophage/monocyte lineage (Cuadros & Navascués, 1998). In the adult mouse retina, blood-derived cells mainly contribute to the turnover of retinal microglia and perivascular macrophages. Proliferation of residential microglia supplies a small portion for the renewal of the microglial population during physiological conditions (Xu *et al.*, 2007). Transformation of microglia from a resting to an activated state involves morphological, immuno-phenotypic and migratory changes (Kreutzberg, 1996). The cartoon below shows the different activity states of microglia (Figure 1-6). In normal human and rat retinas, microglia are located in the ganglion cell layer, and the inner and outer plexiform layers (Ashwell *et al.*, 1989; Provis *et al.*, 1995).
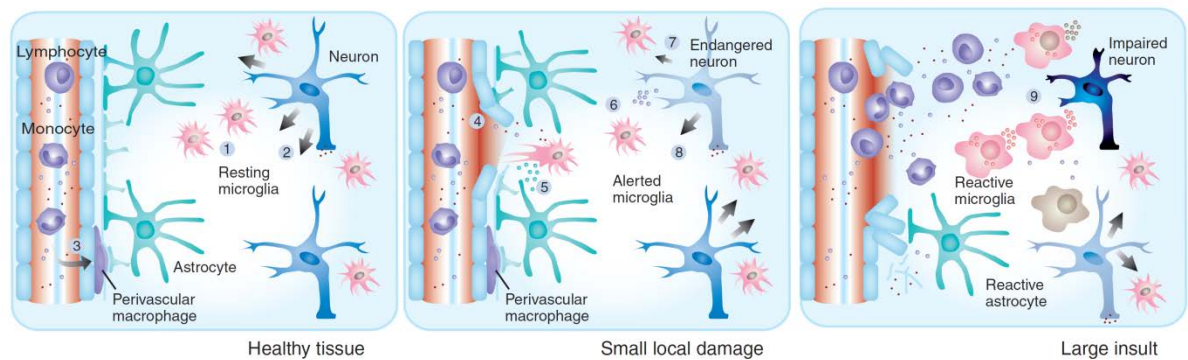
Figure 1-6. A cartoon picture showing activity states of microglia. The resting microglia have fine processes which provide continuous and efficient scanning in the healthy tissue. In small local damage, the microglia are alerted, secreting neurotrophic factors and supporting stressed neurons. In large insults, the microglia become reactive, which leads to substantial damage to the neurons (Hanisch & Kettenmann, 2007). *Copyright License Number: 3241101417898.*

Evidence from mouse models indicates that microglia respond to aging. In the aging mouse retina, resting microglia show smaller and fewer processes morphologically (Damani *et al.*, 2011). In response to focal injury, activated microglia in the aging retina have slower responses and lower rates of motility compared to microglia in the young retina (Damani *et al.*, 2011). In the aging mouse retina, the microglia are located in the sub-retinal space in addition to the inner retina (Xu *et al.*, 2009). This relocation could be associated with an

age-related RPE dysfunction, which increases expression of pro-inflammatory molecules (Ma *et al.*, 2009b). Migration of microglia into the photoreceptor layer has been found in many retinal degeneration mouse models (Karlstetter *et al.*, 2010). Activated microglia with phagocytic activities have even been identified in the normal aged rat retina (Chan-Ling *et al.*, 2007). The activation of microglia in these animal models may be involved in the clearance of neuronal debris, or even earlier events, prior to any signs of degeneration (Gehrig *et al.*, 2007; Karlstetter *et al.*, 2010). Interestingly, in a mouse model of choroidal neovascularisation created using a red diode laser, the density of microglia remained the same as in the normal retina, but blood-derived macrophages were increased in the areas close to activated Müller cells (Caicedo *et al.*, 2005). This indicates that increased permeability of blood vessels may play a more important role in this mouse neovascularisation model compared to the resident microglia.

In addition to retinal glial cells, the complement system is another important component of the innate immune system. It contains more than 20 proteins and protein fragments which are synthesised mainly in the liver and delivered into the circulatory system. The complement system can be activated by three pathways: the classic pathway, the alternative pathway and the mannose-binding lectin pathway (Khandhadia *et al.*, 2012). Full activation of each of these pathways leads to the formation of the membrane-attack complex (MAC), which results in cell lysis and pathogen clearance (Xu *et al.*, 2009; Rutar *et al.*, 2011a).

1.2 Gap junctional communication in physiological and pathological conditions

1.2.1 The structure of gap junctions

Gap junction proteins, also called connexins, form conduits for intercellular communication, allowing rapid exchange of nutrients, metabolites, ions, and small molecules up to 1kDa (kilo Daltons) between cells. One complete intercellular channel is formed by two hemichannels (also known as connexons) located on the membrane of each adjacent cell with about a 2-4nm extracellular gap in the middle. Each hemichannel is a hexamer of six connexin proteins arranged around a central pore. These six connexins can be one or different members of the connexin family (Figure 1-7A) (Goodenough *et al.*, 1996; Evans & Martin, 2002).

Genes encoding mammalian connexins are divided into three classes (α, β and γ) based upon their genetic origin and nucleotide and amino acid sequence similarities (Risek *et al.*, 1990; Eastman *et al.*, 2006). So far, over 21 connexins have been characterised in humans, and are named according to their molecular weights. All the connexin proteins share a common structure, comprising four transmembrane hydrophobic domains (M1 – M4), two extracellular loops (E1 and E2) and one cytoplasmic loop (CL). Both amino- and carboxyl-terminals end in the cytoplasm (Figure 1-7B). The two extracellular loops are cysteine-rich and their amino acid sequences are highly conserved. The amino-terminals show similar lengths between all connexin proteins. The most variable regions, both in length and sequence, include the carboxyl-tail and the cytoplasmic loop (Goodenough *et al.*, 1996; Kumar & Gilula, 1996; Yeager & Nicholson, 1996).
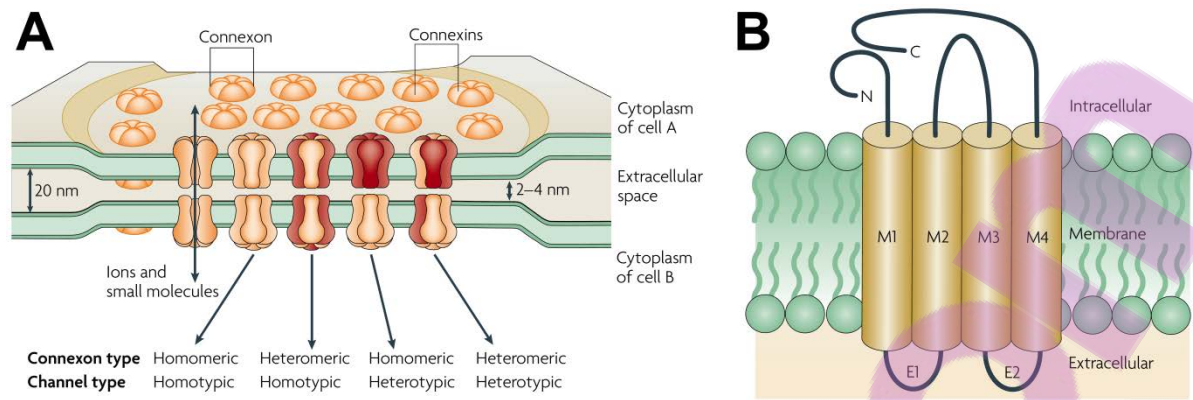
Figure 1-7. Organisation of gap junctions and structure of connexin protein. **A:** Gap junction hemichannels (connexons) may consist of only one type of connexin (homomeric connexons) or a mixture of different connexins (heteromeric connexons). Gap junctional channels can consist of two of the same connexons (homotypic channels) or of connexons with different connexin compositions (heterotypic channels). **B:** Connexin proteins have four transmembrane domains (M1-4), two extracellular loops (E1&2) and one cytoplasmic loop. This image is adopted from (Bloomfield & Volgyi, 2009). *Copyright License Number: 3241110129346.*

1.2.2   The assembly and removal of gap junctions

Gap junctions have a rapid turnover. The half-life of a gap junction in mouse liver was measured to be 5 hours (Fallon & Goodenough, 1981), and the half-life of connexin43 (Cx43) in an adult rat heart was determined to be 1.3 hours, consistent with findings from another study of Cx43 turnover in cultures of cardiac myocytes (Laird *et al.*, 1991; Beardslee *et al.*, 1998). Therefore, gap junctions are constantly formed and removed from the cell surface. The assembly of connexin proteins is a complicated process (Figure 1-8). Similar to other integral membrane proteins, connexin proteins are assembled on the rough endoplasmic reticulum (ER). This is supported by the evidence of connexin existing on microsomes from the ER (Rahman *et al.*, 1993; Falk *et al.*, 1994; Kumar & Gilula, 1996). The formed connexin proteins are transported to the cellular membrane via the Golgi complex (Kumar & Gilula, 1996). The oligomerisation of six connexin proteins into a hemichannel occurs intracellularly and most likely during ER to Golgi transport (Musil & Goodenough, 1993; Kumar & Gilula, 1996). After arrival on the cell surface, connexin proteins can diffuse freely within the membrane. Many hemichannels aggregate at the lateral cellular membrane adjacent to another cell, preparing for junctional channel

24

assembly. How the two hemichannels dock and form a junction is still unclear. One model suggests that the two extracellular loops from each connexin interact with the corresponding loops on the opposed hemichannel, which helps the two hemichannels to dock (Yeager & Nicholson, 1996). Lateral pressure arising from the effects of intermembrane repulsion may also contribute to the process of docking and then opening of two hemichannels in the intercellular membrane of neighbouring cells (Harris, 2001). Intercellular channels cluster into plaques. Newly assembled channels keep adding to the periphery of the plaque, pushing the old channels towards the centre (Gaietta *et al.*, 2002). Gap junctions are removed from the intercellular membrane through a process of internalisation as vesicular-like structures (annular junctions) into one of the two adjacent cells, where they fuse with lysosomes and are finally degraded by lysosomal enzymes (Jordan *et al.*, 2001; Mese *et al.*, 2007).
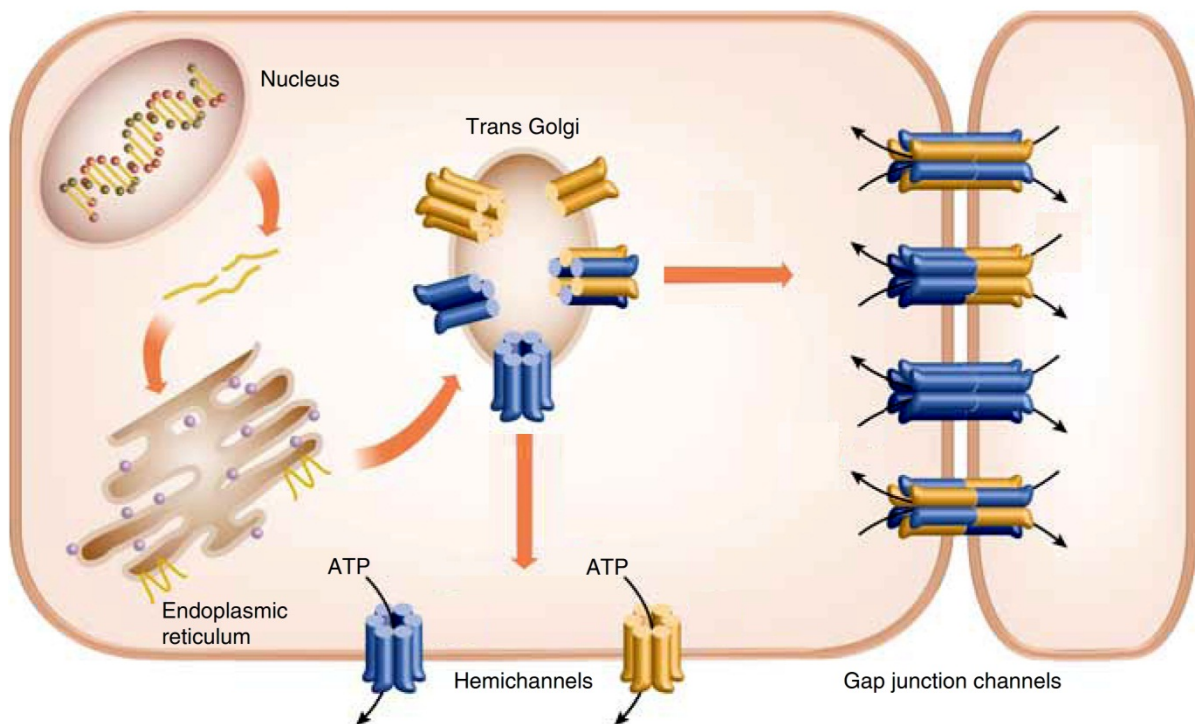
Figure 1-8. A cartoon picture showing the process of gap junction biosynthesis. Connexin proteins are synthesised in the endoplasmic reticulum membrane in the cytoplasm, according to the message carried by the transcript template (mRNA) from the nucleus. The newly formed connexin proteins are transported onto the cytoplasm membrane by the Golgi complex. Oligomerisation occurs during transporting. The oligomerised hemichannels diffuse freely to regions of cell-to-cell contact to form gap junctional channels. This image is adapted from (Mese *et al.*, 2007). *Copyright License Number: 3241110380902.*

1.2.3 The function of intercellular gap junction channels

Intercellular gap junction channels allow the rapid exchange of ions, messengers and metabolic molecules between neighbouring cells. The role of intercellular communication affects a wide range of cellular activities, including signalling, differentiation and growth (Goodenough *et al.*, 1996).

Rapid signal transmission   Electrically excitable cells, such as neurons, cardiac and smooth muscle cells permit rapid intercellular exchange of ions, which causes electrical transmission between adjacent cells to avoid synaptic delays. In the retina, gap junctions are expressed in five major types of neurons and participate in electrical coupling between cells for light sensation. Gap junction-coupled cells can be detected in the retina by injecting biotinylated tracers. Intercellular junctional channels are found between horizontal cells, and between cone bipolar cells and AII amacrine cells (Mills & Massey, 2000). In addition, direct signal transmission has been detected from AII amacrine cells to ON-cone bipolar cells. These gap junctions demonstrate strong electrical coupling and very low steady-state voltage sensitivity (Veruki & Hartveit, 2002).

Both calcium and inositol 1,4,5-trisphosphate (IP_3) are signalling messengers and can move through gap junctions between adjacent cells (Leybaert & Sanderson, 2012). An increase in intracellular calcium concentration in one cell can be passed onto surrounding cells, in a manner similar to creating a propagation wave. This provides one form of intercellular communication. In cultured hepatocytes, for example, injected calcium in one hepatocyte moves to the adjacent cells through transjunctional diffusion (Sáez *et al.*, 1989). A calcium wave is initiated by IP_3 in the stimulated cell, which can also move through junctional channels and communicate intercellular waves (Boitano *et al.*, 1992; Leybaert & Sanderson, 2012). Diffusion of IP_3 from the initiator cell into an adjacent cell via a gap junction is necessary for the propagation of intercellular calcium waves (Boitano *et al.*, 1992).

Passage of metabolic molecules   Sharing nutrients and metabolic molecules across groups of cells is another key function of gap junctions. Intercellular gap junction channels are permeable to glucose, glucose-6-phosphate and lactate in astrocytes, which are the main

metabolic source of energy for brain development and activity (Tabernero *et al.*, 1996). Gap junction inhibitors increase the rate of glucose uptake in astrocytes (Tabernero *et al.*, 1996). This may take place through regulation of glucose transporters located on the astrocyte cellular membrane (Sánchez-Alvarez *et al.*, 2004). In dissociated astrocytes, where there are no intercellular gap junction channels, glucose uptake is not affected by the gap junction inhibitors (Tabernero *et al.*, 1996). Another example of the crucial functions of intercellular channels is the junctional channels on fibre cells on lens. A residue mutation on connexin50 (Cx50) affects intercellular coupling and this non-junctional Cx50 leads to failure of microcirculation of nutrients and metabolites required for lens transparency and may result in dominant congenital cataracts in humans (Banks *et al.*, 2009). Furthermore, enhanced Cx46 expression in lenses by transgenic knock-in alleles increases the intercellular gap junction communication. This has been found to improve small metabolite transport through junctional channels and prevent or delay nuclear cataract formation (Li *et al.*, 2010).

1.2.4   The function of non-junctional hemichannels

Hemichannels that have not been incorporated into intercellular gap junctions have been identified by several studies (Paul *et al.*, 1991; DeVries & Schwartz, 1992; Musil & Goodenough, 1993). In general, the non-junctional hemichannels remain closed and their opening, under some conditions, leads to plasma membrane depolarisation and small molecule leakage from the cytoplasm. When these non-junctional hemichannels are active and open, they may perform diverse functions in various cell types and tissues (Goodenough & Paul, 2003).

Release of signalling molecules into the extracellular space Ca^{2+} wave propagation is a widespread form of intercellular communication between adjacent cells. In addition to the direct intercellular channel mechanism, many studies suggest an alternative mechanism involving non-junctional hemichannels (Suadicani *et al.*, 2000; Bruzzone *et al.*, 2001; Fry *et al.*, 2001; Goodenough & Paul, 2003; Evans *et al.*, 2006). Activation of the non-junctional hemichannels may result in the release of ATP as a primary active messenger into the

extracellular space, where ATP activates P2 purinergic receptors on the surrounding cells and leads to an increase in intracellular Ca^{2+} concentration in these cells (Guthrie *et al.*, 1999; Suadicani *et al.*, 2000; Fry *et al.*, 2001). Opening of the non-junctional Cx43 hemichannels may also cause the release of nicotinamide-adenine dinucleotide (NAD^+), which can be converted to cyclic ADP-ribose (cADPr), a second messenger for mobilising Ca^{2+} from intracellular stores to increase intracellular Ca^{2+} concentration (Lee *et al.*, 1994; Bruzzone *et al.*, 2001).

Promoting cell survival   Non-junctional hemichannels play critical and complex roles in controlling cell death and survival. Most of the studies are focused on Cx43 hemichannels. Bisphosphonates are, for example, a type of drugs used for the treatment of bone diseases. They prevent apoptosis of osteoblasts and osteocytes through extracellular signal-regulated kinase (ERK) activation (Plotkin *et al.*, 1999). Many studies have shown that phosphorylation of the Cx43 cytoplasmic domain results in the activation of ERK and cell survival (Plotkin *et al.*, 1999; Giepmans *et al.*, 2001; Goodenough & Paul, 2003). These results suggest that kinase activation may be linked to hemichannel activities, and phosphorylation of Cx43 may lead to rapid closure of hemichannels and to promote cell survival.

Neuronal signalling in the retina   Non-junctional hemichannels contribute to neuronal signalling in the process of photon transmission in the retina. In the retinal lateral signalling pathway, horizontal cells modulate signals sent from the cone to the bipolar cells through non-junctional hemichannels. One model of the cone synapse suggests that hemichannels are located in the membrane of horizontal cell dendrites, which insert into the cone synapse pedicles. Opening of the hemichannels results in depolarisation of the cone pedicles and Ca^{2+} influx, which causes a subsequent release of neurotransmitters (Kamermans *et al.*, 2001; Goodenough & Paul, 2003).

Overall, gap junctions, both junctional channels and non-junctional hemichannels play important roles for cellular communication within the tissue. Changes to gap junctions may lead to tissue damage and a variety of diseases. Alternatively, tissue injury causes certain micro-conditions where numerous protein kinases modulated by calcium, cyclic AMP and

cyclic GMP result in phosphorylation of gap junction proteins and altering the conductance of junctional channels and non-junctional hemichannels, leading to further tissue damage (Bloomfield & Volgyi, 2009). In Huntington's disease, Cx43 expression is increased compared to the normal control human brain tissue (Vis *et al.*, 1998). Parallel findings have been reported in a mouse model of Parkinson's disease. Both transcript and protein levels of Cx43 are increased in the astrocytes and other glial cells in the injured brain tissue (Rufer *et al.*, 1998). Some gap junctions on astrocytes remain conductive after cerebral ischemia (Cotrina *et al.*, 1998) which enables secondary changes to ionic channels and permits toxic substances generated from injured cells to pass onto the surrounding cells. That disrupts their function, so propagating or amplifying the tissue injury (Lin *et al.*, 1998). These results suggest that modulation of gap junction channels may provide a therapeutic target to rescue the injured tissue from secondary damage.

1.2.5   The expression of gap junctions in the retina

In the vertebrate retina, gap junction proteins are widely expressed on nearly all cell types (Cook & Becker, 1995). Connexins are expressed on neurons in the retina and contribute to electrical coupling in the inner and outer plexiform layers. Cx36 was the first identified connexin in neurons and is the most widely expressed (Söhl *et al.*, 1998; Söhl *et al.*, 2005). In mouse retina, Cx36 and Cx45 are expressed on AII amacrine cells and ON cone bipolar cells (Söhl *et al.*, 1998; Maxeiner *et al.*, 2005). Cx50 is expressed on axon-less horizontal cells and Cx57 is expressed on axon-bearing horizontal cells (Hombach *et al.*, 2004; O'Brien *et al.*, 2006; Bloomfield & Volgyi, 2009). Studies on rat retina showed similar findings for Cx36 and Cx45 on AII amacrine cells and ON cone bipolar cells, as in the mouse retina (Veruki & Hartveit, 2009). In rat retina, Cx36 has also been found in alpha retinal ganglion cells (Hidaka *et al.*, 2004). In addition to neurons, other cell types also express connexins in the retina, playing important roles in normal cellular functions. Some connexins are crucial for endothelial cell structural integrity and physiological functions. Within the rat retina, Cx37 and Cx40 are expressed by endothelium of large radiating arterioles, but they are absent in the mouse retina (Kuo *et al.*, 2008). The glia is another cell type which expresses

connexins widely. In rat retina, Cx43, Cx45 and Cx50 are expressed on Müller cells and astrocytes (Schütte *et al.*, 1998; Zahs *et al.*, 2003; Kuo *et al.*, 2008). Cx43 is also expressed in the vascular endothelium and retinal pigment epithelium (Janssen-Bienhold *et al.*, 1998). Cx30 is limited to the astrocytes in the nerve fibre layer (Zahs *et al.*, 2003; Kuo *et al.*, 2008).

So far, the expression of connexins in human retinal tissue remains largely unexplored. Human Cx36 and Cx45 have been identified in retinal transcripts by Northern blot hybridization, and their protein has been detected in the inner and outer plexiform layers by specific antibodies (Söhl *et al.*, 2010). Cx62 RNA is also detected in human retina (Söhl *et al.*, 2010), which is a true ortholog of mouse Cx57 on horizontal cells (Söhl *et al.*, 2003; Hombach *et al.*, 2004). Cx59 is found by quantitative PCR in total human retinal RNA. The proteins Cx59 and Cx62 need further investigation due to the shortage of specific antibodies (Söhl *et al.*, 2010). Cx43 protein has been localised in astrocytes, Müller cells, blood vessels and pigment epithelium in human retina by immunohistochemistry (Kerr *et al.*, 2010).

1.3 Connexin43

Connexin43 (Cx43) is encoded by the Gja1 gene and is the most ubiquitously expressed connexin protein in mammalian embryos and adults. It is endogenously expressed in at least 35 different tissues, including brain, gut, lungs, skin, kidney and retina (Reaume *et al.*, 1995; Laird, 2006). Cx43 knockout mice die at birth due to blockage of the ventricular outflow tract of the heart (Reaume *et al.*, 1995). Cx43 protein has a short half-life of 1-2 hours in cultured cardiac myocytes (Laird *et al.*, 1991) and about 4 hours in isolated perfused adult rat hearts (Beardslee *et al.*, 1998). Cx43 is a phosphorylated protein. Phosphorylation regulates Cx43 gap junction assembly processes, including trafficking and docking onto the cytoplasm membrane and gating to junctional channels. Phosphorylation of Cx43 also affects permeability of gap junction channels. Cx43 protein has 21 serine and 2 tyrosine residues as targets of phosphorylation. Kinases involved in Cx43 phosphorylation include protein kinase A (PKA), protein kinase C (PKC), p34(cdc2)/cyclin B kinase, casein kinase 1 (CK1), mitogen-activated protein kinase (MAPK), and pp60 (src) kinase (Solan & Lampe, 2005). CK1 is a constitutively active kinase and plays a role in cell cycle progression, intracellular protein trafficking and cell morphogenesis (Solan & Lampe, 2009). In human brain tissue from patients with Alzheimer's disease, CK1-beta transcription increases compared to the control tissue (Yasojima *et al.*, 2000). CK1 has been reported to be involved in phosphorylation of serine residues of Cx43. A specific inhibitor to CK1 decreases the presence of junctional Cx43 and increases the total Cx43 and non-junctional Cx43 (Cooper & Lampe, 2002; Kim & Fishman, 2012). Both Cx43 junctional channels and non-junctional hemichannels respond to tissue injury and micro-environment changes. They also play key roles in a range of secondary processes following the initial injury and in tissue recovery.

1.3.1 The role of connexin43

Cell survival Cx43 gap junctions contribute to the control of germ cell survival and development. Cx43 knockout mice show a deficiency of germ cells even at very early stages

of embryonic development (Juneja *et al.*, 1999). The germ cell deficiency in Cx43 knockout mice is due to cell apoptosis via an increased expression of activated p53 (Francis & Lo, 2006). Cx43 is expressed in human embryonic stem cells. Dissociation of the clustered human stem cells into single cells leads to cell death, which suggests that Cx43 gap junctions may play a key role in cell survival (Wong *et al.*, 2004). Cx43 hemichannels may contribute to cell survival by transducing anti-apoptotic drug effects. A study on bisphosphonates, an anti-apoptotic drug for many bone diseases, has demonstrated that Cx43 hemichannels, but not junctional channels, are vital for passing the anti-apoptotic effect of the drug onto osteoblasts and osteocytes, promoting their cell survival (Plotkin *et al.*, 2002). However, an over-expression of Cx43-formed hemichannels may be involved in ATP-depletion, which causes necrosis and/or apoptosis in cultured human renal cells (Vergara *et al.*, 2003). Likewise, an elevated function of Cx43 hemichannels is associated with pharmacological ATP depletion in cardiac ventricular myocytes and cortical astrocytes in cell cultures (John *et al.*, 1999; Contreras *et al.*, 2002). Increased Cx43 hemichannel opening is also found in endothelia cells exposed to hypoxia. Opening of the Cx43 hemichannel is associated with ATP release into the extracellular space and may be involved in the secondary damage that arises from hypoxia (Faigle *et al.*, 2008). One study has shown that increased Cx43 hemichannel function, but decreased Cx43-related intercellular communication, may be caused by phosphorylation of serine368 residue on the Cx43 protein (Lampe *et al.*, 2000).

Wound healing   In human skin, Cx43 is expressed in basal and lower spinous layers of the skin including epidermal keratinocytes, sebaceous glands, hairs and eccrine sweat ducts (Guo *et al.*, 1992; Salomon *et al.*, 1994). It is also expressed in blood vessels in the skin (Coutinho *et al.*, 2003). After wounding, the Cx43 expression level in keratinocytes at the leading edge of a wound decreases immediately until about two days post-wounding and increases above basal levels from four days up to seven days post-wounding when compared to the control tissue (Goliger & Paul, 1995; Coutinho *et al.*, 2003). In the dermis, the Cx43 level in endothelial cells, smooth muscle cells and fibroblasts around the wound increases transiently within a few hours after wounding and it increases again when granulation tissue maturation starts at four days post-wounding (Moyer *et al.*, 2002; Coutinho *et al.*, 2003). Wound closure can be slow and lead to chronic wounds in diabetic patients. The level of Cx43 expression at the wound edge has been found to be doubled in diabetic rat models

compared to the control animals (Wang *et al.*, 2007). In Cx43 knock-down transgenic mice, keratinocyte migration and proliferation start earlier post-wounding compared to the wild-type mouse. Cx43-formed intercellular junctions may contribute to this process as dye transfer is decreased by 40% in epidermal cells of the skin in the Cx43 knock-down mice (Kretz *et al.*, 2003).

Cx43 also participates in corneal wound healing. In the cornea, Cx43 is predominantly expressed in the basal cell of the epithelium, and is also expressed in corneal keratocytes, stromal fibroblasts and endothelial cells (Dong *et al.*, 1994; Laux-Fenton *et al.*, 2003). Cx43 expression has been investigated following a corneal stromal ablation wound created with an excimer laser in an albino rabbit. At 16-48 hours post-wounding, Cx43 expression is up-regulated in keratocytes under the healing epithelial cells and on the surface of the wound not yet covered by epithelial cells (Grupcheva *et al.*, 2012).

Central nervous system injury   In the central nervous system (CNS), Cx43 is abundantly expressed in astrocytes in both the human and rat brain (Nagy *et al.*, 1992). Data from transgenic mice with a lacZ-reporter gene replacing the Cx43 gene specifically in endothelial cells reveals Cx43 expression in all kinds of vessels in an embryonic brain. In adult mouse brain tissue, Cx43 is absent in large vessels although it is expressed on endothelial cells in small vessels and capillaries. The expression of Cx43 in smooth muscle cells shows a different pattern to the endothelial cells. Smooth muscle cells express Cx43 in large vessels but not in smaller ones (Theis *et al.*, 2001). In human fetal brain tissue, Cx43 is expressed in endothelial cells and perivascular astroglial cells (Virgintino *et al.*, 2001). However, the Cx43 expression appears to be absent in adult human cerebral cortex microvessels (Errede *et al.*, 2002). Under normal physiological conditions, Cx43 is also expressed in about 5% of microglia in the adult rat brain (Eugenín *et al.*, 2001).

Increased Cx43 protein and/or transcript has been associated with several human CNS injuries and diseases, including stroke, epilepsy and Huntington's disease (Elisevich *et al.*, 1997; Vis *et al.*, 1998; Nakase *et al.*, 2006). The increased Cx43 expression in the human brain tissue appears to be mainly limited to the astrocytes. Many studies in animal models for CNS injuries have shown parallel findings (Hossain *et al.*, 1994; Lee *et al.*, 2005;

Ohsumi *et al.*, 2006; Haupt *et al.*, 2007). In astrocyte cell culture under hyperglycaemic conditions and in a diabetic rat brain, dye transfer through gap junctional channels is significantly reduced compared to the controls (Gandhi *et al.*, 2010). In addition to astrocytes, microglia may be another cell type showing changes in Cx43 expression in the CNS following injury. Four days after brain stab wounding, increased Cx43 protein expression is detected at cell interfaces at the edge and around the wound (Eugenín *et al.*, 2001). Up-regulated Cx43 protein is also seen in the primary culture of microglia after treatment with bacterial lipopolysaccharide (LPS) plus interferon-γ (INF-γ) or tumour necrosis factor-α (TNF-α) plus INF-γ (Eugenín *et al.*, 2001). However, these findings about Cx43 on microglia may not be universal. In one rat model of a complete transection of spinal cord injury, both transcript and protein of Cx43 are found up-regulated in astrocytes within hours, but rarely up-regulated in microglia (Lee *et al.*, 2005).

Retinal damage   Under physiological conditions, Cx43 is expressed in retinal pigment epithelium (RPE) and blood vessels of vascularised retinas ubiquitously in many vertebrates (Janssen-Bienhold *et al.*, 1998). The same study also demonstrated that Cx43 is located in astrocytes in the nerve fibre layer of the rabbit retina and in Müller cells of the fish retina. Interestingly, amacrine cells from the zebrafish retina express Cx43, indicating Cx43 may also be expressed in retinal neurons (Janssen-Bienhold *et al.*, 1998). Other groups have further revealed that Cx43 is co-localised with GFAP in astrocytes and vimentin in Müller cells in adult rabbit and rat retinae (Johansson *et al.*, 1999; Zahs *et al.*, 2003). Findings from transgenic mice with a lacZ-reporter gene replacing the Cx43 gene specifically in endothelial cells indicate that Cx43 is expressed in the endothelial cells in the ganglion cell layer and the outer plexiform layer, and colocalised with the blood vessel marker Von Willebrand factor (vWF) (Theis *et al.*, 2001). In human retinal tissue, Cx43 expression has been identified on GFAP-positive astrocytes in the ganglion cell layer and on the processes of glutamine synthetase-positive Müller cells. Human retinal blood vessels and retinal pigment epithelium also strongly express Cx43 (Kerr *et al.*, 2010).

An abnormal expression of Cx43 has been found associated with many human health conditions and in many animal models for ocular diseases. Cx43 immunoreactivity is up-regulated in human retina from patients with glaucoma compared to normal retinal tissue

34

(Kerr *et al.*, 2011). Increased Cx43 expression is mainly in the astrocytes located in the retinal ganglion cell layer of peripapillary and mid-peripheral regions. In the peripapillary region, up-regulated Cx43 is also expressed along GFAP-labelled Müller cell processes throughout the whole retina. Retinal endothelial cells retain the same expression level of Cx43 in the glaucomatous retina as the controls (Kerr *et al.*, 2011). Elevated Cx43 expression is detected in the rat retina, in parallel with changes in GFAP immuno-reactivity and ganglion cell loss following optic nerve injury (Chew *et al.*, 2011).

Down-regulation of Cx43 has been associated with a high-glucose environment. Both protein and transcript Cx43 expression are decreased in human and bovine retinal pericyte cell cultures and rat microvascular endothelial cells cultured in high-glucose containing media (Sato *et al.*, 2002; Li *et al.*, 2003). The Cx43 protein level decreases about 50% in bovine endothelial cells in culture when they are exposed to a high glucose concentration compared to the control (Fernandes *et al.*, 2004). Consistent with the *in vitro* data, streptozotocin-induced diabetic animals also have decreased Cx43 protein and transcript from four weeks onwards of the diabetes onset (Bobbie *et al.*, 2010; Ly *et al.*, 2011). However, it is of note that the Cx43 level is significantly up-regulated compared to control animals at two weeks of diabetes before it drops (Ly *et al.*, 2011).

Connexin43 expression in damaged tissue   Immediately after tissue injury, the immune system is activated around the injured region and responds to the events such as cell damage or tissue repair. The immune response to injuries may be of two types. The quick immune response involves direct activation of tissue-residential immune cells, mainly glial cells when considering the CNS. The activated glial cells around the lesion may release secondary messengers, chemokines and cytokines including ATP, nitric oxide, glutamate and prostaglandin E_2, which leads to increased permeability of the microvasculature (Xu *et al.*, 2003; Abbott *et al.*, 2006; Cronin *et al.*, 2008). The slower immune response involves local microvascular leakage and recruitment of leukocytes from the circulation. An increased neutrophil count correlates with the extent of leakage of the capillary bed, for example, in skin wounds (Qiu *et al.*, 2003; Coutinho *et al.*, 2005; Mori *et al.*, 2006).

In the CNS and the retina, the residential immune cells are mainly glial cells, including astrocytes, Müller cells and microglia cells. Cx43 has been found to be highly expressed in glial cells and responds to damage as described above. Up-regulation of Cx43 expression and/or reduced Cx43-formed junctional communication is generally seen in most injuries at the early stage. Phosphorylation of Cx43 residues may contribute to the dysfunction of junctional channels and the opening of the hemichannels (Lampe *et al.*, 2000; Cooper & Lampe, 2002). Opening of Cx43-formed hemichannels leads to passage of secondary messengers onto adjacent cells through Ca^{2+} influx and ATP release, which may cause secondary damage following the initial tissue injury. Altering the Cx43 response of glial cells may, therefore, ameliorate cell damage and improve or promote tissue repair following injury.

Studies with Cx43-definicient ($Cx43^{-/-}$) transgenic mice have shown that Cx43 protein plays a key role in the circulatory system (Reaume *et al.*, 1995), and the expression of Cx43 in microvasculature in the CNS and in the retina also suggests its critical function in the nervous system (Theis *et al.*, 2001). Increased Cx43 expression in endothelial cells is associated with the inflammatory response. Cx43 transcript has been found up-regulated in endothelial cell primary culture incubated with LPS (De Maio *et al.*, 2002). Increased junctional communication is essential for capillary endothelial cell migration following a mechanically induced wound in an *in vitro* monolayer cell culture model (Pepper *et al.*, 1989). A later study has demonstrated that this increased junctional coupling is associated with increased expression of Cx43 protein and transcript (Pepper *et al.*, 1992). In addition, this endothelial cell coupling can be inhibited by genetically created chimeric connexin and a fusion protein, which leads to a significantly prolonged time being required for complete wound closure (Kwak *et al.*, 2001).

Cx43 expressed on the endothelial cell may also take part in the processes of guiding and adhesion of leukocytes in order for them to migrate from the circulation into the injured tissue. For example, Cx43 expression has been found in LPS-treated leukocytes *in vitro*, and also in leukocytes obtained from the peritoneal cavity of LPS-injected animals (Jara *et al.*, 1995). The process is likely to be driven by inflammation-induced expression of Cx43 in leukocytes forming heterotypic or homotypic intercellular gap junctional communication to

36

aid leukocyte migration from microvessels. Furthermore, Cx43 expression has also been seen in leukemic cells from the human adult T-cell leukemia/lymphoma, a tumour characterised by its high frequency of cutaneous and visceral invasion (Bazarbachi *et al.*, 2004). Direct adhesion and junctional communication has been detected between leukemic-mimic cells and endothelial cells in cell culture models, which indicates a mechanism of tumour cell extravasation (Anderson & Vingrys, 2001; Bazarbachi *et al.*, 2004). The key roles of Cx43 in the residential cellular immune response, blood vessel leakage and circulating leukocyte recruitment further indicate that manipulating the function of Cx43 may reduce tissue damage and/or improve tissue repair following injury.

1.3.2 Modulation of connexin43

While the role of connexin43 (Cx43) following injury and during recovery has been investigated in an extensive range of tissues, specific modulation of Cx43 expression or function has only recently become a very interesting means of treatment for various diseases. To date, Cx43 specific antisense oligodeoxynucleotides (AsODN) and Cx43 mimetic peptides are the two major strategies for specific attenuation of Cx43. These have been studied in cell lines and in animal models of diseases, and even used to treat human health conditions.

Cx43 AsODN   Cx43 AsODN decreases Cx43 protein levels at the process of transcription (Figure 1-9). AsODN is a single-stranded synthesised DNA. It has a sequence which enables it to hybridise specifically to Cx43 messenger RNA (mRNA). This hybridisation stops the Cx43 mRNA sliding through cytoplasmic ribosome and translation into proteins. The hybridised Cx43 AsODN/mRNA complex is then cleaved by RNaseH (Phillips *et al.*, 2000). AsODNs can be used as drugs and have a dose-response. They have been reported to down-regulate the protein level by 15-50% (Phillips *et al.*, 2000). Pluronic gel, for slow release of drugs, has been established to provide an efficient way to deliver Cx43 AsODN onto chick embryos in windowed eggs and causes substantial developmental

defects. The defects are shown more often in the areas with normally high expression levels of Cx43 protein (Becker *et al.*, 1999).
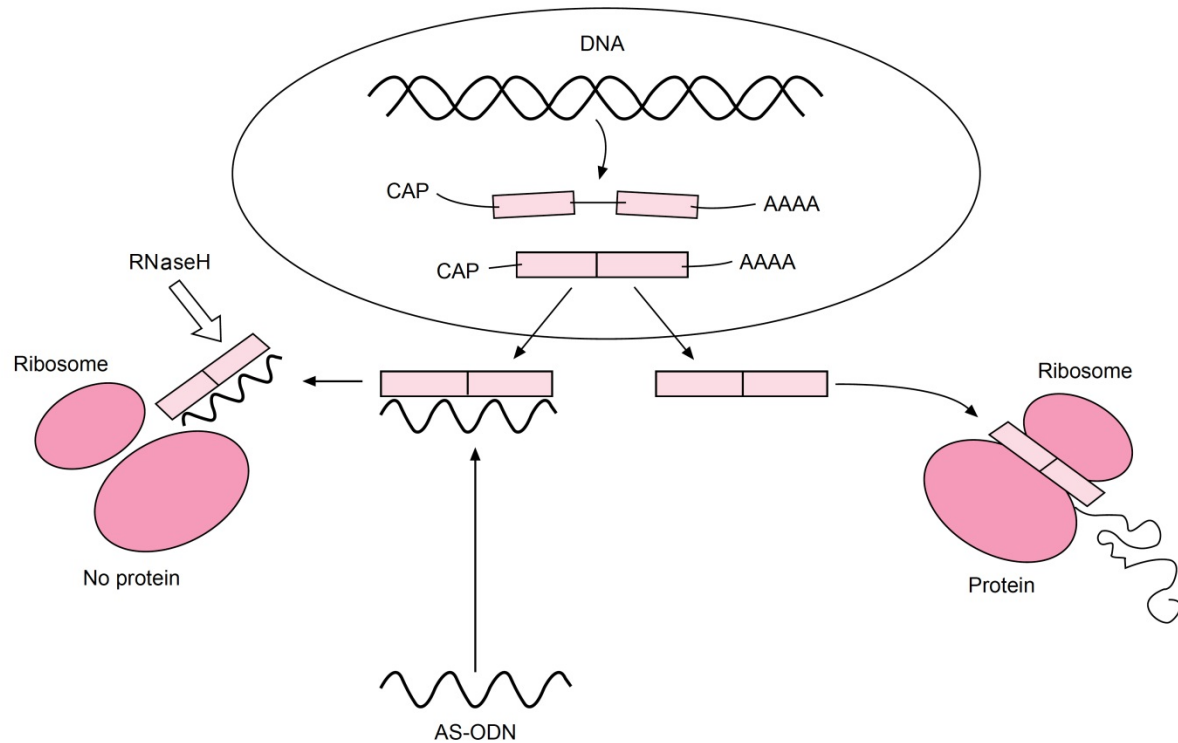
Figure 1-9. The mechanism of antisense oligonucleotides function. The hybridisation of Cx43 AsODN with Cx43 mRNA stops the Cx43 mRNA sliding through cytoplasmic ribosome and translation into proteins. Binding of AsODN to mRNA also stimulates RNaseH to hydrolyse the mRNA and, thereby, reduces the total amount of mRNA. This picture is adopted from (Phillips *et al.*, 2000). *Copyright License Number: 3241110782311.*

Cx43 AsODN application significantly accelerates skin wound healing and reduces scarring (Coutinho *et al.*, 2003; Qiu *et al.*, 2003; Coutinho *et al.*, 2005; Mori *et al.*, 2006). A single topical administration of Cx43 AsODN soaked gel dramatically increases wound closure in both incisional and excisional lesion mouse models (Qiu *et al.*, 2003). It also works efficiently on a burn lesion mouse model. Wound repair is 50% more advanced in Cx43 AsODN-treated wounds compared to the control at four days post-wounding (Coutinho *et al.*, 2005).

Cx43 AsODN has also been used for the treatment of corneal wounds in both an animal model and for human severe ocular surface burns, in parallel with the findings for skin wound healing (Grupcheva *et al.*, 2012; Ormonde *et al.*, 2012). In a rat corneal endothelial

injury model, knock-down of Cx43 by AsODN increases the endothelial cell proliferation rate and reduces corneal fibrosis by inhibiting the endothelial-mesenchymal transformation (Nakano *et al.*, 2008). Cx43 AsODN significantly improves the rate of reepithelialisation of the wound bed from mechanical scrape wounding. In excimer laser ablation wounds, Cx43 AsODN-treated rats exhibit less epithelial hyperplasia and stromal edema, and reepithelialisation occurs 24 hours earlier than in untreated animals (Grupcheva *et al.*, 2012). The results from five compassionate use human cases of Cx43 AsODN-treated severe ocular chemical or thermal burns are exciting. All five subjects did not show corneal recovery with best-practice clinical management in 1-8 weeks post-injury. With either one or two administrations of Cx43 AsODN, all five subjects showed rapid recovery of the vascular bed and full restoration of ocular surface integrity (Ormonde *et al.*, 2012).

Cx43 mimetic peptide   Connexin mimetic peptides are short synthetic amino acid peptides designed against sequences matching regions of either of the two extracellular loops (Evans & Boitano, 2001). By targeting the extracellular domains, the mimetic peptides interfere with either docking or gating processes of docked hemichannels located in the plasma membrane of the adjacent cells and impair intercellular communication (Berthoud *et al.*, 2000). It is unlikely that mimetic peptide separates formed gap junctions into the constituent hemichannels as docked gap junction connexons are difficult to separate (Evans & Boitano, 2001). Mimetic peptides may work on gap junctions in the intercellular space between neighbouring cells and lead to internalisation and breakdown of the gap junction (Evans & Boitano, 2001). More recent studies suggest that Cx43 mimetic peptides regulate cellular plasma membrane permeability through working on hemichannels (Retamal *et al.*, 2007; O'Carroll *et al.*, 2008). In this section of "Cx43 mimetic peptide", two topics will be discussed. First, there is a brief review on all the Cx43 mimetic peptides that have been designed and studied up to date. Second, a review of previous investigations on one specific Cx43 mimetic peptide, peptide5, is presented.

There are about seven mimetic peptides designed against Cx43, which have been established to be efficient inhibitors of gap junction communication and/or hemichannels (Table 1-1). The first and most widely studied two mimetic peptides against Cx43 are Gap 26 and Gap 27. These two peptides are designed against extracellular loop 1 and loop 2 respectively.

They are efficient in interrupting synchronous beating of chick embryonic cardiomyocytes (Warner *et al.*, 1995). Both Gap 26 and 27 also exhibit an inhibitory effect on rhythmic vasomotor activity of smooth muscle cells of rabbit superior mesenteric artery (Chaytor *et al.*, 1997). Gap 27 has an inhibitory effect on endothelium-dependent relaxation of rabbit arteries and endothelium-dependent smooth muscle hyperpolarisation/relaxation (Chaytor *et al.*, 1998; Dora *et al.*, 1999). Activated microglial cells show up-regulation of Cx43 hemichannel activity on astrocyte membrane permeability, and Gap 26 and 27 have been found to inhibit the effects of Cx43 hemichannel opening and to stabilise the cellular membrane (Retamal *et al.*, 2007). *In vivo* studies have found that a single jugular vein injection of Gap 26 or 27 significantly reduces the infarction size in rat myocardial infarction models (Hawat *et al.*, 2012). However, the sequences of Gap 26 and 27 are not specific to Cx43. The majority sequence part of Gap 27 (SRPTEK) is also expressed in Cx37 and Cx40. Therefore, these mimetic peptides may also work on other connexin proteins (Dora *et al.*, 1999; Evans & Boitano, 2001).

Another Cx43 mimetic peptide is designed against extracellular loop 2 (P180-195), which has shown to decrease diffusion of the fluorescent tracers Lucifer Yellow in embryonic rat aortic smooth muscle cells (Kwak & Jongsma, 1999). This peptide also suppresses the function of progesterone production in rat ovarian granulosa cells by inhibiting Cx43 activity (Ke *et al.*, 2005). A distinct Cx43 mimetic peptide corresponding to extracellular loop 1 has also been investigated (Mendoza-Naranjo *et al.*, 2007). This peptide blocks intercellular dye transfer between adjacent cells and diminishes the capacity for human dendritic cells to acquire tumour antigen from neighbouring cells (Mendoza-Naranjo *et al.*, 2007).

A peptide mimetic of the carboxyl terminal of Cx43, named αCT1, has been reported (Hunter *et al.*, 2005; Soder *et al.*, 2009; O'Quinn *et al.*, 2011). This mimetic peptide is 25 amino acids long and designed against the last 9 amino acids (374-382 residues) of the Cx43 carboxyl terminus. αCT1 also contains a cell-permeabilisation sequence, which allow the peptide to easily travel through the cellular membrane and bind to the carboxyl tail in the cytoplasm (Hunter *et al.*, 2005). αCT1 has been shown to modulate wound-healing processes in a rat silicone implant model and to reduce the inducible-arrhythmia in a mouse model following cardiac injury (Soder *et al.*, 2009; O'Quinn *et al.*, 2011).

A recent study has shown that intercellular administration of a Cx43 mimetic peptide designed against a calmodulin binding site on the cytoplasmic loop stops hemichannels docking and gap junction formation in neonatal mouse myocytes (Xu *et al.*, 2012). Although this peptide shows efficient blocking effects of Cx43 gap junctions, the delivery method may limit its potential usage as a therapeutic drug.

Table 1-1. Cx43 mimetic peptides

Sequence/Amino acid site	*Location/Domain*	*Reference*
VCYDKSFPISHVR (Gap 26)	Extracellular loop 1	(Chaytor *et al.*, 1997)
SRPTEKIFII (Gap 27)	Extracellular loop 2	(Chaytor *et al.*, 1997)
P180-195	Extracellular loop 2	(Kwak & Jongsma, 1999)
RPRPDDLEI (αCT1)	Carboxyl terminal	(Hunter *et al.*, 2005)
CNTQQPGCENVCY	Extracellular loop 1	(Mendoza-Naranjo *et al.*, 2007)
VDCFLSRPTEKT (peptide5)	Extracellular loop 2	(O'Carroll *et al.*, 2008)
Amino acids 136-158	Cytoplasmic loop	(Xu *et al.*, 2012)

The Cx43 mimetic peptide used for experiments described in this thesis is named peptide5 here to distinguish it from other mimetic peptides. Peptide5 was designed against the last several amino acids of extracellular loop 2. The first study with this Cx43 mimetic peptide has demonstrated that it significantly reduces tissue damage following spinal cord injury in an *in vitro* organotypic culture model (O'Carroll *et al.*, 2008). It has been shown to reduce tissue swelling and astrogliosis with less GFAP immunoreactivity compared to the sham-treated control after mechanical injury. Peptide5 also significantly improves neuron survival seen as more neuronal N- and neurofiliment H-positive cells (O'Carroll *et al.*, 2008). Interestingly, the same study also compared peptide5 and Gap 27 in the spinal cord *in vitro* organotypic culture where peptide5 is more effective at reducing tissue swelling (O'Carroll *et al.*, 2008). A further study with peptide5 on another organotypic culture model, hippocampal slice cultures, prevents the tissue from epileptiform lesion spread and promotes cell survival (Yoon *et al.*, 2010). The remarkable finding is that peptide5 shows a protective effect during the primary damage that mimics epileptiform seizures (Yoon *et al.*, 2010).

In addition to the *in vitro* evidence, peptide5 has also been shown to improve outcomes and protect tissue from damage after injury in various animal models (Danesh-Meyer *et al.*,

2012; Davidson *et al.*, 2012a; Davidson *et al.*, 2012b). Local administration of peptide5 via an external pump significantly improves electroencephalographic power and brain function in a model of sheep fetal global cerebral ischemia induced by bilateral carotid artery occlusion, although neuron survival has not been shown to be significantly improved (Davidson *et al.*, 2012a). A further study has shown that peptide5 delivered systemically has powerful neuroprotective effects for retinal ganglion cells in a rat model of retinal ischemia-reperfusion (Danesh-Meyer *et al.*, 2012).

Peptide5 selectively works on Cx43 hemichannels and stops the opening of hemichannels at low concentration (5 µM) and non-selectively works on both hemichannels and gap junctional channels at higher concentration (500 µM) (O'Carroll *et al.*, 2008). Evidence for this comes from *in vitro* results. The NT2/D1 cell line is a human testicular embryonal carcinoma cell line, which has high levels of Cx43 expression. Incubating with peptide5 (5 or 500 µM) in low calcium levels significantly inhibits dye uptake into NT2/D1 cells and the inhibition level is comparable with incubating with non-specific connexin hemichannel blockers, such as carbenoxolone and lanthanum chloride. At higher concentrations of peptide5 only, is dye transfer between cells blocked (O'Carroll *et al.*, 2008). Up-regulation of Cx43 expression has been detected in and associated with dysfunction of astrocytes and blood vessels in all the models following injury (O'Carroll *et al.*, 2008; Yoon *et al.*, 2010; Danesh-Meyer *et al.*, 2012; Davidson *et al.*, 2012a). Therefore, it is suggested that peptide5 protects the tissue from the damage resulting from the inflammatory response that follows the primary injury (Danesh-Meyer *et al.*, 2012).

1.4 Age-related macular degeneration

Age-related macular degeneration (AMD) clinically presents as central vision loss, affecting the region of the retina required for detailed vision tasks such as reading and face recognition. Pathological change in AMD is characterised by the accumulation of extracellular deposits between the pigment epithelium and the choroid, called drusen. During early AMD, drusen can be hard with distinct margins, and the presence of drusen represents the dry form of AMD. Subsequently, choroidal neovascularisation (CNV) develops and is accompanied by vascular leakage, which is characterised as wet AMD (de Jong, 2006). Clinically, AMD is classified into three stages: retinal pigment epithelium detachment (PED), geographic atrophy (GA) and CNV (Figure 1-10) (Bird, 2010). Retinal pigment epithelium detachment is the early stage of dry AMD, in which drusen accumulates between the RPE and Bruch's membrane. Patients with retinal pigment epithelium detachment do not necessarily have marked vision loss (Bird, 2010). GA is the late stage of dry AMD. It is characterised by one or several well-defined areas of RPE and photoreceptor atrophy. GA tends to progress with time. Patients with GA usually show severe vision loss (Bird, 2010; Biarnés *et al.*, 2011). CNV is characterised by drusen deposition, subretinal and choroidal haemorrhage, and fibrotic scarring (Jager *et al.*, 2008).
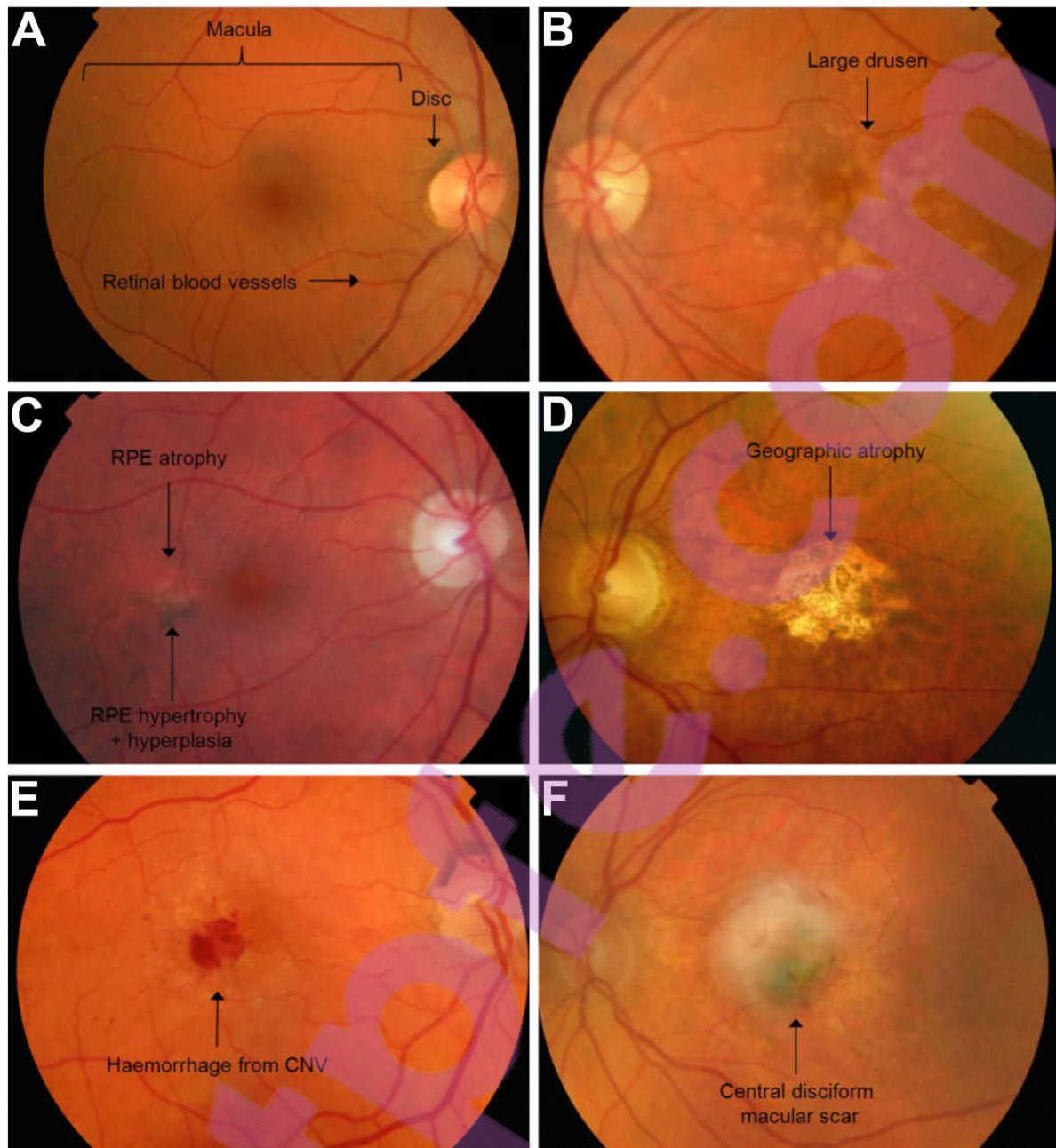
Figure 1-10. Fundus images showing different stages of AMD. **A:** Normal right eye. **B:** Drusen in early AMD. Large drusen can be seen. **C:** Early AMD pigmentation irregularities. **D:** Geographic atrophy (GA) in late stage of dry AMD. **E:** Choroidal neovascularisation (CNV) in late AMD. **F:** A permanent macular scar in late AMD. This image is adopted from (Khandhadia *et al.*, 2012). *Copyright License Number: 3241111063828.*

AMD is a multi-factorial disorder with many risk factors involved in triggering the disease. Research data has been accumulating on this age-related and vasculature-related disease (Xu *et al.*, 2009; Lin *et al.*, 2011; Coorey *et al.*, 2012). These suggest that there are several features of AMD that could be managed. The following paragraphs are mainly focused on

44

inflammatory responses and vascular changes involved in the pathogenesis of AMD. Recently findings on changes in intercellular communication in AMD are also included.

1.4.1 Inflammatory responses in AMD

Lipofuscin is related to lysosomal function along with photoreceptor phagocytosis and digestion in the RPE. The amount of lipofuscin in human RPE tends to increase with age (Weiter *et al.*, 1986). Lipofuscin deposits in the RPE and on Bruch's membrane, where drusen forms, indicating its association with drusen and AMD pathogenesis. Histochemically, drusen contains a mixture of protein, lipid and lipoprotein, including complement factors (C1q, C3a and C5a), complement regulators (complement factor H, clusterin, vitronectrin), immunoglobulins and apolipoprotein E (Johnson *et al.*, 2001; Lotery & Trump, 2007). These components suggest that drusen results from an inflammatory element in AMD development (Anderson *et al.*, 2002a). Two components in the retinal immune system are mainly involved, the complement system and the residential glial cells. Both have been identified to play important roles in the pathogenesis of AMD (McGeer *et al.*, 2005).

Complement factor H (CFH), one of the complement regulatory factors, is the first complement protein implicated in the pathogenesis of AMD (Hageman *et al.*, 2005). It is associated with 50-70% of cases of AMD in population studies (Edwards *et al.*, 2005; Haines *et al.*, 2005; Klein *et al.*, 2005; Gold *et al.*, 2006). CFH is present in drusen, in the sub-retinal space and around the capillaries in the choroid (Hageman *et al.*, 2005). Some variants of the CFH gene also have a close association with the pathology of AMD (Hageman *et al.*, 2005). The membrane-attack complex (MAC), formed after full activation of each complement pathway, has been found in drusen and in the RPE-choroid interface in AMD eyes (Mullins *et al.*, 2000; Hageman *et al.*, 2005). MAC leads to cell lysis through the formation of transmembrane pores. Another gene associated with AMD is complement component 1 (C1), which is the trigger for the classical complement pathway. The C1q subunit has been detected using immunohistochemistry in choroidal neovascular membranes

surgically removed in wet AMD patients (Baudouin *et al.*, 1992; Lommatzsch *et al.*, 2008). Complement component 3 (C3) is the key component in the complement system. All three complement pathways (classical, lectin and alternative pathways) result in cleavage of C3 into C3a and C3b. Deposition of C3 is also found in surgically removed choroidal neovascular membranes (Baudouin *et al.*, 1992; Lommatzsch *et al.*, 2008). Plasma levels of C3a in AMD patients have been found to be elevated compared to the control group, which may suggest that systemic complement activation can trigger AMD development (Sivaprasad *et al.*, 2007; Scholl *et al.*, 2008). C3 gene variants are highly associated with AMD in both English and Scottish populations (Yates *et al.*, 2007). Cleavage of complement component 5 (C5) into C5a and C5b is a marker of activation of the terminal complement pathway (Khandhadia *et al.*, 2012). Elevated plasma levels of C5a have been shown to be significantly associated with AMD (Reynolds *et al.*, 2009; Hecker *et al.*, 2010). Interestingly, a recent study has reported that C5a promotes the expression of interleukin (IL)-22 and IL-17 on T lymphocytes which may contribute to the increased plasma levels of IL-22 and IL-17 seen in AMD patients (Liu *et al.*, 2011). These interleukins have been shown to induce apoptosis and cellular dysfunction of RPE *in vitro* (Li *et al.*, 2008; Liu *et al.*, 2011).

Residential glial cells of the retina include microglia and macroglia. The retinal macroglia is mainly comprised of Müller cells and astrocytes (Coorey *et al.*, 2012). In AMD donor tissue, microglia have been shown to be enlarged and amoeboid-shaped. They migrate from the inner retina to the outer retina and subretinal space, which may be associated with photoreceptor degeneration and removal of cell debris (Gupta *et al.*, 2003; Buschini *et al.*, 2011). In dry AMD (GA and PED), microglia immunoreactivity has been found to be greatly increased (Penfold *et al.*, 1997). Activated microglia have secretory functions and may "cross-talk" with endangered neurons by secretion of pro-inflammatory cytokines, chemokines, complement receptors and chemokine receptors (Langmann, 2007). One chemokine receptor located on microglia has been found closely associated with AMD, the CX3CR1 chemokine receptor (Ding *et al.*, 2009). CX3CR1 is a protein that binds the chemokine ligand 1 (CX3CL1) and is involved in leukocyte adhesion and migration (Buschini *et al.*, 2011). Two variants of CX3CR1 are involved in harbouring single nucleotide polymorphisms (SNPs)-associated variants of complement proteins, which are

46

closely linked to AMD (Tuo *et al.*, 2004). A further study has demonstrated that one of the variants increases the risk of AMD, but not the other (Combadière *et al.*, 2007). In addition to secretion from activated microglia to support neurons, endangered neurons may also emit signals to microglia for assistance (Hanisch & Kettenmann, 2007). Many cytokines and chemokines, Ca^{2+} elevation, ATP elevation and nitric oxide can increase microglia activity (Nakamura, 2002). In addition, a recent study has reported that some neurotransmitters are able to modulate microglia activity in an indirect way (Fontainhas *et al.*, 2011). The ionotropic glutamatergic neurotransmission increases the activation of microglia and the ionotropic GABAergic neurotransmission decreases microglia activity (Fontainhas *et al.*, 2011).

In addition to microglia, astrocytes and Müller cells also have been found to play important roles in the pathogenesis of AMD. GFAP is a common marker for astrocytes in the ocular tissue, and in the normal retina, Müller cells express little or no GFAP (Dahl, 1979). An early report has shown that GFAP-immunoreactivity is associated with Müller cells in AMD donors, but absent in normal young and aged donor tissues (Madigan *et al.*, 1994). A later study has further clarified that increased GFAP-immunoreactivity is associated with AMD, and Müller cells express GFAP in both early (retinal pigment epithelium detachment) and late stages (geographic atrophy) of dry AMD (Wu *et al.*, 2003). Interestingly, some neurons, such as amacrine cells have been noticed to migrate from the inner retina into the outer retina, and this migration is associated with increased GFAP-immunoreactivity (Sullivan *et al.*, 2003). This may suggest a key role of Müller cells in neuronal migration and retinal remodelling (Jones & Marc, 2005). An investigation into astrocytes in human AMD donor tissue has suggested that the processes of astrocytes in AMD do not show any difference from the normal aged retina. However, the cell bodies are enlarged, suggesting its phagocytosis activity (Ramírez *et al.*, 2001). Astrocytes are also, in conjunction with pericytes, involved in maintaining the structure and function of the blood-retinal barrier (Paula *et al.*, 2010; Runkle & Antonetti, 2011).

1.4.2   Vascular factor in AMD

AMD is recognised as a vascular disease and blood vessel changes are highly associated with the pathogenesis and progress of the disease (Coorey *et al.*, 2012). In early stages of AMD, a greater number of non-functional retinal capillaries have been detected using histological methods, and they have thicker vascular walls compared to those in the normal aged retina (Ramírez *et al.*, 2001). Dysfunction of the choriocapillaris may contribute to the formation of drusen and atrophy of RPE (Penfold *et al.*, 2001; Bhutto & Lutty, 2012). A hemodynamic model has also suggested that the increased resistance of blood flow in the choroid may contribute to the accumulation of metabolic waste and the deposit of drusen and lipofuscin (Friedman, 1997; Bhutto & Lutty, 2012). In hypertension and cardiovascular diseases there is constriction of blood vessels with increased resistance to blood flow. Many population studies have found that hypertension and cardiovascular diseases are high risk factors associated with AMD (Hyman *et al.*, 2000; Tan *et al.*, 2007; Hogg *et al.*, 2008; Carresi *et al.*, 2009). Furthermore, a study of human donor tissues with late stage dry AMD has shown that the density of the choriocapillaris is reduced by 50% in the areas with RPE loss compared to the same area in the control eye (McLeod *et al.*, 2002). The surviving choriocapillaris in the RPE atrophy area are highly constricted (McLeod *et al.*, 2002). Nitric oxide (NO) is an important molecule for vasodilation in blood vessels. It is mainly produced by nitric oxide synthases (NOSs) located in endothelial cells and perivascular nitrergic neurons (Alderton *et al.*, 2001). Low expression of nitric oxide synthases (NOSs) in AMD leading to low production of NO, may contribute to the constriction in the choriocapillaris (Bhutto *et al.*, 2010). In wet AMD, similarly, a 50% reduction in choriocapillaris density has been noticed in areas with complete RPE loss (McLeod *et al.*, 2009). However, the luminal diameters of the remaining choriocapillaris in the RPE atrophy area are not significantly different to those in control eyes (McLeod *et al.*, 2009). This finding suggests that some angiogenesis factors may be involved in the disease progress and development of the late stage of AMD (Bressler, 2009; McLeod *et al.*, 2009; Bhutto & Lutty, 2012).

Surviving RPE in dry AMD has been suggested to be associated with development of choroidal neovascularisation (CNV) (Sunness *et al.*, 1999). A four-year study on determining the rate of developing CNV from eyes with geographic atrophy (GA) with an

annual follow-up has demonstrated some interesting results (Sunness *et al.*, 1999). One patient had both eyes with GA. CNV developed in one eye in areas with surviving RPE while no CNV developed in the other eye with GA and instead the RPE and Bruch's membrane were penetrated (Sunness *et al.*, 1999). Another patient from the same study had retinal pigment epithelium detachment (PED) prior to GA in both eyes. CNV developed in one in which the PED resolved while the other eye remained with only GA (Sunness *et al.*, 1999). In GA, reduction of the choriocapillaris may lead to hypoxia in the local microenvironment. Local hypoxia may up-regulate the production of VEGF by RPE cells (Blaauwgeers *et al.*, 1999). In human donors with age-related maculopathy, expression of VEGF is significantly increased in the RPE compared with the normal control (Kliffen *et al.*, 1997). Various isoforms of VEGF (A, C and D) have also been identified in the RPE of a human AMD donor while they are absent in age-matched controls (Ikeda *et al.*, 2006). Both transcription and protein translation of VEGF-A are up-regulated under hypoxia *in vitro* (Ikeda *et al.*, 2006). Animal models with an over-expression of VEGF in the RPE exhibit CNV and enhanced vascular leakage (Spilsbury *et al.*, 2000; Schwesinger *et al.*, 2001).

1.4.3   Current management for AMD

The pathogenesis of AMD is complicated and multiple risk factors are involved. So far, there is no strategy that can cure AMD or even a particularly effective treatment for AMD. Current management for the disease is focused mainly on the late stage CNV. However, there are some established and potential approaches under investigation. They are listed below.

Intravitreal injection of anti-angiogenic agents   This is the primary therapy for CNV. Targeting vascular endothelial growth factor (VEGF) and its pathway is the traditional way of generating anti-angiogenic agents. This procedure has been established to be clinically efficient. One type of agents countering the function of VEGF is pegaptanib sodium (Macugen), which is a small interfering RNA molecule (siRNA) targeting $VEGF_{165}$, the most abundant variant of VEGF-A (Konerding, 2004; Nowak, 2006). VEGF antagonists

such as specific antibodies against either a particular VEGF-A isoform (bevacizumab/Avastin) or all the isoforms of VEGF ranibizumab/rhuFab V2/Lucentis) have positive effects on reducing vascular leakage in CNV (Nowak, 2006). In addition to the siRNA and antibodies, corticosteroid (triamcinolone acetonide) is also used in CNV. Its anti-inflammatory effect can inhibit the formation of prostaglandins and leukotrienes (Maloney *et al.*, 2007). A novel cortisone, anecortave acetate (Retaane), devoid of glucocorticoid activity, which shows a clear advantage over triamcinolone, has effects on inhibiting vascular endothelial cell migration, thereby inhibiting progress of CNV (Nowak, 2006; Maloney *et al.*, 2007).

Photodynamic therapy   This therapeutic method involves intravenous infusion of verteporfin, a photosensitive dye, followed by activation of the dye using infrared light (Lim *et al.*, 2012). Verteporfin accumulates on the neovascular membranes and its activation process generates reactive singlet oxygen species which result in direct damage to the endothelium (Nowak, 2006; Lim *et al.*, 2012). Based on a 343 patients study in New Zealand, this treatment has been shown to be effective, with 70% verteporfin-treated patients avoiding moderate vision loss in 12 months compared to 46% placebo group reported previously (Sharp *et al.*, 2007; Hagigit *et al.*, 2010). Photodynamic therapy was introduced in the late 1990s but is rarely used now (Lim *et al.*, 2012). It has many adverse events, including a 4% chance of acute severe vision loss (Lim *et al.*, 2012).

Laser photocoagulation   This treatment is to create closure of the newly formed blood vessels in CNV by using an argon laser (Lim *et al.*, 2012). Laser photocoagulation is effective in preventing long-term severe vision loss in eyes with small classic extra-foveal and juxta-foveal choroidal neovascularisation lesions (Lim *et al.*, 2012).

Nevertheless, further molecular targets need to be identified for the management of AMD, especially treatments for the early stage of this disease. Since considerable research has been done on intercellular communication in the central nervous system, this field can be explored in the retina and choroid, with the hope of finding a novel therapy for early stages of AMD. Animal models are a useful research tool for investigating human health conditions. I chose the intense light-exposed albino rat as the animal model for this thesis.

1.5   Intense light-exposed albino rat as an animal model for AMD

In the 1960s, Noell et al. reported that intense fluorescent light was able to cause retinal degeneration (Figure 1-11) (Noell *et al.*, 1966). It has since been demonstrated that prolonged light exposure can cause severe damage in the retina. Electroretinograms (ERG) were used in Noell's study for analysis of photoreceptor function. Albino rats exposed to intense fluorescent light with a green plastic filter for four hours had decreased a-waves and b-waves. The damage started to show immediately after light exposure and became progressively severe from 24 hours up to 3-4 weeks post-exposure (Noell *et al.*, 1966). More interestingly, the same amount of total light exposure duration interrupted with dark intervals generate more severe damage than continuous light exposure without interruptions (Noell *et al.*, 1966). Histological analysis showed that a continuous four-hour, intense fluorescent light exposure caused loss of photoreceptors and pigment epithelium, and breakage of the Bruch's membrane, in a pattern similar to that is found in age-related macular degeneration (AMD) patients (Noell *et al.*, 1966; Marc *et al.*, 2008). More detailed pathological changes in light-induced retinal degeneration in albino rats were studied and reported by Robert Marc in 2008. He found that light damage triggered retinal pigment epithelium and choriocapillaris losses, changes to Müller cells, and retinal neuron death. The damage was regional, mainly limited to the central and superior area of the retina. The entire lesion closely resembled the human retinal atrophy that occurs in human AMD (Marc *et al.*, 2008). Although the light-induced retinal damage in the albino rats has been extensively used as a good model for investigating mechanisms of retinal degeneration (Ng & Streilein, 2001; Marc *et al.*, 2008; Rutar *et al.*, 2010) and assessing the efficacy of various therapeutic compounds (Xu *et al.*, 2008a; Albarracin *et al.*, 2011), the mechanisms of retinal degeneration induced by light damage remain unclear.
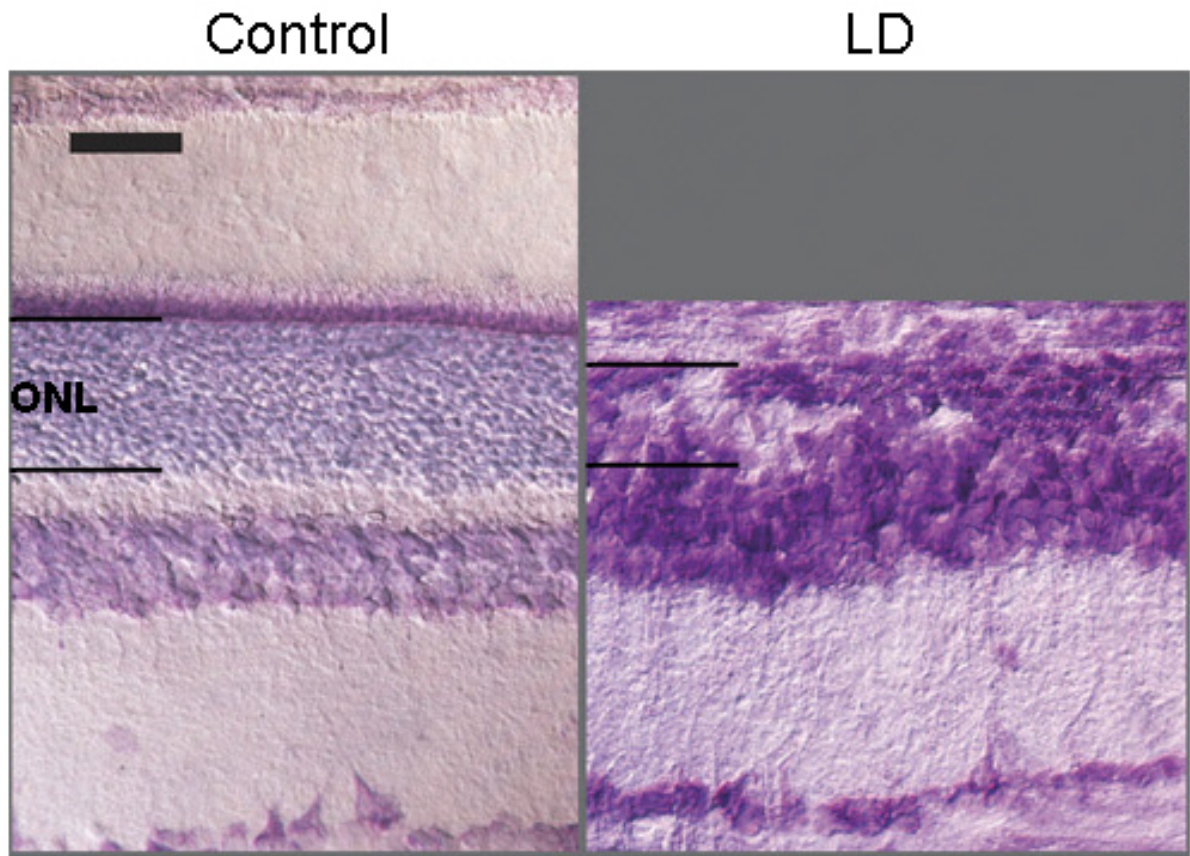
Figure 1-11. Rat retinal sections stained with toluidine blue showing the photoreceptor degeneration following light-damage. The light-damaged (LD) retina shows an obvious thinner outer nuclear layer (ONL) compared to the control (Albarracin *et al.*, 2011). *Copyright License Number: 3266170870812.*

1.5.1 Altered metabolic function in both photoreceptors and Müller cells

Continuous intense light exposure may cause alterations in retinal metabolic functions (Fain & Lisman, 1993; Yu *et al.*, 2007). Agmatine, an endogenous neuromodulator, is packaged and released into synapses upon neuronal depolarisation, and it may become unregulated under stress and inflammatory conditions (Halaris & Plietz, 2007). It is a marker for assessing photoreceptor cation channel permeability (Kalloniatis *et al.*, 2002; Acosta *et al.*, 2005a). Light damage increases the expression level of agmatine in the albino rats, indicating changes in photoreceptor metabolic function (Yu *et al.*, 2007). Studies have shown that extracellular pH modulates photoreceptor output synapse and the release of neurotransmitters (Barnes *et al.*, 1993; DeVries, 2001). Light damage induces elevation of

52

cations (i.e. H$^+$) in the retina and thereby affects the functions of photoreceptors (Ugarte & Osborne, 1999; Ettaiche *et al.*, 2004). Continuous intense light also causes alterations in Müller (glial) cells in the retina (Grosche *et al.*, 1995; Yu *et al.*, 2007). Glutamine synthetase (GS) is confined exclusively to the Müller cells in rat retina (Riepe & Norenburg, 1977) where it plays a role in inactivating the photoreceptors' neurotransmitter, glutamate, and transforming it into glutamine. The expression of GS has been found to be reduced in isolated Müller cells from the light-damaged rat retinae (Grosche *et al.*, 1995). Intense light exposure in rats led to morphological changes in the Müller cells, including distal migration of the nuclei and cell hypertrophy (Jones *et al.*, 2006). Vimentin is a specific marker of astrocytes in the normal retina (Pekny, 2001), but Müller cells also express high levels of vimentin following intense light exposure (Albarracin & Valter, 2012).

Prolonged light exposure leads to an increased metabolic rate, high oxygen flux and occurrence of high levels of polyunsaturated fatty acid (PUFA) in the retina (Yu & Cringle, 2001). Docosahexaenoic acid (DHA) is the most preferentially used n-3 PUFAs and is efficiently transferred from blood lipids to the outer segments (Pifferi *et al.*, 2012). DHA is generated from the metabolism and is more abundant in rod outer segments than in any other mammalian membrane (Fliesler & Anderson, 1983). In many animal models of retinal degeneration, low membrane DHA levels are detected (Anderson *et al.*, 2001; Anderson *et al.*, 2002b). Interestingly, low retinal DHA protected albino rats from intense light exposure. These metabolic alterations in the light-damaged animal model match the changes observed in human AMD (Bidwell III & Raucher, 2010).

1.5.2   Rhodopsin bleaching

Noell et al. has suggested that the damage induced by light is rhodopsin-mediated (Noell *et al.*, 1966). A later study has shown that the damaging effect of light followed the rhodopsin absorption curve. The extent of damage depended on the wavelength relevant to the rhodopsin absorption curve (Kaitz & Auerbach, 1979). The rhodopsin levels are matched to dark adaptation. Dark-reared albino rats had about 50% higher rhodopsin content (Battelle

& LaVail, 1978) and are more susceptible to light damage (Penn *et al.*, 1987) than those reared in cyclic light. The suggestion that rhodopsin bleaching is associated with damage from light is supported by other findings. Two different types of rhodopsin-deficient transgenic mice (*Rpe65*$^{-/-}$ and *Rho*$^{-/-}$), with and without expression of the apoprotein opsin respectively, are both protected against light-induced apoptosis in the retina (Grimm *et al.*, 2000b). Therefore, light could be the trigger for retinal degeneration and the absence of rhodopsin in photoreceptors could lead to protection against light damage. Yet, vision starts with the bleaching of rhodopsin and therefore the balance between physiological vision process and retinal damage is a naturally accruing process. Studies have shown that excessive exposure to blue light and visible light in early human life could increase the risk of AMD in later life (Taylor *et al.*, 1990; Taylor *et al.*, 1992; Simons, 1993; Tomany *et al.*, 2004). Another human study based on more than four thousand participants has reported that there is a significant association between blue light exposure and vascular AMD (Fletcher *et al.*, 2008). In addition, a study has demonstrated that a black population showed a lower risk of getting AMD than did a white population (Schachat *et al.*, 1995). The most accepted theory on the retinal damage caused by photo-bleaching is that it is due to the consequence of released oxidants from photoreceptors responding to light.

1.5.3   Photo-oxidative stress

Like many other sources of reactive oxygen species (ROS), including radiation, toxic chemicals and drugs, light triggers rhodopsin bleaching and generates ROS as side-products in the retina. The reactive species include lipid peroxidation, which leads to membrane instability (Delmelle, 1977). The constant phagocytosis and degradation of rod outer segments results in an accumulation of the oxidative damage in the RPE.

Lipofuscin is an autofluorescent lipid-protein deposit. It occurs naturally and is believed to be associated with aging. Its presence was confirmed in human RPE where it is typically located in the basal half of the RPE cells in older individuals (Feeney-Burns *et al.*, 1980). Intense blue light exposure increases photoreactivity and the presence of lipofuscin in human

54

RPE cells *in vitro* (Rózanowska *et al.*, 1995). Another study has demonstrated that the apoptosis of RPE caused by blue light was mediated by lipofuscin fluorophore A2E (Sparrow *et al.*, 2000), which is present in ocular lipofuscin (Sakai *et al.*, 1996; Reinboth *et al.*, 1997). It has been suggested that singlet oxygen is involved in the RPE damage, either directly or through the generation of A2E. This is supported by results showing that the death of A2E-containing RPE induced by blue light can be blocked in oxygen-depleted media (Sparrow *et al.*, 2002). In addition, *in vivo* data from macaque retinas also showed that visible light induced permanent RPE damage which was thought to be via photo-oxidation of lipofuscin (Morgan *et al.*, 2008). Permanent retinal injury caused by laser exposure was demonstrated in brown Norway rats which exhibit an age-related accumulation of lipofuscin (Boretsky *et al.*, 2011). Photo-oxidative stress mainly involves generating ROS in the photo-transduction pathways and RPE damage from excess ROS, possibly through lipofuscin or other reactive photo-products. Lipofuscin and other oxidised phospholipids are implicated in stimulating inflammatory responses, especially activation of the innate immune response.

1.5.4   Inflammation

Oxidatively modified lipids can be recognised by the macrophages and other phagocytes which form the first line of immune defence in the body. Identifying the enhanced activity of retinal glial cells is a critical approach in determining inflammatory responses in light damaged ocular tissue. Astrocytes show enhanced activity in the albino rat retina after intense light exposure. GFAP immuno-reactivity significantly increased following light damage, and the staining expands from the nerve fibre layer in the normal control tissue to the outer retinal layers in the light-damaged retina (Figure 1-12) (Rutar *et al.*, 2010).

Figure 1-12. Light-damaged rat retina shows increased GFAP immunoreactivity in Müller cells. **A:** GFAP immunoreactivity in the control rat retina without intense light exposure. **B:** Increased GFAP immunoreactivity in the retina after 24 hours intense light exposure. **C:** Dramatically increased GFAP immunoreactivity throughout all retinal layers at 3 days after 24 hours intense light exposure. Images are adopted from (Rutar *et al.*, 2010).

Microglia also respond rapidly to light damage (Figure 1-13). In normal rat retina, microglia are limited in the inner plexiform layer, outer plexiform layer and ganglion cell layer and the primate retina has microglia in the outer nuclear layer and nerve fibre layer in addition to the layers listed in the rat retina (Ashwell *et al.*, 1989; Chen *et al.*, 2002). The subretinal space is the area between the photoreceptors and the RPE, which is devoid of immune cells under physiological conditions (Xu *et al.*, 2009). Many results have demonstrated that intense light exposure is a sufficient stimulus to turn microglia from resting-phase to activated-phase. In albino mice exposed to bright light (500 Lux), 5D4-positive microglia were observed in the subretinal space (Ng & Streilein, 2001). Pigmented Balb/cJ mice exposed to intense light (3500 Lux) for a short period (3 hours) showed activation and migration of the microglia from 6 hours to 3 days after the light exposure. The morphology of CD11b-positive microglia presented a round or oval shape from 6 hours to 1 day and changed to be ramified 3 days after light exposure (Zhang *et al.*, 2005). 24 hours intense light exposure (1000 Lux) leads to ED1-positive macrophages being detected in the retinal vasculature and underlying the choriocapillaris in the choroid in albino rats immediately after exposure. These cells were then detected in the outer nuclear layer by 3 days after light damage (Rutar *et al.*, 2010). Inhibition of microglia activation by delivering minocycline protected photoreceptor loss from light damage (Zhang *et al.*, 2004).
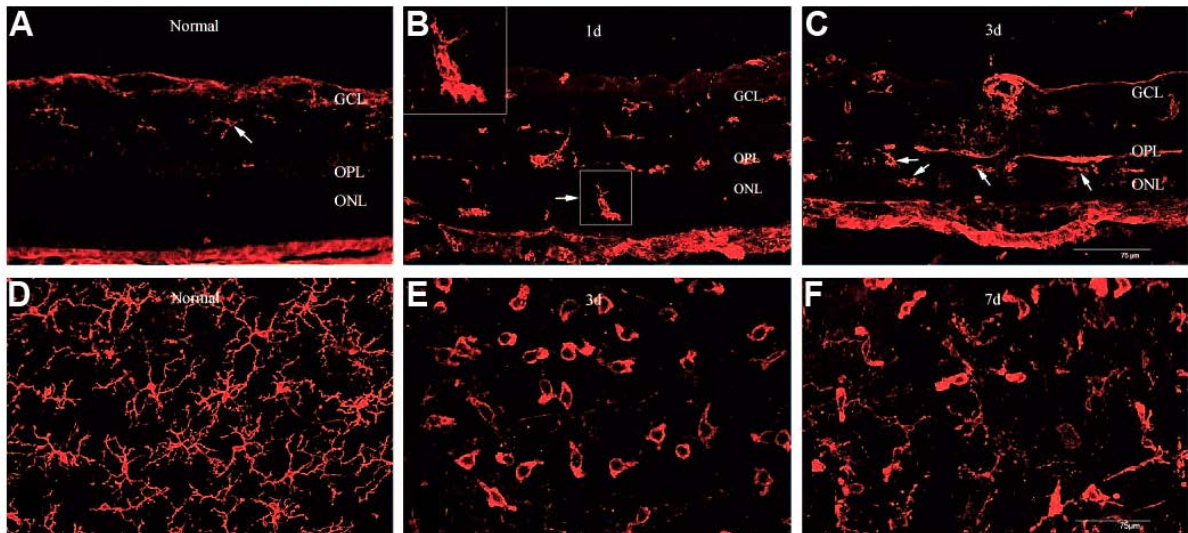
Figure 1-13. Reactive microglia shown in the rat retina following light damage. Increased microglia activity observed in the light-damaged rat retina. The images show microglia immuno-labelled with OX42 antibody. **A-C:** retina cross sections; **D-F:** retina flat-mounts. **A&D:** normal rat retinae without intense blue light exposure; **B&E:** rat retinae at 1 day after 24 hours intense blue light exposure; **C&F:** rat retinae at 7 days after 24 hours intense blue light exposure. Images are adopted from (Ni *et al.*, 2008). *Copyright License Number: 3266170954731.*

More excitingly, these research findings on microglia/macrophage activation from the light-damaged animal models are comparable with many results from aging studies. Major histocompatibility complex (MHC) class II- and ED1-positive microglia, activated T cells, and monocyte-like cells were found in aged (24 to 30 months old) albino rat retinas (Chan-Ling *et al.*, 2007). Aged pigmented mice also showed Iba-1-and ED1-positive microglia in the subretinal area (Xu *et al.*, 2007; Xu *et al.*, 2008b). Microglial activation and migration have been observed in a transgenic animal model of AMD, the *rd* mice. The microglia migrates from the inner retinal layers to the outer retinal layers and to the subretinal layer during photoreceptor degeneration is occurring (Zeng *et al.*, 2005). In addition to microglia, Müller cells also respond to light damage. An increased expression of Ccl2 has been found in the Müller cells in a light-damaged albino rat eye by using immunohistochemical methods (Rutar *et al.*, 2011b). This elevated secretion of Ccl2 in Müller cells may promote activation and recruitment of microglia into the injured area following light-damage (Rutar *et al.*, 2012b).

The complement system, another component of the innate immune system, also plays a critical role in light-damaged ocular tissue. Albino mice with continuous bright light

exposure (1000 Lux) showed increased transcript levels of C1qβ and C3, which are complement components of the alternative pathway (Rohrer *et al.*, 2007). 24 hours bright light exposure (1000 Lux) in the albino rats led to the up-regulation of complement proteins, including C1s, C3, C4b, C3ar1, and C5r1 in the retina and a deposit of C3 synthesised by microglia/macrophages in the outer nuclear layer and subretinal space (Rutar *et al.*, 2011a). All studies on phagocytes and the complement system from the light-damaged animal models showed close similarities to the inflammatory responses observed in the human AMD condition, which further indicates that the light-damaged animal model may be a good model for the study of human retinal degeneration.

1.5.5 Blood vessels

The retinal microvasculature has been recognised as one structure compromised in human AMD. Many conditions altering the vasculature affect the onset, progress and outcome of AMD, such as cardiovascular disease, smoking, alcohol consumption, dietary fat intake and some of the female sex hormones (Evans, 2001). There are a number of studies on the light-damaged animal model that have shown interesting findings related to pathological changes in the blood vessels. A photoactive compound, which naturally exists as a haemoglobin precursor in the blood, was demonstrated to generate superoxide anion and singlet oxygen in the light-exposed areas such as the retina (Gottsch *et al.*, 1990). Retinal capillaries were found to be particularly vulnerable to oxidative stress (Fukumoto *et al.*, 2012), and therefore, all the reactive oxygen species or reactive nitrogen species generated from photo-oxidative stress within the tissue and blood alter the endothelial cells of the retinal microvasculature. Another study showed that an oxidative stress marker, 8-hydroxy-2-deoxyguanosine (8-oxoG) was detected in mouse choroidal endothelial cells after green light exposure (Wu *et al.*, 2005). All the injuries to the endothelial cells in the ocular tissue subsequent to light damage may lead to vascular leakage and could be associated with the inflammatory responses in that area.

Light-induced ocular damage can be achieved in rats (Noell *et al.*, 1966; Frank *et al.*, 1989; Grimm *et al.*, 2000a; Organisciak *et al.*, 2000; Yu *et al.*, 2007; Marc *et al.*, 2008; Rutar *et al.*, 2010), mice (Ng & Streilein, 2001; Zeng *et al.*, 2005; Zhang *et al.*, 2005; Rohrer *et al.*, 2007; Xu *et al.*, 2008b) and many other species (Fite *et al.*, 1993; Criswell *et al.*, 2004; Thomas *et al.*, 2012). Unlike transgenic animal models for AMD (Strettoi *et al.*, 2003; Yu *et al.*, 2004), the light-damaged animal model does not have to involve any modified genes as the pathogenic factors. It closely mimics the dystrophies and degenerations present in the human AMD condition in many aspects, including photoreceptor apoptosis, RPE damage, cellular and tissue oxidative stress, microvasculature injury and inflammatory responses. Therefore, the albino rat exposed to intense light (2700 Lux) for 24 hours has been used as an animal model of AMD in this thesis.

1.5.6   Gap junctions responding to light

Gap junctions or electrical synapses provide an efficient and low-noise form of inter-neuronal signal transmission in the retina (Völgyi *et al.*, 2013). Horizontal cells are second-order neurons that contact both rods and cones in the outer plexiform layer providing signal modulation through gap junction hemichannels in the lateral pathway for processing visual signals (Kamermans *et al.*, 2001; Bloomfield & Volgyi, 2009). Light modulates the density of gap junctions located on the horizontal cells. By using a quantitative freeze-fracture replica method, enhancement in the density of gap junctions on horizontal cells in goldfish has been found to be associated with short-term dark adaptation (Kurz-Isler & Wolburg, 1986). Further electrophysiological studies have demonstrated that darkness results in a larger coupling field of horizontal cells and brightness decreases the coupling field. In this way, light-modulated horizontal coupling maximises the local contrast detection (Balboa & Grzywacz, 2000; Bloomfield & Volgyi, 2009). Cx50 and Cx57 have been identified on mouse horizontal cells (Hombach *et al.*, 2004; O'Brien *et al.*, 2006). Therefore, these two connexin proteins may primarily contribute to the light-modulated changes. After long-term dark adaptation for several days, the transcript level of Cx50 is significantly increased, while both transcript and protein of Cx57 are decreased in the mouse retina (Kihara *et al.*, 2006;

Janssen-Bienhold *et al.*, 2009). Light-adaptation leads to a significant increase in the number of Cx57-immunostained plaques in the mouse retina (Janssen-Bienhold *et al.*, 2009).

In addition to horizontal cells, AII-AII amacrine cell coupling through gap junctions also plays key roles in the retinal lateral pathway (Vaney, 2002; Wässle, 2004), and the coupling can be modulated by light (Bloomfield & Völgyi, 2004). Gap junctional coupling on AII amacrine cells measured by electrophysiological methods has shown cells to be relatively uncoupled in the dark-adapted retina with dramatically increased coupling in scotopic conditions and then uncoupled again under light-adapted conditions (Bloomfield & Völgyi, 2004). In rat and mouse retina, both Cx36 and Cx45 are expressed on AII amacrine cells (Feigenspan *et al.*, 2001; Mills *et al.*, 2001; Maxeiner *et al.*, 2005). Hence, both connexin proteins may contribute to the coupling function changes in response to light. The transcript of Cx45 is significantly decreased in the mouse retina following prolonged dark-adaptation (Kihara *et al.*, 2006). Both transcript and protein of Cx36 are also significantly decreased after dark-adaptation in the mouse retina (Kihara *et al.*, 2006). However, results from dark-adapted chick retina demonstrate conflicting findings to the mouse retina. Both transcript and protein levels of Cx36 are markedly increased following dark-adaptation (Kihara *et al.*, 2009). Cx36 may play a role in neuronal survival following traumatic injury of the retina. Increased Cx36 protein has been demonstrated to be associated with a laser-created retinal lesion, and Cx36-deficient (Cx36$^{-/-}$) mice exhibit a significant increase in cell death after the trauma (Striedinger *et al.*, 2005).

Cx36 and Cx45 are also involved in retinal ganglion cell coupling (Schubert *et al.*, 2005a; Schubert *et al.*, 2005b; Völgyi *et al.*, 2005). Ganglion cell coupling in the retina has been examined by detecting tracer labelling after injection into a single cell (Hu *et al.*, 2010). The light-adapted retina shows an overall increase in alpha ganglion cell coupling in the dark-adapted retina (Hu *et al.*, 2010).

Endothelial cell-associated connexin proteins, Cx37 and Cx43, both respond to prolonged dark-adaptation (Kihara *et al.*, 2006). The transcript of Cx37 is significantly increased, while the transcript and protein of Cx43 is markedly decreased in the mouse retina following 7 days of dark-adaptation (Kihara *et al.*, 2006). The other connexin protein expressed on the

endothelial cells, Cx40, does not show any change with dark-adaptation (Kihara *et al.*, 2006).

1.6 Objectives of this study

The pathogenesis of AMD is multi-factorial and current management is limited primarily to the late stage of the disease. It has been established that intercellular communication plays a key role in many injuries and that modulation of the function of Cx43 is efficient in minimising tissue damage and accelerating tissue repair following injury. The hypothesis of this investigation is that oxidative stress and inflammation are vital factors in the pathogenesis and progress of AMD. In fact, inflammation is clearly associated with the up-regulation of Cx43. By reducing the function of Cx43 channels, inflammatory responses are down-regulated and the tissue injury can be reduced. Therefore, the primary objective of this thesis is to provide the evidence for a new therapeutic approach for early AMD by targeting Cx43. To achieve this, some specific aims have been undertaken:

1) *To further characterise the light-damaged albino rat model to confirm its suitability as an animal model for studying the early stages of AMD.*

To validate that the light-damaged albino rat used in our laboratory is a suitable model for the study, I have tested the retinal function in the animal model following light damage with various recovery periods (0, 6, 24, 48 hours and 7 days) using electroretinograms (ERG). I have investigated the localisation and expression levels of Cx43 in the model by using immunohistochemistry and Western blotting. The levels of oxidative damage, inflammation and cell death that are reported to be involved in the etiology of AMD have been analysed by immuno-labelling specific markers for these factors. The expression of an oxidative stress marker, nitrotyrosine has been quantified by Western blotting and cell counts of Iba-1-immuno-labelled microglia has been used to measure inflammation levels. As RPE atrophy has been found to be one of the first histological signs of AMD, I have examined the morphological changes of the RPE in the light-damaged animal model. In addition to Cx43, some other connexin proteins, including Cx36, Cx40 and Cx45 have also been investigated.

2) *To characterise the functional and molecular effect of Cx43 modulation in the light-damaged albino rat model.*

Intravitreal injection of a mimetic peptide, which blocks hemichannels of Cx43, was used to locally modulate hemichannel function. First, I verified the delivery of the mimetic peptide to the posterior segment of the eye via tracing fluorescence-conjugated peptide injected intravitreally. Following this, ERG tests were used to see if the retinal function could be improved with either a single or double dose of the Cx43 mimetic peptide, peptide5, compared to the sham-treated animals. Tissue samples collected from the treated animals following ERG were then further analysed to check for Cx43 and other connexin protein expression levels and the degree of inflammation using an immunohistochemistry method.

3) *To verify the findings from the animal model in human AMD eyes.*

I investigated the general pathological changes in a late dry AMD donor tissue using toluidine blue staining. Then, I further checked oxidative stress and glial cell responses in human AMD donor tissue and compared this with an age-matched control donor tissue by detecting the immunoreactivity of specific markers in the retina. Up-regulated oxidative stress and inflammation were found to be closely associated with an increased expression of Cx43 in the retina from AMD donors compared to the age-matched control. Although the most damaged macular area showed the most severe photoreceptor degeneration, this area did not offer evidence of the strongest oxidative stress and inflammatory responses. It was the macular surrounding area with lots of surviving neurons that showed the maximum increased Cx43 immunoreactivity and glia-mediated inflammation, showing comparable findings to that of the light-damaged albino rat model.

Overall, the results collected from this project have confirmed that Cx43 plays a critical role in tissue damage in the light-damaged albino rat retina and human AMD condition. The light-damaged albino rat appears to be a suitable animal model of AMD as it closely mimics the inflammatory responses that occur in the early stages or progressive areas of human AMD. The Cx43 mimetic peptide used in this study appears to be effective in protecting the

neuroretina by reducing the level of inflammation following light damage. Cx43 regulation, therefore, has potential for therapeutic treatment of early and progressive AMD.

Chapter 2: Material and methods

The general outline of experimental procedures used throughout this thesis and the basic concepts behind the protocols are described in this chapter. Specific procedures and animal treatment strategies are described in the method sections in each of the following chapters.

2.1 Animals and light damage procedure

Adult Sprague-Dawley (SD) rats (200-250 grams, male or female) were used in this study. The SD rat is an albino strain. The animals lack pigments in the retinal pigment epithelium. In comparison with pigmented strains, the albino rat ensures the adult onset and coherent timing of photoreceptor degeneration for our study (Noell *et al.*, 1966; Marc *et al.*, 2008). Animals were sourced from the Vernon Jansen Unit at the University of Auckland. Animals were born and housed in normal cyclic light conditions [12 hours light (174 Lux):12 hours dark (< 62 Lux)] for the duration of the study, except where otherwise stated. All experimental procedures described in this study were approved by the University of Auckland Animal Ethics Committee. Every effort was made to use the minimum numbers of animals necessary to optimise procedures and obtain results. Analysis of biological data suggest a minimum of 6 samples per experimental condition are required for statistical validation of the results (Anderson & Vingrys, 2001). Experimental groups and the numbers of animals used in each group are listed in each experimental chapter.

2.1.1   Light damage procedure

The intense light-damaged albino rat has been demonstrated to be a good model for studying AMD, based on the resulting structure change, molecular pathology and retinal dysfunction (Noell *et al.*, 1966; Marc *et al.*, 2008). This animal model was used in the present study. Light damage experiments started consistently around 9:00 am. The luminance was 2700 Lux, created by placing fluorescent light lamps (Philips Master TLD 18W/965) directly above the rat cages. The light source covered broad band fluorescence, from 380 to 760 nm (Figure 2-1), with no extra heat generated from the light source. This broad band

fluorescence light source has been demonstrated in a previous study (Yu *et al.*, 2007). There was no hiding area in the cages. Animals were able to move freely in the cage and had free access to food and water. All the experimental protocols consisted of 24 hours light-exposure with variable post-exposure recovery periods are described in the method section of the following chapters. During recovery, animals were returned to normal light and housing conditions.
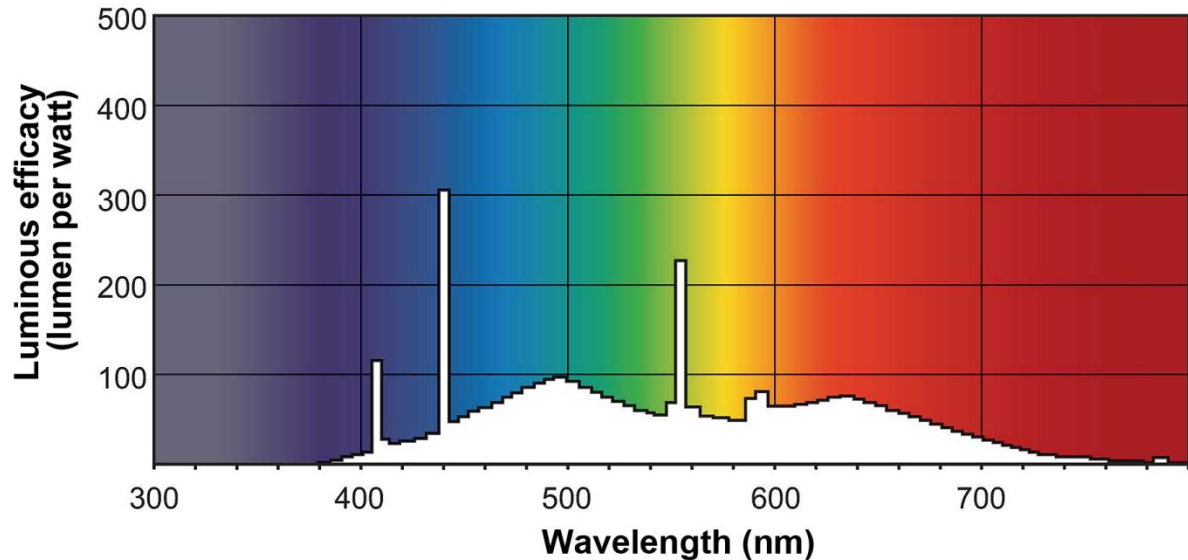
Figure 2-1. Wave length range and efficacy of the fluorescent light source used for inducing light damage in the animal model. This image is adapted from Philips manufacturer's product information sheet.

2.1.2 Cx43 mimetic peptide preparation

Peptide5, the Cx43 mimetic peptide used in this study was designed against the end amino acids of extracellular loop 2 of the Cx43 protein. The peptide has been found to be neuro-protective in animal models for spinal cord injury, glaucoma and stroke (O'Carroll *et al.*, 2008; Danesh-Meyer *et al.*, 2012; Davidson *et al.*, 2012a). The sequence of the unmodified mimetic peptide is H-Val-Asp-Cys-Phe-Leu-Ser-Arg-Pro-Thr-Glu-Lys-Thr-OH (molecular weight: 1396). This 12 amino acids sequence corresponds to residues 196 and 207 of Cx43 from both human and rats, which are both 382 amino acids long and share 98% identity. A

67

fluorescence-conjugated peptide was employed to show the penetration of the peptide following delivery into the vitreous. The sequence of the FITC-conjugated peptide was FITC-βAla-Val-Asp-Cys-Phe-Leu-Ser-Arg-Pro-Thr-Glu-Lys-Thr-OH (molecular weight: 1856). Both mimetic peptides were custom made by Auspep Pty. Ltd, Australia.

To assess the permeability of peptide5, the FITC-conjugated peptide was prepared at two different concentrations: a working concentration (280 µM) and a ten times higher concentration (2.8 mM). The working concentration was determined by targeting 20 µM as the final concentration to be achieved in the vitreous. To achieve this final concentration in the vitreous, 4 µL of 280 µM working solution was injected assuming that the vitreous volume is 56 µL in the rat (Hua *et al.*, 2003).

The unmodified peptide5 was prepared at working concentration (280 µM) following the same protocol as for the FITC-conjugated peptide. All the peptides were prepared in saline (0.9% NaCl solution) as described previously (O'Carroll *et al.*, 2008). Saline was used as sham treatment with 4 µL of saline was injected in control groups.

2.1.3   Intravitreal injections

The animals were anesthetised by intraperitoneal injection (i.p.) with a combination of ketamine (75 mg/kg) and domitor (0.5 mg/kg). After the animals were fully anaesthetised, 4 µL of mimetic peptide or sham (saline) was injected into the vitreous in both eyes either during or after the light exposure. A Hamilton syringe with maximal volume of 10 µL attached to a 30 G x ½ needle (BD PrecisionGlide™) was used for the injection. To avoid damage to the lens, the injection was done gently onto the temporal side of each eye after rotating the eyeball to the nasal side by holding the bulbar conjunctiva. A dissection microscope was used for a good surgical view. The animals were injected with atipamezole (1 mg/kg) after the intravitreal injection, and returned back to the cage for recovery from the anaesthesia. Warm water bottles were used to keep a steady body temperature during recovery.

2.2 Electroretinogram (ERG) procedure and data analysis

2.2.1 Introduction

The electroretinogram (ERG) is a useful tool for measurement of retinal function following light stimulation. It represents serial neural responses and can be used to evaluate the retinal function of different retinal neurons. The light stimulus for ERG is characterised by a high luminous output over a short period of time which allows retinal neurons to saturate within their fast integration times. Cones have a very fast recovery time (about 15-20 milliseconds) (Friedburg *et al.*, 2004), and in contrast, rods need a much longer recovery time from bright flashes (about 2.3 seconds) (Birch *et al.*, 1995). Based on the fact that rods and cones have different recovery time courses, the cone component can be extracted from the mixed rod and cone waveforms by using a twin-flash paradigm (less than 1 second inter-stimulus interval). The theory is that the first flash is to saturate the rods and the second flash is to define the cone photo-response during the transient period of rod extinction (Birch *et al.*, 1995; Pepperberg *et al.*, 1997; Nixon *et al.*, 2001). This twin-flash paradigm was utilised in the current study.

2.2.2 ERG recording

The procedure was adapted and modified based on a previous study (Vessey *et al.*, 2011). The animals were dark-adapted overnight for 12-14 hours before the ERG recording, apart from the groups of animals that were dark-adapted for 5 hours (6 hours recovery post-light with or without intravitreal injections) and groups that were not dark-adapted (0 hour recovery post-light with or without intravitreal injections). The different recovery times would allow for assessment of injury development following onset of light damage. A dim red light generated by a light-emitting diode ($\lambda_{max} = 650$ nm) was used for all manipulations on dark adapted animals during the ERG recording. Following the dark-adaption, animals were anesthetised by intraperitoneal injection (i.p.) with a combination of ketamine (75 mg/kg) and domitor (0.5 mg/kg). The cornea was maintained hydrated with 1%

carboxymethylcellulose sodium (Celluvisc, Allergan, CA) throughout the whole ERG recording. ERG tests were recorded on the left eye of each animal using custom-made silver chloride electrodes (Grass Electrodes, West Warwick, RI). The active electrode was U-shaped and kept in contact with the centre of the cornea. The inactive electrode was V-shaped and was hooked around the front teeth and in contact with the wet tongue. Body temperature was kept at 37°C with warm water bottles. Full-field ERG responses were elicited by a twin-flash (0.8 ms second stimulus interval) generated from a photographic flash unit (Nikon SB900 flash, Japan), via a Ganzfeld sphere. In Ganzfeld method, an integrating sphere approximately 650 mm in diameter, painted white internally was used to reflect the state of the entire retina (Bergoffen *et al.*, 1993). The flash intensity range was from -2.9 to 2.1 log cd.s/m^2 and was attenuated using neutral density filters (Kodak Wratten, Eastman Kodak, Rochester, USA), to obtain light intensities of -3.9, -2.9, -1.9, 0.1, 1.1, 1.6, 1.8 and 2.1 log cd.s/m^2. The flash intensity was calibrated using an IL1700 research radiometer (UV Process Supply Inc., USA). This study utilised a twin-flash paradigm for the isolation of rod and cone pathways. Paired flashes of identical luminous energy were triggered from the flash unit. The rod and cone mixed response was recorded after the initial flash, and the response from the second flash was recorded and represented function from the cone only. The rod response was derived through digital subtraction of the cone response from the initial mixed response. Recording was performed in a faraday cage to reduce electrical noise. Signals were amplified 1,000 times by a Dual Bio Amp (AD Instruments, NSW, Australia) and waveforms were recorded by using the Scope software (AD Instruments, NZ). The collected data were copied into and analysed using Excel software.

2.2.3   ERG data analysis

The method used in the ERG data analysis has been reported in a previous study (Vessey *et al.*, 2011) and adapted to our experimental conditions. The a-wave (fast PIII) is a cornea-negative potential, which reflects the photoreceptor response (Weymouth & Vingrys, 2008). Post-photoreceptor responses from both rod and cone pathways were reflected by the b-wave

(PII), a corneal-positive potential. The summed activities of ON-bipolar cells together with lateral input from the horizontal cell contribute to the b-wave generation (Green & Kapousta-Bruneau, 1999; Hanitzsch *et al.*, 2004). Müller cells have also been suggested to contribute to the b-wave indirectly (Kofuji *et al.*, 2000).

The amplitude of the a-wave was measured between the pre-stimulus baseline and the trough of the waveform. The amplitude of the b-wave was measured between the a-wave trough and the peak of the waveform, or between the baseline and the peak of the waveform if there was no a-wave. The implicit times of a- and b-waves were measured from the stimulus onset to the trough of the a-wave or the peak of the b-wave respectively (Sun *et al.*, 2007; Vessey *et al.*, 2011).

The amplitudes of a- and b-waves from the mixed rod and cone responses were analysed using the Michaelis-Menten function evaluating the amplitude-energy relationship (Naka & Rushton, 1966). The equation was:

$$R = R_{max} \times I^n / (I^n + K^n)$$

where R_{max} (μV) is the maximum amplitude, I (log cd.s/m^2) is the stimulus intensity, n is an exponent related to the slope of the function, and K (log cd.s/m^2) is the intensity for semi-saturation.

As the twin-flash paradigm is utilised in this study, the rod a-wave was extracted from the mixed photoreceptor response by subtracting the cone-only response to the second flash under a range of rod-saturating stimuli: 1.6, 1.8 and 2.1 log cd.s/m^2. The rod a-wave was modelled using a nonlinear function (Hood & Birch, 1990). The equation was:

$$PIII\ (i \times t) = \{1 - exp[-1/2 \times i \times S \times (t - t_d)^2]\} \times R_{max}$$

In this equation $PIII$ represents the current generated by all the photoreceptors as a function of stimulus intensity $(i, cd.s/m^2)$; and time $(t, seconds)$. $Rmax$ (μV) is the saturated amplitude from the stimulus; S (sensitivity) characterises the gain of the photo-transduction process $(m^2/cd \times s^3)$ and $t_d (seconds)$ is the time latency between the stimulus onset and the start of the response. The cone photoreceptor response in rodents is too small to be analysed using ERG.

71

Post-photoreceptoral function PII was isolated by digitally subtracting PIII from the raw waveform and then further extracting the oscillatory potentials (OPs) from the positive PII-OP complex at the highest stimulus intensity, 2.1 log cd.s/m^2 (Weymouth & Vingrys, 2008). The inverted gamma function was used to model both rod and cone PII before the extraction of OPs (Weymouth & Vingrys, 2008). The equation was:

$$R(t) = R_{m_{PII}} \left[\frac{C}{(d+1)(t - T_{max}) + c} \right]^{d+1} \times exp \left[\frac{(t - T_{max})(d+1)^2}{(d+1)(t - T_{max}) + c} \right]$$

In this equation, R (µV) is the response at time, t (ms), after flash onset. $R_{m_{PII}}$ (µV) is the peak amplitude. T_{max} (ms) is the implicit time. Constants c and d are shape factors of the curve (Weymouth & Vingrys, 2008).

The oscillatory potentials (OPs) reflect ON-pathway neurons and lateral inhibitory circuits of inner retinal neurons (Weymouth & Vingrys, 2008). The axon terminals of the bipolar cells, the processes of the amacrine cells and the dendrites of the ganglion cells contribute to the generation of OPs (Wachtmeister, 1998). Generally, five OPs can be extracted from the PII-OP complex (Weymouth & Vingrys, 2008; Vessey *et al.*, 2011). In this study, only OP2, OP3, OP4 and summed OPs were analysed at the highest stimulus intensity, 2.1 log cd.s/m^2, as OP1 and OP5 were too small to be accurately measured in the animal model. Both amplitude and implicit time was analysed. Isolated rod responses and OPs were not analysed in the 0 hour recovery group, as they were not dark-adapted.

2.3 Immunohistochemistry

2.3.1 Introduction

This study employed well-established immunohistochemical techniques to investigate the expression of connexin proteins, oxidative stress markers and inflammatory markers in the animal model and human post-mortem ocular tissues. For the animal experiments, both eyes were collected from each animal.

2.3.2 Animal tissue collection and processing

After completion of any *in vivo* test procedures, the animals were deeply anesthetised by intraperitoneal injection (i.p.) with a combination of ketamine (75 mg/kg) and domitor (0.5 mg/kg). The rat's chest cavity was opened and a perfusion needle was inserted into the left ventricle. An outlet was made in the right atrium to enable the flush solution and fixative to circulate through the vasculature. The animals were perfused with saline for 2-3 minutes followed by further perfusion with 4% paraformaldehyde (PFA) in a 0.1 M phosphate buffer (PB). This transcardial perfusion is an established protocol for neuronal tissue collection and has been used for Cx43 immunoreactivity analysis in the brain (Nakase *et al.*, 2003).

After perfusion, the eyes were dissected from the orbit. The posterior eyecup was flattened by making several radial cuts. With the sclera side up, the tissue was gently mounted on filter paper (0.8 µm pore size, Gelman Sciences, Ann Arbor, MI, USA) to keep the tissue flat for cryo-sectioning. The tissue was then further fixed in 4% PFA for 30 minutes at room temperature and washed in 0.1 M phosphate buffer saline (PBS) pH 7.4. The tissue was cryo-protected using graded sucrose solutions 10%, 20% for 30 minutes each at room temperature and 30% overnight at 4°C, and frozen in Tissue-Tek optimum cutting temperature (O.C.T.) compound (Sakura Finetek, USA) at -20°C. Tissue was then cryo-sectioned in the vertical plane of the retina (16 µm thick sections) using a cryostat (Leica

CM3050S, Heidelberg, Germany). The sections were collected on Superfrost Plus slides (Labserv, New Zealand) and stored at -20°C until the start of the immunolabelling or the staining procedures.

2.3.3   Primary antibodies used in this study

Primary antibodies used in this study include a range of connexin proteins (Cx43, 36, 40 and 45), oxidative stress markers (nitrotyrosine, 8-oxoguanine and superoxide dismutase-1), inflammation markers (CD45 and ionised calcium-binding adaptor molecule-1) and endothelial cell marker (CD31). The detailed information of each antibody is shown in Table 2-1.

To explore intercellular communication in the retina in both light-damaged animals and in human AMD diseased tissues, antibodies against a range of connexin proteins have been employed in this study. Anti-Cx43 antibody is developed in rabbits against a synthetic epitope, corresponding to a C-terminal segment of the cytoplasmic domain of human and rat Cx43 protein. This antibody has been used in previously published studies where specificity was demonstrated in human and rat ocular tissues (Kerr *et al.*, 2010; Kerr *et al.*, 2011; Danesh-Meyer *et al.*, 2012). The anti-Cx36 antibody is designed against the C-terminus of rat and mouse Cx36 protein, which contains a single amino acid different from the human Cx36. This antibody has been successfully used for identifying Cx36 in rat brain tissue in a previous study (Rash *et al.*, 2007). The anti-Cx40 antibody is custom-designed against conserved residues 257–271 of rat Cx40 protein, and was kindly gifted by RG Gourdie (The Medical University of South Carolina). This antibody has specificity for Cx40 as demonstrated in rat heart tissue (Gourdie et al., 1998; Camelliti et al., 2004). Anti-Cx45 antibody is a synthetic sequence. It corresponds to human Cx45 near the C-terminus located in the cytoplasm. Its specificity has been demonstrated in the rat retina in a previously published study (Zahs *et al.*, 2003).

74

To investigate the process of oxidative stress in the animal model and human AMD, a series of oxidative stress markers were used in this study. The anti-nitrotyrosine monoclonal antibody recognises nitrated proteins. This antibody's specificity has been demonstrated in rat retina tissue in a diabetic model from a previously published study (Gonçalves *et al.*, 2012). Superoxide dismutase-1 (SOD-1) facilitates the dismutation of oxygen radicals to hydrogen peroxide and it has been used as a marker for oxidative stress in neurodegenerative diseases (Orrell *et al.*, 1995). The epitope of the anti-SOD-1 polyclonal antibody used in this study maps to near the N-terminus of SOD-1 of human origin. The specificity of this antibody has been demonstrated in a previously published study on human breast cancer cells (Rao *et al.*, 2008). The anti-8-oxoguanine monoclonal antibody recognises nuclear oxidative base lesions, which are the most abundant and well-characterized DNA lesions generated by oxidative stress (Kasai & Nishimura, 1984). This antibody has been used for identifying DNA damage from oxidative stress in a transgenic mouse model expressing a mutated version of the human mitochondrial DNA repair enzyme UNG1 (Lauritzen *et al.*, 2011).

Two markers were employed to investigate the inflammatory response in the light-damaged animal model and human AMD ocular tissue. The ionized calcium-binding adapter molecule-1 (Iba-1) labels all dendritic-derived macrophages and has been proven to be a reliable marker for microglia in the nervous system (Ahmed *et al.*, 2007). The polyclonal anti-Iba-1 antibody used in this study is a synthetic peptide against amino acids 135-147 of the human Iba-1 protein. Its specificity in recognising microglia in rat and aged mouse retina has been demonstrated in published studies (Sappington & Calkins, 2008; Xu *et al.*, 2008b). The anti-CD45 antibody was the second inflammation marker used in this study. An alternate name for CD45 is leukocyte common antigen. This antibody recognises all hematopoietic cells except erythrocytes. A previously published study has successfully used this antibody to show leukostasis in the retina in a diabetic rat model (Ma *et al.*, 2009a).

In order to determine precise localisation of the oxidative stress marker, nitrotyrosine, in AMD-affected retinal tissue, the anti-CD31 antibody was used as an endothelial cell specific marker and double-labelled with nitrotyrosine. This antibody has been used to identify endothelial cells in the human retina in a previously published study (Dong *et al.*, 2012).

Table 2-1. List of primary antibodies used in this study.

Antibody	Production	Host	Working dilution	Company	Cat No.	Immunogen	Reference
Anti-Cx43	Polyclonal	Rb	1:1000	Sigma-Aldrich, USA	C6219	Synthetic peptide corresponding to amino acids 363-382 of human and rat connexin43	(Kerr *et al.*, 2010)
Anti-Cx36	Polyclonal	Rb	1:400	Life Technologies, USA	51-6300		
Anti-Cx40	Polyclonal	GP	1:500	Given by Rober Gourdie's group	N/A	Rat Cx40 protein	(Jay *et al.*, 2004)
Anti-Cx45	Polyclonal	Rb	1:100	Life Technologies, USA	40-7000	Synthetic peptide derived from the C-terminal region of the mouse, rat, Chinese hamster, and golden hamster Cx45	(Rash *et al.*, 2001)
Anti-ED1	Monoclonal	Ms	1:200	AbD Serotec, Oxford, UK	MCA341 GA	Purified IgG1 from tissue culture supernatant, recognising tissue macrophages	(Cao *et al.*, 2011)
Anti-GFAP	Monoclonal, clone G-A-5	Ms	1:1000	Sigma-Aldrich, USA	C9205	Purified GFAP from pig spinal cord	(Danesh-Meyer *et al.*, 2008)
Anti-CD45	Monoclonal, clone OX-1	Ms	1:20	BD Pharmingen, USA	550566	CD45-enriched glycoprotein fraction from Wistar rat thymocytes	(Adamis *et al.*, 2003)
Anti-Iba1	Polyclonal	Gt	1:250	Abcam, USA	Ab5076	Synthetic peptide corresponding to amino acids 135-147 of human Iba1	(Xu *et al.*, 2008b); (Sappington & Calkins, 2008)
Anti-nitrotyrosine	Monoclonal, clone 1A6	Ms	1:2000	Millipore Corporation, MA, USA	05-233	Nitrated KLH (Keyhole Limpet Hemocyanin)	(Dick *et al.*, 2002); (Kern *et al.*, 2002)
Anti-SOD1	Polyclonal	Gt	1:100	Santa Cruz Biotechnology, Inc.	sc-8636	Mapping near the N-terminus of SOD-1 of human origin	(Raoul *et al.*, 2005)
Anti-8-oxoguanine	Monoclonal	Ms	1:100	Millipore Corporation, MA, USA	MAB 3560	8-oxoguanine adsorbed onto alumina	(Conlon *et al.*, 2003)
Anti-CD31	Polyclonal	Rb	1:100	Abcam, USA	Ab28364	Synthetic peptide corresponding to C terminus of mouse CD31	(Dong *et al.*, 2012)

2.3.4   Immunohistochemical labelling of tissue sections

Immunohistochemical labelling was conducted by using the indirect immunofluorescence technique. The Primary antibody specifically recognises and binds to the epitope on the targeted protein (antigen). The secondary antibody (anti-immunoglobulin antibody) that is conjugated with fluorochromes is used to detect the specific antigen binding. This is a more sensitive method compared to the direct detection (Berry *et al.*, 1999).

Frozen tissue sections were air-dried at room temperature for 10 minutes and then washed in 0.1 M PBS. The tissue sections were encircled with a PAP pen (Invitrogen, New Zealand) after wiping off the excess moisture around the sections. Non-specific binding sites in the tissue were blocked with 6% normal goat serum or normal donkey serum (Invitrogen, USA), 1% bovine serum albumin (BSA) and 0.5% triton X-100 in 0.1 M PBS for 1 hour at room temperature. The primary antibodies were diluted in antibody solution containing 3% normal goat serum or normal donkey serum, 1% BSA and 0.5% triton X-100 in 0.1 M PBS (primary antibody details – Table 2-1) and were applied carefully to cover the tissue section. Tissue sections were incubated with the primary antibody overnight at room temperature. The negative control for each antibody was conducted by incubating sections with antibody solution only following the same protocol as if applying a primary antibody. Subsequent to overnight incubation, the slides were washed three times for 5 minutes each in 0.1 M PBS and once for 15 minutes in 0.1 M PBS to remove excess primary antibodies. The secondary antibodies conjugated to either Alexa[TM] 488 or Alexa[TM] 594 (Invitrogen, New Zealand) were diluted 1:500 in antibody solution and applied to the tissue for 2 hours at room temperature. Slides were washed thoroughly with 0.1 M PBS to remove all excess secondary antibodies. Following the washes, tissue sections were incubated with 4',6-diamidino-2-phenylindole dihydrochloride (DAPI) (Sigma, USA) 1 µg/mL in 0.1 M PBS for 15 minutes to label cell nuclei, followed by another thorough wash with 0.1 M PBS. The slides were then mounted in a non-fluorescence-fading medium (Citifluor Ltd, London, UK) and sealed with nail polish to avoid leakage and evaporation.

2.3.5   Animal tissue collection for flat-mount staining

After perfusion and dissection of the eye from the orbit, the posterior segment of the eye was kept as the eyecup. Flat-mount staining allows the identification of the spatial arrangement of the immuno-labelled cells. For this procedure, the posterior segment of the eye was fixed in 4% PFA for 30 minutes at room temperature and washed in 0.1 M PBS. Then, the eyecup was flattened by making several radial cuts. The retina was carefully separated from the sclera. The sclera had the choroid and the retinal pigment epithelium attached onto it. The tissues were permeabilised via incubation in 0.5% triton X-100 in 0.1 M PBS for 15 minutes at -80°C. Following thorough washing with PBS, free floating retinas were incubated with a primary antibody diluted in an antibody solution containing 10% normal goat serum and 2% triton X-100 in 0.1 M PBS solution overnight at 4°C. Subsequent to several thorough washes with 0.1 M PBS, secondary antibodies were diluted with antibody solution and applied to the floating tissues for 3 hours at room temperature. Following thorough washes with 0.1 M PBS, DAPI (Sigma, USA) diluted at 1 µg/mL with PBS was applied to the floating tissue for 30 minutes at room temperature. Then, the tissues were washed three times for 15 minutes each and once for 40 minutes in 0.1 M PBS, and gently transferred and mounted onto the slides. Lastly, the flat-mount tissue was coverslipped in a non-fluorescence fading medium (Citifluor Ltd, London, UK) and sealed with nail polish to avoid leakage and evaporation.

2.3.6   Cell counts and staining intensity measurements

In order to quantify the oxidative stress affected cells and recruited inflammatory cells in the retinal and choroidal tissue following light damage, nitrotyrosine, Iba-1 and CD45 immuno-labelled cells were counted in the light-damaged animal groups and the control groups. Cell counting was performed using low magnification confocal images. All images were taken from a central area around the optic nerve. Cells were counted manually and recorded using Microsoft Excel 2010. Data was presented as labelled cells per mm^2 and represent cell

counts in 0.186 mm^2 of retina and 0.043 mm^2 of choroid. A minimum of 6 eyes from each group were used for the cell counting.

2.4   Specific staining

In this study, staining techniques were used to visualise particular tissue structures and some specific cell types. This enabled comparison between overall tissue morphology, specific cell localisation, and immunohistochemical results.

2.4.1   Toluidine blue staining

Toluidine blue, which stains nucleic acids blue and polysaccharides purple, has been employed to show the tissue histological structure. Frozen sections mounted on slides were air-dried for 10 minutes at room temperature and then washed with 0.1 M PBS. The sections were stained for 2-3 minutes with 1 mg/mL toluidine blue solution prepared in MilliQ water. This was followed by three washes of 3 minutes each in 0.1 M PBS. Finally, the stained tissue sections were coverslipped and images were taken immediately after the staining procedure, using a bright field microscope.

2.4.2   Phalloidin staining

Phalloidin is a high-affinity filamentous actin (F-actin) probe which selectively stains F-actin. Alexa Fluor 488$^®$-conjugated phalloidin (Life Technologies, USA) was used in this study to identify the structure of RPE on the flat-mount tissue. The Alexa Fluor 488$^®$ phalloidin was diluted at 1:200 with 0.1 M PBS, and then incubated with flat-mount choroid tissue for 1 hour at room temperature. Phalloidin staining was usually performed after immunohistochemistry and before the DAPI labelling on the flat-mount tissue.

2.4.3 TUNEL staining and cell death analysis

Signs of apoptosis were investigated in the tissue collected from light-damaged animals. The TdT-mediated dUTP nick end labelling (TUNEL) technique (In Situ Cell Death Detection Kit from Roche Applied Science, Germany) was used to detect cell death in light-damaged and control groups. Tissues were processed using a commercial In Situ Cell Death Detection Kit, Fluorescein (Roche Diagnostics GmbH, Mannheim, Germany). During apoptosis, single strand breaks and double-stranded low molecular weight DNA fragments may be generated from cleavage of genomic DNA. TUNEL reaction is based on an enzymatic reaction to identify the DNA strand breaks by labelling free 3'-OH termini with modified nucleotides. TUNEL reaction detects apoptosis at the single-cell level in histological specimens. Tissue sections were washed twice with 0.1 M PBS before being permeabilised with 0.1% triton X-100 and 0.1% tri-sodium citrate in 0.1 M PBS for 5 minutes on ice. The sections were washed and incubated with the TUNEL reaction mixture (TdT enzyme solution and fluorescein nucleotide label solution at 1:17 dilution) for 20 minutes at 37°C in a dark humid chamber. Negative controls were incubated with the label solution only. The sections were rinsed several times in 0.1 M PBS, and then mounted in Vectashield HardSet Mounting Medium with DAPI (Vector Laboratories, Burlingame, CA). The stained sections were visualised using confocal microscopy.

2.5 Imaging

All the images were acquired from immuno-labelled, phalloidin stained and TUNEL labelled sections using a high-resolution laser scanning confocal microscope (Olympus FluoView FV1000, Olympus Corporation, Tokyo, Japan) with 488 nm and/or 594 nm excitation from an argon ion laser. A series of 4-8 optical sections with 1 µm intervals were collected for each specimen and image analysis was performed on a stack image of intensity projection over the z-axis. Six retinas obtained from different animals were analysed for each group, and the representative images shown.

2.6 Collection of human normal and AMD ocular specimens

Human ocular samples were obtained through the New Zealand National Eye Bank according to the tenets of the Declaration of Helsinki and approved by the Institutional Ethics Review Committee Board of the University of Auckland and Northern District Human Ethics Committee. Age-related macular degeneration (AMD) ocular samples were obtained from three Caucasian donors, who were diagnosed with dry AMD. Clinical history indicated no previous treatment for the condition. Normal age controls were obtained from three age-matched Caucasian donors with no ocular disease (Table 2-2). There is morphological degradation associated with post-mortem neurological tissue, including a jagged appearance to stained cellular soma and reduced definition in the dendritic pattern as described in previous publications (de Souza *et al.*, 2012; Souza *et al.*, 2013). The posterior segment of ocular tissues was fixed in 4% PFA for 30 minutes at room temperature, washed with 0.1 M PBS, and cryo-protected in graded sucrose solutions 10%, 20% for 30 minutes each at room temperature and 30% overnight at 4°C. The tissue was then embedded and mounted in Tissue-Tek optimum cutting temperature (O.C.T.) compound (Sakura Finetek, USA) and serial transverse cryo-sections were cut at 16µm thickness using a cryostat (Leica CM3050S, Heidelberg, Germany). The sections were collected on Superfrost Plus slides (Labserv, New Zealand) and stored at -20°C until the start of the staining procedure.

Table 2-2. Human AMD donors' demographics

Donor	Age	Gender	Ethnicity
1. Dry AMD	82	Female	Caucasian
2. Wet AMD	81	Female	Caucasian
3. Dry AMD	80	Male	Caucasian
4. Control	67	Female	Caucasian
5. Control	76	Male	Caucasian
6. Control	82	Female	Caucasian

2.7 Western blot

Western blot of retinal and choroidal tissue was used to quantify or semi-quantify the oxidative marker nitrotyrosine and Cx43 protein expression in order to characterise the light-damaged animal model. A minimum of 6 eyes were used for data analysis from each group.

Rats were deeply anaesthetised by intraperitoneal injection (i.p.) with a combination of ketamine (75 mg/kg) and domitor (0.5 mg/kg), and then transcardially perfused through the left ventricle with saline. After dissection of the eye from the orbit, the posterior segment of the eye was isolated. The retina was carefully separated from the choroid and sclera with the use of a dissection microscope. The retinal pigment epithelium remained attached to the choroid and sclera.

2.7.1 Protein extraction and measurement

Rat retina and choroid were extracted from the eye and homogenised in a cold, freshly prepared homogenising buffer (10 mM 4-(2-hydroxyethyl)-1-piperazineethanesulfonic acid/HEPES; 0.25 M sucrose in MilliQ water, pH 7.4) containing 1× protease inhibitor cocktail (Complete mini tablet; Roche Diagnostics, Germany) using a teflon homogeniser. This protocol for tissue homogenisation has been used for retinal tissue in a previously published study (Acosta *et al.*, 2005b). Samples were then centrifuged twice (16,000 rpm for 2 minutes at 4°C) to sediment any unhomogenised tissue, and the supernatant was stored at -20°C until use.

Following protein extraction, the protein concentration of each sample was measured using a Pierce® BCA Protein Assay Kit (Thermo Scientific, USA). This assay is a detergent-compatible formulation based on bicinchoninic acid (BCA). BCA can form a purple-coloured complex by the chelation of two molecules of BCA with one cuprous ion with amino acids in the protein sample responsible for the reaction. This water-soluble purple-coloured complex has a strong absorbance at 562 nm that is nearly linear with increasing

protein sample concentrations. In accordance with the manufacturer's protocol, 10 µL of each protein sample was used to set the microplate reactions and absorbance was read at 562 nm using a Synergy HTMulti-Mode Microplate Reader (BioTek). Protein concentrations of the samples were interpolated from the calibration plot constructed from a series of known bovine serum albumin (BSA) protein dilutions 125-2000 µg/mL prepared in the same homogenising buffer and run in the same 96-well microplate. Following protein concentration assays of the samples, all the retinal and choroidal samples were diluted to 450 µg/mL.

2.7.2 Western protocol

Samples were mixed with a loading buffer (10:1) containing 0.1% bromophenol blue, 20% v/v glycerol and 2% sodium dodecyl sulphate (SDS). Typically, 9 µg of retinal or choroidal sample protein in a total volume of 20 µL was gently loaded into the leading wells of a 10% Mini-PROTEAN® TGX™ Precast Gel (Bio-Rad Laboratories, New Zealand). Proteins were separated according to molecular weight under electrophoresis using a Mini-Protean Tetra Cell (Bio-Rad Laboratories, USA) with an SDS gel running buffer (25 mM Tris base; 19mM glycine; 0.1% SDS in MilliQ water) which applies a negative charge to each protein in proportion to its molecular weight. A Precision Plus Protein™ All Blue Standard (Bio-Rad Laboratories, USA) containing proteins with known molecular weights ranging from 10 to 250 kDa was loaded alongside the protein samples in each gel. The separated proteins were transferred from the gel to a polyvinylidene difluoride (PVDF) membrane (Roche Diagnostics, USA) using a semi-dry transfer system – Trans-Blot® Turbo™ Transfer Starter System (Bio-Rad Laboratories, USA) with a small amount of transfer buffer (25 mM Tris base; 190 mM glycine; 15% methanol in MilliQ water, pH 8.4).

The membrane containing separated and transferred protein samples was incubated with a blocking solution (5% non-fat milk powder; 2% v/v normal goat serum in Tris-buffered saline-tween (TBS-T), containing 20 mM Tris hydrochloride; 137 mM sodium chloride; 0.1% v/v tween-20, pH 7.2) for 2 hours at room temperature. This was followed by

incubating the membrane with the primary antibody overnight at 4°C. The primary antibody (either anti-Cx43 antibody 1:4000 dilution or anti-nitrotyrosine antibody 1:2000 dilution) was diluted with an antibody solution containing 2% non-fat milk powder, 2% v/v normal goat serum in TBS-T. Following three washes each of 15 minutes and one wash for 40 minutes in TBS-T, the membrane was incubated with a horseradish peroxidase-conjugated secondary antibody (either donkey anti-rabbit IgG or sheep anti-mouse IgG; 1:5000 dilution; Amersham Biosciences, USA) for 1 hour at room temperature. The membrane was then washed with another series of TBS-T.

The immuno-blot was detected using an ECL Plus Western Blot Detection Reagents Kit (Amersham Biosciences, USA). The horseradish peroxidase-conjugated to the secondary antibody catalyses oxidation of the Lumigen PS-3 Acridan substrate and this reaction produces a sustained, high intensity chemiluminescence with maximum emission at a wavelength of 430 nm, which was subsequently detected on a FujiFilm LAS-4000 imager.

A loading control blot was performed following the imaging of the first immuno-blot for anti-Cx43 or anti-nitrotyrosine. The blot membrane was stripped out from the membrane by incubating it with stripping buffer (2% SDS, 100 mM β-mercaptoethanol, 62.5 mM Tris hydrochloride, pH 6.7) for 30 minutes at 37°C. The loading control was then blotted with an anti-tubulin antibody (1:5000 dilutions in antibody solution) on the same membrane.

Quantification of the immuno-blot images was conducted using ImageJ 1.45 s software (Wayne Rasband, National Institute of Health, USA). Histograms indicating the intensity of each of the bands were obtained and converted into numerical values indicating the intensity of the bands with the ImageJ program. The blots for Cx43 or nitrotyrosine were divided by the loading controls for each well, and then were statistically analysed between experimental groups.

84

2.8 Statistical analysis

Graphing and statistical analyses were performed using GraphPad Prism 6 (GraphPad Software, San Diego, CA). All data was presented as the mean ± the standard error of the mean (SEM). The comparison of the effects of stimulus intensity and recovery from the ERG data was performed using a two-way ANOVA followed by a Bonferroni post-test. Comparison of recovery after light exposure at the intensity of 2.1 log cd.s/m^2, and comparison between normal and light-damaged tissue Western blots for Cx43 and nitrotyrosine were conducted using a one-way ANOVA followed by a Tukey's test. A Student's unpaired t-test assuming unequal variances was used to compare cell counts of nitrotyrosine, Iba-1 and CD45 immuno-stained cells in the retina and choroid.

Chapter 3: Characterisation of the light-damaged albino rat as an animal model of age-related macular degeneration

3.1 Introduction

Age-related macular degeneration (AMD) is the major cause of blindness in people aged 75 years or older in developed countries and the third cause of blindness in the world, following cataract and glaucoma (Klaver *et al.*, 1998b; Biarnés *et al.*, 2011). Pathologically, AMD is characterised by accumulation of deposits between the retinal pigment epithelium (RPE) and the choroid, called drusen. During early AMD, drusen can be hard with distinct margins, which is characteristic of the dry form of AMD. Subsequently, choroidal neovascularisation develops and is accompanied by increased vascular leakage, which represents the wet form of AMD (de Jong, 2006). So far, there is no strategy that can cure AMD or an established effective treatment for early stage of AMD. The current management for the disease is mainly focused on the pathological progression in the late stage. The aim of this study is to analyse how the damaging process is initiated and progresses at the early stage of AMD by using a light-damaged albino rat model.

The albino rat exposed to intense fluorescent light has been an animal model of retina degeneration since the 1960s (Noell *et al.*, 1966). Histological analysis of the light-damaged animal model has shown changes to Müller cells, loss of photoreceptors and pigment epithelium, breakage to Bruch's membrane, and choroidal damage. These are all very similar characteristics to those observed in human AMD (Noell *et al.*, 1966; van Best *et al.*, 1997; Wu *et al.*, 2005; Marc *et al.*, 2008). In the light-damaged albino rat eye, the injured area is regional and mainly limited to the central and superior segments of the retina (Marc *et al.*, 2008). In addition to the histological changes, neural dysfunction has been found in this animal model, particularly seen as a reduction in the a- and b-waves in a full-field retinal electroretinogram (ERG) (Noell *et al.*, 1966; Penn *et al.*, 1989). The mechanisms of retinal degeneration in the animal model induced by light-damage, however, still remains unclear. We hypothesise that in the light-damaged animal model there is a complex procedure involving oxidative stress, inflammation and vascular reactions that mimics the disease process. The retinal stress initiated by excessive rhodopsin bleaching will consequently spread damage into the RPE and choriocapillaris.

Oxidative stress in photoreceptors results from the process of photo-oxidation generated by rhodopsin bleaching in photoreceptor outer segments and is also observed in the RPE as a result of phagocytosis of the outer segment (Beatty *et al.*, 2000; Khandhadia & Lotery, 2010). In addition to photoreceptor outer segments, oxidative stress has also been found in the mitochondrial DNA (mtDNA) in photoreceptors from aged human donor tissues (Barron *et al.*, 2001). In the light-damaged animal model, protein nitration has been found to be increased in the photoreceptor outer segment and the RPE when compared to the animals maintained in the dark (Miyagi *et al.*, 2002; Palamalai *et al.*, 2006).

Inflammation is involved in the pathogenesis of AMD (Anderson *et al.*, 2002a; Gupta *et al.*, 2003; Wu *et al.*, 2003; Coorey *et al.*, 2012; Khandhadia *et al.*, 2012), and has also been found in the light-damaged animal model (Zhang *et al.*, 2005; Ng *et al.*, 2009; Rutar *et al.*, 2010; Rutar *et al.*, 2011a; Rutar *et al.*, 2012a). Although the adult retina is regarded as an immune-privileged tissue, it has residential glial cells to provide support and protection of the retinal neurons by supplying nutrients, removing neural waste products and phagocytosis of neuronal debris (Coorey *et al.*, 2012). Retinal microglia become activated after light damage and migrate to the outer retina in a number of animal models (Ng & Streilein, 2001; Zhang *et al.*, 2005; Ni *et al.*, 2008; Xu *et al.*, 2008a; Rutar *et al.*, 2010). Studies of human post-mortem tissue from AMD diagnosed donors have revealed comparable findings with microglial migration to the outer nuclear layer and subretinal space (Gupta *et al.*, 2003; Milam *et al.*, 2003). The inflammatory response is present in both the retina and the choroid following light damage (Rutar *et al.*, 2010), suggesting residential microglia/macrophage activation and migration may play an important role in the process of tissue damage in the light-damaged albino animal model.

Intercellular gap junction channels allow rapid exchange of ions, messengers and metabolic molecules between neighbouring cells. The role of intercellular communication affects a wide range of cellular activities, including signalling, differentiation and growth (Goodenough *et al.*, 1996). In the retina, gap junctions participate in electrical coupling between cells for light sensation (Veruki & Hartveit, 2002; Goodenough & Paul, 2003). Within the rat retina, Cx37 and Cx40 are expressed in the endothelium of large radiating arterioles (Kuo *et al.*, 2008). In rat and mouse retina, both Cx36 and Cx45 are expressed on

AII amacrine cells (Söhl *et al.*, 1998; Maxeiner *et al.*, 2005; Veruki & Hartveit, 2009), which are the key elements of the light signal transduction pathways. Hence, both connexin proteins may contribute to coupling function changes in response to light. For example, light modulates the density of gap junctions located on the horizontal cells. By using quantitative freeze-fracture replica methods, enhancement in the density of gap junctions on horizontal cells in gold fish has been found to be associated with dark adaptation (Kurz-Isler & Wolburg, 1986). The light-adapted retina shows an overall increase in alpha ganglion cell coupling at coupled cell number and coupled field compared with the dark-adapted retina (Hu *et al.*, 2010). However, there are very few reports of changes in connexin proteins in the light-damaged animal model.

Cx43 is the most ubiquitous gap junction protein and is expressed by astrocytes and endothelium in the nervous system. Previous studies have demonstrated that it is expressed on Müller cells, astrocytes, vascular endothelium and retinal pigment epithelium in both human and rat retinas (Zahs *et al.*, 2003; Kuo *et al.*, 2008; Kerr *et al.*, 2010). Cx43 plays an important role in modulating response to injury (Danesh-Meyer *et al.*, 2008; O'Carroll *et al.*, 2008; Kerr *et al.*, 2011; Ly *et al.*, 2011; Danesh-Meyer *et al.*, 2012; Davidson *et al.*, 2012a). Increased Cx43 protein and/or transcript have been found in many human CNS injuries and diseases, including stroke, epilepsy and Huntington's disease (Elisevich *et al.*, 1997; Vis *et al.*, 1998; Nakase *et al.*, 2006).

Based on previous studies, we hypothesise that the injury process in the light-damaged animal model is happening through a complex procedure involving oxidative stress, inflammation and vascular reaction. The retinal stress may be initiated by excessive bleaching of rhodopsin in the photoreceptors from prolonged exposure to the intense light, which would consequently impact on the RPE and choroidal capillaries (Noell *et al.*, 1966; Williams & Howell, 1983). A disruption of the outer retinal blood barrier, mainly the RPE, which involves processes of abnormal cation influx, oxidative damage, and activation of inflammatory response, would lead to secondary injury of the retinal neurons and result in retinal degeneration (Ablonczy *et al.*, 2000; Vaughan *et al.*, 2003; Zhang *et al.*, 2005; Rutar *et al.*, 2010; Rutar *et al.*, 2011a; Rutar *et al.*, 2011b; Rutar *et al.*, 2012a). Oxidative damage and its associated inflammatory response are sufficient to produce retinal lesions in the retina

and the choroid (Hollyfield *et al.*, 2008). Alterations in gap junctions expressed on retinal neurons together with photoreceptor degeneration may contribute to the photoreceptor and post-photoreceptor dysfunction in the retina in the animal model. Similar to other animal injury models, Cx43 expression may be affected following intense light-induced injury.

The features of the animal model and its usefulness for its understanding the mechanisms that contribute to AMD are investigated in this chapter. The aim of this study was to evaluate changes in neuronal function, oxidative stress, inflammatory response and the expression of connexin proteins, especially Cx43, in the light-damaged rat retina. In particular, ERG was used to characterise the function of rod and cone pathways; immunohistochemistry and Western blot were employed to correlate the retinal function with cell death, changes in gap junction proteins, oxidative stress, inflammatory responses and RPE alterations.

3.2 Materials and methods

3.2.1 Animal handling and light exposure protocol

The experimental protocol consists of exposing animals to intense light followed by variable periods of recovery. Briefly, the 24 hours intense light exposure protocol was employed (Yu *et al.*, 2007). Non-exposed animals were used in the control group. The rats were culled after ERG testing either immediately (0 hour), at 6, 24, 48 hours or 7 days after light-exposure. The number of animals used to characterise this light-damaged model is listed in Table 3-1. Animal groups in this study are described in Figure 3-1.
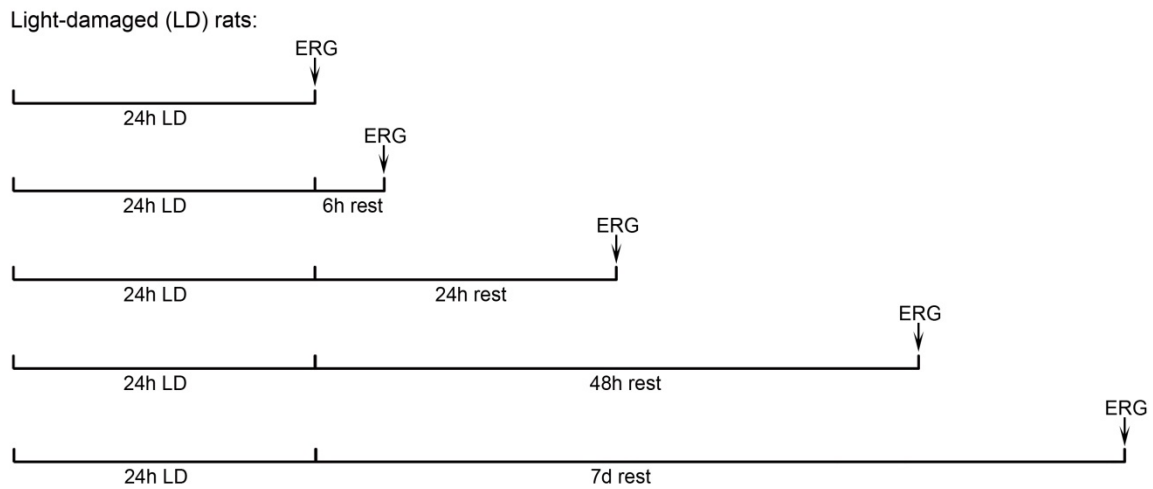
Figure 3-1. Experimental groups of the light-damaged rats. All the animals had 24 hours light damage. The signs of ERG↓ indicate time points at which ERGs were recorded.

Table 3-1. Animal numbers used to characterise the light-damaged albino rat model.

Non-LD control	0h post-LD	6h post-LD	24h post-LD	48h post-LD	7d post-LD
n=9	n=9	n=9	n=6	n=6	n=6

3.2.2   ERG recording

The animals were dark-adapted overnight for 12-14 hours before the ERG recording using a procedure adapted from a previous study (Vessey *et al.*, 2011).   Briefly, the animals were anesthetised and ERGs were recorded on the left eye.   The light stimulus was elicited by twin-flashes (0.8 ms second stimulus interval) via a Ganzfeld sphere.   Flash intensity range was from -2.9 to 2.1 log cd.s/m^2.   Waveforms were recorded and amplitudes of a- and b-waves from the mixed rod and cone responses were analysed using the Michaelis-Menten function.   The implicit times of a- and b-waves were measured from the stimulus onset to the trough of the a-wave or the peak of the b-wave respectively (Sun *et al.*, 2007; Vessey *et al.*, 2011).   Oscillatory potentials (OPs) were collected at 2.1 log cd.s/m^2.

3.2.3   Tissue collection and processing

At the end of the ERG recording the rats were still deeply anesthetised.   We perfused them transcardially with saline for 2-3 minutes followed by 30 minutes incubation in 4% paraformaldehyde (PFA) in a 0.1 M phosphate buffer (PB).   The eyes were dissected from the orbit, eyecups were further fixed in 4% PFA for 30 minutes and washed in 0.1 M phosphate buffer saline (PBS) pH 7.4.   After cryoprotection tissues were used in flat mount immunocytochemistry or were cryo-sectioned and collected on slides before the immunocytochemical procedure.

3.2.4   Immunohistochemistry

The procedure was conducted as explained in Section 2.3, Chapter 2.   Briefly, after washing with 0.1 M PBS, sections were blocked with a solution containing normal goat serum or donkey serum (Invitrogen, USA), 1% bovine serum albumin (BSA) and 0.5% triton X-100 in 0.1 M PBS for 1 hour at room temperature.   The tissues were immune-labelled with primary antibodies, including mouse anti-nitrotyrosine, mouse anti-rat CD45, goat anti-Iba1,

rabbit anti-Cx43, mouse anti-ED1, guinea pig anti-Cx40, rabbit anti-Cx36 and mouse anti-Cx45 antibodies. The primary antibody details are given in Table 2-1, Chapter 2. Tissue sections were incubated with the primary antibody overnight at room temperature. The secondary antibodies were diluted 1:500 and were applied for 2 hours in the dark at room temperature. Slides were rinsed several times in 0.1 M PBS, mounted in non-fluorescence fading medium and sealed.

3.2.5 TUNEL labelling

TdT-mediated dUTP nick end labelling (TUNEL) was used to detect cell death in light-damaged and in control animals. The sections were washed and incubated with the TUNEL reaction mixture as the protocol described in Chapter 2. Negative controls were performed and data was visualised using confocal microscopy.

3.2.6 Imaging

All the images were acquired from immuno-labelled sections using a high-resolution laser scanning confocal microscope (Olympus FluoView FV1000, Olympus Corporation, Tokyo, Japan) with 488 nm and/or 594 nm excitation from an argon ion laser. A series of 4-8 optical sections with 1 µm intervals were collected for each specimen and image analysis was performed on a stack image of intensity projection over the z-axis. Six retinas obtained from different animals were analysed for each group, and the representative images shown.

3.2.7 Cell counts

Nitrotyrosine, Iba-1 and CD45 immuno-labelled specific cells were counted in all experimental and control groups. Cell counting was performed using low magnification confocal images. All images were taken from a central area around the optic nerve. Data is

presented as labelled cells per mm^2 and represent cell counts in 0.186 mm^2 of retina and 0.043 mm^2 of choroid.

3.2.8   Western blot

Rat retina and choroid were extracted and homogenized separately in homogenizing buffer containing 10 mM HEPES; 0.25 M sucrose in MilliQ water, pH 7.4 and 1× Complete protease inhibitor cocktail (Roche Diagnostics, Germany).   Equal amounts of proteins (9 µg) were separated by 10% SDS-PAGE precast gel (Bio-Rad Laboratories, New Zealand), and electrophoretically transferred to a PVDF membrane (Roche Diagnostics, USA).   After blocking with 5% non-fat milk and 2% normal goat serum in Tris-buffered saline with Tween 20 (TBS-T) (20 mM Tris hydrochloride, 137 mM NaCl, 0.1% Tween 20, pH 7.2) for 1 hour, the membrane was probed for 2 hours with anti-nitrotyrosine antibody (1:2,000) or anti-Cx43 (1:4,000).   The blotted membrane was washed with TBS-T and incubated for 1 hour with horseradish peroxidase-conjugated goat anti-mouse secondary antibody (dilution 1:5,000) before the immune-blot were detected using ECL Plus Western Blotting Detection Reagents (Amersham Biosciences, USA). To determine exact loading of protein blots were produced with anti-tubulin (1:5000) on the same membrane, but after it was first stripped of primary blots by incubating with stripping buffer (2% SDS, 100 mM β-mercaptoethanol, 62.5 mM Tris hydrochloride, pH 6.7) for 30 minutes at 37°C. The bands were imaged on a Fuji Film LAS-4000 imager.

3.2.9   Statistical analysis

Graphing and statistical analyses were performed using GraphPad Prism 6 (GraphPad Software, San Diego, CA). All data was presented as the mean ± standard error of the mean (SEM). The comparison of the effects of stimulus intensity and recovery from the ERG data was performed using a two-way ANOVA followed by a Bonferroni post-test.   The

94

comparison of recovery from the light-exposure at the intensity of 2.1 log cd.s/m^2 was conducted by using a one-way ANOVA followed by a Tukey's test. A Student's unpaired t-test assuming unequal variances was used to compare cell counts of nitrotyrosine, Iba-1 and CD45 immuno-stained cells in the retina and choroid. A Student's unpaired t-test was also used for comparison of Cx43 and nitrotyrosine proteins tested by Western blot.

3.3   Results

3.3.1   The activities of both rod and cone pathways are reduced in light-damaged rats

ERG was used to determine changes in rod and cone function at various time-points after light damage. Representative rod and cone mixed wave forms for control and light-damaged rats are presented in Figure 3-2A. A comparison with the control group showed a general loss of ERG amplitude at all intensities and at all recovery periods. Mixed a-waveforms illustrate that all light-exposed rats had reduced photoreceptor-derived amplitude at each stimulus intensity. In particular, at the last four intensities, from 1.1 to 2.1 log cd.s/m^2, the a-wave reduction was significant (two-way ANOVA, $p < 0.05$; Figure 3-2B). Further rod and cone responses were analysed to determine whether the rod- or cone-pathway contributed to the decreased a-waveform (Figure 3-3 and Figure 3-4). The rod response was isolated at the highest intensity (2.1 log cd.s/m^2). Representative raw waveforms of rod responses from each animal group are shown in Figure 3-3A. There was a significant reduction in the rod PIII amplitude in all recovery groups compared with the non-exposed control rats (one-way ANOVA, $p < 0.001$; Figure 3-3B). The substantial change in PIII amplitude indicated that function of rod photoreceptors was significantly impaired and this impairment was long-term or permanent. The sensitivity of PIII did not show a significant change between control and light-damaged rats or between light-damaged groups (Figure 3-3C). A reduction in the rod PII amplitude was observed in the light-damaged groups compared to the control group (one-way ANOVA, $p < 0.01$; Figure 3-3D). There was a transient delay of PII implicit time at 6 hours after light damage which was not seen at 24, 48 hours or 7 days recovery (one-way ANOVA, $p < 0.01$; Figure 3-3E). The oscillatory potentials (OPs) were isolated from the rising edge of rod b-wave in response to the 2.1 log cd.s/m^2 flash. There was a significant reduction in the amplitude of summed OPs from all the light-damaged rats compared to control (one-way ANOVA, $p < 0.05$; Figure 3-3F). However, the implicit time of summed OPs did not show any delay (Figure 3-3G). These results showed that retinal functions are dramatically reduced following intense light exposure.
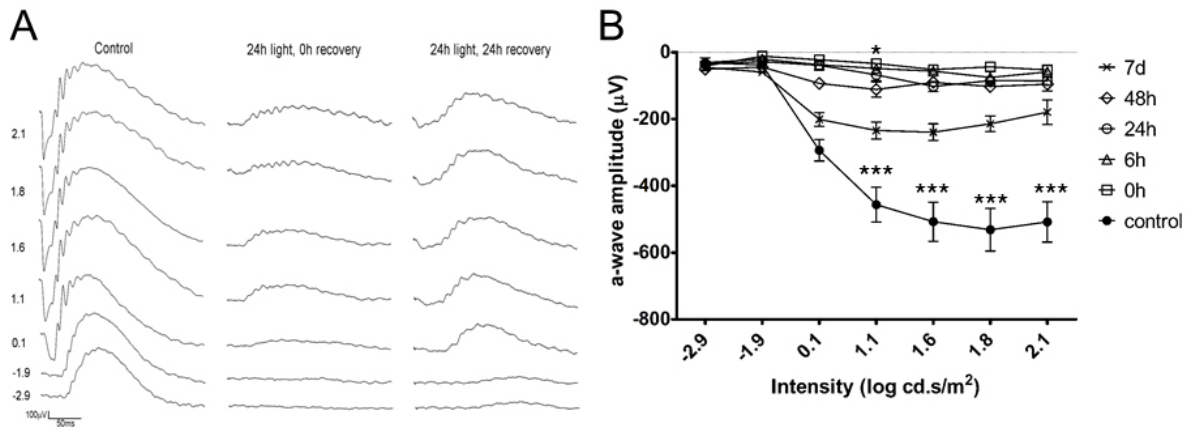
Figure 3-2. ERG analysis in the intense light-exposed rats with various recovery periods.
A: Representative mixed ERG wave forms for control, 0 and 24 hours recovery after light damage at intensity from -2.9 to 2.1 log cd.s/m^2. **B:** The average a-wave response from the mixed waveforms showed significant reduction in the amplitude at the four brightest intensities from all the light-damaged groups compared with the control group $p < 0.001$. Data are expressed as means ± SEM (n=6). A two-way ANOVA and a Bonferroni post-test were used for comparisons of mixed a-wave responses and mixed b-wave responses. Significant values are indicated with asterisks: * $p < 0.05$; ** $p < 0.01$; *** $p < 0.001$.
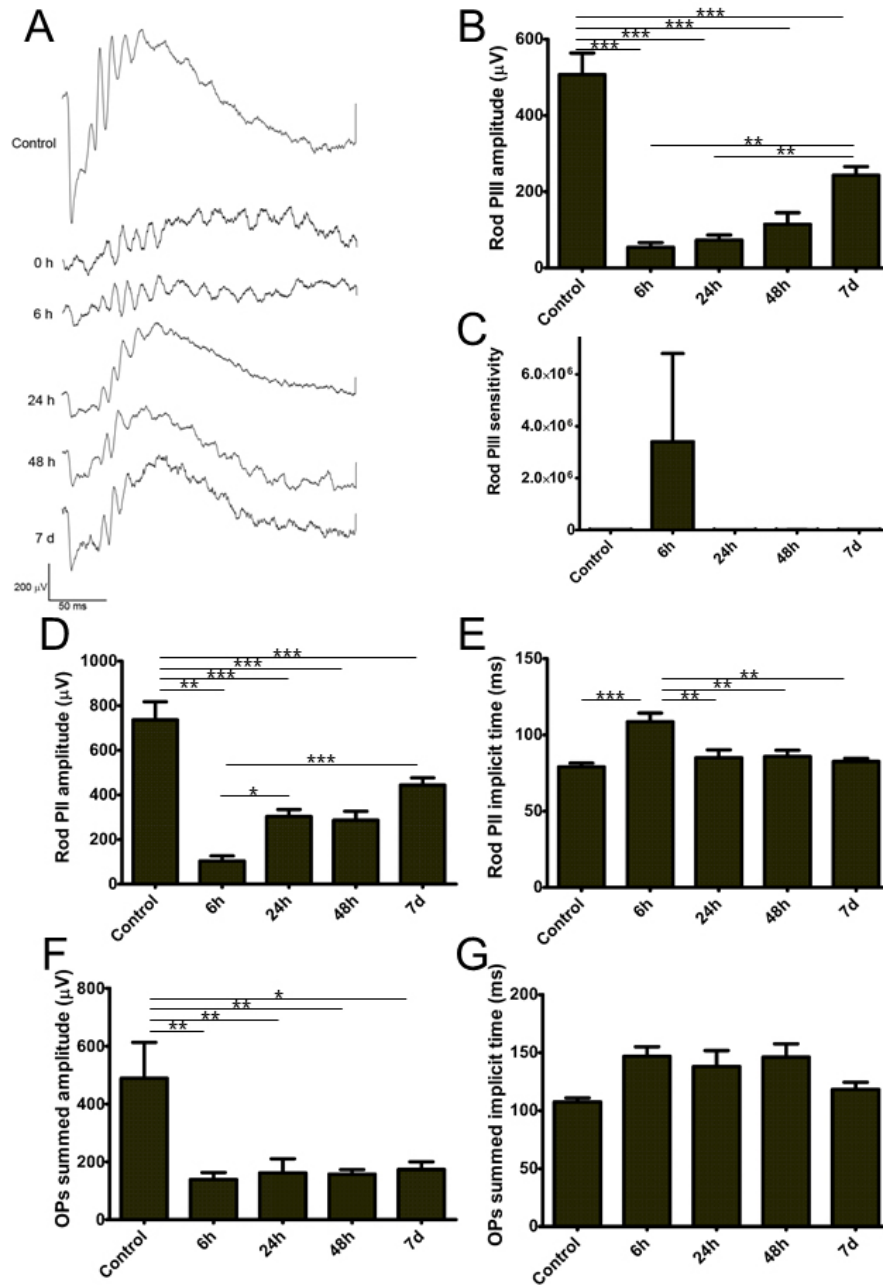
Figure 3-3. Rod photoreceptor functional response. **A:** Representative ERG isolated rod response wave forms for control, and light-damaged retinas at several recovery times. **B:** Extracted average rod a-wave response at intensity of 2.1 log cd.s/m^2 from light-damaged rats showed significant reduction in the amplitude at all the recovery time-points post-exposure compared to the control rat eyes ($p < 0.001$). **C:** There was no difference in the sensitivity of the rod a-wave at all recovery time-points. **D:** Rod b-wave amplitude was significantly decreased at all the time-points post-exposure. **E:** Rod b-wave implicit time was significantly increased at 6 hours post-exposure ($p < 0.001$) and was reduced to control values at all other recovery times. **F:** The amplitudes of summed oscillatory potentials OP2, OP3 and OP4 at intensity of 2.1 log cd.s/m^2 showed significant reduction at most recovery time-points ($p < 0.05$). **G:** There were no significant differences in the OPs implicit time. A one-way ANOVA followed by a Tukey's test were used for comparisons of extracted rod and OPs. Data are expressed as means ± SEM (n=6). Significant values are indicated with asterisks: * $p < 0.05$; ** $p < 0.01$; *** $p < 0.001$.

Isolated cone responses were also inspected at the highest flash intensity (2.1 log cd.s/m^2). There was a general reduction in cone responses in light-damaged eyes compared with control rats and representative waveforms as shown in Figure 3-4A. There was a significant reduction in cone PII amplitude in the light-exposed rats (one-way ANOVA, $p < 0.01$; Figure 3-4B). However, the timing of the PII response did not vary from control rats (Figure 3-4C). These results indicate that cone post-photoreceptor response was affected by intense light exposure.
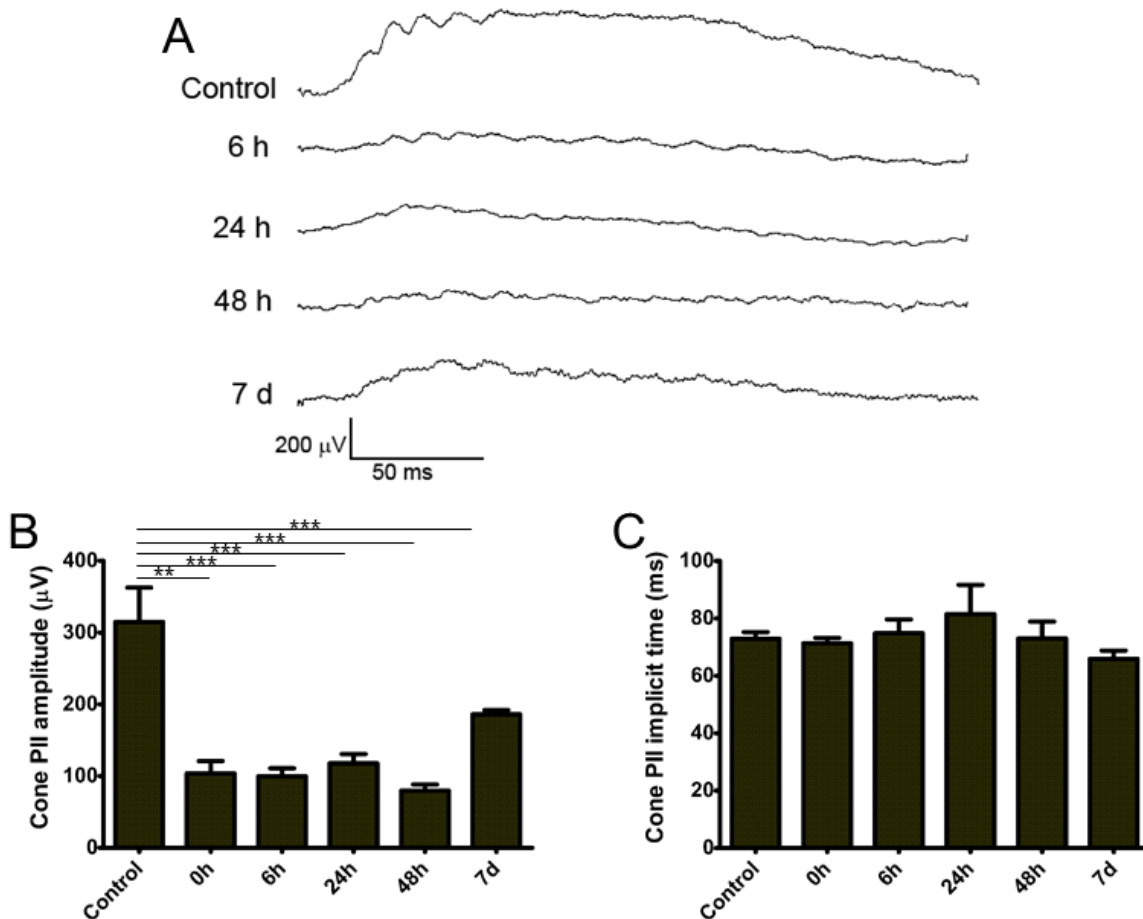
Figure 3-4. Cone photoreceptor functional response. **A:** Representative ERG isolated cone response wave forms for control, and light-damaged retinas at several recovery times. **B:** The amplitude of cone b-wave response showed significant reduction from all groups post-exposure comparing to the control rat eyes $p < 0.01$. **C:** The implicit timing was not altered. A one-way ANOVA followed by a Tukey's test were used for comparisons of extracted cone responds. Data are expressed as means ± SEM (n=6). Significant values are indicated with asterisks: ** $p < 0.01$; *** $p < 0.001$.

3.3.2 Photoreceptors were processing cell death at the highest rate soon after light damage

TUNEL labelling was performed on central retina in the same tissue where ERG was conducted to provide an indication of the amount of photoreceptor cell loss (Figure 3-5). Light damage caused photoreceptor cell death was evident at each recovery time-point, but most prominent at 6 hours post-exposure (Figure 3-5C). At 6 hours post-exposure, there was significant TUNEL labelling possibly contributing to the big loss of retinal function (Figure 3-3B). However, the number of TUNEL labelled cell counts at 48 hours and 7 days post-exposure (Figure 3-5E&F) did not explain recovery in ERG function at those time-points (Figure 3-3 and Figure 3-4). The results highlighted that in addition to cell death, other mechanisms than purely cell death may contribute to abnormal retinal function. The expression of inflammatory markers in the light-exposed rats was then explored.

TUNEL-positive cell counts were different along the retina from light-damaged rats (Figure 3-5A). Central area showed obviously more TUNEL-positive cells compared to the peripheral areas. 24 hours intense light exposure caused a significant increase in TUNEL-positive cells in the outer retina compared to the control non-light-damaged retina ($p < 0.001$; Figure 3-5B).
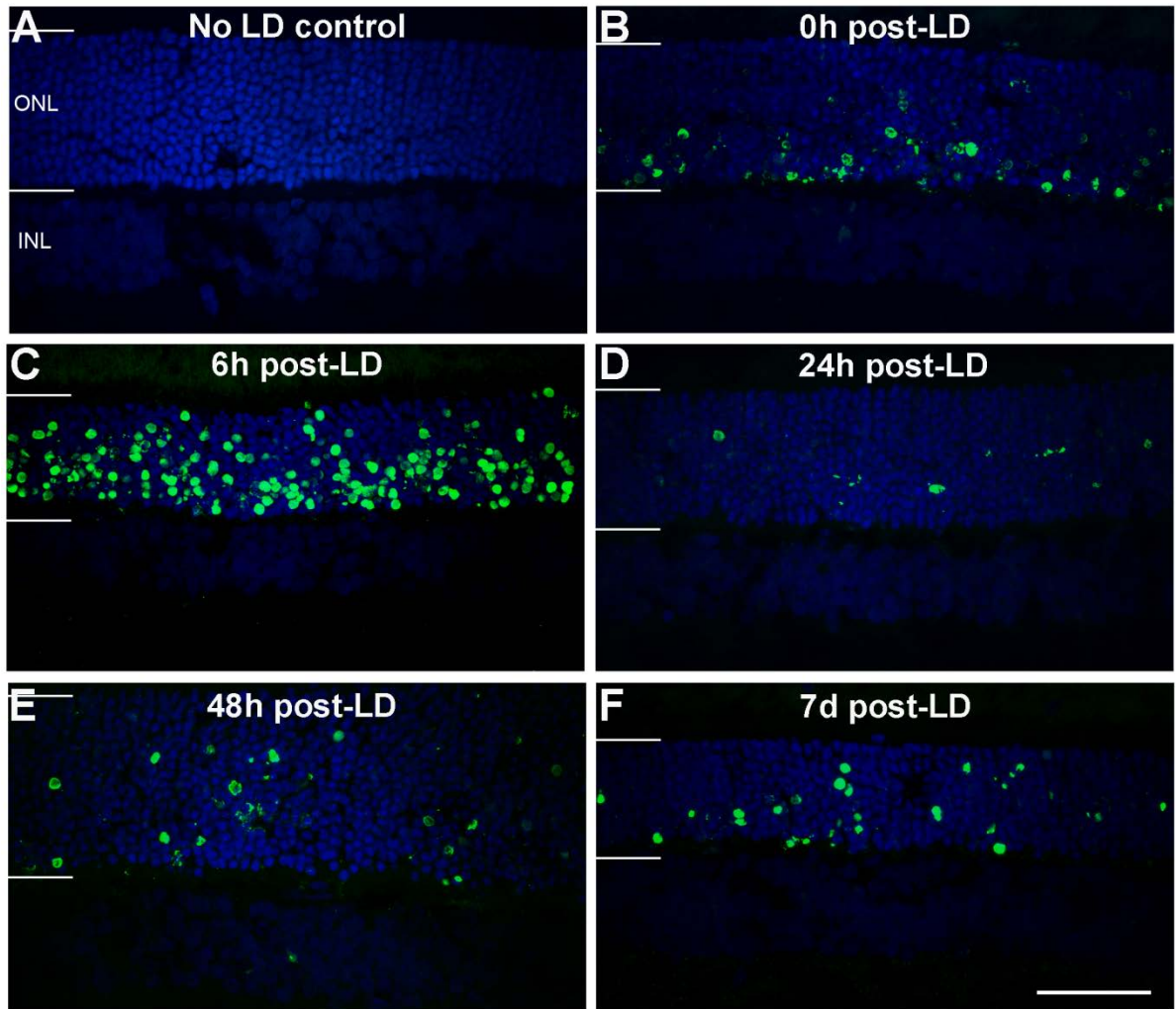
Figure 3-5. TUNEL staining in the retina of the control and light-damaged rats. **A:** TUNEL staining was absent in the control rat. **B-F:** Low magnification images showed that TUNEL positive cells were present in the light-damaged rats in the inner part of ONL immediately after damage (**B**) and spread throughout the whole ONL with prolonged recovery (**C-F**). Apoptotic activity reached its peak at 6 hours post-exposure (**C**). Abbreviations: **ONL**, outer nuclear layer; **INL**, inner nuclear layer. Scale bar = 50 µm.
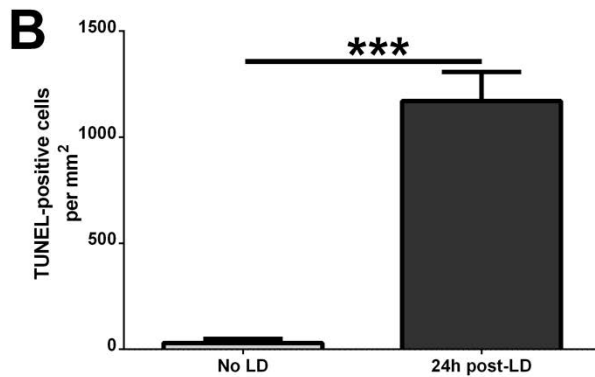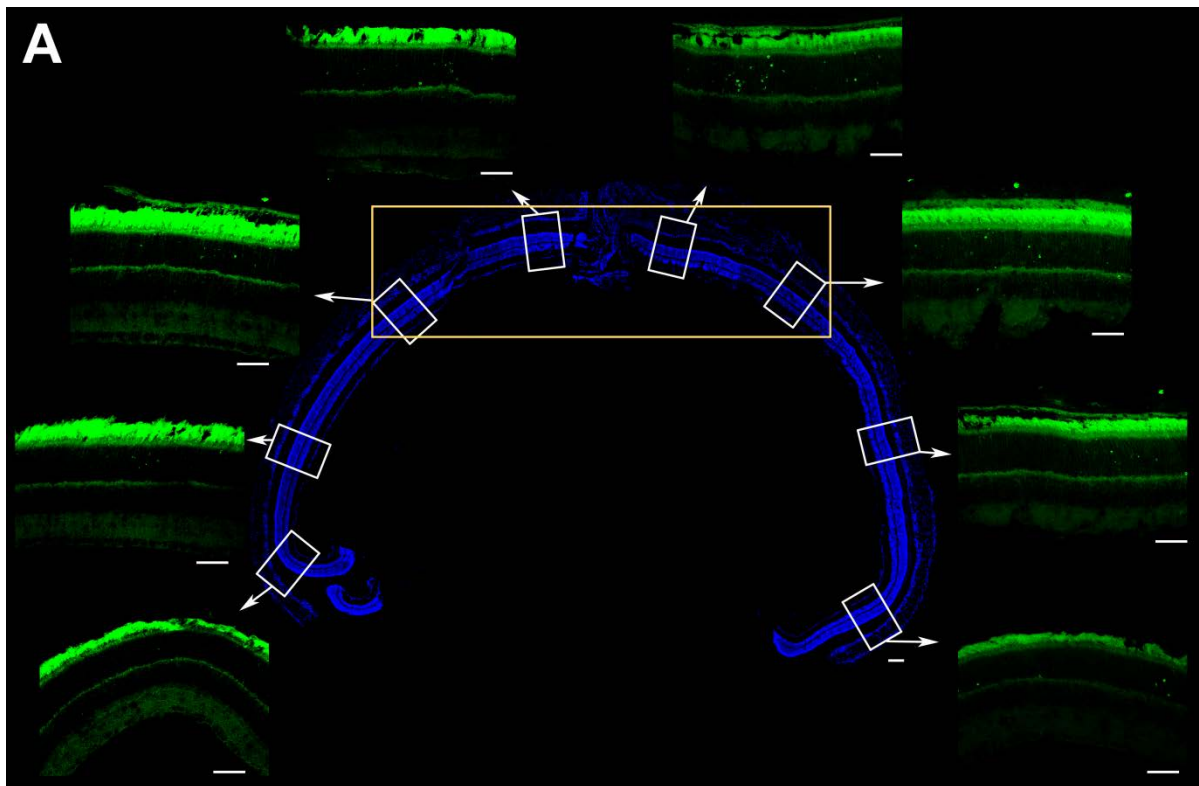
Figure 3-6. TUNEL staining in the retina 24 hours following light damage. A: TUNEL staining showed different labelling patterns along the retina. **B:** Quantification analysis showed significantly increased TUNEL-positive cell counts in the group of 24 hours post-LD compared to control group without light damage (unpaired t-test, $p < 0.001$; n = 5 in each group). The quantification refers to the central area of the retina that has been used in this study (yellow box). Scale bar = 50 µm in TUNEL images and scale bar = 100 µm in the constructed DAPI image.

3.3.3 Microglia respond immediately post-exposure

Ionised calcium-binding adaptor molecule-1 (Iba-1) is a marker for microglia in the retina (Xu *et al.*, 2007; Ibrahim *et al.*, 2011). In the control retina, Iba-1 expression was limited to

the ganglion cell layer, inner plexiform layer and outer plexiform layer (Figure 3-7A). To determine the proportion of microglia activated in the retina the cells immuno-labelled with Iba-1 were counted in the inner, middle and outer parts of the retina. In the control rats, the majority of the microglia cells were located in the ganglion cell layer and inner plexiform layer (Figure 3-7G) with hardly any in the outer nuclear layer and IS/OS area (Figure 3-I). The shape of these microglia cells tended to be round or oval and with few thin projecting processes. Immediately after light damage (0 hour), many Iba-1 stained cells were observed in the outer nuclear layer (Figure 3-7B). These were activated microglia as demonstrated by their polarised and decreased primary and terminal projecting processes, which has been presented in a previous study (Wong *et al.*, 2008). The microglia seems to move from the ganglion cell layer and inner plexiform layer as their number decreased in these layers compared with the control retina (Student's t-test, $p < 0.05$; Figure 3-7G). At 6 hours after light damage, the projecting processes were thicker (Figure 3-7C). Iba-1-labelled cells continued to move to the outer and the inner nuclear layer at 24 hours and 48 hours post-exposure and many more microglia were observed in the IS/OS area (Figure 3-7D&E). These cells had thickened projecting processes and enlarged cell bodies (Figure 3-7D&E, arrows). The number of microglia significantly and progressively increased in the INL, OPL and OS/IS after light damage until 48 hours post-exposure (Student's t-test, $p < 0.05$; Figure 3-7H&I). However, the outer layers of the retina, including the outer plexiform layer and the IS/OS area, showed the most dramatic increase in the number of microglia compared to the control rats (Student's t-test, $p < 0.01$; Figure 3-7I). After 7 days, Iba-1-labelled cells were almost absent from the inner and outer nuclear layers and the morphology of the cells were similar as those in control (Figure 3-7F). The results suggest that 24 to 48 hours post-exposure is a critical time-point when the inflammatory response reaches its peak in the retina.
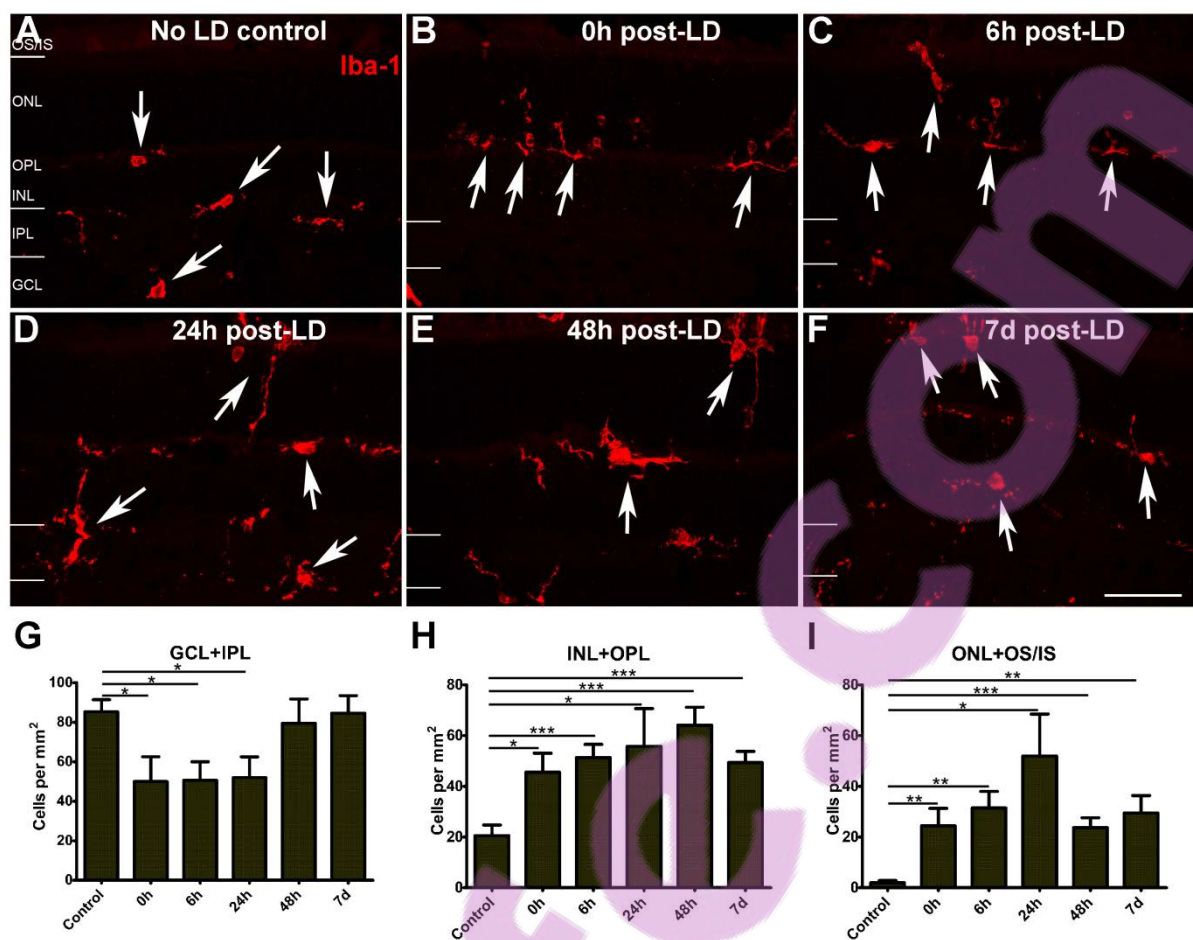
Figure 3-7. Iba-1 immuno-labelled microglia in the retina and microglia cell counts in inner, middle and outer retina layers. A: Control retinas showed microglia in the plexiform layers. **B:** Immediately post-exposure, microglial processed extended towards the ONL. **C:** At 6 hours post-exposure, microglial somata migrated in the ONL, OPL. **D:** At 24 hours post-exposure, microglia migrated in the ONL and were also shown in the OS/IS. **E:** At 48 hours post-exposure, there were activated microglia in the ONL and throughout the retina. **F:** 7 days after light damage, many microglia were still found in the outer retina. **G:** Quantification of number of cell per unit area showed a significant decrease in the number of microglia in the GCL and IPL up to 24 hours post-exposure ($p < 0.05$), returning to control values 48 hours post-exposure. **H:** In the INL and OPL, the number of microglia significantly increased at all time-points tested compared with the control. **I:** In the ONL and OS/IS, the amount of microglia rose following light damage and peaked at 24 hours post-exposure. Abbreviations: **OS/IS**, outer segment/ inner segment; **ONL**, outer nuclear layer; **OPL**, outer plexiform layer; **INL**, inner nuclear layer; **IPL**, inner plexiform layer; **GCL**, ganglion cell layer. Scale bar = 50 μm. Statistical analysis was completed by using an unpaired Student's t-test. Data are expressed as means ± SEM (n=6). Significant values are indicated with asterisks: * $p < 0.05$; ** $p < 0.01$; *** $p < 0.001$.

Another specific marker for activated microglia and macrophages, ED1 (CD68), was employed in this study to further analyse the inflammatory response. The immunoreactivity of ED1 has been investigated in tissues collected from both non-exposed control animals and animals culled at 6 hours post-exposure to intense light. In the retina, ED1 immuno-staining

104

was hardly detectable, with only faint labelling in the ganglion cell layer in the normal eye, which was associated with glial fibrillary acidic protein (GFAP) in astrocytes. There were also some macrophages showing immunoreactivity to ED1 in the inner plexiform layer in the non-light-damaged control tissue (Figure 3-8A). The ED1 immunoreactivity in the ganglion cell layer was increased markedly following light damage compared to the non-light-damaged control (Figure 3-8A&B). This increased ED1 immunoreactivity was thought to be associated with increased astrocyte activity due to their specific localisation in the nerve fibre layer of the rat retina (Stone & Dreher, 1987). In the choroid, there were some ED1 stained cells in the normal control tissue. These cells had large, oval-shaped cell body (Figure 3-8C). At 6 hours post-exposure, the amount of ED1 immuno-labelled cells in the choroid was increased and the cell bodies tended to be amoeboid in shape (Figure 3-8D).
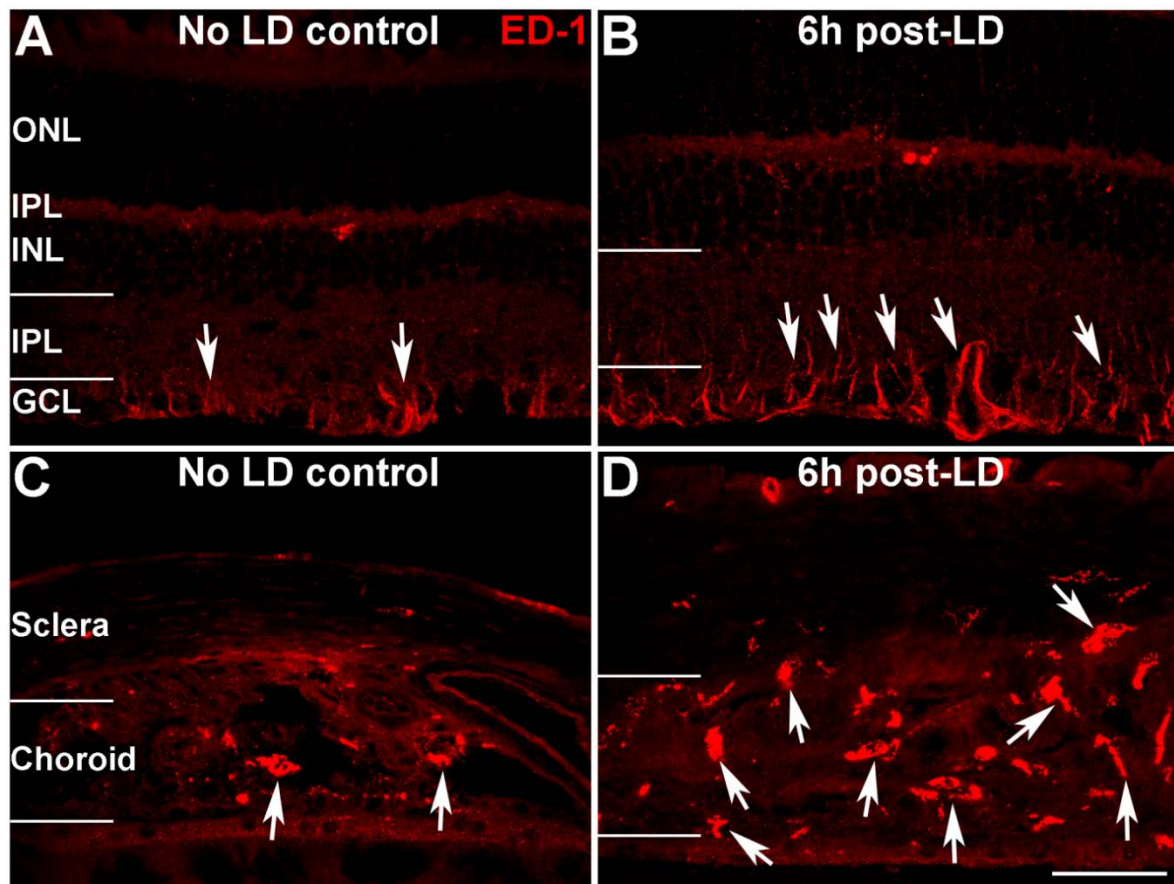
Figure 3-8. ED1 immunoreactivity in the retina and the choroid. A&C: ED1 immunoreactivity in the normal control eye without light damage showed low levels of immunoreactivity in the ganglion cell layer (GCL) of the retina with a few ED1 immuno-stained cells in the choroid. **B&D:** Higher immunoreactivity of ED1 in the GCL in the retina and more ED1 immuno-stained cells in the choroid following light damage. Abbreviations: **OS/IS**, outer segment/ inner segment; **ONL**, outer nuclear layer; **OPL**, outer plexiform layer; **INL**, inner nuclear layer; **IPL**, inner plexiform layer; **GCL**, ganglion cell layer. Scale bar = 50 µm.

3.3.4 Activated retinal microglia lose their CD45 expression in response to light damage

Iba-1 labels all dendritic-derived macrophages (Ahmed *et al.*, 2007). To confirm whether the increase in macrophages was due to a turnover of residential or vascular derived macrophages, the tissue was double-labelled with Iba-1 and CD45. CD45, also called the common leukocyte antigen, is expressed on all hematopoietic cells. Expression of CD45 and its co-localisation with Iba-1 were investigated in control rats and intense light-exposed rats with various recovery periods. In the retina of control rats, cells labelled with Iba-1 were also CD45-positive in the inner and outer plexiform layers (arrows in Figure 3-9A-C). However, microglia labelled with Iba-1 in the ganglion cell layer did not express CD45 (Figure 3-9A-C). Immediately after light damage, expression of CD45 was much weaker in the inner and outer plexiform layers compared to control retinas. At this time-point, microglia cells labelled with Iba-1 were located in the outer nuclear layer and had no CD45 labelling (Figure 3-9D-F). At 6 hours and 24 hours after light damage, there was some co-localisation of CD45 and Iba-1, but there were still a number of Iba-1-expressing cells that were CD45-negative (Figure 3-9G-I, data of 6 hours not shown). At 48 hours and 7 days post-exposure, CD45 was expressed weakly in the retina and the co-localisation of CD45 and Iba-1 was rare (Figure 3-9J-L, data of 48 hours not shown). As with the control rats, CD45 immuno-labelling was absent in the Iba-1 positive microglia cells in the ganglion cell layer at all the time-points post-exposure (Figure 3-9C, F, I and L).
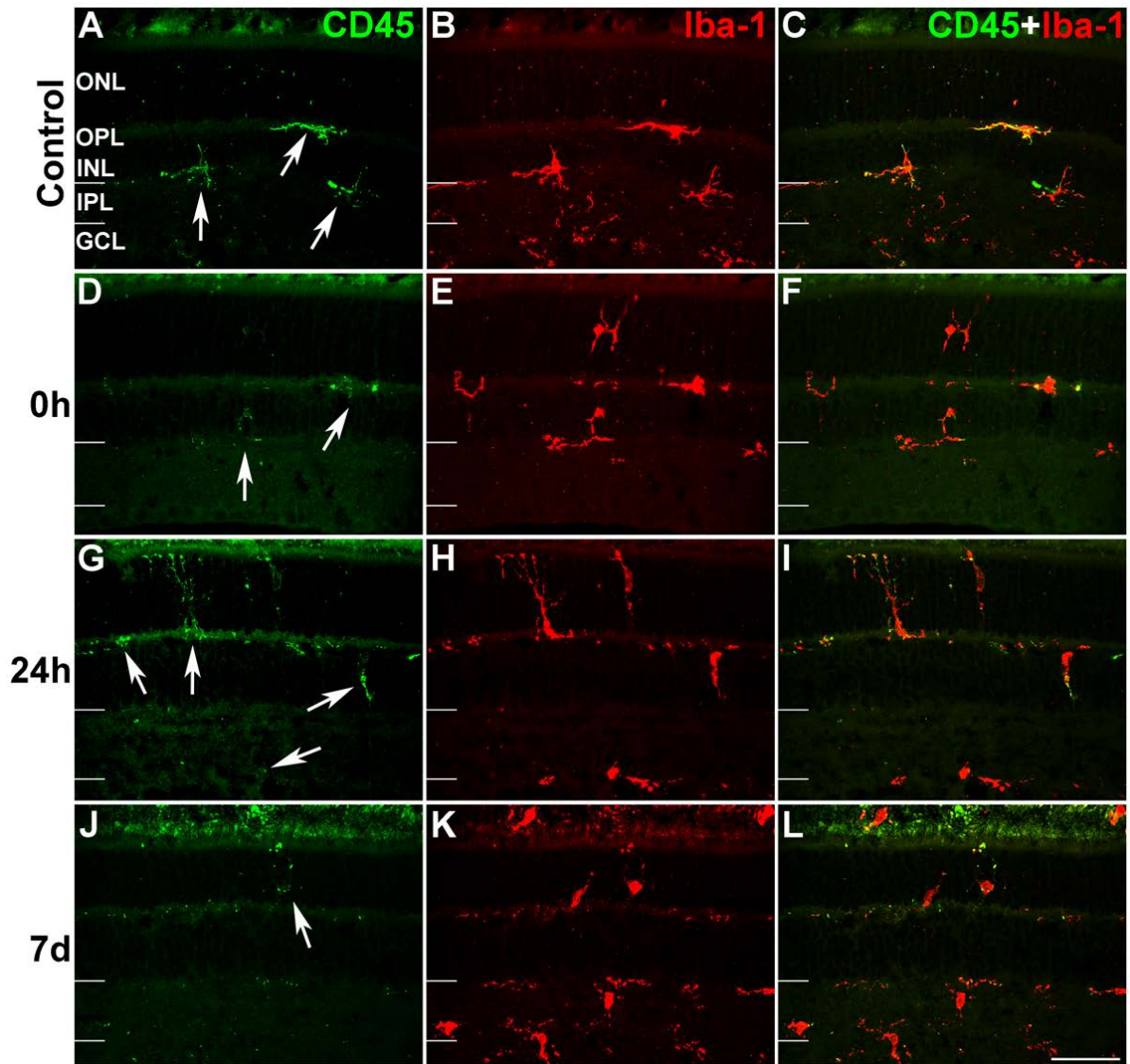
Figure 3-9. CD45 and Iba-1 immuno-labelling in the retina. **A-C:** Control rat retina had a few cells with co-localisation of Iba-1 and CD45 (arrows). **D-F:** Iba-1-labelled microglia lost most CD45 expression immediately after light damage (arrows). **G-I:** At 24 hours post-exposure, CD45 immuno-labelling was weakly observed only on some microglia (arrows). **J-L:** There was minimal CD45 labelling of microglia cells at 7 days post-exposure (arrow). Abbreviations: **OS/IS**, outer segment/ inner segment; **ONL**, outer nuclear layer; **OPL**, outer plexiform layer; **INL**, inner nuclear layer; **IPL**, inner plexiform layer; **GCL**, ganglion cell layer. Scale bar = 50 µm.

In the choroid, Iba-1 labelled macrophage-phenotype microglia were not expected as Iba-1 is a marker for dendritic-derived macrophages (Ahmed *et al.*, 2007). Interestingly, however, co-localisation of Iba-1 and CD45 was observed in the choroid. In control animals, a few CD45 immuno-stained cells were detected, which were limited to the inner capillary layer of the choroid (Figure 3-10A-C). These cells became spread throughout vessel layers and microcapillary layers of the choroid after light damage (Figure 3-10D-F). Double-labelling of Iba-1 and CD45 in the light-damaged tissue showed co-localisation of the markers on large, round cells. After 7 days, the pattern of co-localisation was unchanged (Figure 3-10G-I). The number of CD45 immuno-positive cells was elevated in light-damaged groups, although this was only significant at 6 hours post-exposure compared with the control ($p < 0.05$; Figure 3-10J). It is concluded that both Iba-1 and CD45 can be used to identify residential macrophages in the choroid.
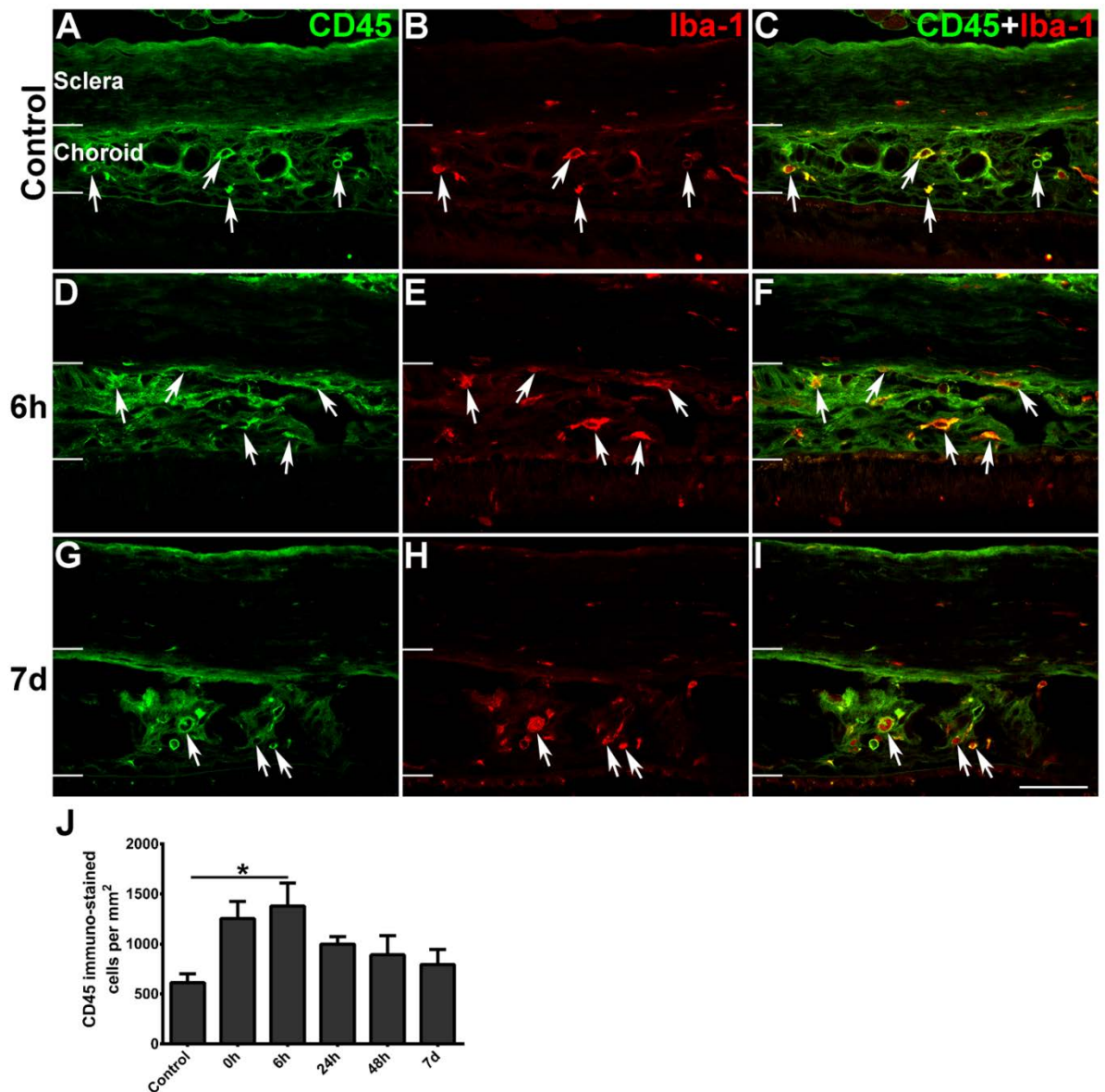
Figure 3-10. Confocal images showing CD45 and Iba-1 double immuno-labelled cells in the choroid at various recovery time-points following light damage. A-C: There were a few cells showing co-localisation of CD45 and Iba-1 in the control choroid. **D-F:** At 6 hours after light damage, increased CD45 immunoreactivity seemed to be associated with lba-1 immuno-labelling and the labelled cells showed ameboid-shaped morphology. **G-I:** At 7 days following the light damage, the morphology of CD45 and Iba-1 labelled cells was similar to the control. **J.** CD45-labelled cell counts in the choroid at various time-points following the light damage. There was a significant increase at 6 hours post-exposure ($p < 0.05$). Statistical analysis was completed by using a Student's t-test. Data are expressed as means ± SEM (n=6). Significant values are indicated with asterisks: * $p < 0.05$. Scale bar = 50 µm.

3.3.5 Oxidative stress expression following light-damage

In addition to the inflammatory responses, oxidative damage was investigated using immunohistochemistry and Western blot with an anti-nitrotyrosine antibody. Animal tissue collected over various recovery time-points following the light damage was analysed. Nitrotyrosine, a marker for endogenous nitrosation and nitration, has been used to quantify oxidative stress in the blood and tissue proteins (Ohshima *et al.*, 1990). In the aging mouse retina, nitrotyrosine-immunoreactivity has been shown to be remarkably increased (Xu *et al.*, 2009). The present study showed that control rats without light damage displayed nitrotyrosine expression in both the retina and the choroid in a Western blot (Figure 3-11A-C). In the choroid, multiple nitrated proteins with bands at 120 kDa and 55 kDa were detected (Figure 3-11A). A similar pattern was seen the retina (data not shown). Quantification analysis showed that the level of nitrotyrosine expression was significantly increased in the choroid over a short time period (0-6 hours) following the light damage (n=6; Figure 3-6B). However, there was no significant change in the retina (Figure 3-11C). Images of immunohistochemical staining showed nitrotyrosine expression in big cells located in the capillary layer of the choroid, where smaller blood vessels are located (Figure 3-11D). These cells were also labelled with the microglia cell marker, Iba-1 (Figure 3-11D-F). In addition, some capillaries showed nitrotyrosine-immunoreactivity in this area (Figure 3-11D). In the retina, nitrotyrosine-immunoreactivity was only detected at 24 hours post-damage. The immunoreactivity seen in the outer plexiform layer and throughout the inner retinal layers appeared to be associated with retinal blood vessels (Figure 3-11G), and it was also in close proximity to the microglia (Figure 3-11G-I).
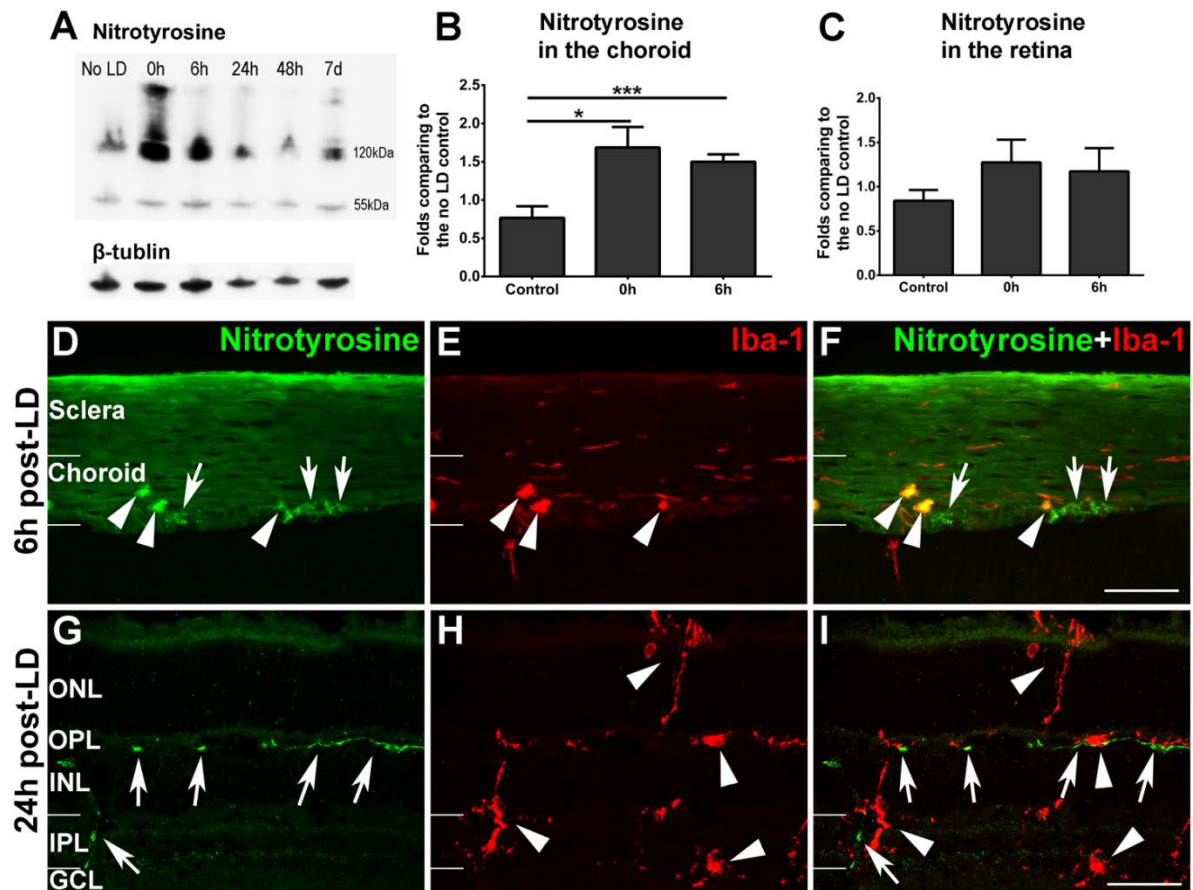
Figure 3-11. Elevated oxidative stress was detected mainly in the choroid following light damage. **A:** Representative image of a Western blot for nitrotyrosine expression in the choroid. β-tubulin (lower bands) was used as a loading control. **B&C:** Quantitative analysis of nitrotyrosine expression in the choroid (**B**) and retina (**C**) in the control animals and animals after a short recovery time following light damage. **D-F:** Nitrotyrosine-immunoreactivity was shown in the blood vessels (**BV**; arrows) in the choroid at 6 hours post-damage. It also showed co-localisation with the microglia marker Iba-1 (arrow heads). **G-I:** At 24 hours following light damage, nitrotyrosine-immunoreactivity (arrows) was seen in the OPL of the retina, where it appears to be associated with blood vessels and increased microglia immunoreactivity (arrow heads). Abbreviations: **OS/IS**, outer segment/ inner segment; **ONL**, outer nuclear layer; **OPL**, outer plexiform layer; **INL**, inner nuclear layer; **IPL**, inner plexiform layer; **GCL**, ganglion cell layer. Scale bar = 50 µm.

3.3.6 Gap junction protein expression is changed following light damage

Gap junction proteins including Cx43, Cx40, Cx36 and Cx45 in the non-light-damaged control group were compared to the light-damaged groups with various recovery periods. Cx43 expression in the retina and the choroid was investigated using Western blot and immunohistochemistry. Cx43 was present in the choroid and the retina (Figure 3-12). Quantification analysis of Western blots using ImageJ showed that Cx43 level in the choroid and RPE was dramatically increased in the short term following light damage (Figure 3-7B). However, the expression level of Cx43 in the retina showed a decrease compared to the control tissue, although this was not significant (Figure 3-12C). Confocal images showed strong Cx43 immunoreactivity in the endothelial cells of larger choroidal blood vessels in the normal control tissue. It was also strongly expressed in the RPE (Figure 3-13A). Following intense light exposure, the localisation of Cx43 did not show much change in the RPE and choroid (Figure 3-13B-F, H & I). In the normal rat retina, Cx43 immunoreactivity was detected primarily in the ganglion cell layer (Figure 3-14A), which may be closely associated with the processes of astrocytes, and the endothelium of blood vessels (Ly *et al.*, 2011; Danesh-Meyer *et al.*, 2012). After light damage and up to 7 days post-exposure, Cx43 immunoreactivity was still detected in this layer and did not seem to be labelled in other cells or layers of the retina (Figure 3-14B-F).
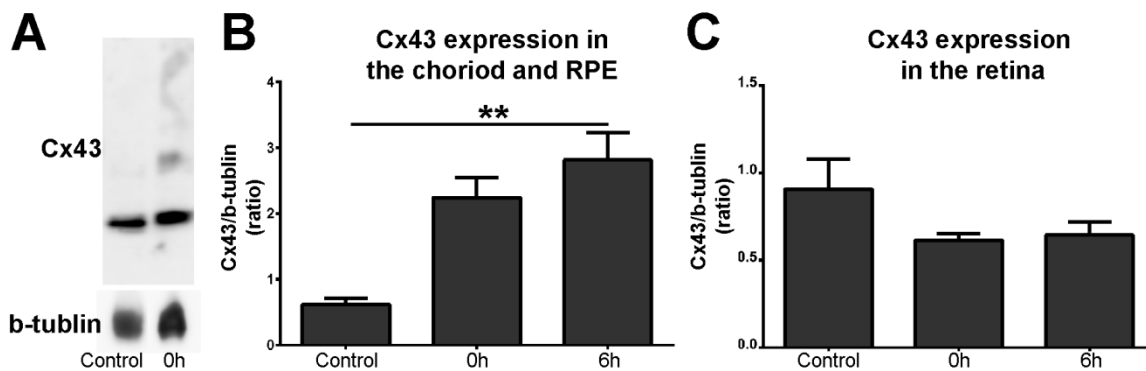
Figure 3-12. Western blot analyse of Cx43 expression in the choroid and retina of control and light-damaged animals. **A:** Representative image showing Western blot detection of Cx43 in the control and light-damaged rat retina. **B:** Quantitative analysis of Western blot for Cx43 protein expression in the choroid and RPE from the control and light-damaged groups. Cx43 expression was significantly increased post-exposure compared to the control (n=6; ** $p < 0.01$). **C:** Quantitative analysis of Western blot for Cx43 expression in the retina from the control and light-damaged groups. The expression of Cx43 tended to be decreased post-exposure, but this change was not significant.
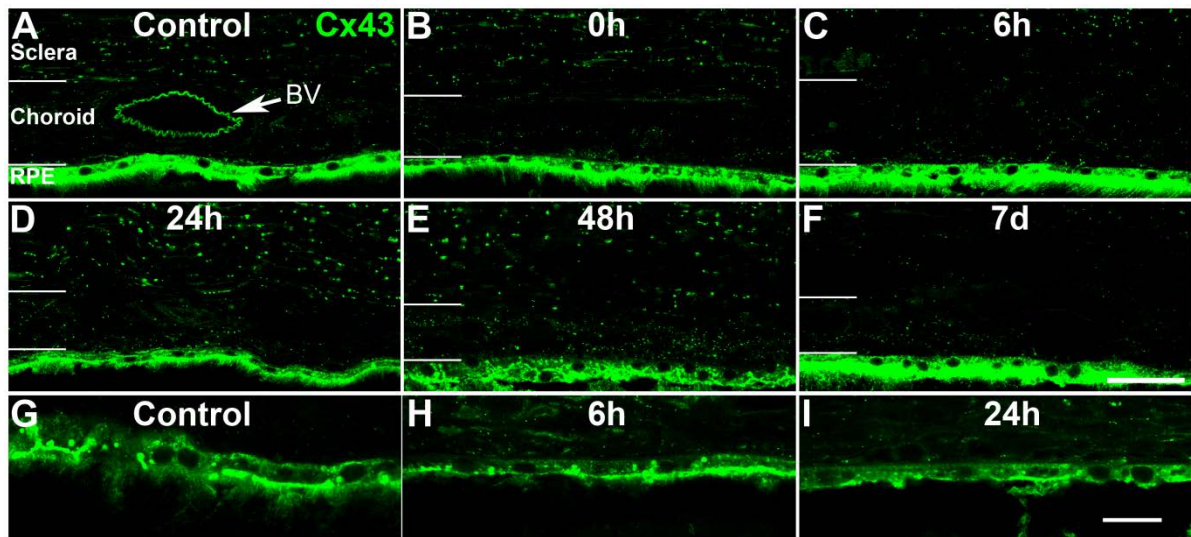
Figure 3-13. Confocal images showing Cx43 expression in the choroid of the control and light-damaged animals. **A:** Cx43 immunoreactivity in normal control RPE and choroid tissue, primarily seen strongly in the endothelium of blood vessels, choroidal capillaries and the RPE. **B-F:** RPE and choroid tissue from the light-damaged group immuno-labelled for Cx43. **G-I:** Higher magnification images showing Cx43 immunoreactivity on the endothelium of the choroidal capillaries and RPE. Abbreviations: **OS/IS**, outer segment/ inner segment; **ONL**, outer nuclear layer; **OPL**, outer plexiform layer; **INL**, inner nuclear layer; **IPL**, inner plexiform layer; **GCL**, ganglion cell layer; **BV**, blood vessels. **A-F:** scale bar = 50 µm; **G-I:** scale bar = 20 µm.

113
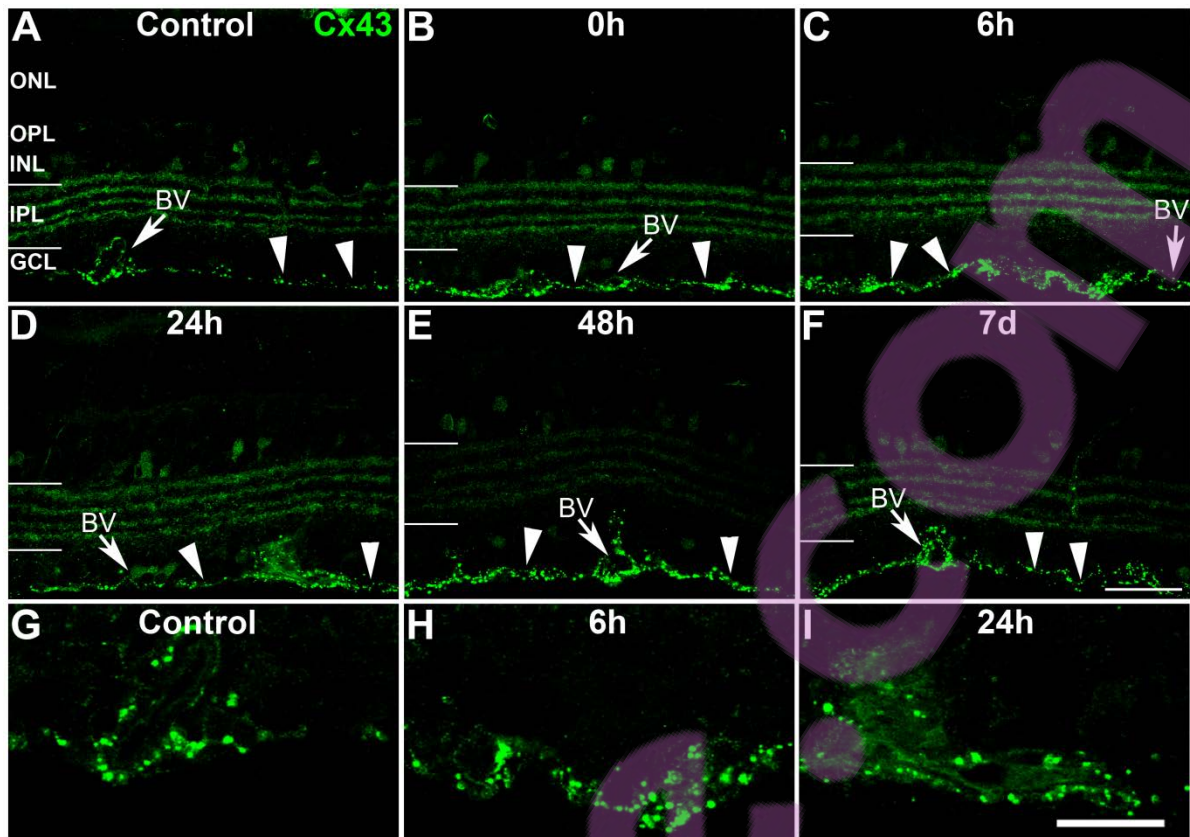
Figure 3-14. Confocal images showing Cx43 expression in control and light-damaged retinas.
A: Cx43 immunoreactivity was limited to the ganglion cell layer in the normal control retina.
B-F: Cx43 immuno-labelling in the retina at various time-points following light damage. **G-I:**
Higher magnification images showing Cx43 immunoreactivity on the endothelium of the retinal
capillaries and astrocytes. Abbreviations: **OS/IS**, outer segment/ inner segment; **ONL**, outer nuclear
layer; **OPL**, outer plexiform layer; **INL**, inner nuclear layer; **IPL**, inner plexiform layer; **GCL**,
ganglion cell layer; **BV**, blood vessels. **A-F:** scale bar = 50 µm; **G-I:** scale bar = 20 µm.

In addition to Cx43, the expression of Cx36, Cx45 and Cx40 were also investigated using
immunohistochemistry in the control and the light-damaged animals. Cx36
immunoreactivity was low and limited to the inner plexiform layer of the control retina
(Figure 3-15A). At 24 hours following intense light exposure, the immunoreactivity of Cx36
had obviously increased. Big blood vessels in the ganglion cell layer also showed Cx36
immunoreactivity (Figure 3-15B). At 7 days post-exposure, Cx36 immunoreactivity
dropped back to a level which was comparable to that of the control tissue (Figure 3-15C).
In the control retina Cx45 was mainly expressed in the inner plexiform layer and the nerve
fibre layer (Figure 3-15D). The immunoreactivity was strong. At 24 hours following
intense light exposure, Cx45 immunoreactivity was obviously decreased compared to the
control tissue (Figure 3-15E). Interestingly, at 7 days post-exposure, the expression of Cx45

114

in the inner plexiform layer was increased to a similar level to that of the control (Figure 3-15F). However, Cx45 immunoreactivity in the nerve fibre layer remained low, compared to the control retina.
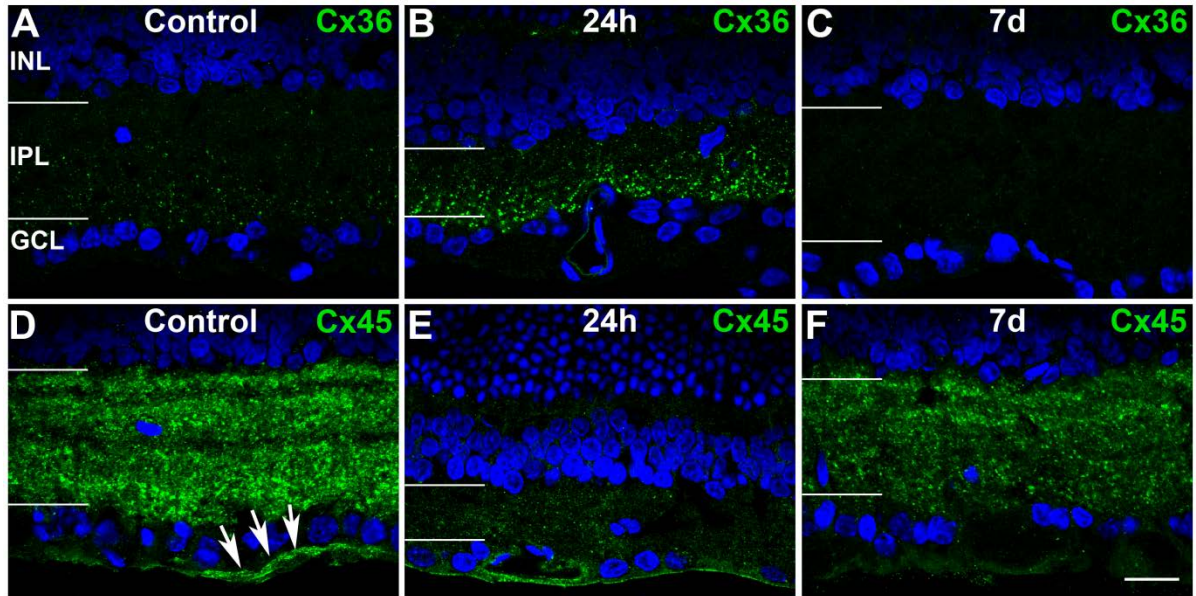
Figure 3-6. Cx36 and Cx45 expression in control and light-damaged retinas with 24 hours and 7 days recovery periods. A-C: Cx36 immunoreactivity in control retina (**A**), and retinas at 24 hours (**B**) and 7 days (**C**) following intense light exposure. The Cx36 immunoreactivity levels are comparable between the control and 7 days post-exposure, but it was obviously increased at 24 hours following light damage. **D-F:** Cx45 immunoreactivity in the control retina (**D**), and the retinas at 24 hours (**E**) and 7 days (**F**) following intense light exposure. The expression levels of Cx45 in the inner plexiform layer were similar between control retina and 7 days post-exposure. However, the control tissue showed stronger Cx45-labelling in the nerve fibre layer (arrows). Cx45 immunoreactivity was decreased in the retina at 24 hours following the light damage. Abbreviations: **INL**, inner nuclear layer; **IPL**, inner plexiform layer; **GCL**, ganglion cell layer. Scale bar = 20 µm.

In the normal retina and choroid, Cx40 did not show any immunoreactivity (data not shown). At 24 hours following light damage, the retina still had no Cx40 immunoreactivity but Cx40 was now detected on the large blood vessels in the vascular layer of the choroid (Figure 3-16A) where the large and medium-sized arteries and veins are located. Cx40 immunoreactivity was also noticed on some large, round cells in the choroid (Figure 3-16B). By 7 days post-exposure, Cx40 immunoreactivity was again undetectable in either the retina or the choroid (data not shown).
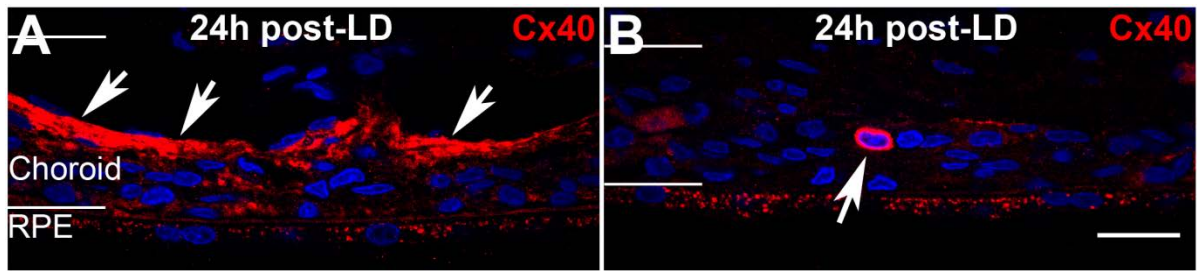
Figure 3-7. Confocal images showing Cx40 immunoreactivity in the choroid at 24 hours following the intense light exposure. A: At 24 hours post-exposure, large blood vessels showed strong Cx40 immunoreactivity (arrows). **B:** Some oval or round shaped large cells showed Cx40 immunoreactivity at 24 hours following the light damage (arrow). Abbreviations: **RPE**, retinal pigment epithelium. Scale bar = 20 µm.

3.3.7 Cx43 expression is detected on the macrophage following light damage

In addition to up-regulated expression level of Cx43, it was noticed that Cx43 is expressed by some CD45 immuno-labelled macrophages in the choroid and the retina following the light damage (Figure 3-17). Expression of Cx43 was also detected on the nitrotyrosine immune-labelled cells in the choroid post-exposure (Figure 3-18). These cells may be the same type of macrophages, as results from this study have shown that immunoreactivity of nitrotyrosine and Iba-1 are co-localised on some cells in the light-damaged choroid (Figure 3-11D-F).
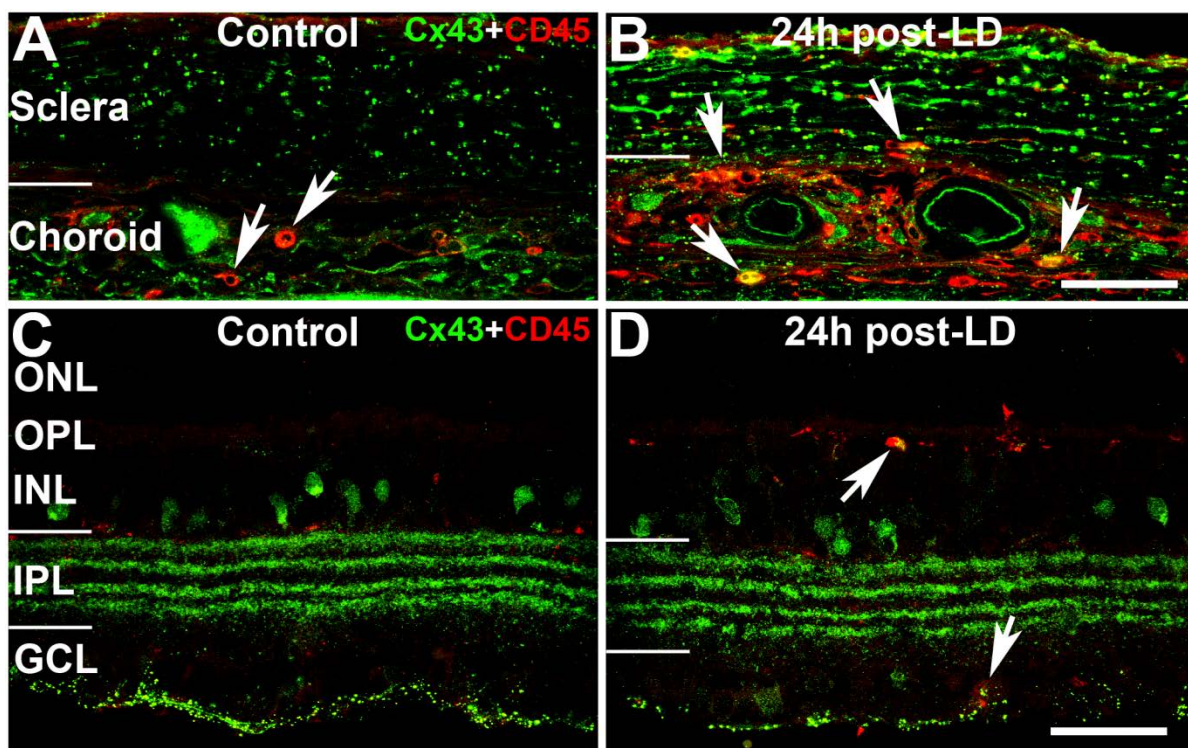
Figure 3-8. Confocal images showing co-localisation of Cx43 and CD45 in the choroid and retina following the light damage. **A:** In normal choroid, the CD45 immuno-labelled macrophages did not show any Cx43 expression. **B:** Many CD45 immuno-labelled macrophages (arrows) showed Cx43 immunoreactivity in the choroid at 24 hours post-exposure. **C:** Co-localisation of Cx43 and CD45 immuno-labelling was detected in the normal retina. **D:** Some CD45 immuno-labelled macrophages/microglia (arrows) showed Cx43 immunoreactivity in the retina at 24 hours following the light damage. Abbreviations: **OS/IS**, outer segment/ inner segment; **ONL**, outer nuclear layer; **OPL**, outer plexiform layer; **INL**, inner nuclear layer; **IPL**, inner plexiform layer; **GCL**, ganglion cell layer. Scale bar = 50 µm.
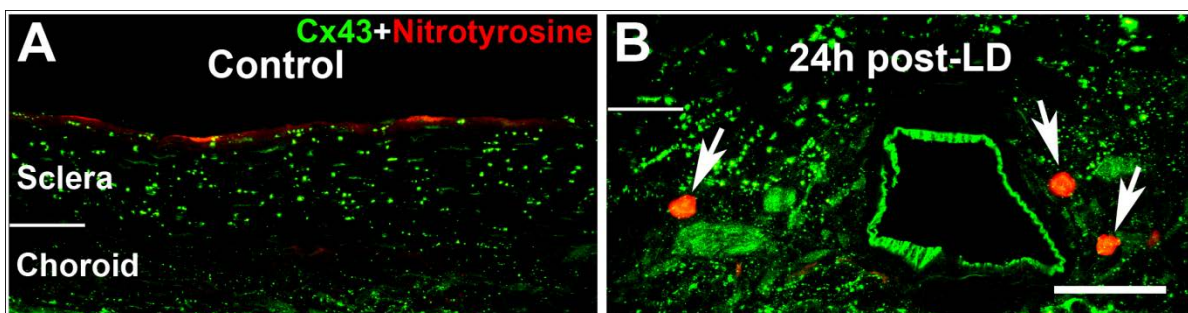
Figure 3-9. Confocal images showing co-localisation of Cx43 and oxidative stress marker, nitrotyrosine in the light-damaged choroid. **A:** In control choroid, nitrotyrosine immunoreactivity was barely detectable. **B:** At 24 hours following the light damage, nitrotyrosine immune-labelled cells showed expression of Cx43 (arrows) in the choroid. Scale bar = 50 µm.

3.3.8   Intense light exposure leads to RPE changes

RPE morphology and expression of connexin proteins were compared in tissues collected from the control and light-damaged groups. In the normal tissue, phalloidin staining showed that RPE cells were hexagonal or pentagon-shaped and with one or two nuclei (Figure 3-19). At 24 hours following light damage, some patches of cells showed stronger phalloidin staining in the light-damaged RPE tissue (Figure 3-19B, arrows), while the staining for phalloidin was even in the undamaged control tissue (Figure 3-19A). More intense staining for phalloidin in some parts of the control tissue was due to difficulties of imaging the waving tissue. In addition, some of the cells were swollen and had more than two nuclei (Figure 3-19H, arrows) as if cells had become merged or were dividing.

As Cx43 was the only connexin protein found expressed in the RPE of all the connexin proteins which were investigated in this study, further examination of Cx43 expression changes was made through immunohistochemistry on the flat-mount RPE/choroid tissue. There was no distinguishable difference for Cx43 expression patterns between light-damaged RPE and control RPE (Figure 3-19C&F). The immunoreactivity of Cx43 was mainly located on cell plasma membrane, co-localising with the phalloidin staining. Little Cx43 immunoreactivity was detected in the cytoplasm of the RPE cells (Figure 3-19E&H).
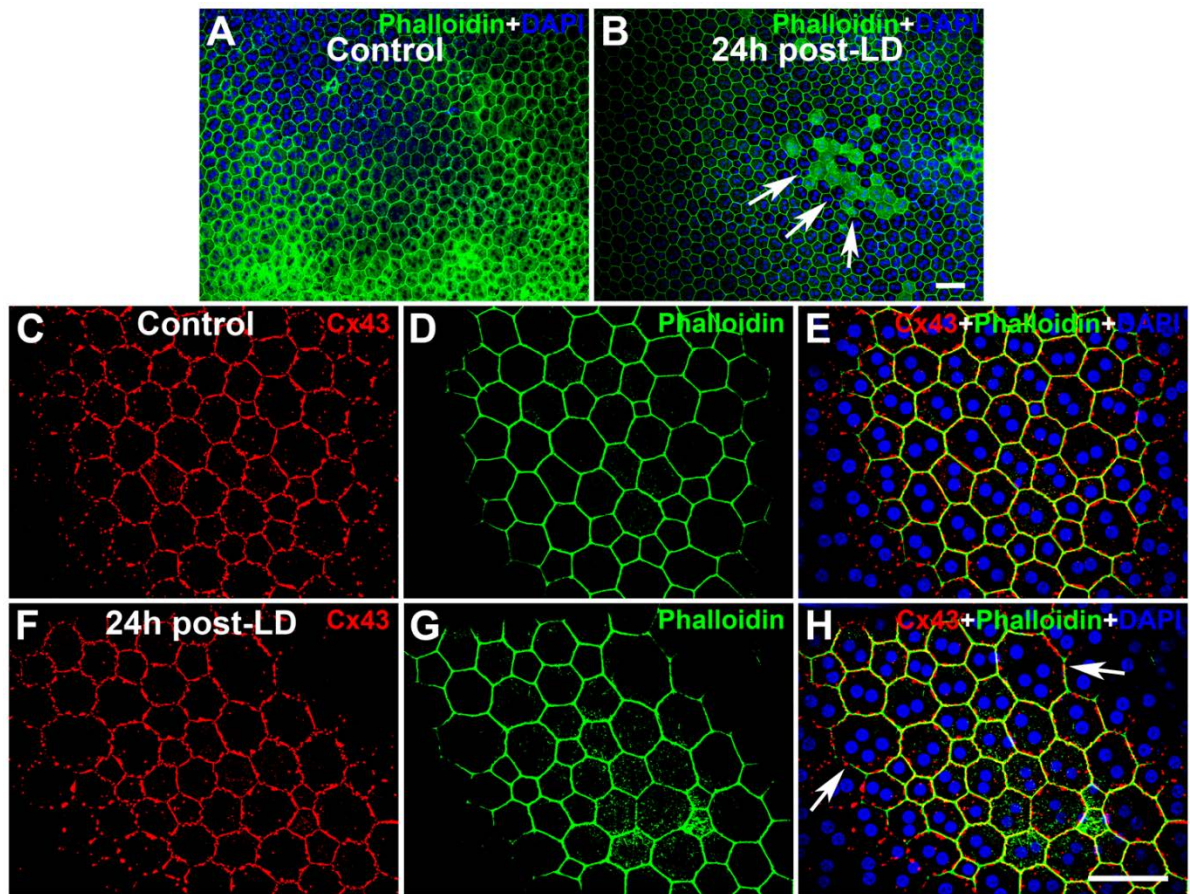
Figure 3-10. Confocal images of flat mounts showing RPE changes following the light damage and Cx43 immunoreactivity in the RPE. **A&B:** Phalloidin staining showing the morphology of RPE in the control (**A**) and light-damaged tissue (**B**). Some patches of RPE cells were strongly stained with phalloidin following the light damage (arrows in **B**). **C-E:** The control RPE tissue was immuno-labelled for Cx43 (**C**), stained for phalloidin (**D**) and the overlay of Cx43, phalloidin and DAPI (**E**). **F-H:** Tissue collected at 24 hours following light damage was immune-labelled for Cx43 (**F**), stained for phalloidin (**G**) and the overlay of Cx43, phalloidin and DAPI (**H**), which did not reveal any differences to the control. Scale bars = 50 μm.

3.4   Discussion

This study has demonstrated that 24 hours intense light exposure significantly reduced the function of both rod and cone photoreceptors in the albino rat.   Oxidative stress was primarily observed in the choroid and RPE, while in the retina only a transient increase was observed at 24 hours post-exposure.   In the choroid, the oxidative stress was co-localised with inflammatory cells and patchy areas around blood vessels that were close to the RPE.   It was evident that the residential retinal microglia cells had tracked to the outer retina immediately following the light damage.   In the normal retina these microglia cells were recognised by both Iba-1 and the common leukocyte antigen CD45.   Intense light exposure led to activation of these cells and a loss of CD45.   ED1 showed many inflammatory cells in the choroid but failed to detect activated microglia in the retina.   Gap junction proteins showed response to the intense light exposure.   Immunoreactivity of Cx36 and Cx45 demonstrated obvious change in the inner plexiform layer of the retina at 24 hours following light damage, compared to control and 7 days post-exposure retinas.   This may be associated with impaired light signal transduction and reduced inner retinal function detected by ERG. Significant up-regulation of Cx43 was found in the choroid and RPE at 0 and 6 hours following light damage, while little change was detected in the retina.   This may indicate that intense light exposure causes more stress on the Cx43-expressing cells in the choroid and RPE than those in the retina.   Cx40-expressing cells in the choroid also showed response to the light damage by exhibiting increased Cx40 immunoreactivity relative to control.

3.4.1   Reduced neuronal responses from both the rod and cone pathways

This study has demonstrated that the intense light exposed albino rat retinas show significantly reduced amplitudes of a-waves, b-waves and OPs with little change in implicit times in the electrophysiological activity (Figure 3-2, Figure 3-3 and Figure 3-4). Interestingly, similar findings on ERG changes with human AMD have been reported in previous studies, which showed decreased a- and b-waves, especially reduced amplitudes of b-wave with normal implicit times, and also significantly reduced amplitudes of OP2

120

(Walter *et al.*, 1999; Jackson *et al.*, 2006). Despite previous histological findings on human AMD donor tissue showing that rods located in the periphery of the macula start degenerating first and are more vulnerable than cones (Curcio *et al.*, 1996; Curcio *et al.*, 2000), the isolated rod and cone ERG data presented here indicate a simultaneous attenuation of neuronal responses from both rod and cone pathways in our light-damaged animal model. This would be mainly due to the fact that the rat retina does not have the macula arrangement.

TUNEL labelling demonstrated that increased photoreceptor cell loss may be associated with impaired retinal function (Figure 3-5). Cell death was observed at various recovery periods but the amount of cell death was not enough to account for the significant reduction in ERG waveforms. This suggests that other mechanisms could also be involved in the impaired retinal function. One possible mechanism affecting rod photoreceptor responses is the structurally disorganised rod outer segment in the light-damaged retina which has been suggested as a source of ERG abnormalities in an earlier study on infant rats (Fulton *et al.*, 1999). Alternatively, we suggest that oxidative stress and inflammatory responses may additionally affect the microenvironment where the photoreceptors sit and subsequently affect neuronal functions in the retina. To date, there is not enough evidence supporting the idea that oxidative stress can directly alter retinal function. However, many studies have indicated a close association between ERG abnormalities and oxidative stress. Edaravone (3-methyl-1-phenyl-2-pyrazolin-5-one), a free radical scavenger, can protect against retinal dysfunction and improve ERG responses after light damage in the mouse (Imai *et al.*, 2010). In addition, an antioxidant component extracted from green tea, epigallocatechin gallate (EGCG), improves otherwise reduced neuronal functions in the ischemic rat retina (Osborne *et al.*, 2008). Transgenic mice carrying a superoxide dismutase transgene showed less oxidative stress-induced reduction in ERG amplitudes, conferring high importance to oxidative stress in the outcome of the ERG (Dong *et al.*, 2006).

3.4.2 Alterations in Cx36 and Cx45 expression levels may contribute to the reduced post-transductional activities seen on ERG PII waveforms

The significantly reduced amplitudes of the rod and cone PII waveforms demonstrated in this study indicates that post-transductional activities are attenuated in both rod and cone pathways in our light-damaged animal model (Figure 3-3 and Figure 3-4). Furthermore, OPs have been proven to be generated from bipolar cells, amacrine cells and ganglion cells located in the inner retina (Wachtmeister, 1998). Therefore, the reduction in OPs in the light-damaged animal model indicates that the inner retina is injured and probably the OFF-pathway involving amacrine cells is mostly affected (Wachtmeister, 1998). The result from immunohistochemical labelling for Cx36 and Cx45 in the inner plexiform layer in our light-damaged animal model supports the attenuated ERG record for the post-photoreceptor neuronal function. Obvious changes in Cx36 and Cx45 immunoreactivity have been noticed in the light-damaged retina, compared with the control tissue (Figure 3-15). Previous studies on rat retina have demonstrated that Cx36 and Cx45 are expressed on AII amacrine cells and ON cone bipolar cells (Veruki & Hartveit, 2009). Cx36 has also been found in alpha retinal ganglion cells in the rat retina (Hidaka *et al.*, 2004). This current study has found that Cx36 is increased at 24 hours following intense light exposure (Figure 3-15B), consistent with previous reports on Cx36 expression levels in dark or light adapted animals (Striedinger *et al.*, 2005; Kihara *et al.*, 2006; Hu *et al.*, 2010). Both transcript and protein of Cx36 are significantly decreased after dark-adaptation in the mouse retina (Kihara *et al.*, 2006). Increased Cx36 protein has been demonstrated to be associated with laser-created retinal lesions, and Cx36-deficient (Cx36$^{-/-}$) mice exhibit a significant increase in cell death after trauma (Striedinger *et al.*, 2005). In our light-damaged animal model Cx45 immunoreactivity was decreased at 24 hours post-exposure (Figure 3-15E). Thus far, to the best of our knowledge, there has not been any report on alterations in Cx45 expression in the light-damaged animal. Findings in the mouse retina following prolonged dark-adaptation are not parallel with our results but have shown that the transcript of Cx45 is significantly decreased in response to dark-adaption (Kihara *et al.*, 2006).

3.4.3   In the light-damaged animal model nitration of phospholipids occurs first in the choroid

Oxidative stress is the damage caused by reactive oxygen species (ROS) or reactive nitrogen species (RNS) in cells or tissues. The retina is a high oxygen consumption tissue and it generates high levels of ROS and NOS through normal cellular metabolism and photochemical reactions. Normally rhodopsin bleaching initiates visual transduction and triggers changes in the RPE. Under normal light conditions, the disks are shed from the distal tips of the outer segments of the photoreceptors and cleared mainly by the RPE. Intense light exposure leads to permanently shed disks and causes an overall decrease in rod length (Organisciak & Vaughan 2010). It also results in large numbers of phagosomes accumulating in the RPE, a process closely associated with the formation of lipofuscin (Ng *et al.*, 2008). Oxidative stress could also induce mitochondrial DNA damage in both human AMD and light-damaged animal models (Barron *et al.*, 2001; Godley *et al.*, 2005). Many studies of human donor tissue have suggested that oxidative stress is the trigger for AMD (Beatty *et al.*, 2000; Olsen *et al.*, 2007; Suzuki *et al.*, 2007; Khandhadia & Lotery, 2010). Pioneer studies have demonstrated that light-damaged animals show extraordinary histological similarity to human AMD (Noell *et al.*, 1966; Marc *et al.*, 2008; Organisciak & Vaughan, 2010) and oxidative stress markers including lipofuscin and nitrotyrosine have been detected in the retina in light-damaged animal models (Fite *et al.*, 1993; Xu *et al.*, 2009). This study employed nitrotyrosine as the oxidative stress marker. Nitrotyrosine is a marker for endogenous nitrosation and nitration, and is mainly associated with oxidised phospholipids (Ohshima *et al.*, 1990; Greenberg *et al.*, 2008). The experimental evidence presented here suggests that oxidative stress induced by nitric oxide, a damaging reactive nitrogen species with cytotoxic and pro-angiogenic properties, in the light-damaged rats affects the retinal endothelial cell (Figure 3-11G). This is comparable to the findings on the aging mouse retina in that nitrotyrosine-immunoreactivity has been shown to be remarkably increased along retinal blood vessels (Xu *et al.*, 2009). The results from Western blot and immunohistochemistry have shown that the oxidative stress marker was significantly increased in the choroidal vasculature, macrophages and RPE following the intense light exposure, and it happened much earlier than was detectable along blood vessels in the retina (Figure 3-11). The macrophages in the choroid labelled with Iba-1 also showed intense

123

labelling for nitrotyrosine (Figure 3-11D-F). This results are coincidently matched with findings on choroidal macrophages in human AMD-affected tissue (Cherepanoff *et al.*, 2010). The study has demonstrated that macrophages in AMD patients, but not in the control subjects, have inducible nitric oxide synthase (iNOS), which is a major enzyme converting L-arginine to nitric oxide (Cherepanoff *et al.*, 2010). Studies on lipid peroxidation have suggested that endoplasmic reticulum stress is an important and early event, first seen with choroidal and RPE damage which triggers AMD (Libby & Gould, 2010). Research carried out two decades ago demonstrated that photosensitive compounds in the blood generate oxidants by intense light, which leads to damage to the choriocapillaris. An antioxidant enzyme, glutathione peroxidase was also detected in the choroid (Rao *et al.*, 1988; Gottsch *et al.*, 1990). A more recent study has established that light-induced DNA oxidation occurs in mouse choroidal endothelial cells (Wu *et al.*, 2005). Comparable with these previous findings, results from this study suggest that lipid nitration is occurring in the choroid well before it can be detected in the retina.

3.4.4   Oxidative stress may contribute to the activation of inflammatory responses with microglia playing a key role

Double immuno-labelling of nitrotyrosine and Iba-1 in the choroid confirmed that lipid peroxidation was detectable in the macrophages following intense light exposure. Nitrotyrosine immunoreactivity has shown that free radical production and lipid peroxidation as an end product of NO production are present in the choroid. Co-localisation of nitrotyrosine and the inflammatory cell marker, Iba-1 in the light-damaged choroid (Figure 3-11D-F) indicates a close association between oxidative stress and inflammatory responses. The lipid whisker model suggests that oxidised phospholipids from senescent and apoptotic cells can be recognised by receptors on macrophages and are then cleared up by the innate immune system (Greenberg *et al.*, 2008). In this study, nitrotyrosine immunoreactivity detected in the Iba-1 immuno-labelled cells has provided a good indication of where the oxidised phospholipids end up. These findings suggest that oxidative stress is a preamble for the inflammatory responses that follow.

124

The inflammatory response is directly associated with degenerating cells in the light damage model (Rutar *et al.*, 2011a). The result here has shown that microglial cells are present in the outer nuclear layer immediately following intense light exposure. Accumulating evidence has shown that perivascular and subretinal microglia may play an important role in age-related retinal disease. The accumulated microglia secrete cytokines, such as vascular endothelial growth factor (VEGF), which can promote angiogenesis in the choroid in AMD (Penfold *et al.*, 2001). The number of Iba-1 immuno-labelled microglia is significantly increased in the aging mouse RPE-choroid comparing to young animals (Xu *et al.*, 2008b). The cell counts throughout the retina at 0 and 6 hours following light damage in the current study (Figure 3-7G-I) indicate that these responding microglial cells in the outer nuclear layer are very likely recruited from the inner layers of the retina. The elevation in the total number of microglia counts in the retina though (Figure 3-7G-I) suggests recruitment of monocytes/macrophages across the blood-retina barrier (Xu *et al.*, 2007), and possibly across damaged RPE basal membrane from the choroid (Rutar *et al.*, 2010). Interestingly, this study showed that activated microglial cells induced by the light damage lose the CD45 marker (Figure 3-9). An earlier study has shown that most microglial cells expressing CD45 also express Iba-1 in the normal mouse retina (Gregerson & Yang, 2003). *In vitro* study has found that cultured retinal CD45-positive cells are not actively involved in the antigen-presenting activity (Gregerson *et al.*, 2004). In a more recent study Xu et al (2009) report decreased CD45 expression in a significantly great number of microglia in the aged mouse retina compared to the young, in parallel with the increased number of those cells strongly expressing Iba-1 that they had reported earlier (Xu *et al.*, 2008b). These results are consistent with those in this thesis in the light-damaged albino rat model. Taken together, all these findings suggest that the reduction in expression of CD45 may a very good indicator of microglial activation.

3.4.5 Alterations in Cx43 expression is associated with oxidative stress and inflammation in light-damaged tissue

This study has demonstrated that Cx43 protein expression is increased in the choroid and RPE following light damage but little change has been detected in the retina (Figure 3-12). This finding is paralleled with many studies on animal models for central nervous system injuries (Hossain *et al.*, 1994; Lee *et al.*, 2005; Ohsumi *et al.*, 2006; Haupt *et al.*, 2007). Abnormal expression of Cx43 has been found associated with many human health conditions and in many animal models for ocular diseases. The immunoreactivity of Cx43 is up-regulated in human glaucomatous retina compared to normal retinal tissue. Increased Cx43 expression is mainly seen in the astrocytes located in the retinal ganglion cell layer of peripapillary and mid-peripheral regions. In the peripapillary region, up-regulated Cx43 is also expressed along glial fibrillary acidic protein (GFAP)-labelled Müller cell processes throughout the entire retina. Retinal endothelial cells retain the same expression level of Cx43 in the glaucomatous retina as the controls (Kerr *et al.*, 2011). Elevated Cx43 expression was also detected in the rat retina, paralleled with changes in GFAP immunoreactivity and ganglion cell loss following optic nerve injury (Chew *et al.*, 2011). It is interesting, therefore, to compare the changes seen in Cx43 following light damage in the albino rat model which appeared to be restricted primarily to the choroid and RPE.

This study has found that the up-regulated expression of Cx43 was on CD45-positive macrophages in the choroid and the retina following the light damage (Figure 3-17). In the choroid, the expression of Cx43 was also detected on the nitrotyrosine immune-labelled macrophages post-exposure (Figure 3-18). This finding is parallel with many *in vitro* studies. It has been shown that up-regulated Cx43 protein is detected in primary culture of microglia after treatment with bacterial lipopolysaccharide (LPS) plus interferon-γ (INF-γ) or tumour necrosis factor-α (TNF-α) plus INF-γ (Eugenín *et al.*, 2001). Monocytes/macrophages only express Cx43 after being stimulated by exposure to interferon-gamma (IFN-γ) and tumour necrosis factor-α (TNF-α) but not under physiological conditions (Eugenín *et al.*, 2003). A more recent study has demonstrated that expression of Cx43 by activated phagocytes is critical for the regulation of phagocytosis and rearrangement of the F-actin cytoskeleton (Anand *et al.*, 2008). Cx43 has also been found to

be expressed on many other residential and circulating leukocytes, including neutrophils, dendritic cells and lymphocytes (Pfenniger *et al.*, 2013). However, so far, relatively little has been reported on Cx43 expression by inflammatory cells in tissue from *in vivo* investigation. Results from this study suggests that Cx43 is only expressed on activated macrophages in the choroid following the intense light exposure, which may be critical for the role of these inflammatory cells. Tuning down the function of Cx43 may result in down-regulation of the inflammatory response in the tissue after the light damage as is seen after down regulation of Cx43 in skin and spinal cord wounds (Qiu *et al.*, 2003; Coutinho *et al.*, 2005; Cronin *et al.*, 2008).

In summary, the present study has revealed retinal function changes in the light-damaged albino rat model at various recovery time-points following the injury. The results have demonstrated that oxidative stress starts primarily in the choroid immediately post-exposure. The oxidative stress is closely associated with inflammatory responses, which may lead to further tissue damage. Activated inflammatory cells and the injured tissue following the light damage show increased Cx43 expression which was closely associated with oxidative and inflammatory damage processes. Findings from this study contribute to a better understanding of the injury process occurring in the light-damaged albino rat model, which provides valuable information on pathogenesis mechanisms of human AMD condition. This study also suggests that manipulating the function of gap junction channels, particularly Cx43 channels, has potential to reduce visual deficits in early AMD.

Chapter 4: Connexin43 mimetic peptide improves retinal function in the light-damaged animal model of age-related macular degeneration

4.1 Introduction

Connexin43 (Cx43) is the most ubiquitously expressed gap junction protein in mammalian embryos and adults (Reaume *et al.*, 1995; Laird, 2006). Gap junction proteins form conduits for intercellular communication, which allows rapid exchange of nutrients, metabolites, ions, and small molecules up to 1 kDa between cells. One complete intercellular channel is formed by two hemichannels located on the membrane of each adjacent cell (Goodenough *et al.*, 1996; Evans & Martin, 2002). In general, the non-junctional hemichannels remain closed under physiological conditions. However, cells may respond to metabolic inhibition, such as hypoxia and ischemia, by opening of the hemichannels, which leads to cytomembrane depolarisation and secondary messenger leakage from the intracellular stores into the extracellular space, such as Ca^{2+} and ATP (Contreras *et al.*, 2002; Goodenough & Paul, 2003). Many *in vitro* studies have demonstrated that raised function of Cx43 hemichannels is associated with cell injury and cell death of astrocytes and endothelial cells (Contreras *et al.*, 2002; Vergara *et al.*, 2003; Faigle *et al.*, 2008). Cx43 is found in astrocytes and in the endothelium in the central nervous system (CNS) (O'Carroll *et al.*, 2008; Davidson *et al.*, 2012a), in the retinal pigment epithelium (RPE), endothelium of the blood vessels, astrocytes, and Müller cells (Janssen-Bienhold *et al.*, 1998; Theis *et al.*, 2001; Zahs *et al.*, 2003; Kerr *et al.*, 2011). Amacrine cells from the zebrafish retina likewise express Cx43, indicating Cx43 may also be expressed in neurons (Janssen-Bienhold *et al.*, 1998). Increased Cx43 protein and/or transcript is associated with many human CNS injuries and diseases, including stroke, epilepsy and Huntington's disease (Elisevich *et al.*, 1997; Vis *et al.*, 1998; Nakase *et al.*, 2006). Relevant to retinal disease or injuries, Cx43 has been shown to be up-regulated in glaucoma (Kerr *et al.*, 2011; Danesh-Meyer *et al.*, 2012) and following optic nerve injury (Chew *et al.*, 2011). These findings suggest that down-regulating Cx43, and especially blocking Cx43 hemichannels may provide protection to the tissue following injuries.

Connexin mimetic peptides are short synthetic amino acid peptides designed to match sequences in the two extracellular loops of connexins (Evans & Boitano, 2001). Cx43 mimetic peptides regulate cellular plasma membrane permeability by blocking hemichannels

(Retamal *et al.*, 2007; O'Carroll *et al.*, 2008). Peptide5, the Cx43 mimetic peptide used in this study, has demonstrated neuroprotective effects in both *in vitro* and *in vivo* studies. Applying peptide5 to the culture medium has significantly reduced tissue damage following spinal cord injury in organotypic culture (O'Carroll *et al.*, 2008). Local administration of peptide5 via an external pump significantly improved electroencephalographic power and brain function in a model of sheep fetal global cerebral ischemia induced by bilateral carotid artery occlusion, although the neuron survival has not significantly improved (Davidson *et al.*, 2012a). Another study has shown that peptide5 delivered systematically has neuroprotective effects for retinal ganglion cells in a rat model of retinal ischemia-reperfusion (Danesh-Meyer *et al.*, 2012).

The current study aims to assess whether blocking Cx43 hemichannels with a mimetic peptide through intravitreal injection improves retinal function in the light-damaged albino rat. Based upon the results presented in Chapter 3, it is known that retinal function dramatically drops in the light-damaged rat and there is up-regulation of Cx43 associated with inflammation and oxidative stress occurring mostly in the RPE/choroid. We hypothesised that applying a Cx43 specific mimetic peptide, peptide5, would lead to down-regulation of the inflammatory response in the RPE/choroid reducing the extent of damage and promoting recovery of retinal function following light damage. The penetration of fluorescein isothiocyanate (FITC)-conjugated peptide5 into the retina and choroid following intravitreal injection was checked to ensure that the mimetic peptide reached the targeted RPE/choroid area. Electroretinogram (ERG) was used for assessing the retinal function.

Microglia/macrophage-mediated inflammatory responses were investigated in the tissue collected after the ERG test. This study has shown that intravitreal injection is an efficient means for local delivery of peptide5 into the retina, RPE and the choroid. Blocking Cx43 hemichannels using this specific Cx43 mimetic peptide significantly improved retinal function and decreased the inflammatory response in the choroid.

4.2 Methods

4.2.1 Animal handling

The experimental protocol involved exposing animals to intense light followed by injections with Cx43 mimetic peptide or sham (saline), and variable periods of recovery. Briefly, animals were exposed to intense light for 24 hours and were anaesthetised before delivering the mimetic peptide.

Intravitreal injections were used as described in Section 2.1.3, Chapter 2. For the group that was injected during the light exposure period, animals were returned to light exposure after the intravitreal injection. For other groups, animals were returned to dark-adaption for electroretinogram (ERG) or housing conditions after recovery from anaesthesia (Figure 4-1). For each individual rat, both eyes were either injected with peptide5 or injected with sham (saline). The number of animals used in this study is listed in Table 4-1.

Single dose treatment in the light-damaged rats

Double dose treatment in the light-damaged rats
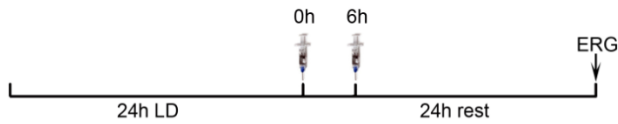
Strategy A:

Strategy B:

Strategy C:
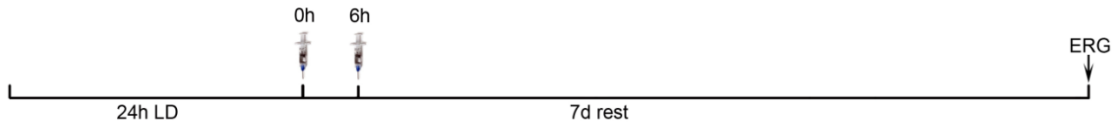
Strategy D:
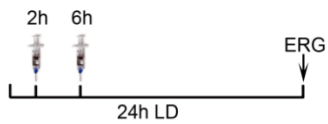
Figure 4-1. Experimental groups of the light-damaged rats with intravitreal treatment. In all treatment groups, half of the animals received intravitreal injection with mimetic peptide (final concentration 20 µM) and the other half received sham (saline) as a control. The syringes indicate time points at which injections were given, and ERG↓ indicates time points at which ERGs were recorded.

Table 4-1. Animal numbers used in the intervention experiments with either peptide5- or sham-treatment.

	1 injection post-LD, 24h rest	2 injections post-LD, 24h rest (Strategy A)	2 injections during LD, 24h rest (Strategy B)	2 injections post-LD, 7d rest (Strategy C)	2 injections during LD, 0h rest (Strategy D)
Peptide5	n=6	n=8	n=5	n=4	n=4
Sham	n=6	n=6	n=5	n=4	n=4

4.2.2   Cx43 mimetic peptide preparation

Peptide5, the Cx43 mimetic peptide used in this study was designed against the end amino acids of extracellular loop 2 of the Cx43 protein and has demonstrated its neuro-protective effect in several organotypic culture and animal models (O'Carroll *et al.*, 2008; Danesh-Meyer *et al.*, 2012; Davidson *et al.*, 2012a). The detailed information and preparation of peptide5 have been described in Section 2.1.2, Chapter 2. The sham control animals were injected with saline.

4.2.3   Electroretinogram (ERG) recording and data analysis

The procedure was adapted from that used in a previous study (Vessey *et al.*, 2011). The animals were dark-adapted overnight for 12-14 hours before the electroretinogram (ERG) recording, apart from two groups which were treated with peptide5 or sham treated during light damage with 0 hour recovery (Strategy C in Figure 4-1).

4.2.4   Immunohistochemistry

The procedure was conducted as described in Section 2.4, Chapter 2. Briefly, after hydration, sections were blocked with a solution containing normal goat serum or donkey serum (Invitrogen, USA), 1% bovine serum albumin (BSA) and 0.5% triton X-100 in 0.1 M PBS for 1 hour at room temperature. The tissues were immuno-labelled with primary antibodies, including rabbit anti-Cx43, guinea pig anti-Cx40, rabbit anti-Cx36, mouse anti-Cx45, mouse anti-CD45, mouse anti-GFAP and goat anti-Iba1 antibodies. The primary antibody details are given in Table 2-1, Chapter 2. Tissue sections were incubated with the primary antibody overnight at room temperature. The secondary antibody, goat anti-rabbit, goat anti-mouse, sheep anti-guinea pig, or donkey anti-goat antibody was diluted 1:500 and

was applied for 2 hours in the dark at room temperature. Slides were rinsed several times in 0.1 M PBS, mounted in non-fluorescence fading medium and sealed.

4.2.5 Imaging

All the images were acquired from immuno-labelled sections using a high-resolution laser scanning confocal microscope (Olympus FluoView FV1000, Japan) with 488 nm and/or 594 nm excitation from an argon ion laser. A series of 4-8 optical sections with 1 µm intervals were collected for each specimen and image analysis was performed on a stack image of intensity projection over the z-axis. Six retinas obtained from different animals were analysed for each group, and the representative images shown.

4.2.6 Statistical analysis

Graphing and statistical analyses were performed using GraphPad Prism 6 (GraphPad Software, USA). All data was presented as the mean $\pm$ standard error of the mean (SEM). The comparison of the effects of stimulus intensity and recovery from the ERG data was performed using a two-way ANOVA followed by a Bonferroni post-hoc test.   The comparison of recovery from the light-exposure at the intensity of 2.1 log cd.s/m^2 was conducted by using an unpaired Student's t-test with a Welch's correction.

4.3   Results

4.3.1   Permeability of Cx43 mimetic peptide following intravitreal injection

To ensure that peptide5, the Cx43 mimetic peptide, was able to reach the targeted tissue by intravitreal injection, the permeability of the peptide was investigated. Both the usual working concentration (280 µM) for the light-damaged animal treatment and a ten times (10x) higher concentration (2.8 mM) were tested for increased imaging sensitivity. At the working concentration, the permeability of peptide5 was assessed in both normal non-light-damaged animals and animals which had been exposed to 24 hours intense light. It was found that the mimetic peptide penetrated readily through the retina, RPE and choroid within 30 minutes of the intravitreal injection at both 10x higher concentration (Figure 4-2) and normal working concentration (Figure 4-3). However, the higher concentration (2.8 mM) showed a wider spread of the peptide in the retina and the choroid and was co-localised with most cell types (Figure 4-2). The working concentration (280 µM) showed a much more specific localisation of the mimetic peptide to the retinal vessels, RPE and choroidal vessels (Figure 4-3 and Figure 4-4). Interestingly, the peptide showed higher affinity to the retinal vessels and RPE in the light-damaged ocular tissue compared to the control in both flat-mount tissue images and cross-sectioned tissue images (Figure 4-3A-D and Figure 4-4). Little difference in the fluorescence intensity was observed in the blood vessels in the choroid between the control and the light-damaged tissue (Figure 4-3E&F and Figure 4-4). Nevertheless, peptide5 showed high penetration through the retina and into the choroid, with some evidence for specificity targeting endothelial cells at the working concentration of 280 µM.
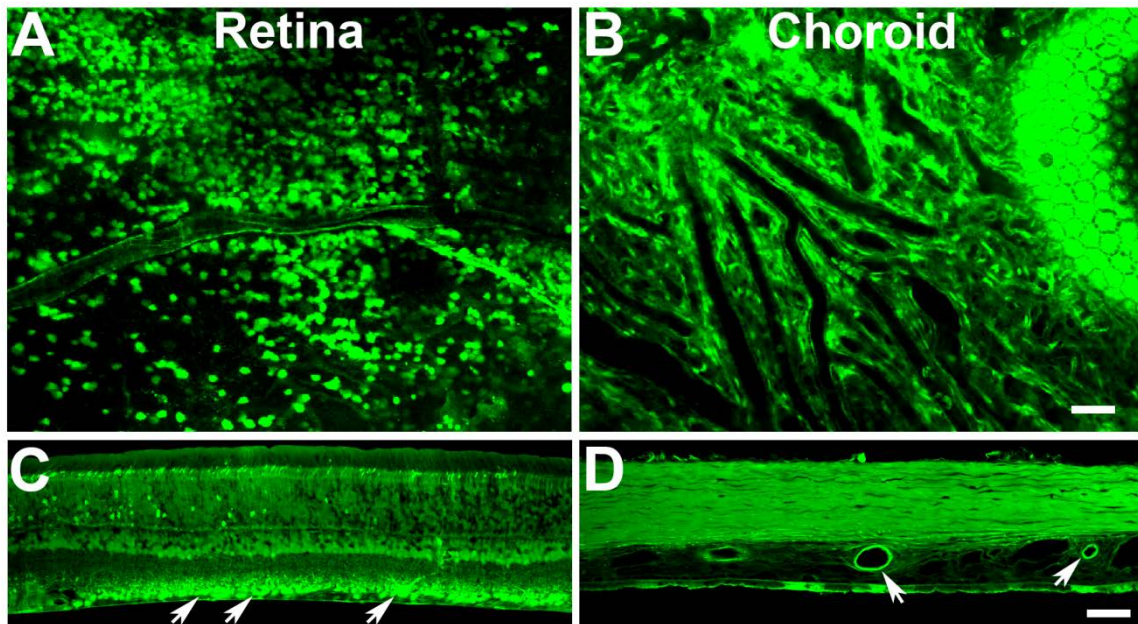
Figure 4-2. Permeability of FITC-conjugated peptide5 at 10x higher concentration following intravitreal injection. FITC-conjugated peptide5 at 10x higher than normal working concentration (2.8 mM) was injected into the vitreous immediately after 24 hours intense light exposure. The final intraocular concentration was 200 µM. Tissues were collected 30 minutes post-injection. **A:** Peptide5 localised in many cells and the retinal blood vessels in the retina flat-mount tissue. **B:** Peptide5 had a wide-spread distribution in the choroid in the choroid flat-mount tissue. **C:** Peptide5 was present in layers of the retina with the highest concentration in the ganglion cell layer (arrows) in a retinal cross section. **D:** Peptide5 penetrated through the retina and RPE, and reached the choroid and sclera with high affinity to the endothelial cells of the choroidal blood vessels (arrows). Scale bars = 50 µm.
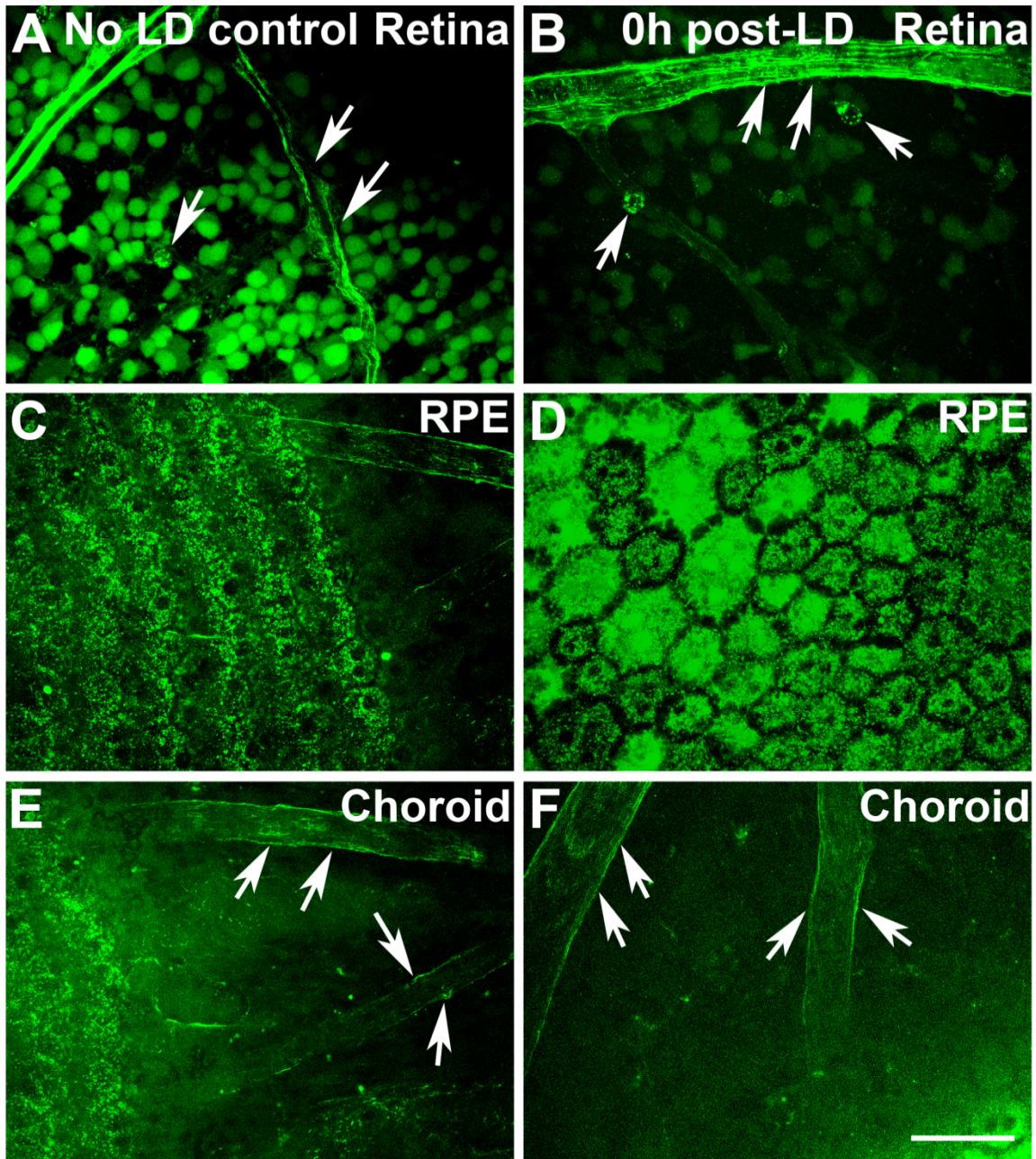
Figure 4-3. Flat-mount tissues showing permeability of FITC-conjugated peptide5 at the working concentration following intravitreal injection. A&B: Peptide5 injected at working concentration (280 µM) distributed in the normal (**A**) and light-damaged retina (**B**). The final intraocular concentration was 20 µM. The blood vessels showed the most intense fluorescence (arrows). **C&D:** The mimetic peptide showed higher affinity to the RPE in the light-damaged tissue (**D**) than the control (**C**). **E&F:** Peptide5 was able to reach the choroid following the intravitreal injection where it mainly localised to the blood vessels (arrows). Scale bar = 50 µm.

137
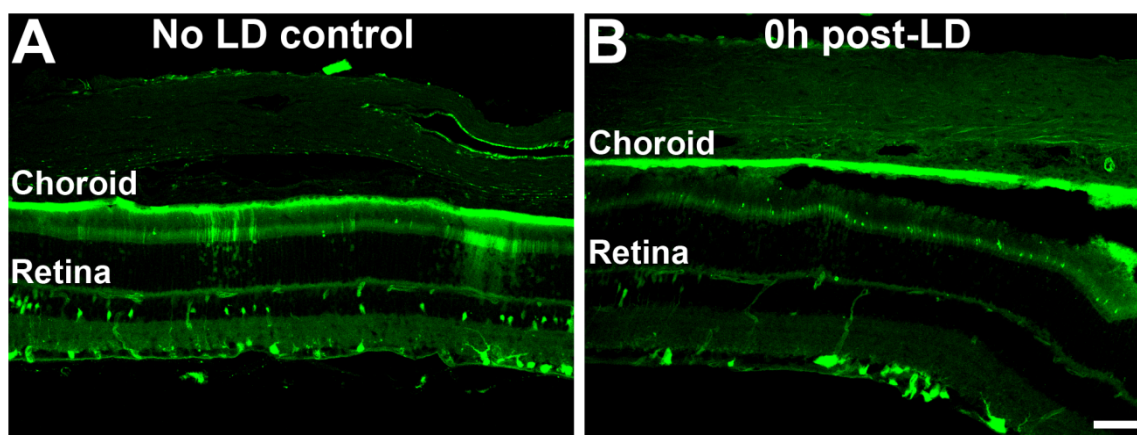
Figure 4-4. Cross sections showing permeability of FITC-conjugated peptide5 at the working concentration following intravitreal injection. The cross sections showed peptide5 injected at working concentration (280 µM) penetrated readily through the retina, RPE and into the choroid and the sclera in both control (**A**) and light-damaged rat tissue (**B**).

4.3.2 A single Cx43 mimetic peptide treatment non-significantly improved retinal function in the light-damaged rats

The electroretinogram (ERG) was used to investigate the effect of the Cx43 mimetic peptide (peptide5) on retinal functions in the light-damaged albino rat model. The first experiment consisted of testing the effect of a single dose of peptide5. Representative waveforms showed improvements in peptide5-treated rats compared to sham-treated animals (Figure 4-5). There were non-significant improvements for the amplitudes of mixed a- and b-waveforms (Figure 4-6A&C). The implicit time showed very similar results in peptide5- and sham-treated animals (Figure 4-6B&D).

The twin-flash paradigm used in this study allowed us to isolate rod responses from mixed waveforms by subtraction of cone responses. The rod PIII response showed that rod photoreceptors exhibited a non-significant increase for both amplitude and sensitivity in peptide5-treated rats comparing to the sham-treated animals (Figure 4-7A&B). The peptide5-treated rats also showed a non-significant increase for the rod PII amplitude and a significantly shorter implicit time (Figure 4-7C&D), suggesting a better recovery in peptide5-treated group for rod post-photoreceptor response.

The cone post-photoreceptor response was reflected by the cone PII waveform. There was no significant difference for both amplitude and implicit time between mimetic peptide- and sham-treated animals (Figure 4-8). However, there was a tendency towards increased amplitude and decreased implicit time (Figure 4-8).

The inner retinal function, including functions of ON-pathway neurons and lateral inhibitory circuits of inner retinal neurons were measured after isolation of the OPs (Weymouth & Vingrys, 2008). The summed OP responses showed a significantly increased amplitude in peptide5-treated rats comparing to sham-treated animals ($p < 0.05$, Figure 4-9A). The implicit time was not different between sham- and peptide5-treated groups (Figure 4-9B).
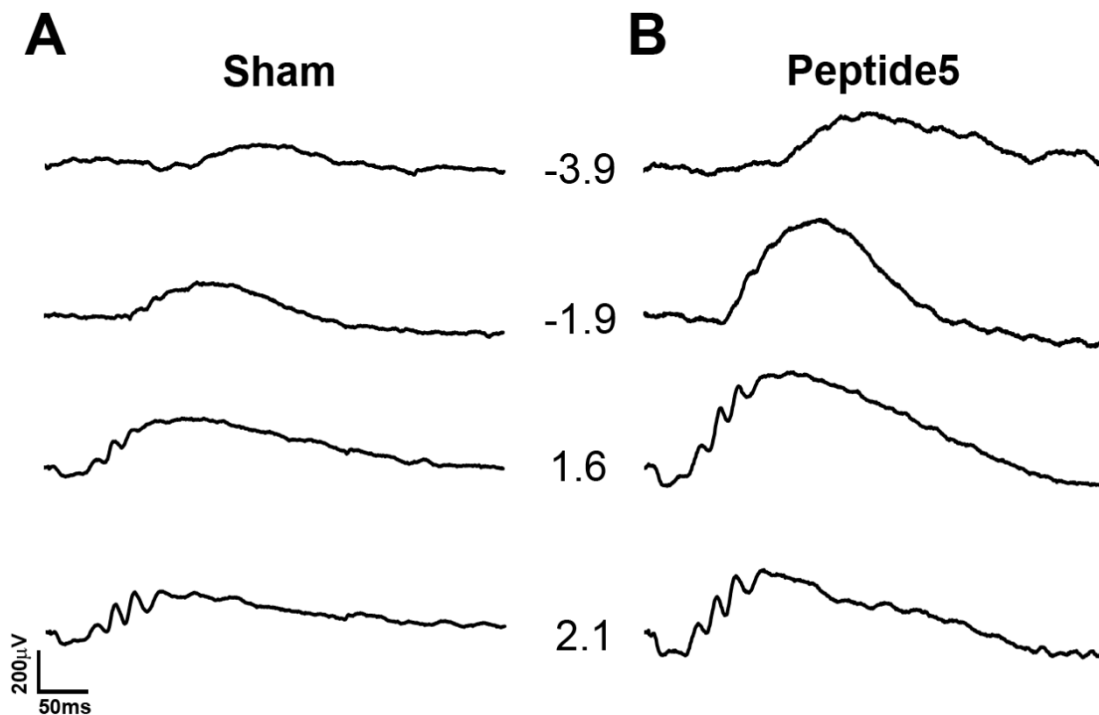
Figure 4-5. Representative mixed ERG waveforms following single dose sham- and peptide5-treated light-damaged rats. Representative mixed ERG waveforms are presented for sham- (**A**) and peptide5-treated rats (**B**) at intensities ranging from -3.9 to 2.1 log cd.s/m^2.
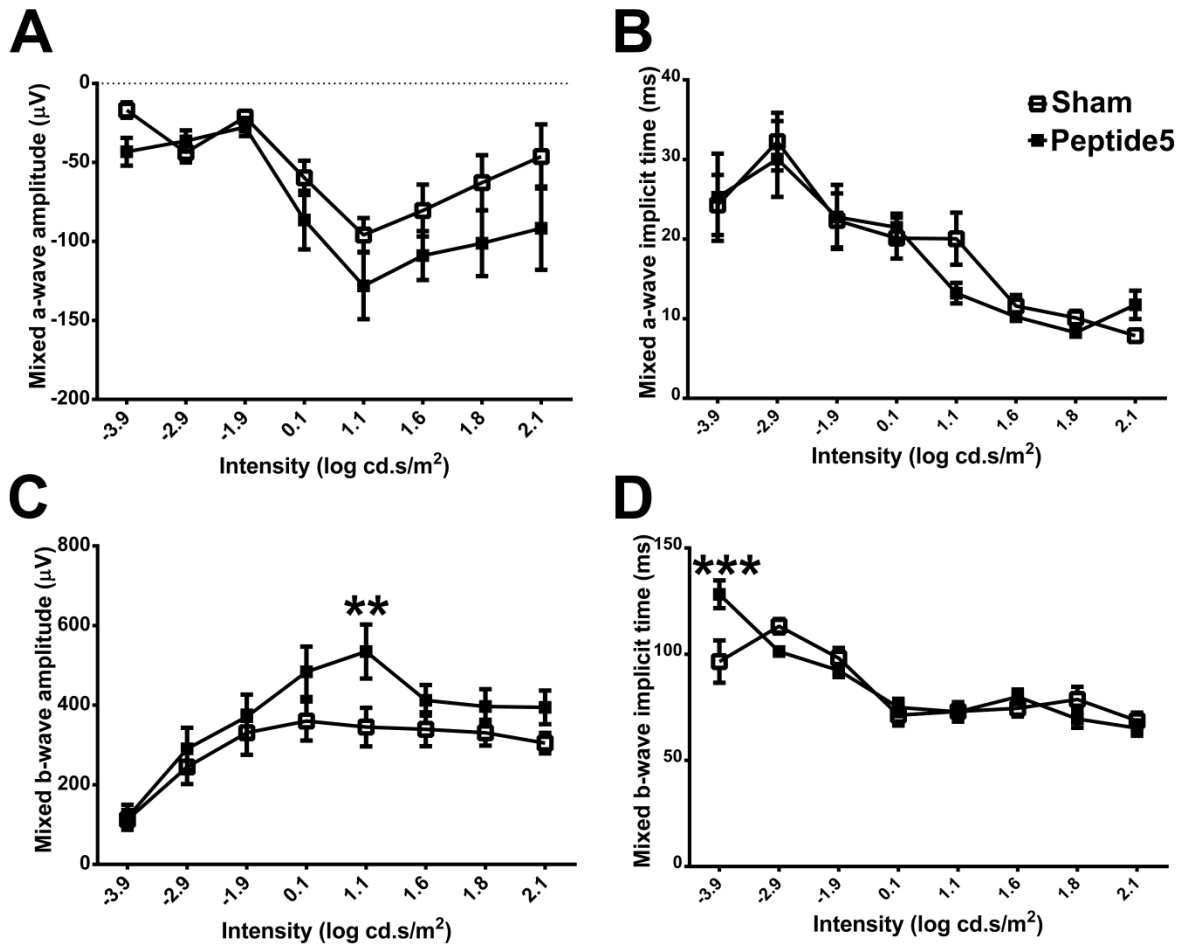
Figure 4-6. The mixed ERG response showed a trend towards improvement in rats treated with a single dose of peptide5 following light damage. **A:** The average amplitude of the a-wave response from the mixed waveforms showed a tendency toward larger amplitude of the photoreceptor derived component in peptide5 treated rats compared with the sham. However, there was no significant difference. **B:** The average a-wave implicit time did not show any difference between mimetic peptide and sham-treated rats. **C:** Peptide5-treated rats also showed a tendency for improvement of mixed b-wave amplitudes. A significant increase showed at the intensity of 1.1 log cd.s/m^2 ($p < 0.01$). **D:** Mixed b-wave implicit times showed no difference between peptide5- and sham-treated rats at all the higher intensities, except at the lowest intensity -3.9 log cd.s/m^2, where the peptide5-treated rats showed a significantly longer implicit time ($p < 0.001$). All average data are expressed as mean ± SEM, n=11 in the sham-treated group and n=12 in the Cx43 mimetic peptide-treated group. Statistical analysis was completed by using a two-way ANOVA and a Bonferroni post-hoc test.
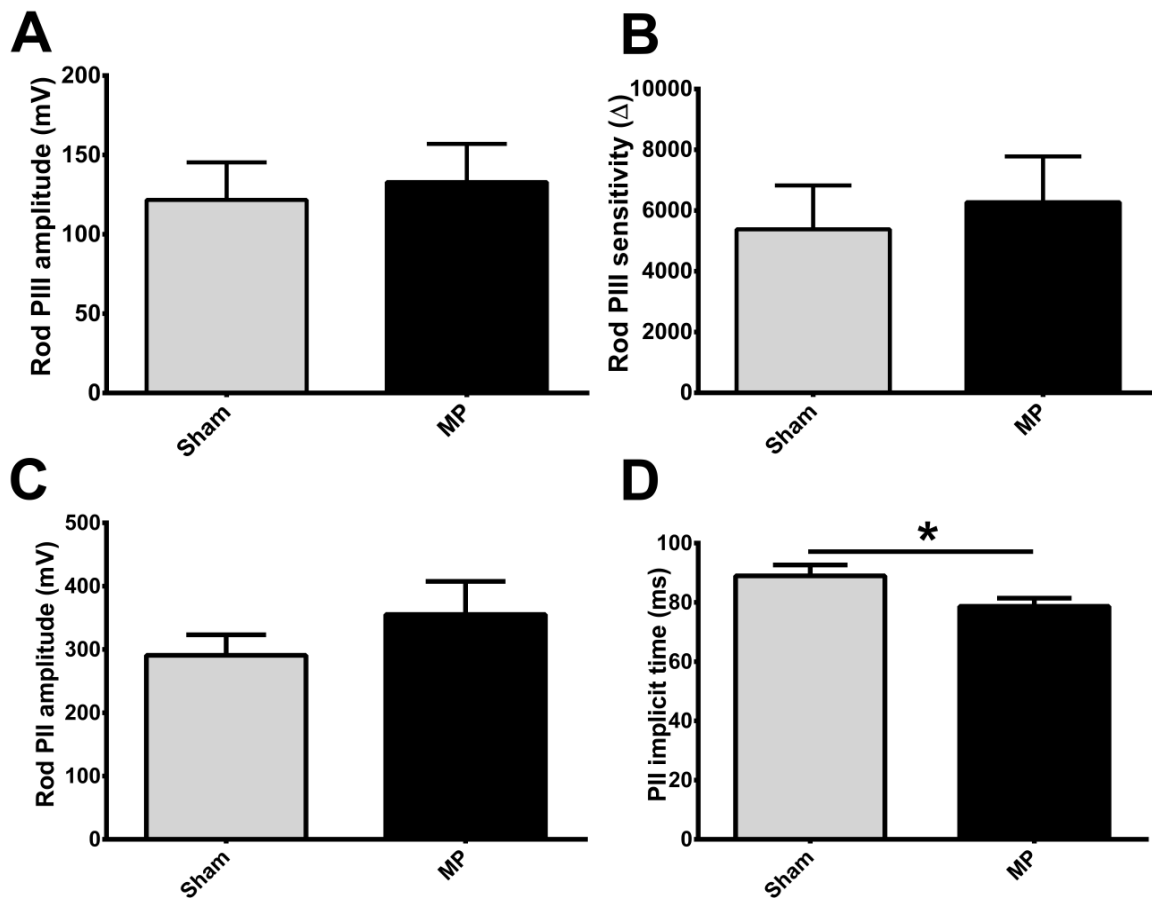
Figure 4-7. A single dose of peptide5-treated rats showed a tendency toward improvement for rod PIII and PII responses. **A:** Rod PIII amplitude showed only a non-significant increase in peptide5-treated rats compared with the sham-treated animals. **B:** Rod PIII sensitivity was also non-significantly higher in the peptide-treated group. **C:** Rod PII showed a trend towards increased amplitude in peptide5-treated rats. **D:** Rod PII implicit time was significantly shorter in the peptide5-treated rats compared with the sham-treated animals, $p < 0.05$. All average data are expressed as mean $\pm$ SEM, n=12 in each group. Statistical analysis was completed by using an unpaired Student's t-test with Welch's correction. Abbreviation: **MP**, Cx43 mimetic peptide.
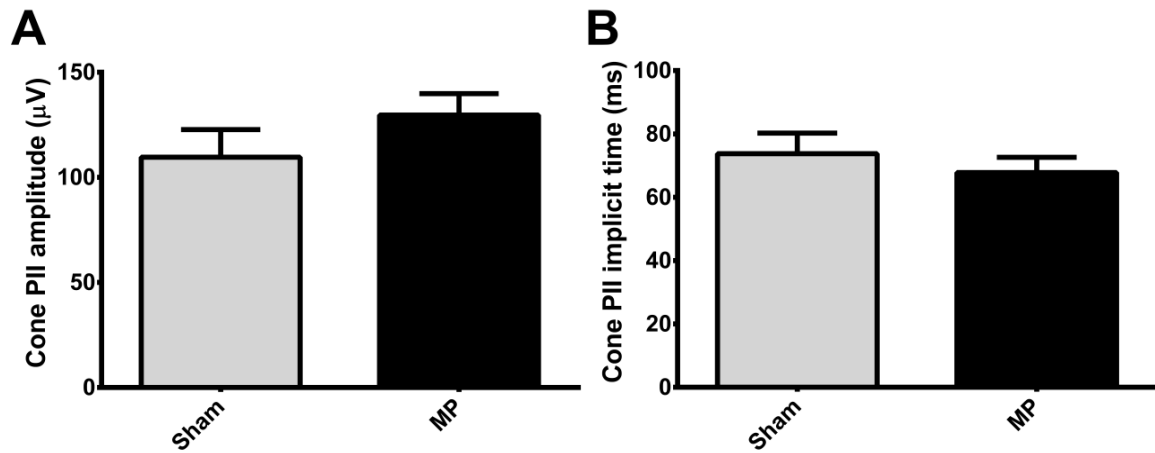
Figure 4-8. The cone PII response showed a non-significant improvement in cone post-photoreceptoral pathway after a single dose of peptide5-treatment. **A:** Cone PII amplitude showed a non-significant increase in peptide5-treated rats. **B:** Peptide5-treated rats showed a non-significantly shorter cone PII implicit time compared to sham-treated animals. All average data are expressed as mean ± SEM, n=12 in each group. Statistical analysis was completed by using an unpaired Student's t-test with a Welch's correction. Abbreviations: **MP**, Cx43 mimetic peptide.
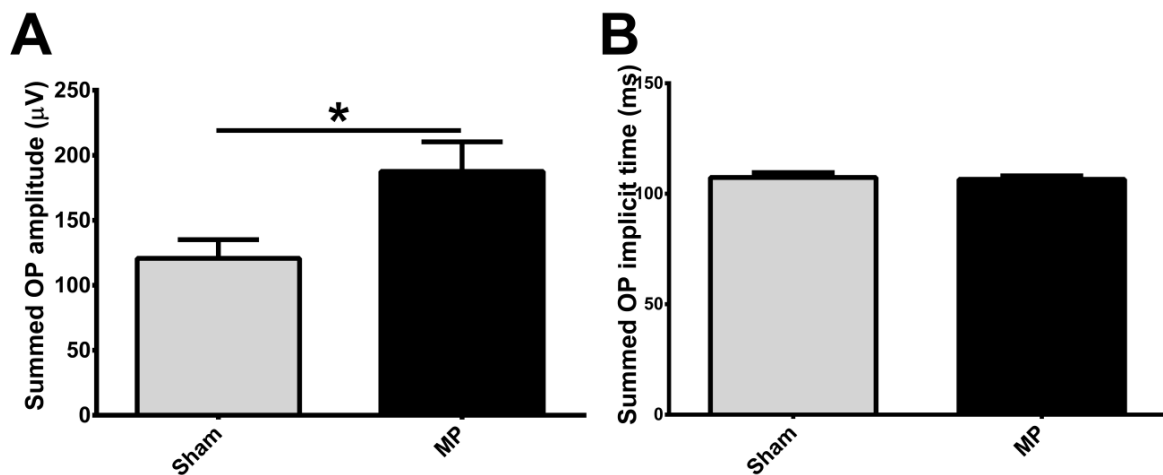
Figure 4-9. A single dose of peptide5-treated rats showed improved summed oscillatory potentials. **A:** The amplitude of summed oscillatory potentials (OPs) was significantly higher in peptide5-treated rats, $p < 0.05$. **B:** Both sham- and peptide5-treated groups showed a similar summed OP implicit time. All average data are expressed as mean ± SEM, n=12 in each group. Statistical analysis was completed by using an unpaired Student's t-test with Welch's correction. Abbreviation: **MP**, Cx43 mimetic peptide.

142

4.3.3 A double dose of Cx43 mimetic peptide significantly improved the mixed a- and b-wave responses in light-damaged rats

To investigate a more sustained dosage effect of Cx43 mimetic peptide (peptide5) on the light-damaged albino rat, two intravitreal injections were applied to the animals with four different strategies (Figure 4-1). Results here compare the retinal function of rats using ERG. Comparison of the mixed waveforms is described first, followed by an explanation of isolated rod and cone responses for each treatment strategy in the following section.

Strategy A consisted of two treatments at 0 and 6 hours after a 24-hour period of intense light exposure (Figure 4-1). Recordings were conducted 24 hours after the offset of light exposure. Representative waveforms from sham- and peptide5-treated groups are presented (Figure 4-10). The amplitude of mixed a-wave showed a general increase in mimetic peptide-treated rats compared to sham-treated animals over intensities from 0.1 to 1.8 log cd.s/m^2, with a significant increase at 1.1 log cd.s/m^2 ($p < 0.01$; Figure 4-11A). Similar implicit times of mixed a-wave were seen for sham- and peptide-treated groups except for an unusual drop at -2.9 log cd.s/m^2 in the control group ($p < 0.0001$; Figure 4-11B). The mixed b-wave, which reflects the inner retina function, showed similar amplitude and implicit time in sham and peptide5-treated groups (Figure 4-11C&D).

Rats treated in Strategy B showed the most obvious improvements out of all the strategies for mixed a-wave and b-wave in peptide5-treated groups compared with sham-treated groups (Figure 4-12). Peptide5 was delivered during light exposure and at the beginning of the recovery period; ERG tests were conducted 24 hours after light damage. The amplitude of mixed a-wave in peptide5-treated rats showed similar responses at the lower stimulus intensities (-3.9 to -1.9 log cd.s/m^2) but a significant increase at all the high intensity responses above 0.1 log cd.s/m^2 compared to the sham-treated group ($p < 0.05$; Figure 4-12A). The peptide5- and sham-treated animals showed similar implicit time for mixed a-waves (Figure 4-12B). In the group treated with peptide5, the amplitude of mixed b-wave was significantly higher than for the sham-treated group at the intensities higher than 0.1 log cd.s/m^2 ($p < 0.01$), although not at the highest intensity (2.1 log cd.s/m^2)

143

(Figure 4-12C). The implicit time of mixed b-waves appeared to have similar results for peptide5- and sham-treated animals throughout all stimulus intensities (Figure 4-12D).

Under Strategy C, rats were treated with two doses of peptide5 or sham after light damage and ERG recordings were conducted 7 days after offset of light exposure (Figure 4-1). The peptide5-treated group showed in general increased amplitudes of a-wave and b-wave responses from the mixed waveforms. However, none of these showed any statistical significance at any of the stimulus intensities (Figure 4-13A&C). The implicit time of a-wave responses was significantly lower in the peptide5-treated group at the intensity of -3.9 and -2.9 log cd.s/m^2 compared to the sham-treated group, but with very similar readings at all the other higher intensities (Figure 4-13B). The implicit time of mixed b-waves appeared similar for peptide5- and sham-treated animals (Figure 4-13D).
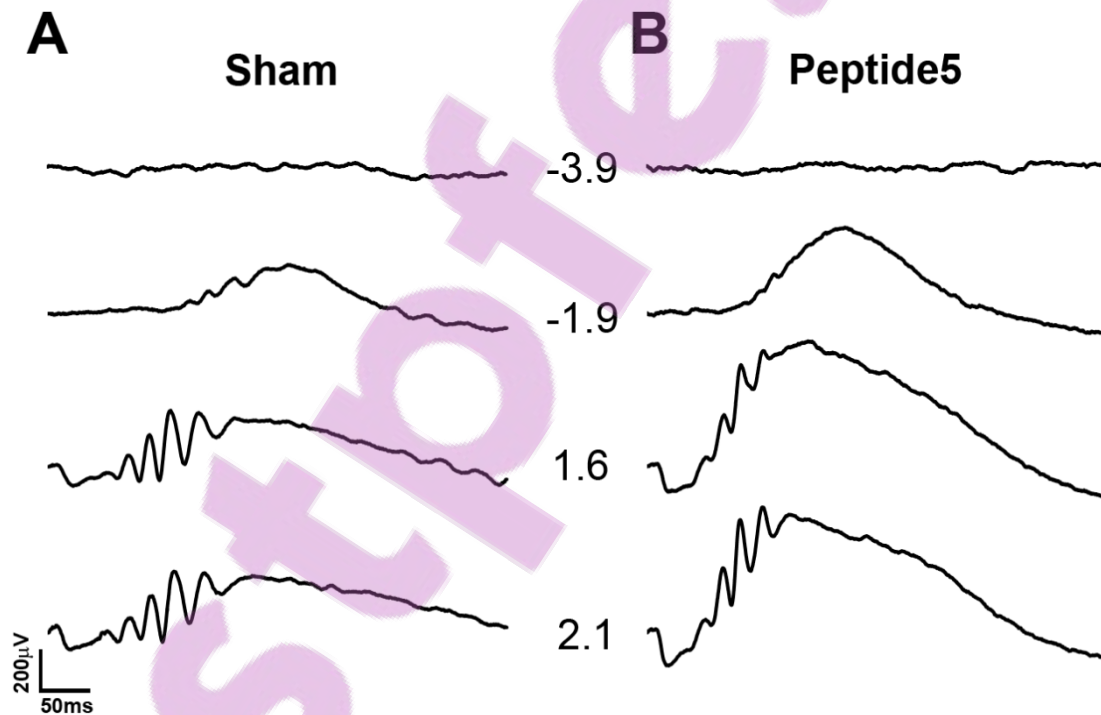
Figure 4-10. Representative mixed ERG waveforms for sham- and peptide5-treated rats after two intravitreal injections following light damage (Strategy A). Representative mixed ERG waveforms are presented for sham- (**A**) and peptide5-treated rats (**B**) at intensities ranging from -3.9 to 2.1 log cd.s/m^2.

144
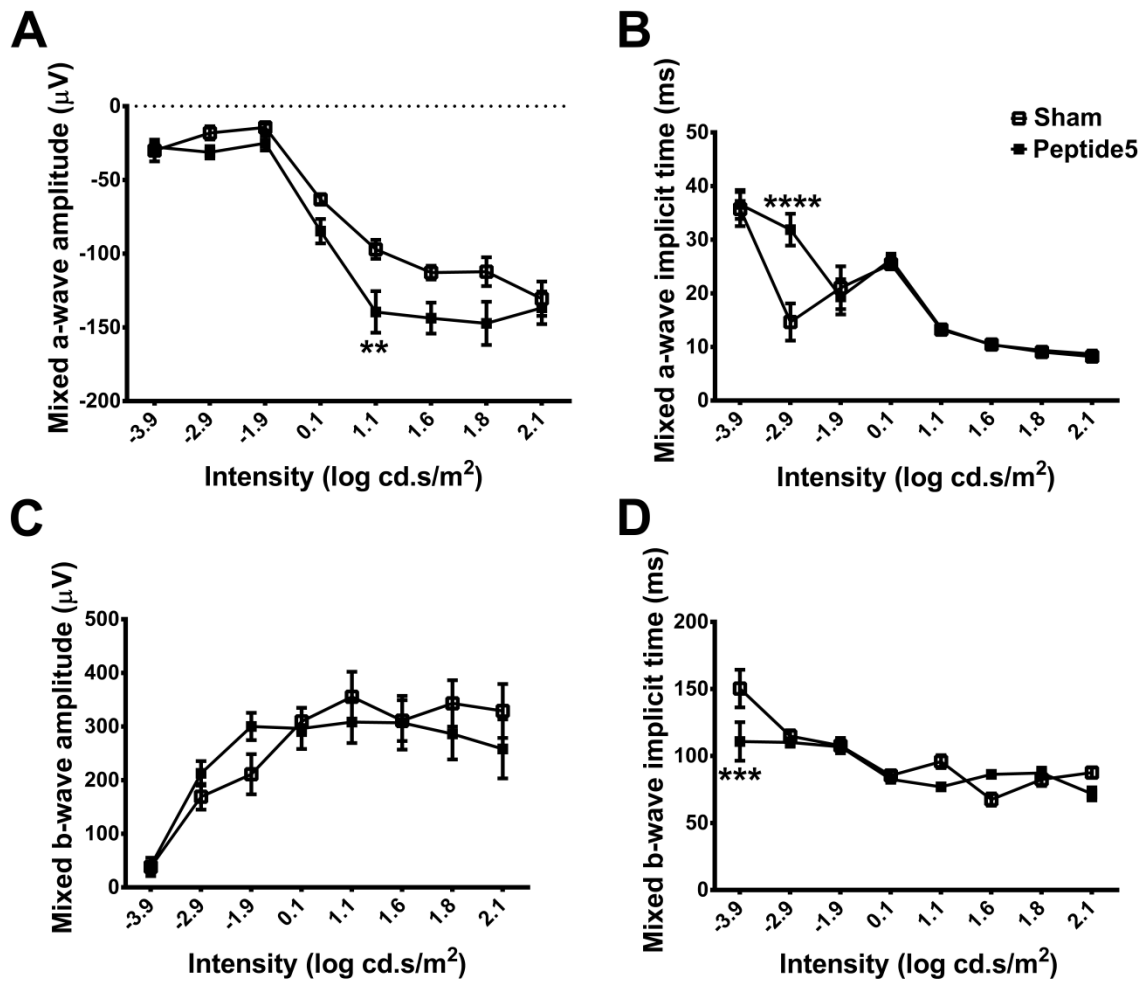
Figure 4-11. The average amplitude and implicit time of mixed a- and b-waves from ERG recordings in rats after two sham- or peptide5-injections (Strategy A). A: The average amplitude of a-wave response from the mixed waveforms was slightly larger in peptide5-treated rats at most intensities ranging from -3.9 to 2.1 log cd.s/m^2. A significant increase showed at intensity of 1.1 log cd.s/m^2 ($p < 0.01$). **B:** The average implicit time of mixed a-wave did not show any difference between sham- and peptide5-treated groups, except at -2.9 log cd.s/m^2 when the peptide5-injected rats had a significantly longer implicit time ($p < 0.0001$). **C:** No difference was apparent for the average amplitude of mixed b-waves between sham- and peptide5-treated groups. **D:** At the intensity of -3.9 log cd.s/m^2, peptide5-treated rats showed significantly shorter implicit time than the sham-treated group ($p < 0.001$). However, there was no difference between the two groups at other higher intensities. All average data are expressed as mean ± SEM, n=11 in sham-treated group, and n=12 in peptide5-treated group. Statistical analysis was completed by using a two-way ANOVA and a Bonferroni post-hoc test.
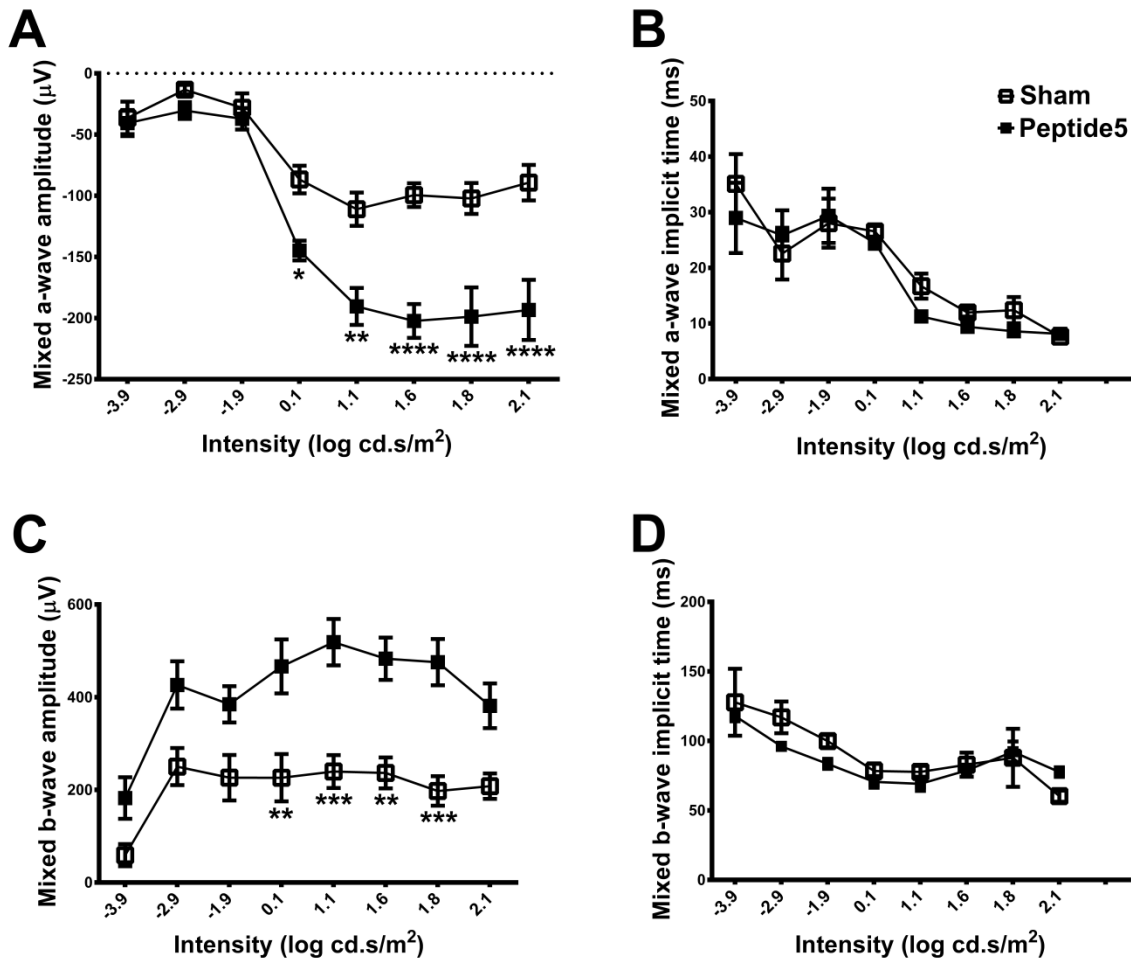
Figure 4-12. The average amplitude and implicit time of mixed a- and b-waves from ERG recordings in rats after two injections of sham- or peptide5 (Strategy B). **A:** The average amplitude of a-wave response from the mixed waveforms was similar at low intensities and significantly larger at higher intensities (over 0.1 log cd.s/m^2) in peptide5-treated rats ($p < 0.05$ at 0.1 log cd.s/m^2; $p < 0.01$ at 1.1 log cd.s/m^2; $p < 0.0001$ at 1.6, 1.8 and 2.1 log cd.s/m^2). **B:** The average implicit time for mixed a-waves did not show only difference between sham- and peptide5-treated groups. **C:** The average amplitude of b-wave response from the mixed waveforms showed a general increase in peptide5-treated animals, with statistical significance shown at 0.1, 1.1, 1.6 and 1.8 log cd.s/m^2 ($p < 0.01$ at 0.1 and 1.6 log cd.s/m^2; $p < 0.001$ at 1.1 and 1.8 log cd.s/m^2). **D:** Similar implicit times of mixed b-waves were apparent for peptide5- and sham-treated groups. All average data are expressed as mean ± SEM, n=6 in sham-treated group, and n=7 in peptide5-treated group. Statistical analysis was completed by using a two-way ANOVA and a Bonferroni post-hoc test.

146
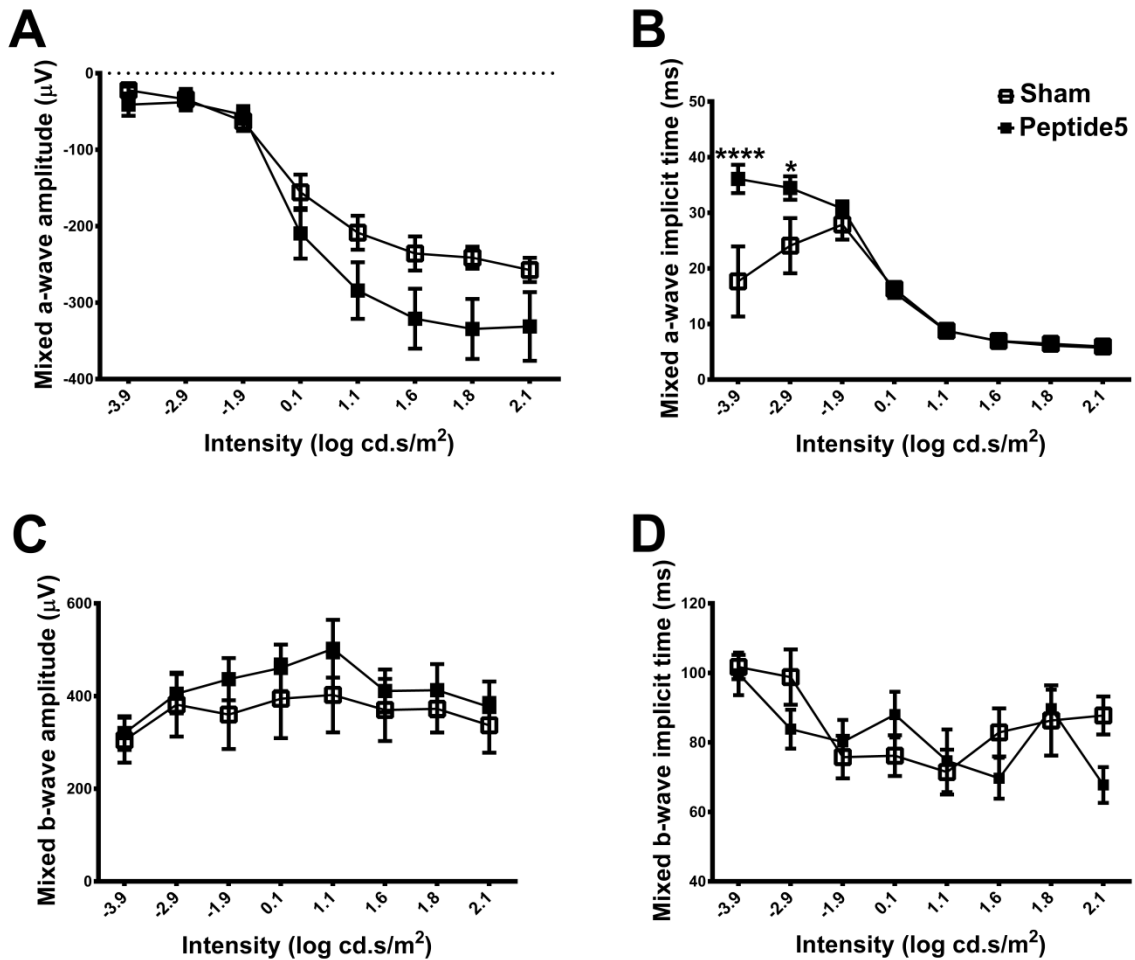
Figure 4-13. The average amplitude and implicit time of mixed a- and b-waves from ERG recordings in rats 7 days following the treatment with a double dose injection (Strategy C). **A:** The average amplitude of a-wave response from the mixed waveforms was slightly larger in peptide5-treated rats at most intensities ranging from -3.9 to 2.1 log cd.s/m^2. **B:** The average implicit time for mixed a-waves did not show any difference between sham- and peptide5-treated groups, except at -3.9 and -2.9 log cd.s/m^2 when the peptide5-injected rats showed a significantly longer implicit time ($p < 0.0001$ at -3.9 log cd.s/m^2 and $p < 0.05$ at -2.9 log cd.s/m^2). **C:** No difference was apparent for the average amplitude of mixed b-waves between sham- and peptide5-treated groups. **D:** There was no difference for the average implicit time of mixed b-waves between sham- and peptide5-treated groups. All average data are expressed as mean ± SEM, n=11 in sham-treated group, and n=12 in peptide5-treated group. Statistical analysis was completed by using a two-way ANOVA and a Bonferroni post-hoc test.

4.3.4 The rod pathway response was significantly improved by a double dose of Cx43 mimetic peptide

For the rats under treatment Strategy A, the isolated rod PIII at the highest flash intensity of 2.1 log cd.s/m^2 showed that rod photoreceptoral activity was improved in peptide5-treated rats compared with sham-treated animals (Figure 4-14A&B). Rod PIII amplitude was significantly increased in the peptide5-treated group ($p < 0.01$; Figure 4-14A). The sensitivity was also increased but a significant difference was not reached (Figure 4-14B). In addition, the rod post-photoreceptoral activity was improved (Figure 4-14C&D). There was a significant increase for rod PII amplitude in peptide5-treated rats compared with sham-treated animals ($p < 0.01$; Figure 4-14C). A slight decrease for rod PII implicit time showed in the peptide-treated group but it was not significant (Figure 4-14D).

Interestingly, cone post-photoreceptor activity showed a significant reduction in the peptide5-treated group compared with the sham-treated group (Figure 4-15). The cone PII amplitude was dramatically decreased ($p < 0.05$; Figure 4-15A), and the implicit time was significantly increased ($p < 0.05$; Figure 4-15B) in the peptide5-treated group. The summed OPs showed non-significantly decreased amplitude and a very similar implicit time in peptide5-treated rats compared with sham-treated animals (Figure 4-16).
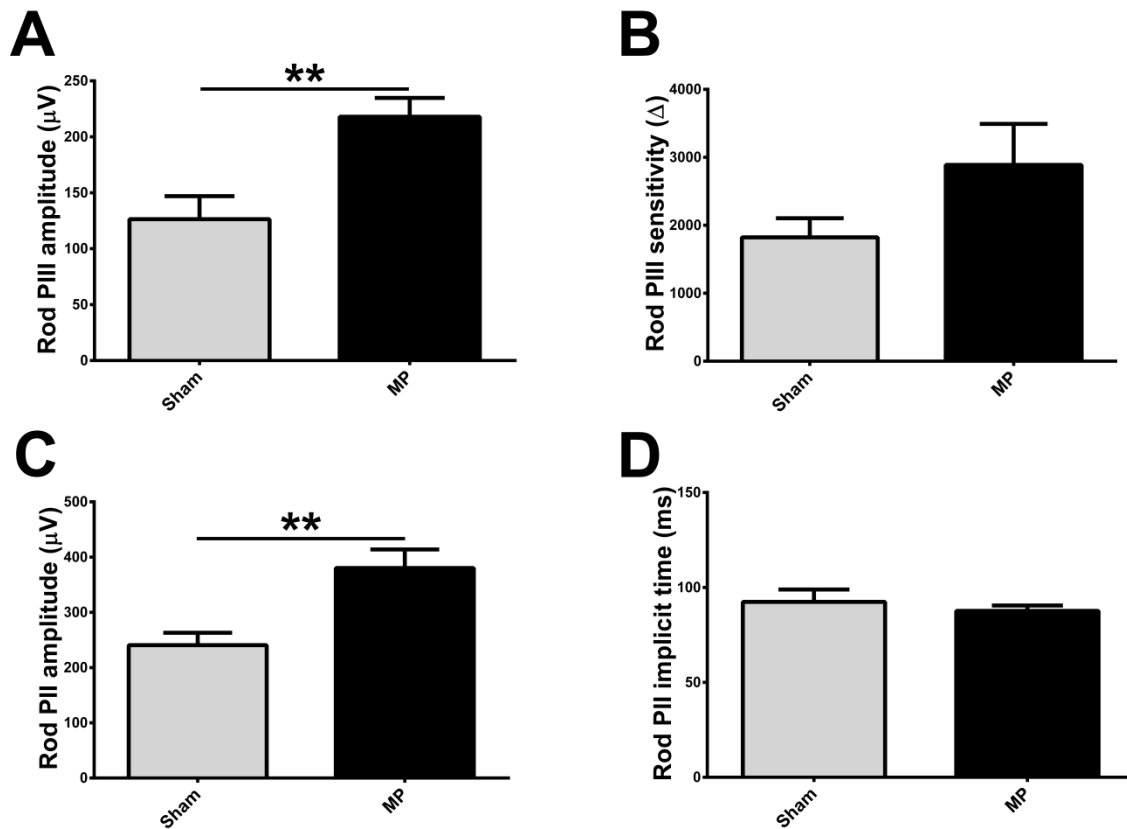
Figure 4-14. The rod pathway showed improved photoreceptoral and post-photoreceptoral responses after two peptide5-injections in the light-damaged rats (Strategy A). **A:** The amplitude of rod PIII was significantly higher in peptide5-treated rats than sham-treated animals ($p < 0.01$). **B:** The peptide5-treated rats showed a trend towards improved sensitivity of rod PIII response compared with sham-treated group. **C:** Rod PII amplitude was significantly higher in the mimetic peptide5-treated group than sham-treated animals ($p < 0.01$). **D:** Rod PII implicit time showed a non-significant reduction in peptide5-treated animals compared to sham-treated rats. All average data are expressed as mean ± SEM, n=11 in sham-treated group, and n=12 in peptide5-treated group. Statistical analysis was completed by using unpaired t-test with Welch's correction. Abbreviation: **MP**, Cx43 mimetic peptide.
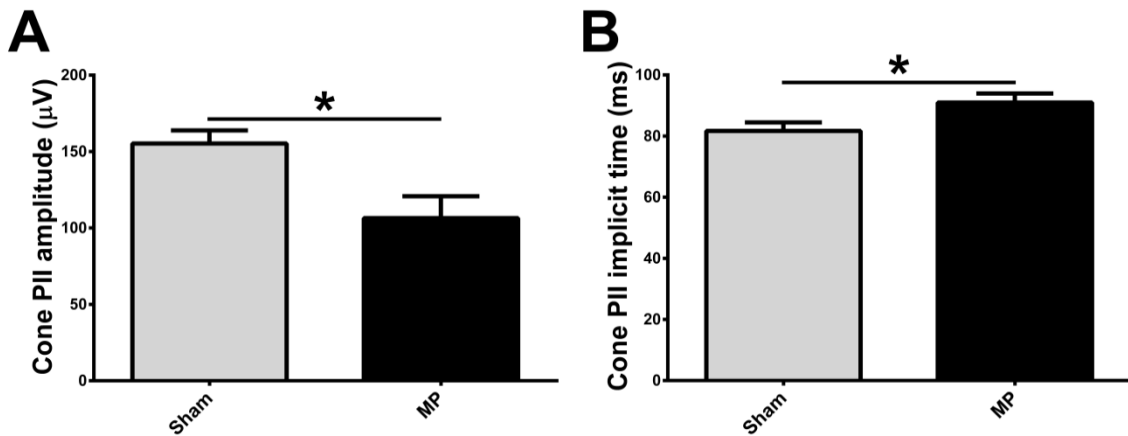
Figure 4-15. Rats with two injections of peptide5 after light damage with 24 hours recovery (Strategy A) showed a decreased cone post-photoreceptoral response. Strategy A consisted of two intravitreal injections with either peptide5 or sham post-LD with 24 hours recovery following light damage. The peptide5-treated group (n=12) showed a significantly decreased cone PII amplitude (**A**; $p < 0.05$) and increased implicit time (**B**; $p < 0.05$) for the cone PII response, compared with the sham-treated group (n=11). All average data are expressed as mean ± SEM. Statistical analysis was completed by using an unpaired t-test with a Welch's correction. Abbreviation: **MP**, Cx43 mimetic peptide.
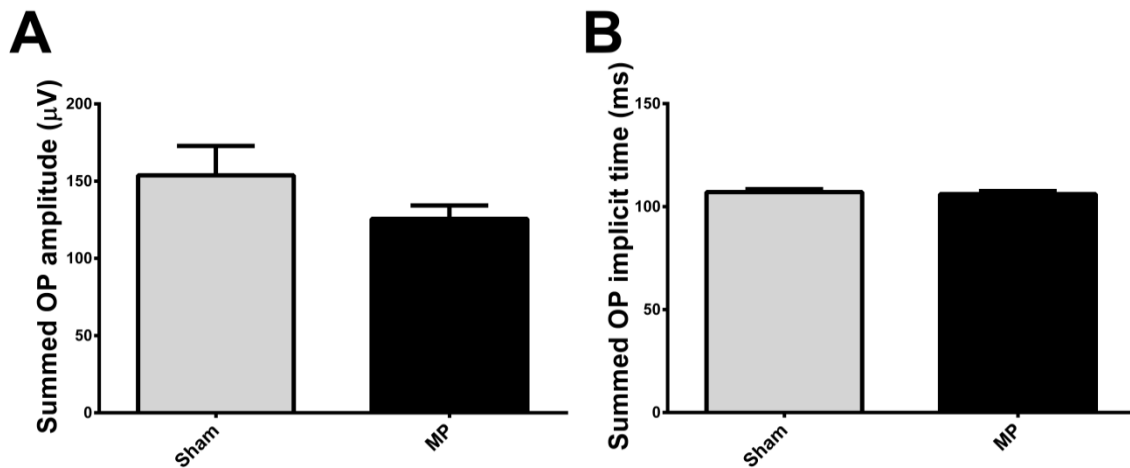
Figure 4-16. Summed OPs showed no difference between sham- and peptide5-treatments after light damage with 24 hours recovery (Strategy A). **A:** The amplitude of summed OPs was slightly lower in peptide5-treated animals than sham-treated animals. However, the difference was not significant. **B:** Sham- and peptide5-treated groups showed similar implicit time for summed OPs. All average data are expressed as mean ± SEM, n=11 in sham-treated group, and n=12 in peptide5-treated group. Statistical analysis was completed by using an unpaired t-test with a Welch's correction. Abbreviation: **MP**, Cx43 mimetic peptide.

The isolated rod and cone functions were also analysed in the groups under treatment Strategy B, which showed the most significantly improved mixed a-wave and b-wave responses (Figure 4-12). The rod PIII response showed a trend towards increased amplitude and significantly increased sensitivity ($p < 0.05$) in peptide5-treated group compared to sham-treated group (Figure 4-17A&B). Peptide5-treated animals also showed significantly increased rod PII amplitude ($p < 0.01$; Figure 4-17C) and similar rod PII implicit time (Figure 4-17D). The isolated cone PII response showed significantly improved amplitude ($p < 0.05$; Figure 4-18A) and very similar implicit time in peptide5-treated group compared to sham-treated group (Figure 4-18B). The summed OPs showed no statistical significance between peptide5- and sham-treated groups (Figure 4-19).

Analysis of isolated rod and cone responses from the group under treatment Strategy C (two injections post-LD with 7 days recovery following the offset of light damage) showed no difference between peptide5- and sham-treated animals (Figure 4-20, Figure 4-21 and Figure 4-22). However, a trend towards improvement of all the amplitudes of rod PIII, rod PII, cone PII and summed OPs was noticed (Figure 4-20A&C; Figure 4-21A and Figure 4-22A).

For the group under treatment Strategy D (two injections during the light damage and no recovery following the light damage), only cone PII responses were analysed as animals were not dark adapted. No statistical significance was detected in the cone PII responses (Figure 4-23). However, the peptide5-treated animals showed a trend towards improved PII amplitude compared to the sham-treated animals (Figure 4-23A), and unexpectedly, the PII implicit time was non-significantly prolonged in the peptide5-treated group (Figure 4-23B).
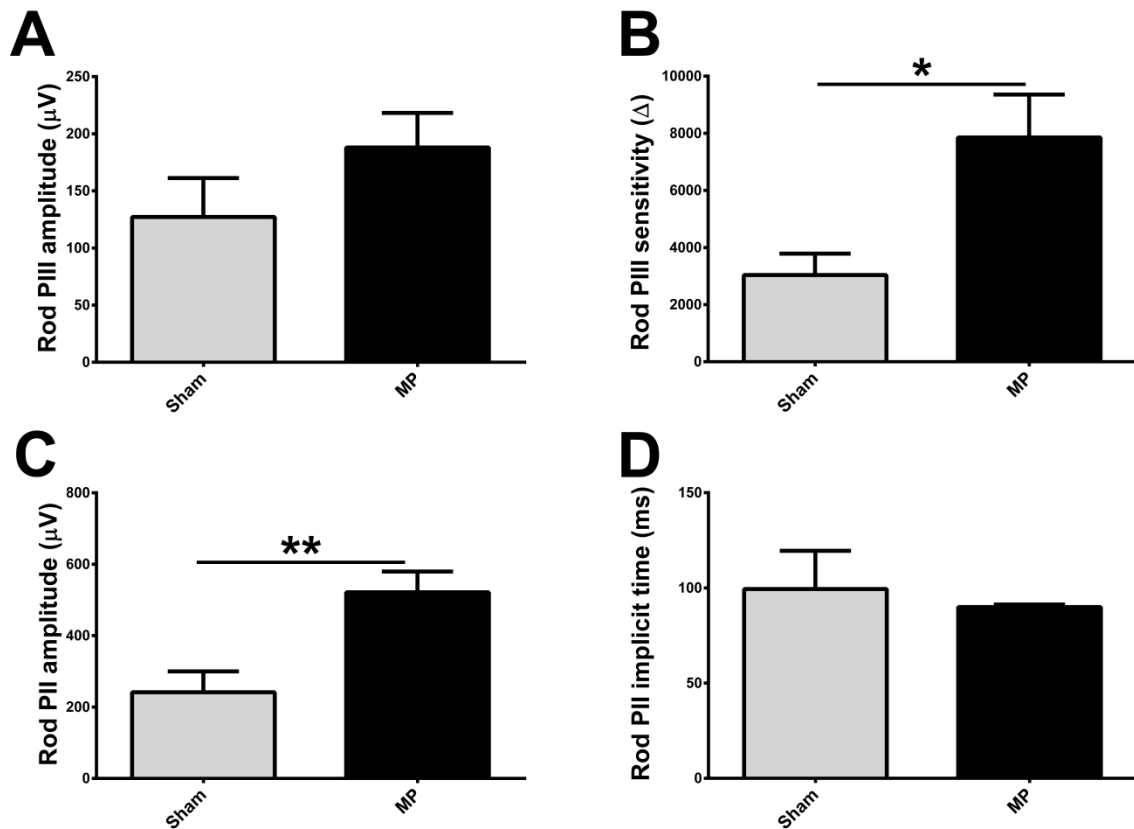
Figure 4-17. The rod pathway showed improved photoreceptoral and post-photoreceptoral responses 24 hours after two injections of peptide5 during light damage (Strategy B). **A:** The amplitude of rod PIII showed a trend towards improvement in peptide5-treated rats compared with sham-treated animals, but no significance was achieved. **B:** The peptide5-treated rats showed significantly improved sensitivity of rod PIII response compared with sham-treated group ($p < 0.05$). **C:** Rod PII amplitude was significantly higher in the mimetic peptide5-treated group compared to sham-treated animals ($p < 0.01$). **D:** Rod PII implicit times showed a non-significant reduction in peptide5-treated animals compared to sham-treated rats. All average data are expressed as mean ± SEM, n=6 in sham-treated group, and n=7 in peptide5-treated group. Statistical analysis was completed by using an unpaired t-test with a Welch's correction. Abbreviation: **MP**, Cx43 mimetic peptide.
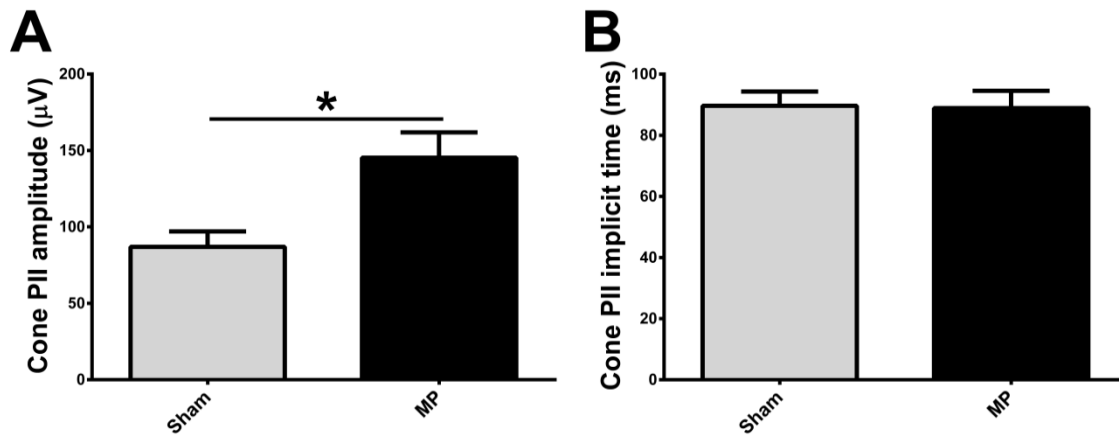
Figure 4-18. Rats with two injections of peptide5 during light damage with 24 hours recovery (Strategy B) showed a significant increase in the cone PII response. Strategy B consisted of two intravitreal injections with either peptide5 or sham during light damage and ERG recordings 24 hours after offset of intense light exposure. The peptide5-treated group (n=7) showed significantly increased amplitude (**A**; $p < 0.05$) and similar implicit time (**B**) for the cone PII response, compared with the sham-treated group (n=6). All average data are expressed as mean ± SEM. Statistical analysis was completed by using an unpaired t-test with a Welch's correction. Abbreviation: **MP**, Cx43 mimetic peptide.
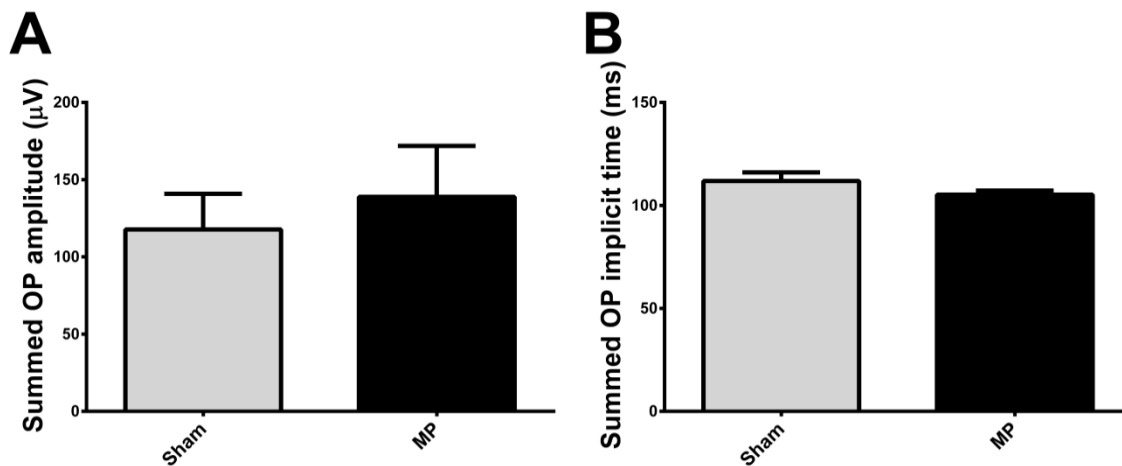
Figure 4-19. Summed OPs showed no difference between sham- and peptide5-treatments during light damage with 24 hours recovery (Strategy B). **A:** The amplitude of summed OPs indicates a trend towards improvement in peptide5-treated animals compared with sham-treated animals. However, no significance was obtained. **B:** Sham- and peptide5-treated groups showed similar implicit times for summed OPs. All average data are expressed as mean ± SEM, n=6 in sham-treated group, and n=7 in peptide5-treated group. Statistical analysis was completed by using an unpaired t-test with a Welch's correction. Abbreviation: **MP**, Cx43 mimetic peptide.

153
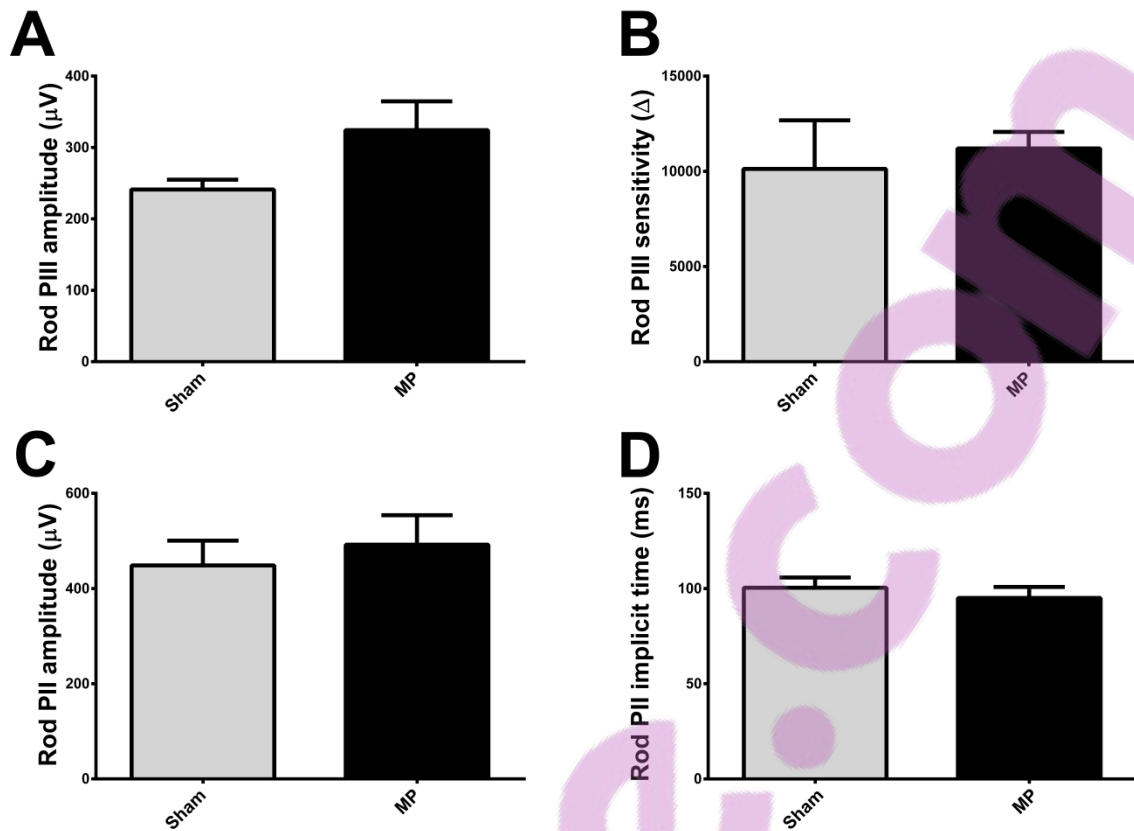
Figure 4-20. The rod pathway showed similar photoreceptoral and post-photoreceptoral responses in the light-damaged rats following two doses of peptide5-treatment post-LD with 7 days recovery (Strategy C). The rod PIII responses in peptide5-treated rats showed a trend towards improved amplitude (**A**) and sensitivity (**B**), but no significance was achieved. The rod PII response showed a non-significant increase in the amplitude (**C**) and similar implicit time (**D**) in peptide5-treated rats compared to sham-treated animals. All average data are expressed as mean ± SEM, n=6 in sham-treated group, and n=6 in peptide5-treated group. Statistical analysis was completed by using an unpaired t-test with a Welch's correction. Abbreviation: **MP**, Cx43 mimetic peptide.

154
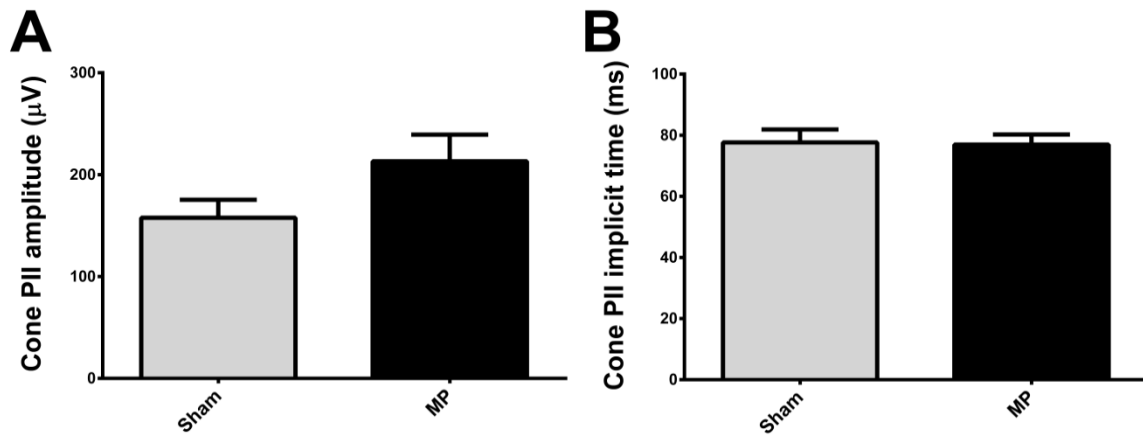
Figure 4-21. Rats with two injections of either peptide5 or sham post-LD and 7 days recovery showed similar cone post-photoreceptoral responses (Strategy C). The treatment followed was Strategy D with two intravitreal injections of either peptide5 or sham/saline post-LD and 7 days recovery following light damage. The peptide5-treated group (n=6) showed a trend towards increased amplitude (**A**) but a similar implicit time (**B**) for the cone PII response, compared with the sham-treated group (n=6). No significance was achieved. All average data are expressed as mean ± SEM. Statistical analysis was completed by using an unpaired t-test with a Welch's correction. Abbreviation: **MP**, Cx43 mimetic peptide.
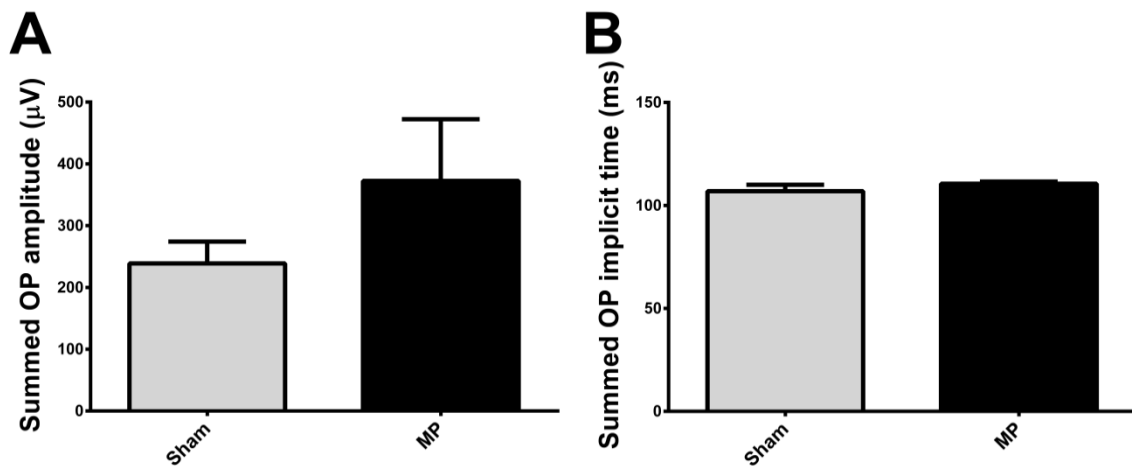
Figure 4-22. Summed OPs showed no difference between sham- and peptide5-treatments post-LD with 7 days recovery (Strategy C). A: The amplitude of summed OPs tended to improve in peptide5-treated animals compared with sham-treated animals. However, no significance was shown. **B:** Sham- and peptide5-treated groups showed similar implicit time of summed OPs. All average data are expressed as mean ± SEM, n=6 in sham-treated group, and n=6 in peptide5-treated group. Statistical analysis was completed by using an unpaired t-test with Welch's correction. Abbreviation: **MP**, Cx43 mimetic peptide.
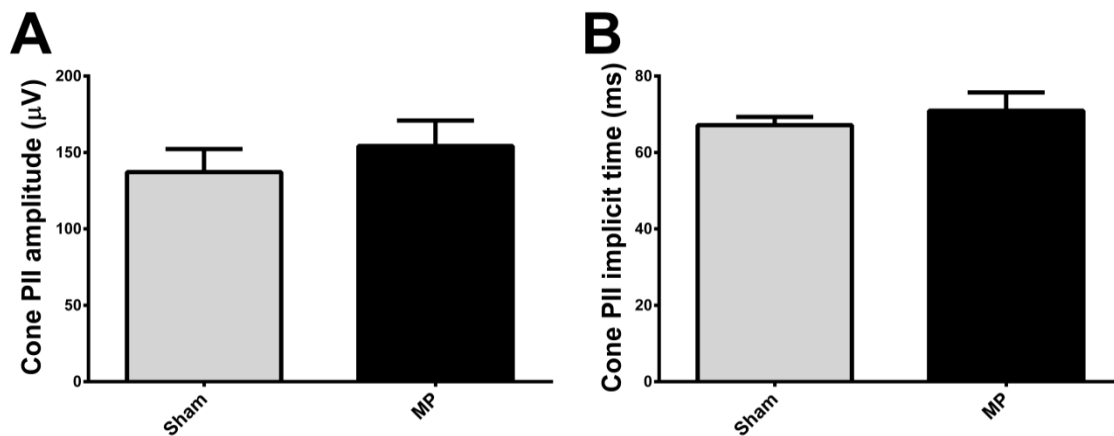
Figure 4-23. Rats with two injections of peptide5 during the light damage period and with no recovery showed no change in cone post-photoreceptoral responses (Strategy D). The treatment followed was according to Strategy A with two intravitreal injections of either peptide5 or sham/saline during the first 6 hours of the light damage, and with no recovery following the light damage. Peptide5-treated group (n=6) showed a trend towards increased amplitude (**A**) and a trend towards increased implicit time (**B**) for the cone PII response, compared with the sham-treated group (n=6). No significance was achieved. All average data are expressed as mean ± SEM. Statistical analysis was completed by using an unpaired t-test with a Welch's correction. Abbreviation: **MP**, Cx43 mimetic peptide.

4.3.5 Cx43 mimetic peptide effects on immunoreactivity of connexin proteins expressed in the rat retina

The immunoreactivity of a range of connexin proteins was investigated in the animals which had two intravitreal injections post-LD (Strategy A in Figure 4-1). Peptide5-treated rats showed lower immunoreactivity for Cx43 in the retinal nerve fibre layer (Figure 4-24B, arrows) compared with sham-treated animals (Figure 4-24A). This Cx43 immuno-labelling was mainly localised on astrocytes and retinal blood vessels similar to previous findings (Kerr *et al.*, 2010; Danesh-Meyer *et al.*, 2012). Cx43 immunoreactivity in the RPE/choroid area showed a similar labelling level in sham- and peptide5-treated groups (Figure 4-24C&D), where the RPE was primarily labelled.

The immunoreactivity of Cx36 and Cx45 were assessed in the inner retinal layers, where the immuno-labelling of these two antibodies was found (Figure 4-25). Peptide5-treated rats showed very similar immunoreactivity of Cx36 to sham-treated rats (Figure 4-25A&B). For

156

the immunoreactivity of Cx45, mimetic peptide-treated rats showed very similar labelling to sham-treated animals in the retinal inner plexiform layer, but stronger labelling in the nerve fibre layer (arrows in Figure 4-25D) than sham-treated rats (Figure 4-25C).

Cx40 immunoreactivity was present on some large, oval-shaped cells in the choroid in both sham- and peptide5-treated rats (Figure 4-26). Some RPE cells also showed Cx40 labelling (arrows in Figure 4-26). Similar labelling patterns of Cx40 immunoreactivity were apparent in sham- and peptide5-treated groups (Figure 4-26).
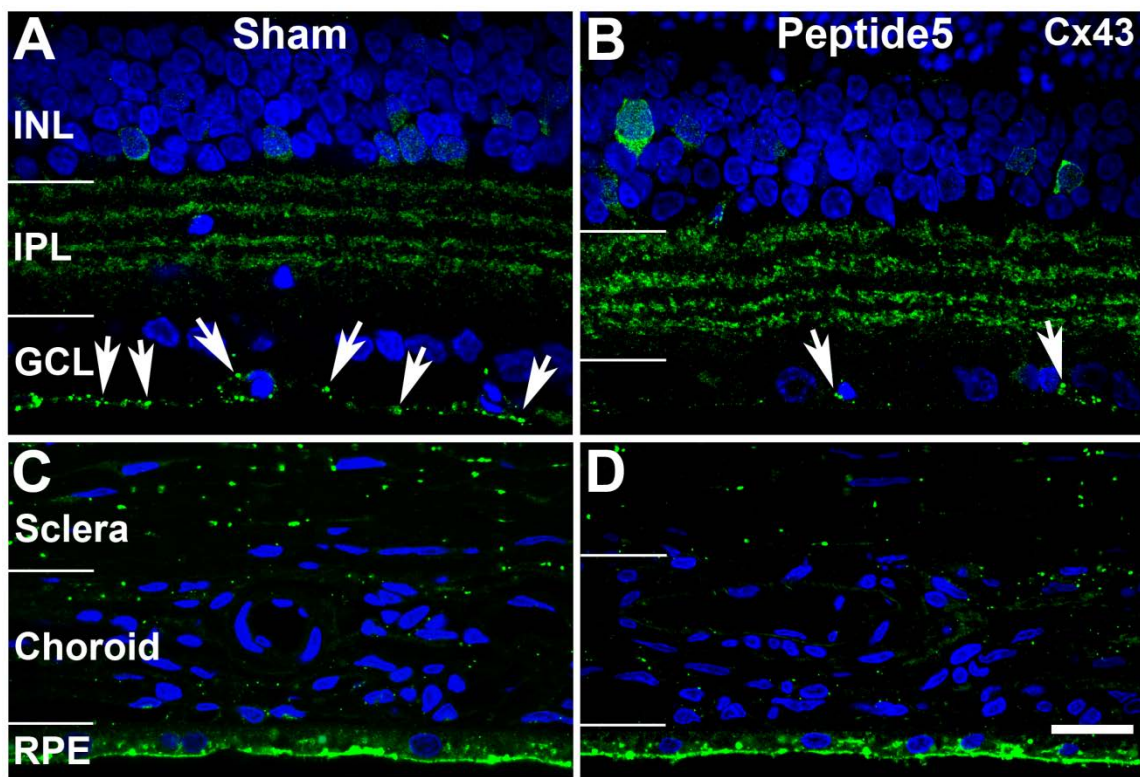
Figure 4-24. Peptide5-treated rats exhibited lower Cx43 immunoreactivity in the retinal nerve fibre layer but similar reactivity in the RPE/choroid compared to sham-treated rats. **A&B:** Cx43 immunoreactivity in the retina in sham- (**A**) and peptide5-treated rats (**B**). Less labelling was detected in the nerve fibre layer (arrows) in peptide5-treated rats than sham-treated animals. The labelling in the inner plexiform layer was due to non-specific binding of the antibody. **C&D:** Similar Cx43 immunoreactivity was detected in the RPE/choroid in sham- (**C**) and peptide5-treated rats (**D**). Abbreviation: **INL**, inner nuclear layer; **IPL**, inner plexiform layer; **GCL**, ganglion cell layer; **RPE**, retinal pigment epithelium. Scale bar = 20 µm.
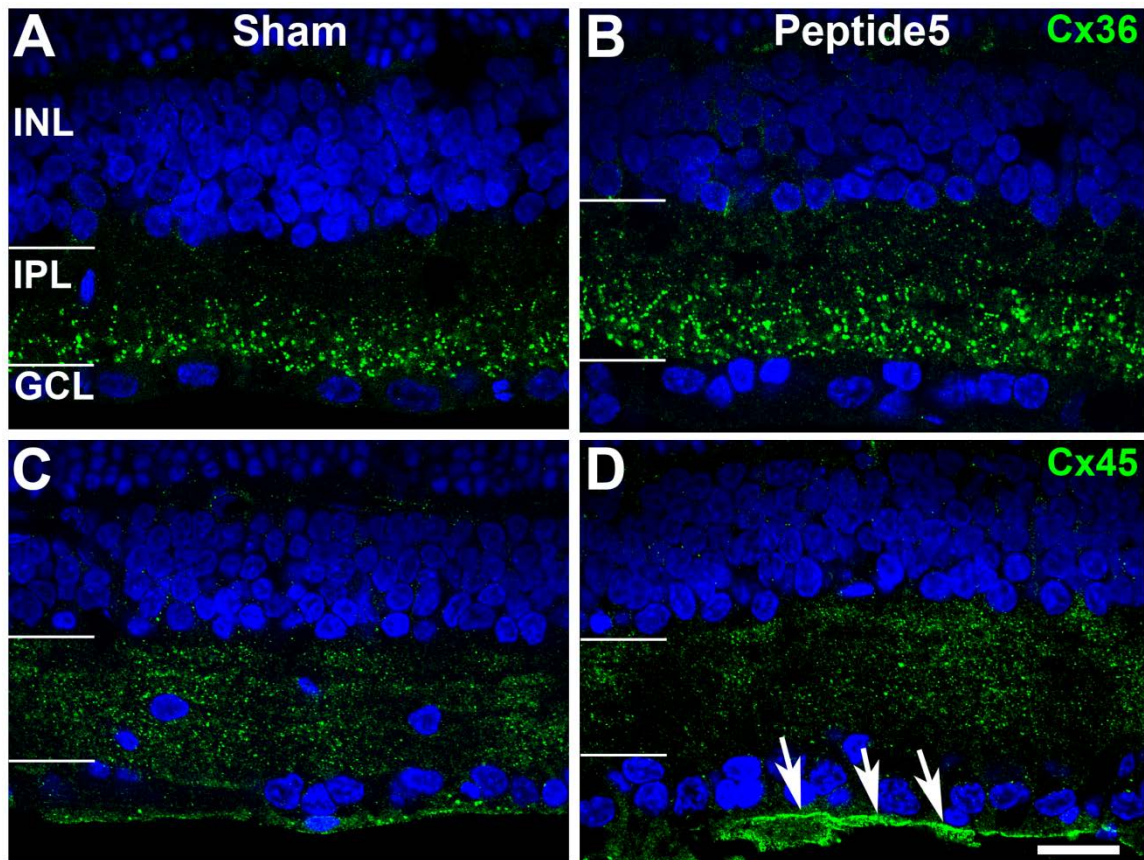
Figure 4-25. No difference in Cx36 and Cx45 immunoreactivity was present between sham- and peptide5-treated rats. **A&B:** Similar immunoreactivity of Cx36 was shown in the retina in sham- (**A**) and peptide5-treated rats (**B**). The labelling was mainly limited in the inner plexiform layer. **C&D:** In the inner plexiform layer, similar Cx45 immunoreactivity was detected in the RPE/choroid in sham- (**C**) and peptide5-treated rats (**D**). In the nerve fibre layer, peptide5-treated rats (arrows; **D**) had stronger Cx45 labelling than sham-treated animals (**C**). Abbreviation: **INL**, inner nuclear layer; **IPL**, inner plexiform layer; **GCL**, ganglion cell layer. Scale bar = 20 µm.
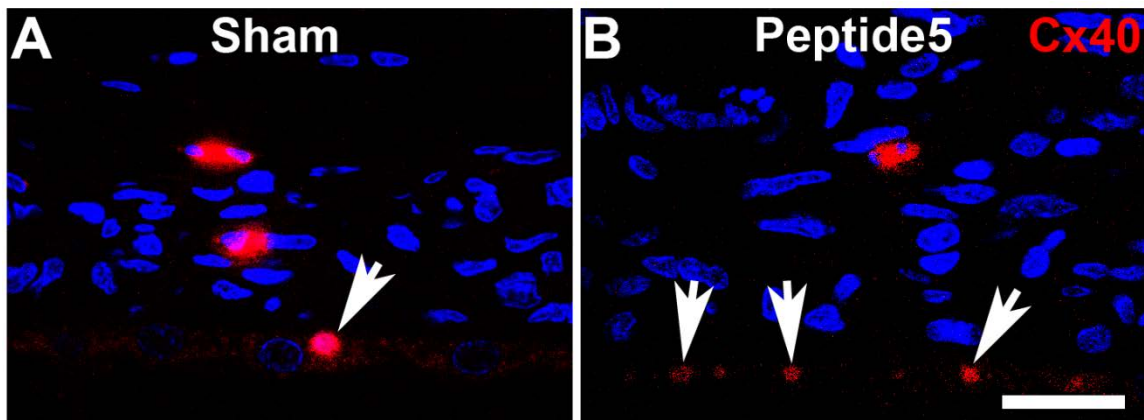
Figure 4-26. **Similar immunoreactivity of Cx40 in sham- and peptide5-treated rats.** **A:** Cx40 immuno-labelling in the RPE (arrow) and choroid in a sham-treated rat. **B:** Cx40 immuno-labelling in the RPE (arrows) and choroid in a peptide5-treated rat. Scale bar = 20 µm.

4.3.6 A double dose of Cx43 mimetic peptide significantly suppressed the inflammatory response in the light-damaged choroid and retina

Following assessment of retinal function, the inflammatory response was investigated by checking the immunoreactivity of several markers in the rats which had two intravitreal injections following (Strategy A) and during light damage (Strategy B in Figure 4-1). In the animals treated post-LD (Strategy A), CD45, a lymphocyte common antigen, showed noticeably fewer labelled cells in the choroid in peptide5-treated rats compared with sham-treated animals (Figure 4-27C&D). Statistical analysis showed CD45 positive cell count was significantly decreased in peptide5-treated animals than sham-treated animals (Figure 4-27E, $p < 0.001$). The retina did not show specific CD45 immunoreactivity in either sham- or peptide5-treated groups (Figure 4-27A&B).

Glial fibrillary acidic protein (GFAP) was used to examine the effect of peptide5 on astrocyte and Müller cell activity in the retina. There was weaker immunoreactivity for GFAP in peptide5-treated rats compared to sham-treated animals (Figure 4-28). Stronger GFAP immunoreactivity associated with the processes of Müller cells were observed in sham-treated retina (Figure 4-28A).   In peptide5-treated retina, the level of GFAP immunoreactivity dropped back to normal and was only associated with astrocytes in the retinal nerve fibre layer (Figure 4-28B).

Ionised calcium-binding adaptor molecule-1 (Iba-1), a marker for residential macrophages and microglia in the retina (Ahmed *et al.*, 2007), was also employed in this study. In sham-treated retina, Iba-1-labelled cells were detected in the retinal outer nuclear layer (Figure 4-29A). However, there were no Iba-1-labelled cells in this area in peptide5-treated animals (Figure 4-29B). Statistical quantification of Iba-1-labelled cells using unpaired t-test showed no change in the inner layers of the retina (the ganglion cell layer and the inner plexiform layer) between sham- and peptide5-treated animals (Figure 4-29E). Unsurprisingly, the middle layers (the inner nuclear layer and the outer plexiform layer) and outer layers (the outer nuclear layer and the outer segment/inner segment) of the retina showed significantly

decreased number of Iba-1-labelled cells in peptide5-treated animals compared to sham-treated animals (Figure 4-29F&G, $p < 0.001$). In the choroid, several Iba-1 immuno-labelled cells were present in the activated-phase with an amoeba-shaped cell body but few processes (Figure 4-29C). In peptide5-treated rat choroid, any Iba-1 immuno-labelled cells that were present had more numerous and larger processes indicating they remained primarily in the resting phase (Figure 4-29D).
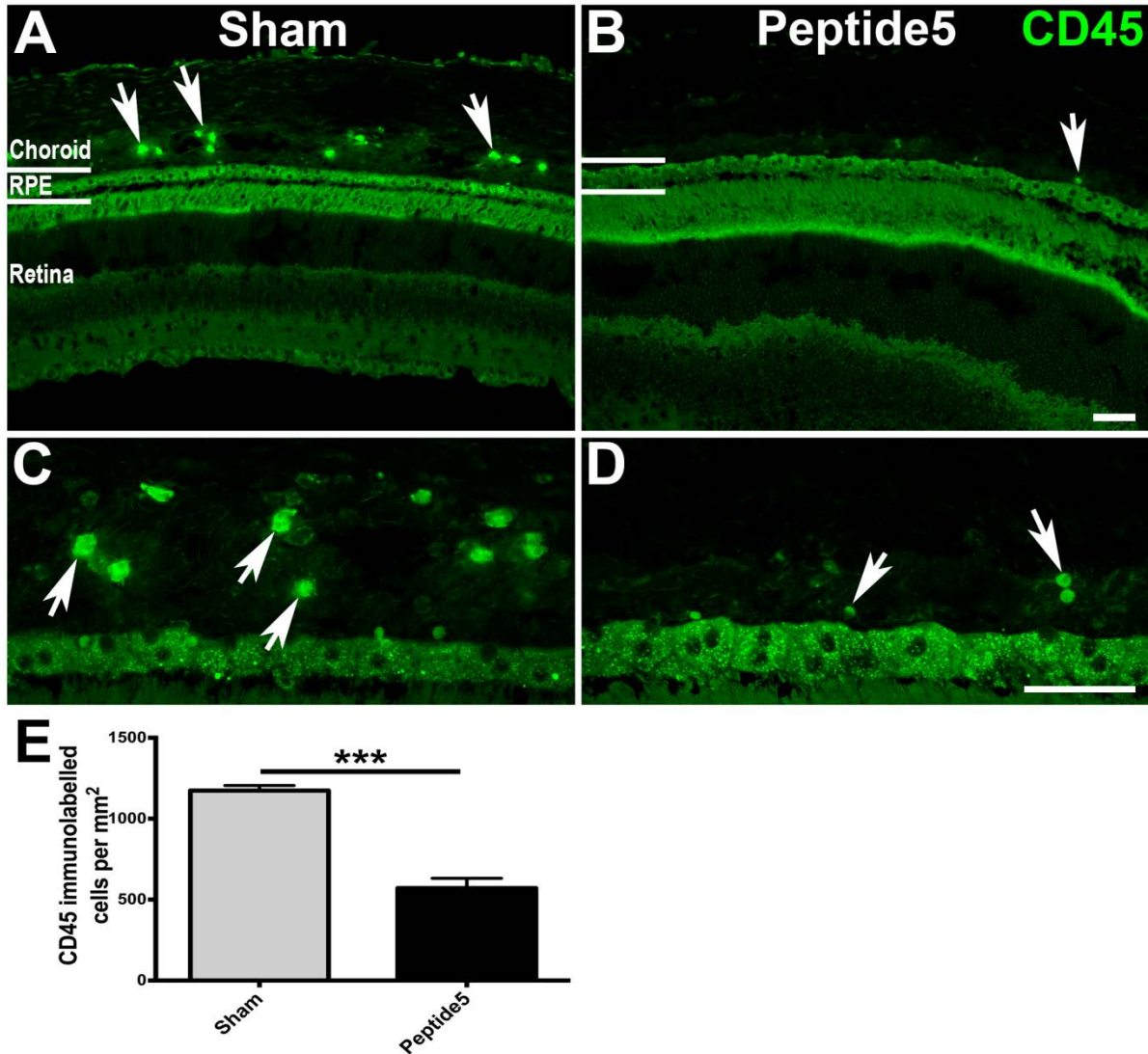
Figure 4-27. CD45 immuno-labelled cells were fewer in number in the choroid of peptide5-treated rats compared with sham-treated rats (Strategy A). A&B: Strong immunoreactivity of Cx45 was detected in the choroid in sham-treated rat (arrows; **A**) but few Cx45 immuno-labelled cells were seen in peptide5-treated rats (arrow; **B**). **C&D**: Higher magnification images showing the Cx45 immuno-labelled cells in the choroid in sham- (arrows; **C**) and peptide5-treated rats (arrows; **D**). **E:** statistical analysis using unpaired t-test showed CD45 cell count was significantly less in the choroid in peptide5-treated animals than sham-treated animals (*** $p < 0.001$). Scale bars = 50 µm.
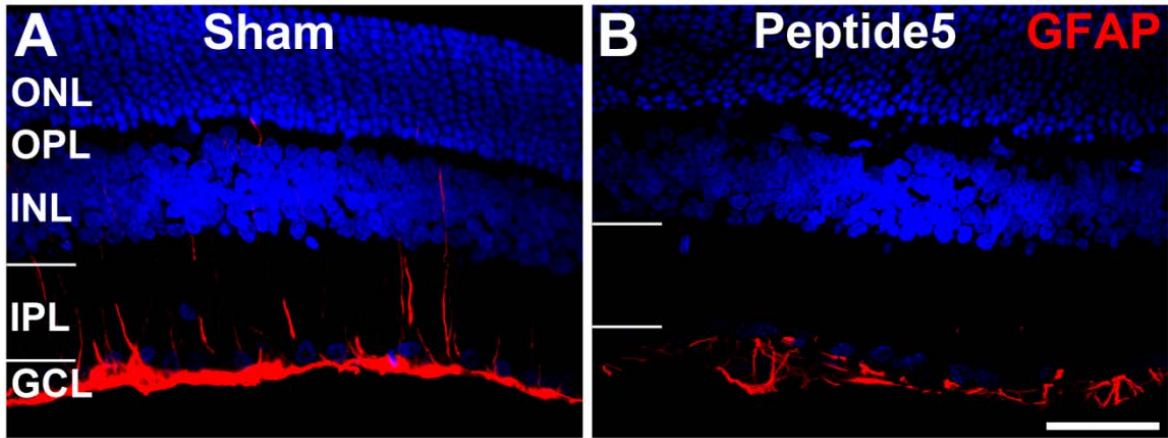
Figure 4-28. GFAP immunoreactivity does not increase as much in the retina of peptide5-treated rats compared with sham-treated rats (Strategy A). A: Elevated GFAP immunoreactivity was seen in sham-treated rats throughout the ganglion cell layer and embedded in the inner plexiform layer. **B:** Apparently normal GFAP immunoreactivity was detected in peptide5-treated rats where it limited to the retinal nerve fibre layer. Abbreviation: **ONL**, outer nuclear layer; **OPL**, outer plexiform layer; **INL**, inner nuclear layer; **IPL**, inner plexiform layer; **GCL**, ganglion cell layer. Scale bar = 50 µm.
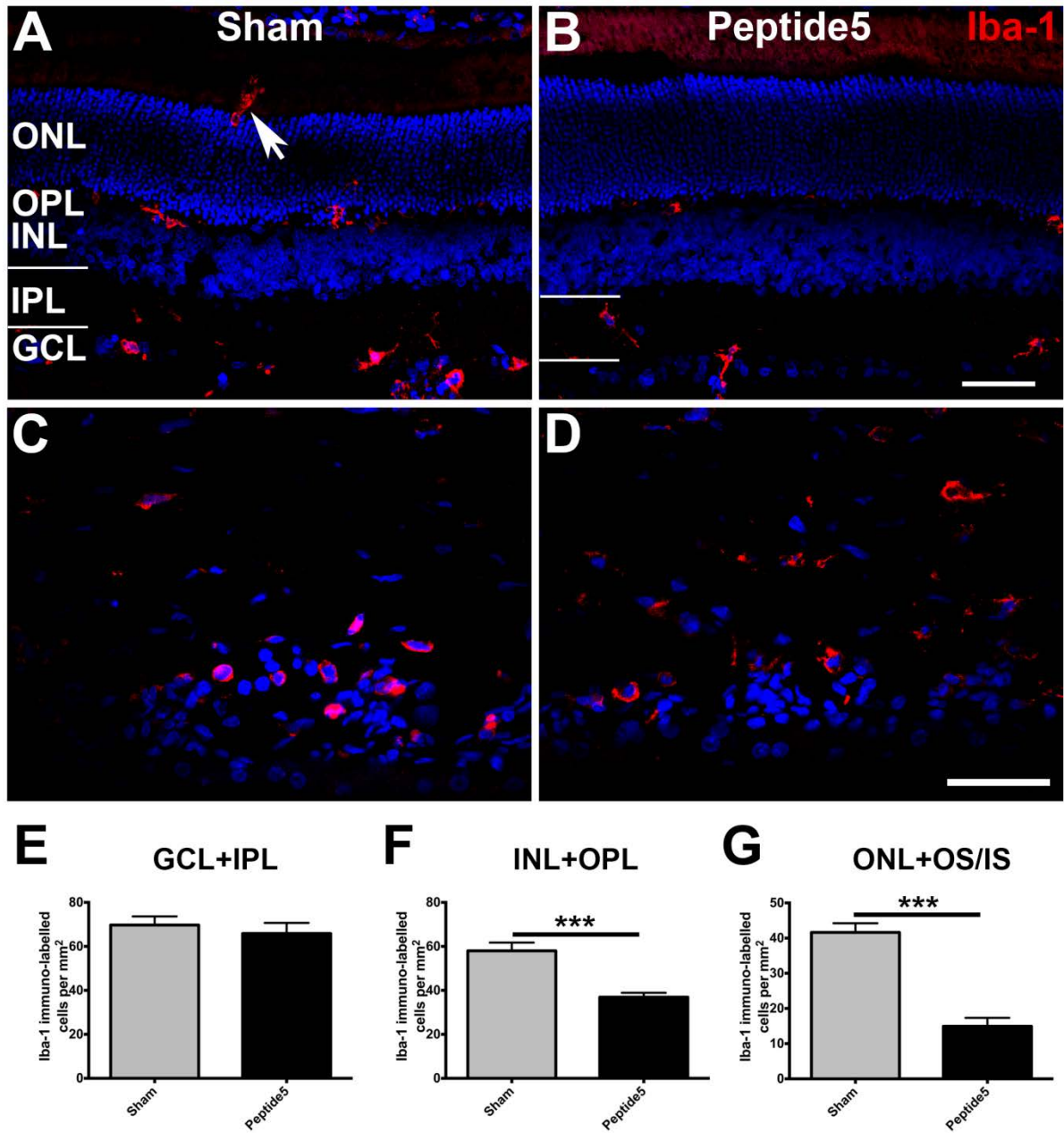
Figure 4-29. Peptide5-treated rats had fewer activated Iba-1 immuno-labelled cells in the retina (Strategy A). **A:** In sham-treated rat retina, Iba-1 immuno-labelled cells were appeared to be migrating into the outer nuclear layer (arrow). **B:** No Iba-1 immuno-labelled cells were detected in the outer retina in peptide5-treated rats. **C:** In sham-treated rat choroid, Iba-1 immuno-labelled cells were present in their activated-phase. **D:** In peptide5-treated rat choroid, Iba-1 immuno-labelled cells were present in their resting phase. **E-G:** Quantification of number of microglia in the inner layers (**E**), middle layers (**F**) and outer layers (**G**) of the retina in sham- and peptide5-treated animals. The inner layers showed no change between sham- and peptide5-treated animals (**E**); however, the middle (**F**) and outer layers (**G**) of the retina showed significantly decreased Iba-1-labelled cells in peptide5-treated animals compared to sham-treated animals (*** $p < 0.001$). Abbreviation: **OS/IS**, outer segment/inner segment; **ONL**, outer nuclear layer; **OPL**, outer plexiform layer; **INL**, inner nuclear layer; **IPL**, inner plexiform layer; **GCL**, ganglion cell layer. Scale bar = 50 µm.

In addition to analysing inflammation in the animals treated following the offset of light damage (Strategy A); the inflammatory response was also investigated in animals treated during the light damage period (Strategy B). This group showed the most significant improvement to ERG mixed responses amongst all the treatment strategies (Figure 4-12).

Not surprisingly, these animals showed a dramatically reduced inflammatory response. There were few CD45-labelled macrophages in the choroid in peptide5-treated rats, and these macrophages were in the resting stage with small and oval-shaped cell body (Figure 4-30B, arrow), and statistical analysis showed significantly decreased in peptide5-treated animals compared to sham-treated animals (Figure 4-30C, $p < 0.001$). Confocal images revealed fewer macrophages in the animals treated with Strategy B (Figure 4-30B) compared to those treated with Strategy A (Figure 4-27B&D). GFAP immunoreactivity from animals treated with a double dose of peptide5 under Strategy B (Figure 4-31B) showed a similar level to those under Strategy A (Figure 4-28B). This was dramatically lower compared to the sham-treated rats (Figure 4-31A).

In sham-treated retina, Iba-1 immuno-labelled microglia were located in the inner and outer nuclear layers, indicating their association with retinal neuronal cellular injury (Figure 4-32A). Quantification analysis using unpaired t-test showed significantly decreased number of microglia in the inner layers (Figure 4-32E, the ganglion cell layer and the inner plexiform layer) and middle layers (Figure 4-32F, the inner nuclear layer and the outer plexiform layer) of the retina in peptide5-treated animals compared to sham-treated animals ($p < 0.05$). The Iba-1-labelled cell count in the outer retina (the outer nuclear layer and the outer segment/inner segment) showed the most significant decrease (Figure 4-32G, $p < 0.001$). The peptide5-treated retina showed microglia were limited to the plexiform layers and ganglion cell layer (Figure 4-32B), parallel to the pattern observed in the retinas of rats treated under strategy A (Figure 4-29A). In the choroid peptide5-treated rats showed noticeably fewer Iba-1-labelled macrophages (Figure 4-32B) compared to sham-treated animals (Figure 4-32A).
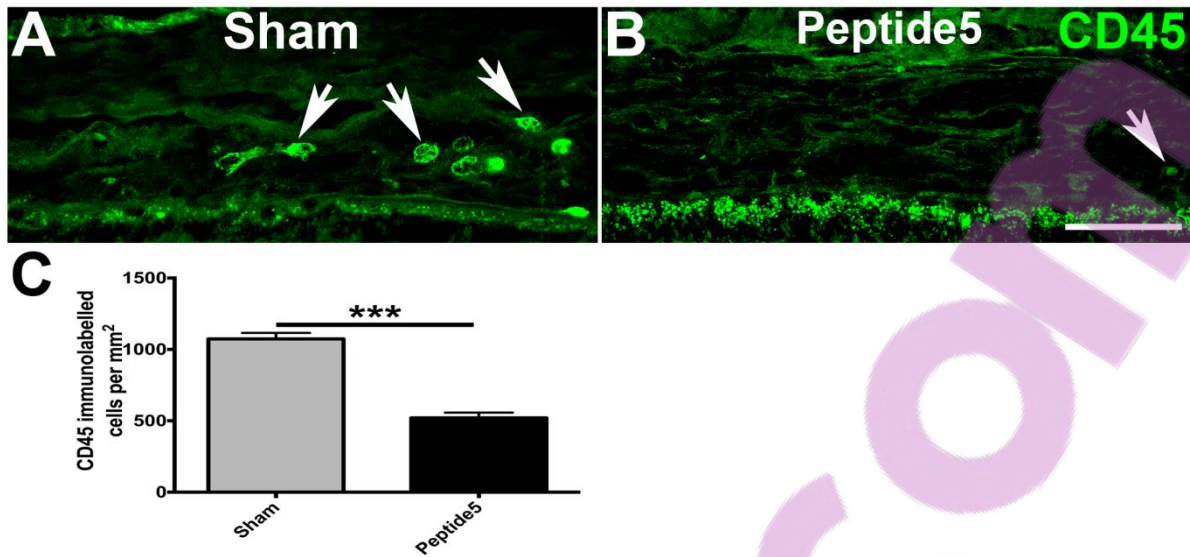
Figure 4-30. CD45 immuno-labelled cells were fewer in number in the choroid of peptide5-treated rats compared with sham-treated rats (Strategy B). Sham-treated rats showed several activated Cx45 immuno-labelled macrophages with enlarged cell bodies (**A**, arrows), whilst few were seen in MP-treated rats (**B**; arrow). **C:** statistical analysis using unpaired t-test showed CD45 cell count was significantly less in the choroid in peptide5-treated animals than sham-treated animals (*** $p < 0.001$). Scale bars = 50 µm.
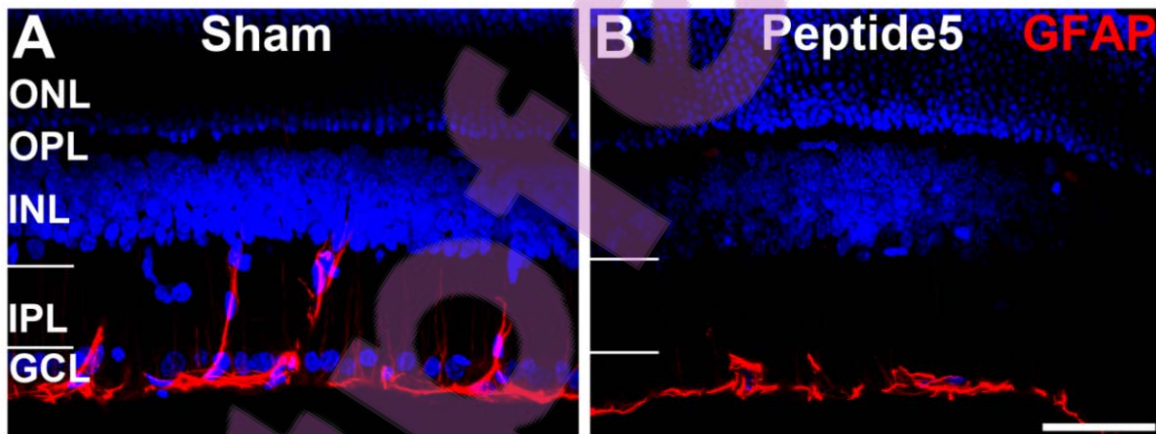
Figure 4-31. GFAP immunoreactivity does not increase as much in the retina of peptide5-treated rats compared with sham-treated rats (Strategy B). **A:** Elevated GFAP immunoreactivity was seen in sham-treated rats. **B:** Apparently normal GFAP immunoreactivity was detected in peptide5-treated rats. Abbreviation: **ONL**, outer nuclear layer; **OPL**, outer plexiform layer; **INL**, inner nuclear layer; **IPL**, inner plexiform layer; **GCL**, ganglion cell layer. Scale bar = 50 µm.
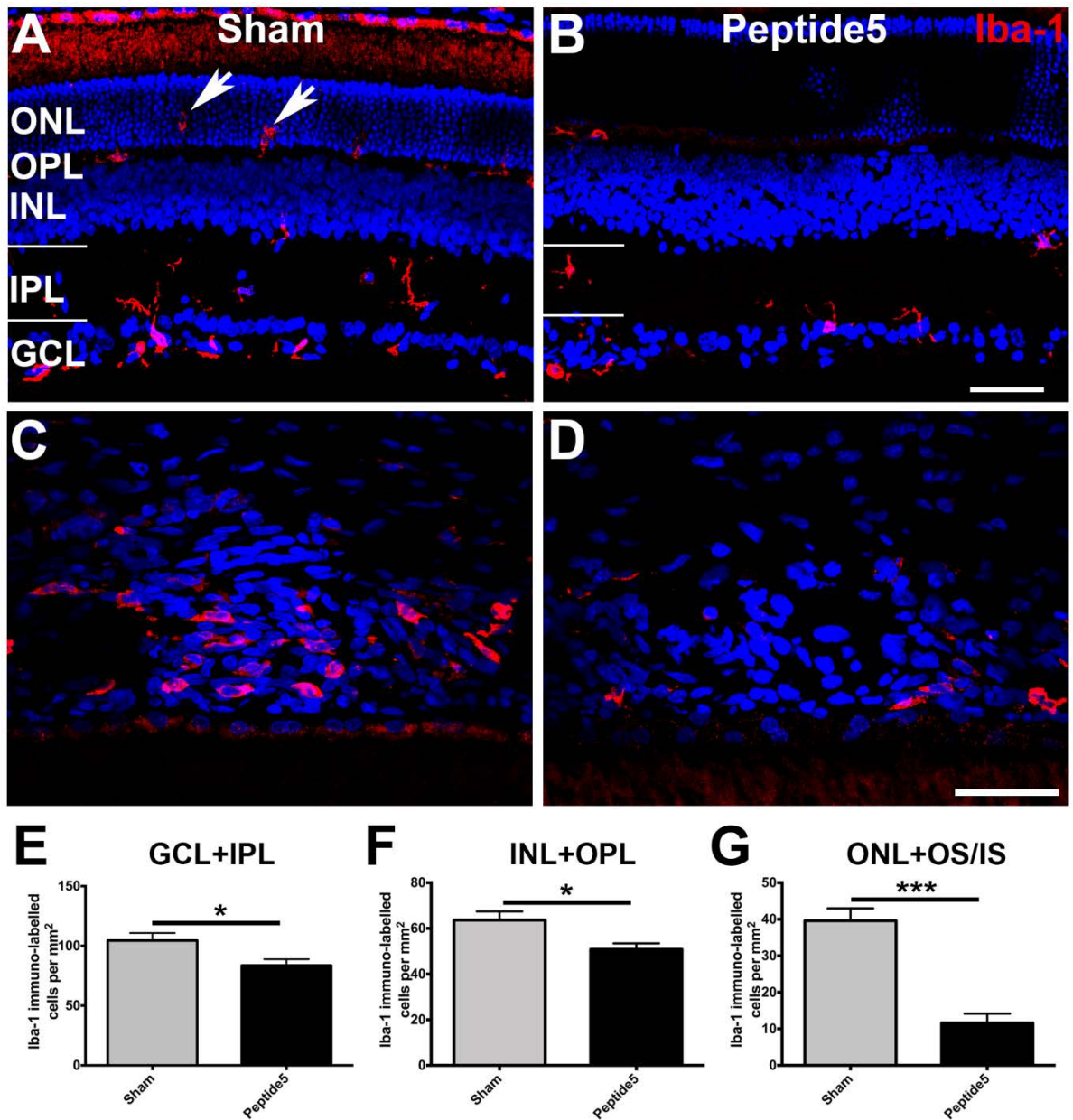
Figure 4-32. Peptide5-treated rats had fewer activated Iba-1 immuno-labelled cells in the retina and choroid (Strategy B). **A:** In sham-treated rat retina Iba-1 immuno-labelled cells were detected migrating into the outer nuclear layer (arrow). **B:** No Iba-1 immuno-labelled cells were detected in the outer retina in peptide5-treated rats. **C:** In sham-treated rat choroid, many cells were Iba-1 immuno-labelled. These cells were present in the activated-phase. **D:** In peptide5-treated rat choroid, Iba-1 immuno-labelled cells were fewer in number and those present remained in the resting phase. **E-G:** Quantification analysis showed significantly decreased number of microglia in all the layers in peptide5-treated animals compared to sham-treated animals (* $p < 0.05$). The cell count in the outer retina showed the most significant decrease (**G,** *** $p < 0.001$). Abbreviation: **OS/IS**, outer segment/inner segment; **ONL**, outer nuclear layer; **OPL**, outer plexiform layer; **INL**, inner nuclear layer; **IPL**, inner plexiform layer; **GCL**, ganglion cell layer. Scale bar = 50 µm.

4.4 Discussion

This study has demonstrated that Cx43 mimetic peptide, peptide5 was able to reach the targeted tissue including the retina, RPE and the choroid following intravitreal injection. Single dose administration with mimetic peptide showed a trend for improvement in ERG recordings of both rod and cone pathways. The effect of increased doses was then examined in light-damaged animals. A double dose of peptide5 treatment (Strategy A in Figure 4-1) showed significant improvement in the photoreceptoral and post-photoreceptoral responses, reflected by isolated rod PIII and PII responses respectively (Figure 4-14). However, the post-photoreceptoral response did not show improvement in the peptide5-treated group, and on the contrary, it showed a significantly reduction (Figure 4-15). Immunohistochemical study on the harvested tissue demonstrated that the Cx43 immunoreactivity was decreased and Cx45 immunoreactivity was increased in the nerve fibre layer of peptide5-treated rats. Interestingly, a significant reduction in monocyte inflammatory response was found in peptide5-treated rats compared with sham-treated group. CD45 in the choroid and GFAP in the retina have proved to be good markers for analysing the inflammatory response in the ocular tissue.

4.4.1 High permeability of the Cx43 mimetic peptide in the ocular tissue

FITC-conjugated peptide5 was employed to investigate the permeability of the mimetic peptide following two different delivery routes, via intraperitoneal and intravitreal injections. This method was adopted and modified from FITC-conjugated dextran, a complex commonly used to test concentration gradients, which has also been used previously in ocular tissue (Olsen *et al.*, 1995). FITC-conjugated antisense oligonucleotide has also been used to measure its permeability in the ocular tissue (Hagigit *et al.*, 2010).

In the light-damaged animal model (Chapter 3) it was evident that the intense light exposure induced oxidative stress and inflammation in the choroid and the retina. This suggested that both the choroid and the retina were likely target tissues for Cx43 mimetic peptide as a

166

treatment. The current study has demonstrated that peptide5 passed readily through the inner limiting membrane into the retina, RPE and the choroid following intravitreal injection. This indicates that intravitreal injection is an efficient way for administration of peptide5.

A previous *in vitro* study on spinal cord injury has demonstrated that both high (500 μM) and low concentrations (5 μM) of peptide5 significantly reduced tissue swelling when peptide5 was present for 24 hours following injury, and only concentrations below 100 μM reduced tissue swelling when peptide5 was present for 4 days post-injury (O'Carroll *et al.*, 2008). In this study, the final concentration of peptide5 in the vitreous was 20 μM, a concentration level expected to prevent hemichannel opening but not to uncouple gap junctions. Peptide5 at this concentration showed specificity to some particular cells in the ganglion cell layer and inner nuclear layer (Figure 4-4A), while peptide5 at ten times higher concentration (200 μM) showed no specificity (Figure 4-2C). Interestingly, peptide5 at the desired concentration (20 μM) showed higher affinity to endothelial cells of the retinal blood vessels in the light-damaged animal compared with non-light-damaged control animals (Figure 4-3). The reason for this is not clear. The more intense fluorescence associated with retinal blood vessels in the light-damage animal could, however, be related to the increased expression of Cx43 on the endothelium in the injured tissue (Danesh-Meyer *et al.*, 2008; O'Carroll *et al.*, 2008; Danesh-Meyer *et al.*, 2012; Davidson *et al.*, 2012a).

4.4.2 Improved rod-pathway responses may be associated with neuronal survival and decreased cone-pathway responses may be related to the non-specificity of the Cx43 mimetic peptide

Cell types in ocular tissue respond differently to damage. Cones are more resistant to cell damage and rods are more susceptible to light damage than cones (Tanito *et al.*, 2007). The current study has demonstrated that two doses of the Cx43 mimetic peptide, peptide5, significantly improved both photoreceptoral and post-photoreceptoral responses in the rod pathway compared to sham-treated groups (Figure 4-14 and Figure 4-17). For rats under

167

Strategy A, the larger rod PIII amplitude in peptide5-treated rats suggested that the mimetic peptide improved survival of rod photoreceptors following the light damage compared to sham-treated animals. Peptide5 also supported a better survival rate and response in the rod-bipolar cells, amacrine cells and other inner retinal neurons, reflected by the significantly improved PII amplitude. Notably, peptide5 significantly increased the amplitudes of rod PIII and PII suggesting that this mimetic peptide significantly enhanced the number of rod photoreceptors and other neurons responding to the stimulus. The function of rods and other neurons reflected by the implicit time was not expected to be changed as neuron function was not affected in the present animal model (Figure 3-3E&G and Figure 3-4C, Chapter 3). It is interesting that the cone PII amplitude is significantly decreased (Figure 4-15A). This will be discussed below with similar results observed from Strategy C. Rats treated with Strategy B, also showed significantly improved rod PII activity (Figure 4-17C). The significantly increased a-wave and b-wave responses from mixed waveforms also verified substantial benefits in the rod pathway (Figure 4-12). Retinal neuron function and survival can be affected by diffusible factors (Li *et al.*, 1995; Mohand-Said *et al.*, 1998). Measurements of the outer nuclear layers against the whole retina thickness showed thicker outer nuclear layer in peptide5-treated rats compared to sham-treated animals following both Strategy B and Strategy C treatments (Figure 4-33), which indicates higher neuronal survival. The mechanism for this neuro-protective effect provided by peptide5 in the rod pathway remains unclear. However, it is thought to be achieved by limiting the glia-mediated inflammatory response. This will be discussed in the Section 4.4.3 below.
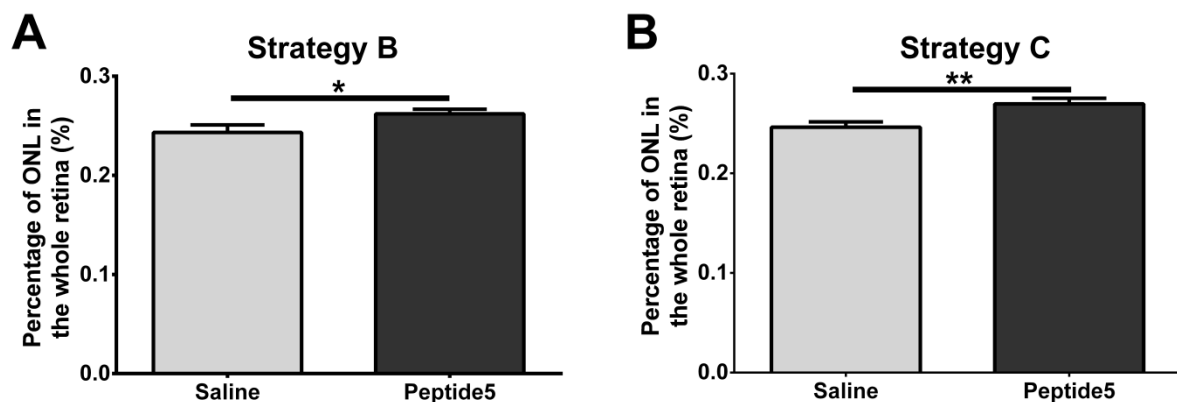
Figure 4-33. Peptide5-treated rats had thicker outer nuclear layer than sham-treated rats (Strategy B & C). In both Strategy B and C, the outer nuclear layer (ONL) is thicker in peptide5-treated groups compared to sham-treated groups ($p < 0.05$ in Strategy B and $p < 0.01$ in Strategy C, n = 4 in each group.)

Gap junctions play a key role in the process of light transduction (Goodenough & Paul, 2009). Cx36 has been identified at the ends of the fine processes of the cone pedicles (Haverkamp *et al.*, 2000; Feigenspan *et al.*, 2004; Li & DeVries, 2004). Co-localisation of Cx36 and Cx45 has been detected on two types of cone bipolar cell terminals and AII amacrine cells, which are involved in relaying the rod signal into the cone pathway under scotopic conditions (Dedek *et al.*, 2006). They may also contribute to electrical coupling between neurons, providing fast conductance and low steady-state voltage sensitivity (Söhl *et al.*, 2005). This electrical coupling works through phosphorylation or dephosphorylation of connexin proteins, which leads to altering the conductance of ionic currents, such as K^+ and Ca^{2+} (Goodenough & Paul, 2009). Hemichannels have been identified on the cone horizontal cell dendrites (Malchow *et al.*, 1993) which extend into the cone pedicles where it has been suggested that they play a key role in the inhibition feedback from the ON horizontal cell to the cones (Kamermans *et al.*, 2001). Responding to the light, the ON horizontal cell stops cones from generating dark current and produce a membrane hyperpolarization through a hemichannel signalling ephaptic feedback (Hagins *et al.*, 1970; Hofer & Dermietzel, 1998; Kamermans *et al.*, 2001; Klaassen *et al.*, 2012). Blocking the hemichannel using carbenoxolone abolishes the feedback from horizontal cells to cones in the carp retina (Kamermans *et al.*, 2001; Goodenough & Paul, 2003; Klaassen *et al.*, 2012). Regarding the molecular effect of peptide5, previous *in vitro* and *in vivo* studies have suggested that peptide5 functions through blocking the opening of Cx43 hemichannels, which are normally kept closed under physiological conditions (Goodenough & Paul, 2003; O'Carroll *et al.*, 2008; Danesh-Meyer *et al.*, 2012; Davidson *et al.*, 2012a). Peptide5 was designed against extracellular loop 2 (O'Carroll *et al.*, 2008) which is highly conserved within the connexin family (Figure 4-34) (Goodenough *et al.*, 1996; Kumar & Gilula, 1996; Yeager & Nicholson, 1996). Therefore, the significantly reduced and delayed cone post-photoreceptoral response in the rats treated with Strategy A (Figure 4-15) may possibly be associated with non-specific blocking of other connexin isoform hemichannels. Especially under this strategy where the two injections were given only four hours apart, there may be enhanced concentration levels if there is remaining peptide from the first injection. A non-significant prolonged cone PII implicit time was also seen in rats treated with Strategy D (two hours apart between the two injections) (Figure 4-23B), which may also be due to the effect of concentration summation, or simply that the peptide levels are sustained for a

prolonged period (this study has not analysed peptide stability). Nevertheless, non-specific blocking of hemichannels by peptide5 may lead to the reduced response in the cone pathway. Other connexin hemichannel roles in light signal transductions may vary at different stages of tissue injury and repair which could be the reason why Strategy D showed a weakly affected cone response while Strategy A showed a significantly reduced cone response. This hypothesis is supported by the mixed wave data and isolated cone data from treatment Strategy B, which showed the effects on cone pathway responses was no longer present when the two injections were given 22 hours apart (Figure 4-12 and Figure 4-15). This non-specific blocking affected both the size and the time course of post-photoreceptoral responses, which were reflected by the significantly reduced amplitude and increased implicit time.

Figure 4-34. Peptide5 has close sequence homology with other connexin proteins in addition to Cx43.

4.4.3 Connexin mimetic peptide may act by suppressing glia/monocyte-mediated inflammatory responses

The RPE and choroid respond quickly to intense light exposure and in this study we validated the animal model in Chapter 3, showing that the oxidative stress and inflammatory response peaks in the RPE/choroid before the retina. Other studies have demonstrated that intense light exposure results in large numbers of phagosomes accumulating in the RPE, which is closely associated with the formation of lipofuscin (Ng *et al.*, 2008). Blue light induces mitochondrial oxidative DNA damage in human RPE cells (Godley *et al.*, 2005). However, the number of Iba-1 immuno-labelled microglia is significantly increased in the

aging mouse RPE/choroid compared to young animals (Xu *et al.*, 2008b). This damage in the RPE/choroid was thought to initiate or accelerate neuronal cell death processes in the retina following light damage. Up-regulation of Cx43 was found in this area of the RPE/choroid too (Figure 3-7 and Figure 3-8 in Chapter 3). The administration of Cx43 mimetic peptide, peptide5, significantly suppressed the macrophage-mediated inflammatory response in the choroid (Figure 4-27 and Figure 4-29C&D). The reduced inflammatory response may provide support for a healthier microenvironment in the retina and improve neuron survival rate, especially of rod photoreceptors which are more susceptible to cell damage (Tanito *et al.*, 2007). This enhanced survival of rod photoreceptors and other inner retinal neurons was reflected in the significantly improved amplitudes of rod PIII and PII in ERG recordings.

Although the adult retina is regarded as an immune-privileged tissue, it has residential glial cells to provide support and protection of the retinal neurons by supplying nutrients, removing neural waste products, and phagocytosis of neuronal debris (Coorey *et al.*, 2012). Müller cells, astrocytes and microglia are the three major types of glial cells in the retina (Coorey *et al.*, 2012). Findings from Chapter 3 and other previous studies have shown that the glial cells are activated following light damage (Ng & Streilein, 2001; Rutar *et al.*, 2010; Santos *et al.*, 2010). Activated microglia may release neurotoxic factors, which may induce neurons to start or continue the cell death process (Marín-Teva *et al.*, 2012). Abundant free radical nitric oxide (NO) and reactive nitrogen oxides have been detected from activated microglia and have been suggested to be neurotoxic agents involved in neurodegenerative diseases (Boje & Arora, 1992; Chao *et al.*, 1992). Peptide5 resulted in reduced GFAP immunoreactivity which was associated with astrocyte activity in the retina (Figure 4-28), and prevented microglia activation and migration into the nuclear layers (Figure 4-29A&B). This suppressed glia-mediated inflammatory response that may diminish the amount of neurotoxins released from activated glial cells and therefore, lead to an increased neuronal survival rate.

It remains unclear how exactly the Cx43 mimetic peptide works on the retina, RPE and choroid to diminish the inflammatory response. The peptide may work on the hemichannels located on glial cells or macrophages directly to control neurotoxic release from these cells.

Cx43 hemichannels have been identified on cytoplasmic processes of the glial cells (Hofer & Dermietzel, 1998; Goodenough & Paul, 2003) which are involved in ATP release and calcium waves during intercellular communication (Guthrie *et al.*, 1999). The calcium signalling is also freely transmitted from glial cells to other connexin-deficient neurons (Cotrina *et al.*, 2000). These findings support the mechanism that peptide5 may inhibit neurotoxic calcium signalling by blocking Cx43 hemichannels on the plasma membrane of these cells.

In addition, peptide5 may also work directly on RPE cells. The present study showed strong Cx43 immunoreactivity on the RPE in the light-damaged rats (Figure 3-8, Chapter 3). Similar to astrocytes, the ATP-mediated paracrine intercellular communication through Cx43 hemichannels also occurs in the RPE (Pearson *et al.*, 2005). RPE cells under oxidative stress increase the release of basic fibroblast growth factor (bFGF), which could lead to sustained pathological angiogenesis in the choroid (Eichler *et al.*, 2008). An increase in the secretion of pro-inflammatory factors, including Interleukin-1 beta (IL-1β), IL-6, tumour necrosis factor-alpha (TNF-α) and granulocyte macrophage-colony stimulating factor (GM-CSF) has been found in stressed RPEs (Ma *et al.*, 2009b). The Cx43 mimetic peptide may support the RPE in maintaining its normal function by blocking hemichannels.

4.4.4   Better effects with earlier administration of the mimetic peptide

The peptide started to work at 2 hours after the onset of light damage when comparing the result from different treatment strategies. An extra injection at 2 hours after the start of light damage significantly improved responses from both cone and rod pathways with comparison of the data from Strategy B to the single injection result. A previous study has demonstrated that the tissue damage process and cellular apoptosis are detectable in the rats within short-term (2 hours) light damage (Yu *et al.*, 2007). Results from the present study indicated that the mimetic peptide started to protect the retinal neurons even when the injury level was low. Therefore, the earlier the mimetic peptide is given following the onset of tissue injury, the better the neuronal protective effects that could be achieved.

An additional dose, such as two injections after 24 hours light damage in rats treated with Strategy C might also result in better retinal function. Several studies have shown that the tissue damage process, such as enhanced glial activity, is on-going even after more than seven days following the light damage (Noell *et al.*, 1966; Marc *et al.*, 2008; Xu *et al.*, 2008a; Rutar *et al.*, 2010). Further suppression of the inflammatory response by extra administrations of the Cx43 mimetic peptide may offer better protection to the retinal neurons from stress. This is especially so as the peptides used in this study were unmodified. There is little data available on their stability but unmodified peptides usually have a fairly short half-life.

In summary, findings from the present study support the idea that locally blocking Cx43 hemichannels using the Cx43 mimetic peptide, peptide5, can significantly improve the function of neurons in the rod phototransduction pathway in the light-damaged animal model. The enhancement of neuronal function may be achieved through suppressing the glia-mediated inflammatory response by blocking Cx43 hemichannel opening in activated glial cells in the retina and macrophages in the choroid. They may also be playing a role in maintaining choroid vascular integrity. The correct timing and dose of mimetic peptide delivery are important and these are yet to be fully determined. The mimetic peptide also inhibited the response from the cone pathway which could be caused by non-specific blocking to other connexin isoform hemichannels on cone horizontal cells. Improving the specificity of the mimetic peptide to Cx43 may eliminate this side-effect.

Chapter 5: Characterisation of gap junction protein connexin43 expression, oxidative stress and inflammation in human age-related macular degeneration

5.1   Introduction

Age-related macular degeneration (AMD) clinically presents as central vision loss. Central vision contributes to detailed vision tasks such as reading and face recognition. AMD is molecularly characterised by the extracellular accumulation of deposits between the pigment epithelium and the choroid, called drusen. During early AMD, drusen can be hard with distinct margins, which represents the dry form of AMD. Subsequently, choroidal neovascularisation develops and is accompanied by increased vascular leakage, characteristic of wet AMD (de Jong, 2006). Clinically, early stage AMD exhibits a few medium-sized drusen or retinal pigment abnormalities (Jager *et al.*, 2008). The late phase of AMD is classified into three stages: retinal pigment epithelial detachment (PED), geographic atrophy (GA) and choroidal neovascularisation (CNV) (Bird, 2010). Patients with drusen do not necessarily have much vision loss (Bird, 2010). GA is the late stage of dry AMD (Biarnés *et al.*, 2011). GA is characterised by one or several well-defined areas of retinal pigment epithelium (RPE) and photoreceptor atrophy. GA tends to progress with time and CNV can be developed. CNV is characterised by drusen deposition, subretinal and choroidal haemorrhage, and fibrotic scaring (Jager *et al.*, 2008).

AMD is the major cause of blindness in people aged 75 years or older in developed countries and the third cause of blindness in the world, following cataract and glaucoma (Klaver *et al.*, 1998b; Biarnés *et al.*, 2011). A population study conducted in 1982 showed a prevalence of 6.4% AMD among people aged 65 years and older in Gisborne, New Zealand and an increasing prevalence with age (Martinez *et al.*, 1982). A recent study reported that the prevalence of late stage AMD in people in their 70s is 1.4%, 5.6% in people in their 80s, and 20% in people in their 90s (Rudnicka *et al.*, 2012). In addition to age, studies have shown that many other risk factors also contribute to triggering of AMD. Genetic influences on AMD are well recognised. A similar incidence of AMD in monozygotic twins has been reported, suggesting a close link between heredity and AMD (Meyers & Zachary, 1988; Klein *et al.*, 1994; de Jong, 2006). Some genes, such as apolipoprotein E (apoE), complement factor H (CFH or HF1), factor B (BF) and complement component 2 (C2) have

been identified as contributing to the onset of AMD (Klaver *et al.*, 1998a; Edwards *et al.*, 2005; Haines *et al.*, 2005; Klein *et al.*, 2005; de Jong, 2006; Gold *et al.*, 2006). External factors, such as smoking were also identified as a significant risk factor for AMD (Thornton *et al.*, 2005; Biarnés *et al.*, 2011). In New Zealand, 26.8% of all registered cases of AMD-caused blindness are associated with current or past smoking history (Wilson *et al.*, 2001). Studies, including a 28,000-case study carried out in Britain have reported a significant risk of developing AMD in smokers compared to non-smokers (Evans *et al.*, 2005; Khan *et al.*, 2006). Increased exposure to sunlight over a lifetime may be another risk factor. It is hard to measure the amount of sunlight exposure in the human population, and there is no certainty as to when light exposure is important during the lifespan (Evans, 2001). Therefore, the link between sunlight exposure and AMD has always been controversial. The Blue Mountain Eye study has reported that there is an association between blue iris colour and late stage AMD (Mitchell *et al.*, 1998). However, the five- and ten-year longitudinal data from the same study have not shown a significant association between iris or hair colour and incidence of AMD (Wang *et al.*, 2003; Pham *et al.*, 2009), though the ten-year study suggested a link between skin sensitivity to sunburn and late stage AMD (Pham *et al.*, 2009). Nonetheless, a recent review has concluded that increased sunlight exposure may increase the risk of AMD (Sui *et al.*, 2012).

Oxidative stress, caused by reactive oxygen species (ROS) or reactive nitrogen species (RNS) has long been considered to be a major factor in the aging process (Haigis & Yankner, 2010). ROS is generated from many sources under physiological conditions, including NADPH-dependent membrane-bound enzymes, mitochondrial metabolism of oxygen during normal cellular activities, and other intracellular oxidases (Finkel, 2011). Cells also possess several antioxidant enzymes to remove ROS, such as superoxide dismutase, which reduces O^{2-} to H_2O_2, catalase, and glutathione peroxidase, which reduces H_2O_2 to H_2O (Finkel, 2011). In the retina, especially the macula, high levels of ROS are generated as a result of rhodopsin bleaching for light signal transduction and cellular metabolism (Beatty *et al.*, 2000; Handa, 2012). This high oxygen consumption coupled with long periods of exposure to light leads to oxidative stress in the RPE, which is responsible for the phagocytosis of photoreceptor outer segments. This, therefore, may result in the

formation of lipofuscin, a lipid-protein aggregate (Beatty *et al.*, 2000; Kinnunen *et al.*, 2011). Lipofuscin is also called "age-pigment" and correlates with a variety of age-related diseases (Beatty *et al.*, 2000; Handa, 2012). In addition to ROS, nitric oxide (NO) is another cytotoxic molecule which is associated with the pathogenesis of AMD. It is mainly produced by nitric oxide synthases (NOSs) located in endothelial cells and perivascular nitrergic neurons (Alderton *et al.*, 2001).

Residential glial cells provide support and protection of retinal neurons by supplying nutrients, removing neural waste products and phagocytosis of neuronal debris (Coorey *et al.*, 2012). There is accumulating evidence that glial activation is playing a key role in pathogenesis of AMD (Madigan *et al.*, 1994; Gupta *et al.*, 2003; Sullivan *et al.*, 2003; Wu *et al.*, 2003; Ding *et al.*, 2009). In AMD donor tissue, microglia have been shown to be enlarged, amoeboid-shaped, and to migrate from the inner retina to the outer retina and subretinal space (Gupta *et al.*, 2003; Buschini *et al.*, 2011). Increased glial fibrillary acidic protein (GFAP)-immunoreactivity is associated with AMD, and Müller cells express GFAP in both early (retinal pigment epithelium detachment) and late stages (geographic atrophy) of dry AMD (Wu *et al.*, 2003). These activated glial cells release neurotoxic factors, such as NO, which has been suggested to be a neurotoxic agent involved in a range of neurodegenerative diseases (Boje & Arora, 1992; Chao *et al.*, 1992).

Gap junction proteins, also called connexins, form a conduit for intercellular communications, allowing rapid exchange of secondary messengers between neighbouring cells. Each channel is formed by two connexons (hemichannels), one contributed by each of the neighbouring cells. The proper intercellular exchange rate is critical for ion homeostasis within neuronal cells and keeping their physiological function and survival. For example, sustained increases in calcium levels within cells caused by over influx of calcium into the cells may lead to mitochondrial toxicity and cell death. The capacity of calcium channel blockers to protect photoreceptors has been recognised (Kelsell *et al.*, 1997). In general, the undocked hemichannels remain closed after their assembled on the cytoplasm membrane. Opening of these undocked hemichannels, under some conditions, leads to cytoplasm

membrane depolarisation and small molecule leakage from the cytoplasm. When these undocked hemichannels are active and open, they may perform diverse functions in various cell types and tissues (Goodenough & Paul, 2003).

Connexin43 (Cx43) is encoded by the Gja1 gene and it is the most ubiquitously expressed connexin protein in mammalian embryos and adults (Kerr *et al.*, 2010). Increased Cx43 protein and/or transcript expression have been found in many human central nervous system injuries and diseases, including stroke, epilepsy and Huntington's disease (Elisevich *et al.*, 1997; Vis *et al.*, 1998; Nakase *et al.*, 2006). In human retinas from donors with glaucoma, Cx43 immunoreactivity is increased in the optic nerve head and retina compared with the tissue from normal donors (Kerr *et al.*, 2011). Modulation of Cx43 hemichannel function with a mimetic peptide has been shown to improve neuronal survival following traumatic and ischaemic injury to the retina, brain and spinal cord in animal models (O'Carroll *et al.*, 2008; Danesh-Meyer *et al.*, 2012; Davidson *et al.*, 2012a; O'Carroll *et al.*, 2013).

Despite greater understanding of the pathology of AMD, there is currently no efficient or effective treatment. Therefore the aim of the current study was to investigate changes in oxidative stress, glia-mediated inflammatory responses and expression of Cx43 in the human retina that could indicate potential therapeutic targets for the disease.

5.2   Materials and methods

5.2.1   Human donors and tissue preparation

Three post-mortem human eyes with a diagnosis of age-related macular degeneration (AMD) with no previous treatment for the disease and three eyes from age-matched normal donors with no recorded ocular disease (subject demographics described in Table 2-2, Chapter 2) were obtained from the New Zealand National Eye Bank (Auckland, New Zealand). All human eyes were handled in accordance with the tenets of the Declaration of Helsinki and approved by the Institutional Review Committee of the University of Auckland and Northern District Human Ethics Committee. There was no known infection or sepsis in any of the donors at the time of death. The cause of death for all donors was not related to a head injury. Eyes were enucleated within 48 hours after death and processed as described in detail in Section 2.6, Chapter 2. Sections comprising central and peripheral retina were processed for analysis.

5.2.2   Toluidine blue staining

Toluidine blue staining was employed to show the human AMD tissue histological structure. The detailed procedure is introduced in Section 2.4.1, Chapter 2. In brief, the sections were stained for 2-3 minutes with 1 mg/mL toluidine blue solution prepared in MilliQ water. This was followed by washes in 0.1 M PBS. Finally, the stained tissue sections were coverslipped and images were taken immediately after the staining procedure, using a bright field microscope.

5.2.3 Immunohistochemistry

The procedure was conducted as explained in Chapter 2. Briefly, after hydration, sections were blocked with a solution containing 6% normal goat serum or donkey serum (Invitrogen, USA), 1% bovine serum albumin (BSA) and 0.5% triton X-100 in 0.1 M PBS for 1 hour at room temperature. The tissues were immuno-labelled with primary antibodies, including mouse anti-nitrotyrosine, goat anti-Iba1, rabbit anti-Cx43, goat anti-superoxide dismutase-1 antibody, mouse anti-8-oxoguanine antibody and rabbit anti-CD31 antibody, as specified in Table 2-1, Chapter 2. Tissue sections were incubated with the primary antibody overnight at room temperature. The secondary antibodies were diluted 1:500 and were applied for 2 hours in the dark at room temperature. Slides were rinsed several times in 0.1 M PBS, mounted in non-fluorescence fading medium and sealed. The labelled sections were viewed and imaged using confocal microscopy.

5.2.4 Imaging

All the images were acquired from immuno-labelled sections using a high-resolution laser scanning confocal microscope (Olympus FluoView FV1000, Japan) with 488 nm and/or 594 nm excitation from an argon ion laser. A series of 4-8 optical sections with 1 µm intervals were collected for each specimen and image analysis was performed on a stack image of intensity projection over the z-axis. Six retinas obtained from different animals were analysed for each group, and the representative images shown.

5.3 Results

5.3.1 Pathological changes were regional in AMD donor's tissue

Transverse sections stained with toluidine blue revealed a pathological morphology in the AMD affected tissue (Figure 5-1 and Figure 5-2). Low magnification observation of the tissue from an advanced dry AMD donor showed a large pale region in the macula (Figure 5-1A). Other regions were comparable with the control tissue (data not shown). The toluidine blue stained sections showed that the lesions in AMD were regional (Figure 5-1 and Figure 5-2). Four different areas were analysed in this study: the temporal peripheral area, the macular drusen area, the central drusen-free area and the nasal drusen area (Figure 5-1B-E). Image of transverse tissue section at lower magnification is shown in Figure 5-2.

The analysis of the temporal peripheral area revealed normal morphology of the retina, retinal pigment epithelium (RPE) and Bruch's membrane (Figure 5-1B). The macular drusen was large and comprised scar tissue. It was located between the retina and the choroid (asterisks in Figure 5-1C and Figure 5-2), and mainly contained fibrocytes and blood vessels, while no remaining RPE or Bruch's membrane evident in this area. The retina had severely degenerated and showed damage extending from the outer nuclear layer to the inner nuclear layer (Figure 5-1C, arrows). Only the ganglion cell layer and nerve fibre layer displayed normal morphology (Figure 5-1C). In the central drusen-free retinal area, the RPE and Bruch's membrane were intact. The retina showed some degeneration in the outer and inner nuclear layers (Figure 5-1D, arrows). Some enlarged retinal blood vessels were also evident in this area (Figure 5-1D, arrow heads). In the nasal drusen area, some isolated drusen were detected between the RPE and Bruch's membrane (Figure 5-1E, arrows), while the retinal layers had a normal histological morphology.
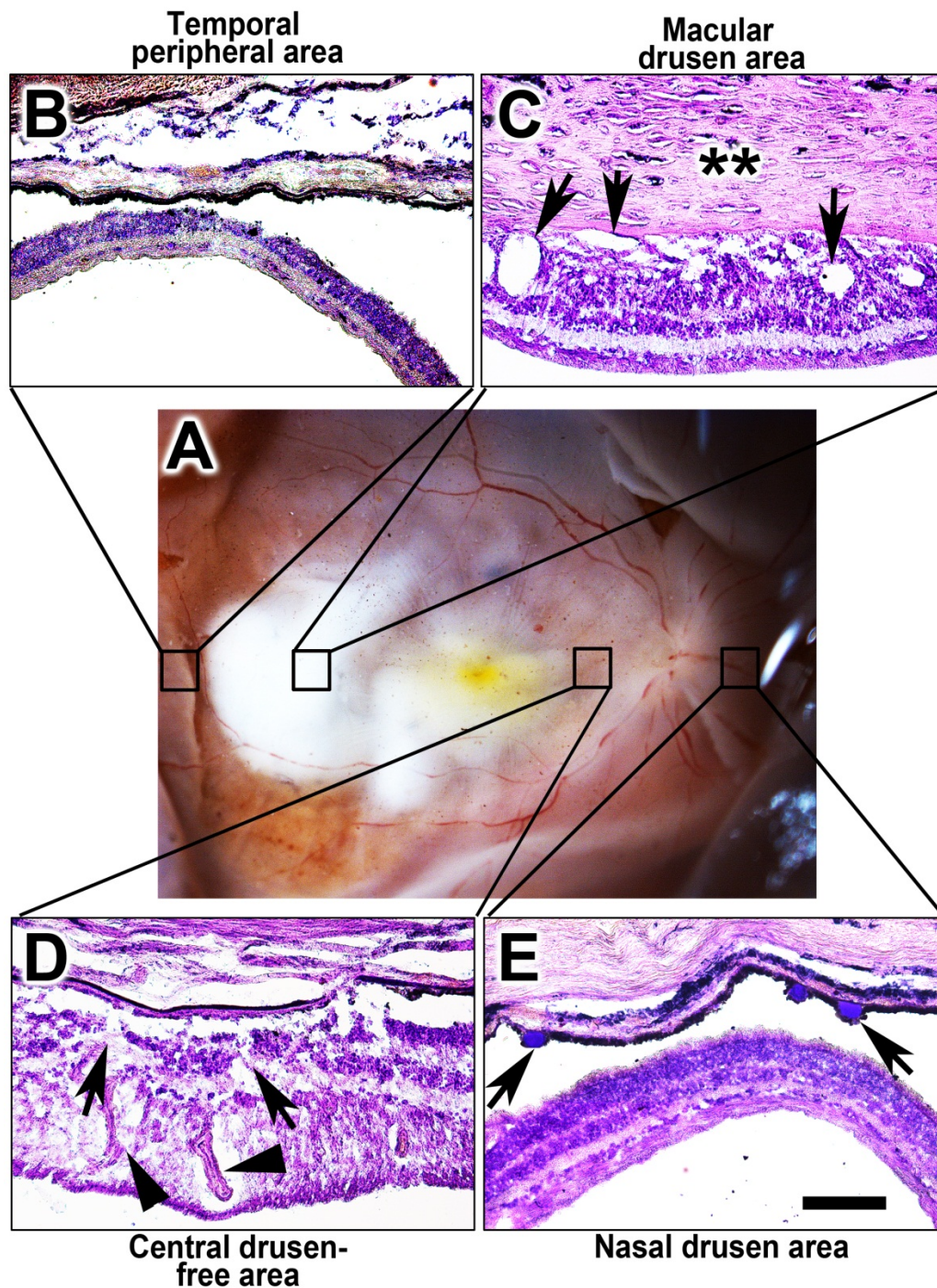
Figure 5-1. Images of toluidine blue staining show regions associated with pathological changes in AMD affected ocular tissue. **A:** View of the posterior pole from an AMD donor eye showing pathological areas. **B:** Temporal peripheral area of the eye showing no obvious morphological changes. **C:** Macular drusen area showing a very large scar (**) between the retina and the choroid as well as obvious neuronal degeneration (arrows). There was no RPE or Bruch's membrane in this area. . **D:** Central drusen-free area near the optic nerve, showing intact RPE and Bruch's membrane and degeneration sites (arrows) and more blood vessels in the retina (arrow heads). **E:** The nasal drusen area showed isolated drusen between the RPE and Bruch's membrane (arrows). Scale bar = 100 μm.
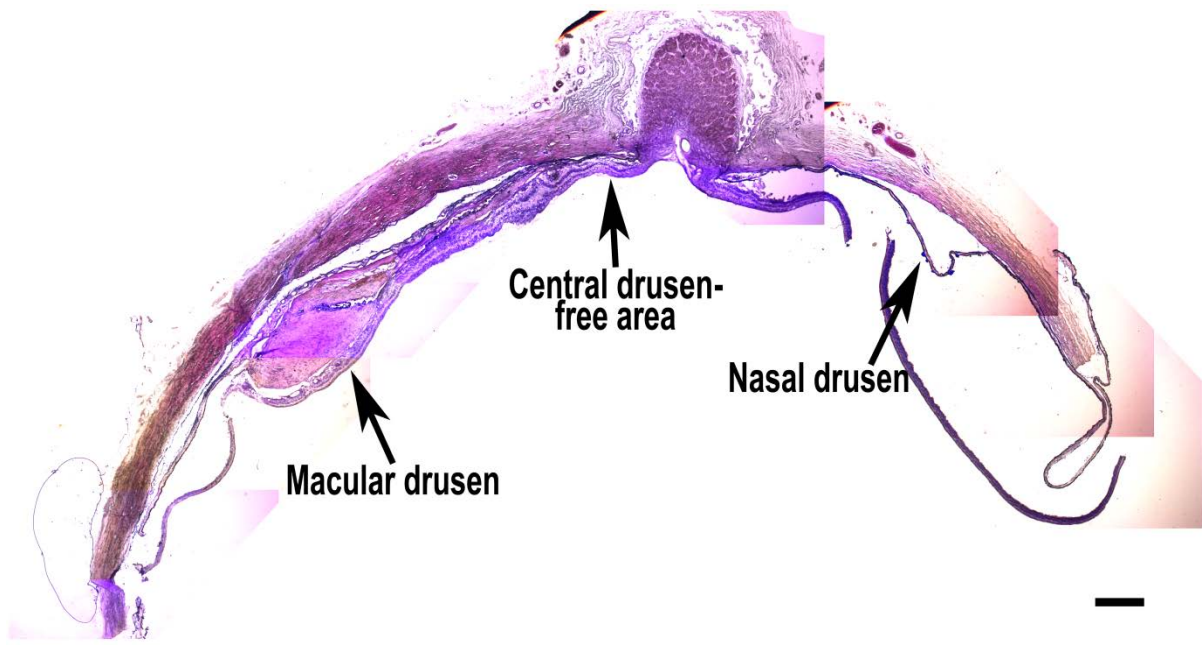
Figure 5-2. Transverse tissue section stained with toluidine blue showing the various regions associated with pathological changes in AMD affected donor tissue. A large drusen is seen in the macula, and small, isolated drusen are present to the nasal side of the eye. Scale bar = 1 mm.

5.3.2 Increased Cx43 immunoreactivity was detected in AMD retina, predominantly in the central drusen-free area

To investigate the expression level of Cx43 in different regions in AMD affected donor retinas compared to the control tissue, immunohistochemistry was performed using an anti-Cx43 antibody. In the control retina, Cx43 was evenly distributed in the nerve fibre layer and ganglion cell layer along the whole tissue (Figure 5-3 and Figure 5-4). Cx43 immunoreactivity was also identified on retinal blood vessels (Figure 5-4). The intensity of labelling was not different between the central and peripheral areas (Figure 5-4).

In AMD affected donor tissue, there was a general increase in the level of Cx43 immunoreactivity (Figure 5-5). In areas of macular drusen, temporal periphery and nasal drusen, Cx43 immunoreactivity was mainly associated with blood vessels in the nerve fibre

layer and ganglion cell layer (Figure 5-6A, G and J), and comparable with both central and peripheral areas in the control retina (Figure 5-4). Interestingly, in the central drusen-free area of the AMD retina, Cx43 immunoreactivity was much higher compared with other regions shown obviously in the low magnification image (Figure 5-5). High magnification image showed that increased Cx43 expression expanded from the nerve fibre layer and ganglion cell layer into the inner plexiform layer and inner nuclear layer (Figure 5-6D, arrows).
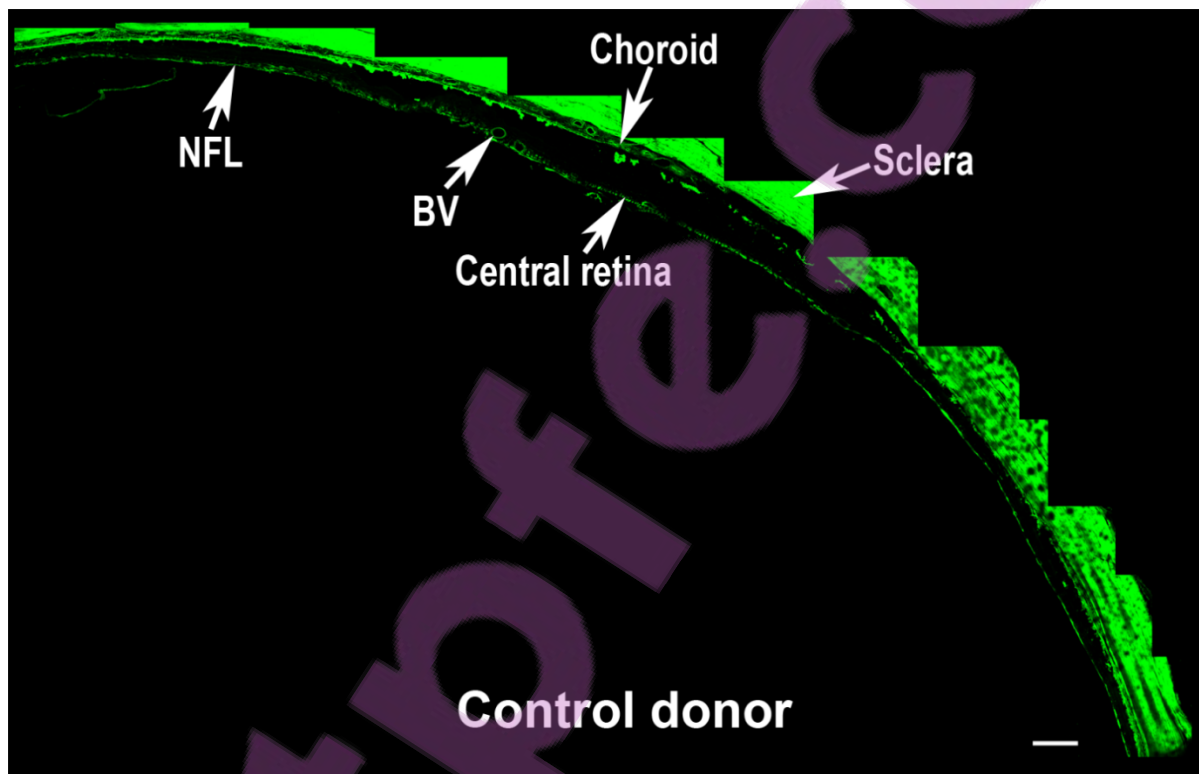
Figure 5-3. Montaged confocal images showing Cx43 labelling in the control donor's tissue. In the retina from control donor, Cx43 immunoreactivity was evenly distributed in the nerve fibre layer (**NFL**). Retinal blood vessels (**BV**) were also labelled. Scale bar = 400 µm.
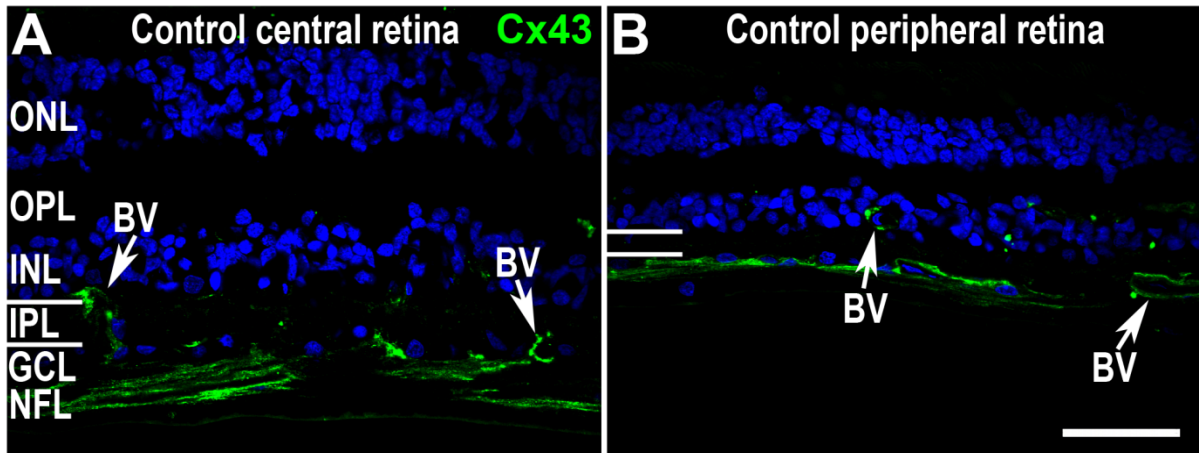
Figure 5-4. Cx43 immunoreactivity in control human retina. **A:** The central retina from a control donor showed Cx43 labelling mainly in the nerve fibre layer (NFL) and was associated with retinal blood vessels. **B:** The peripheral control retina showed a similar intensity of Cx43 immunoreactivity in the NFL to the central area (**A**). Abbreviations: **ONL**, outer nuclear layer; **OPL**, outer plexiform layer; **INL**, inner nuclear layer; **IPL**, inner plexiform layer; **GCL**, ganglion cell layer; **NFL**, nerve fibre layer; **BV**, retinal blood vessels. Scale bar = 50 µm.
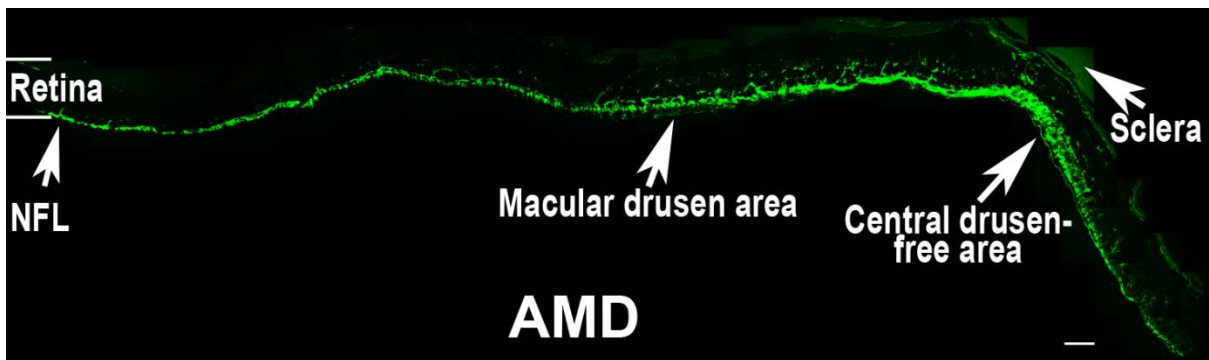
Figure 5-5. Montaged confocal images showing Cx43 labelling in AMD affected donor tissue. In the retina from an AMD donor, Cx43 immunoreactivity was mainly associated with nerve fibre layer (NFL) and was increased in the central drusen-free area, compared to other areas in the same piece of tissue. Scale bar = 400 µm.
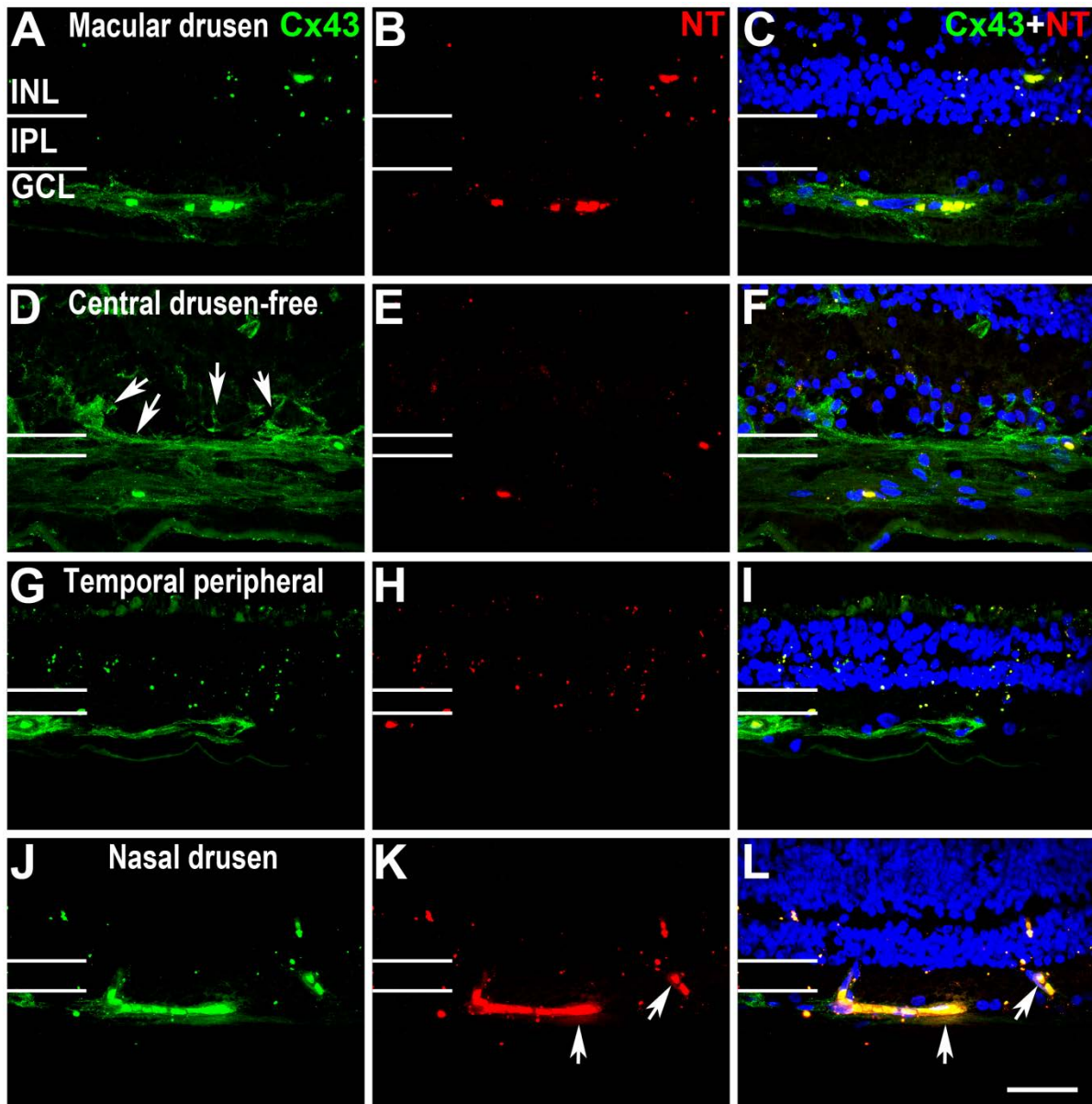
Figure 5-6. Confocal images showing Cx43 and nitrotyrosine in different areas of the retina from AMD affected donor retina. A-C: In the macular drusen area, Cx43 immunoreactivity was mainly associated with blood vessels in the GCL and NFL (**A**), and no nitrotyrosine labelling was detected (**B**). **D-F:** In the central drusen-free area, a higher level of Cx43 immunoreactivity was shown associated with GCL and IPL (**D, arrows**), and no nitrotyrosine labelling was seen in this area (**E**). **G-I:** In the temporal peripheral area, Cx43 labelling was limited to the GCL and NFL (**G**), and no nitrotyrosine labelling was shown in this area (**H**). **J-L:** In the nasal drusen area, Cx43 immunoreactivity was associated with blood vessels in the GCL (**J**), and it was co-localised with nitrotyrosine (**K&L, arrows**). **A, D, G and J:** Cx43 immunoreactivity **B, E, H and K:** Nitrotyrosine immunoreactivity; **C, F, I and L:** Double labelling with Cx43 and nitrotyrosine and DAPI was used to indicate the retinal layers. Abbreviations: **INL**, inner nuclear layer; **IPL**, inner plexiform layer; **GCL**, ganglion cell layer; **NFL**, nerve fibre layer. Scale bar = 50 µm.

5.3.3 Nitrotyrosine, an oxidative stress marker associated with endothelial cells, was specifically seen in AMD affected retina

Nitrotyrosine, a marker for endogenous nitrosation and nitration, has been used to quantify oxidative stress in blood and tissue (Ohshima *et al.*, 1990). In the present study, nitrotyrosine was employed to investigate damage from reactive nitrogen species (RNS). Nitrotyrosine immunoreactivity was only detected in AMD affected retinas (Figure 5-6) and did not show any labelling in the tissue from control donors (Figure 5-7). The specific nitrotyrosine labelling in AMD retina was only detected in the nasal drusen area (Figure 5-6K), where it co-localised with the endothelial cell marker, CD31 (Figure 5-8A-C). None of the other areas in AMD affected retinas showed immunoreactivity to nitrotyrosine (Figure 5-6B, E&H and Figure 5-8D-F). Interestingly, this nitrotyrosine immunoreactivity also co-localised with Cx43 immunoreactivity (Figure 5-6J-L).
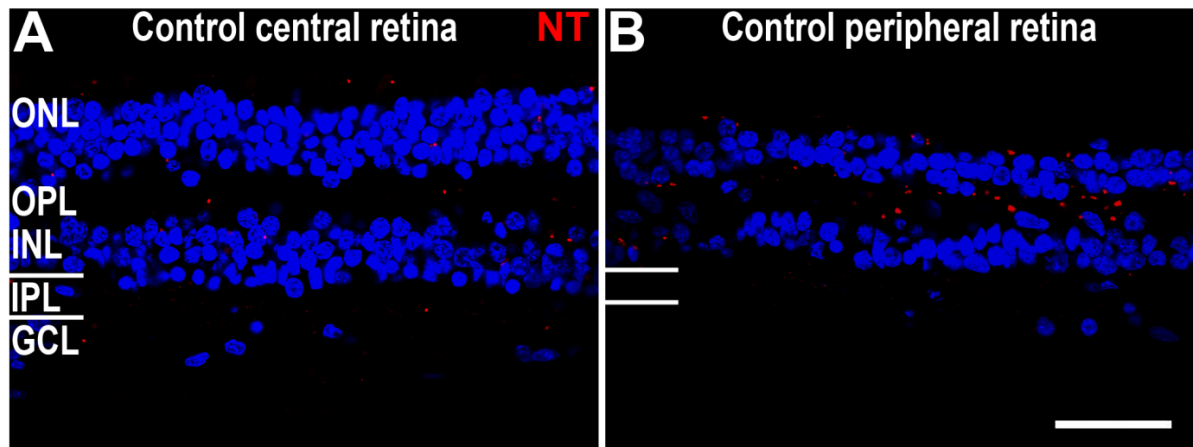
Figure 5-7. The retina from a control donor retina was the absent of nitrotyrosine immunoreactivity. Both the central area (**A**) and the peripheral area of the control retina (**B**) did not show any nitrotyrosine labelling. The red dots on the images are the pigment from the retinal pigment epithelium displaced during tissue processing and cryosectioning. These pigments are nonspecific and can be visualised through all the confocal channels. Abbreviations: **ONL**, outer nuclear layer; **OPL**, outer plexiform layer; **INL**, inner nuclear layer; **IPL**, inner plexiform layer; **GCL**, ganglion cell layer. Scale bar = 50 μm.
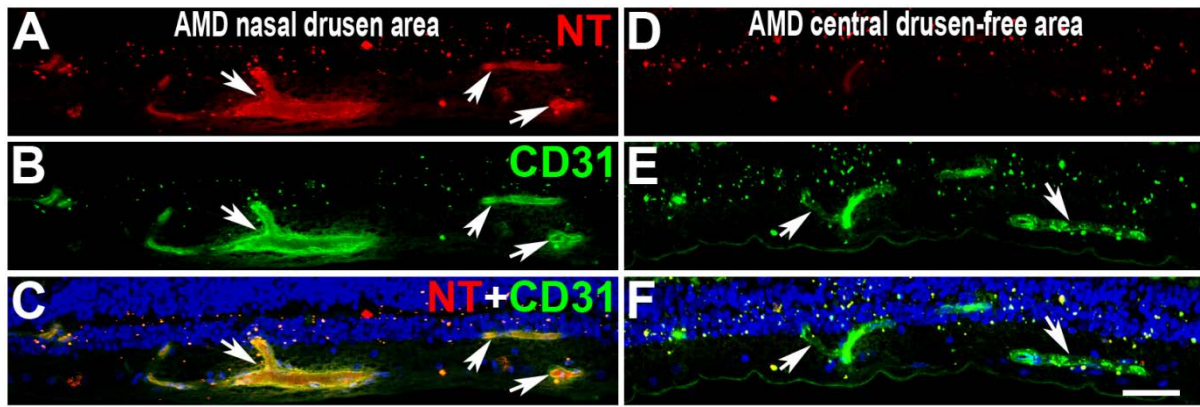
Figure 5-8. Co-localisation of nitrotyrosine with endothelial cells in the nasal drusen area of AMD retina. **A-C:** In the nasal drusen area of AMD retina, nitrotyrosine immunoreactivity was detected along blood vessels (**A**) which were identified with CD31 labelling (**B**). Double labelling of nitrotyrosine and CD31 showed the co-localisation of these two markers (**C**). **D-F:** In the central drusen-free area, no nitrotyrosine immunoreactivity was detected (**D**). The CD31-labelled retinal blood vessels (**E**) had no nitrotyrosine labelled (**F**). The red dots on the images of nitrotyrosine labelling are the pigment from the retinal pigment epithelium displaced during tissue processing and cryosectioning. These pigments are nonspecific and can be visualised through all the confocal channels. Abbreviations: **NT**, nitrotyrosine. Scale bar = 50 µm.

In addition to nitrotyrosine, two other oxidative markers, superoxide dismutase 1 (SOD-1) and 8-oxoguanine (8-oxoG) were used to assess different aspects of oxidative damage. SOD-1 is an antioxidant enzyme, which facilitates the dismutation of oxygen radicals to hydrogen peroxide and reduces superoxide levels in cells (Rao *et al.*, 2008). In this study, SOD-1 immunoreactivity was seen in both central and peripheral retina from control donors (Figure 5-9A&B, arrows). The labelling was mainly in the inner retina, including the inner plexiform layer and ganglion cell layer (Figure 5-9A&B). The retina from an AMD affected donor showed a similar pattern of SOD-1 labelling (Figure 5-9C-E, arrows). There was no difference between the various areas of AMD affected retina, such as the macular drusen area, central drusen free area and nasal drusen area (Figure 5-9C-E).

8-oxoguanine (8-oxoG) is a DNA lesion product arising from oxidative stress (Hübscher & Maga, 2011) and was used in this study to assess nuclear damage from oxidative stress. 8-oxoG immunoreactivity was seen in the inner layers of the retina from control donors (Figure 5-10A&B, arrows). The central retina did not shown any difference to the peripheral retina (Figure 5-10A&B). In the retina from an AMD affected donor, 8-oxoG

188

immunoreactivity was also seen in the inner retina (Figure 5-10C-E, arrows) at similar levels to the control tissue (Figure 5-10A&B). The central drusen-free area showed slightly more labelling than other areas of the AMD retinal tissue (Figure 5-10D).
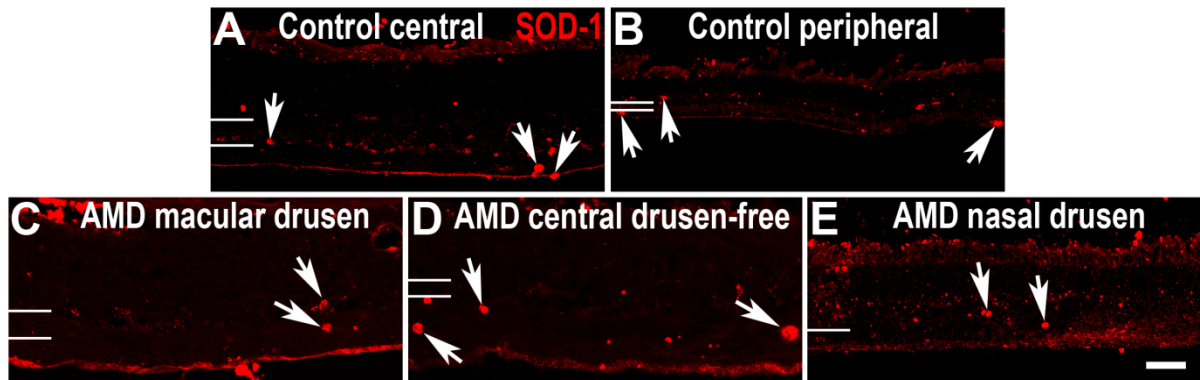
Figure 5-9. SOD-1 immunoreactivity in control and AMD retina. A-B: The central (**A**) and peripheral (**B**) area of the retina from a control donor showed SOD-1 immunoreactivity mainly in the inner retina. **C-E:** In the retina from an AMD affected donor, different areas including macular drusen area (**C**), central drusen-free area (**D**) and nasal drusen area (**E**) all showed similar inner retinal labelling of SOD-1. Scale bar = 50 µm.
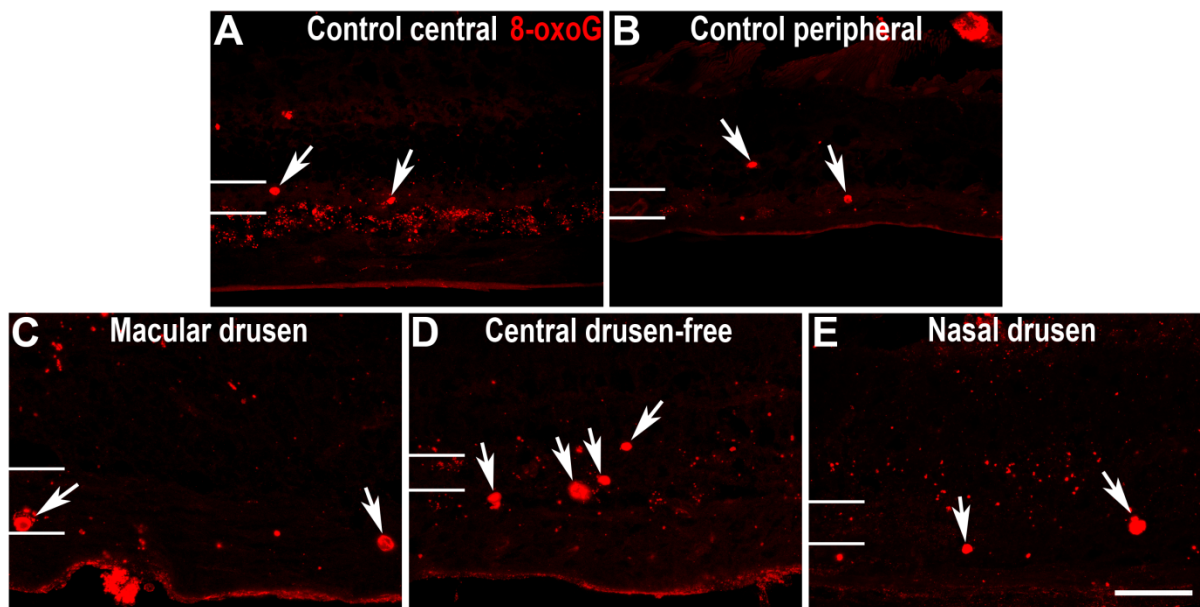
Figure 5-10. 8-oxoG immunoreactivity in control and AMD affected retina. A-B: The central (**A**) and peripheral (**B**) area of the retina from a control donor showed 8-oxoG immunoreactivity mainly in the inner retina. **C-E:** The retina from an AMD affected donor showed immunoreactivity to 8-oxoG was still mainly in the inner retina, with slightly enhanced labelling in the central drusen-free area (**D**). Scale bar = 50µm.

5.3.4. Changes in Cx43 immunoreactivity were closely associated with increased inflammatory responses in AMD affected retina

Glial fibrillary acidic protein (GFAP) is a specific marker of astrocytes (Trivino *et al.*, 1996) and reactive astrocytes are usually associated with increased expression of GFAP (Kaur *et al.*, 2008). GFAP immunoreactivity and its association were examined in the control and AMD affected donor tissue (Figure 5-11). In the aged, normal retina, GFAP immunoreactivity was limited in the inner retina. In the control central retina, GFAP was detected in the nerve fibre layer, ganglion cell layer and inner plexiform layer (Figure 5-11A), while it was only detected in the nerve fibre layer and ganglion cell layer in the control peripheral retina (Figure 5-11B). The GFAP immunoreactivity was associated with Cx43 labelling in the control tissue (Figure 5-11A&B). In the retina from an AMD affected donor, clearly enhanced GFAP immunoreactivity was evident mainly in the central retina. This included the macular-drusen area (Figure 5-11C) and the central drusen-free retina (Figure 5-11D) where GFAP labelling had expanded throughout all the retinal layers. This enhanced GFAP immunoreactivity was closely associated with increased Cx43 expression. The temporal peripheral area showed moderately increased GFAP immunoreactivity, as exhibited abnormally in the inner plexiform layer and the nuclear layers (Figure 5-11E). The nasal drusen area was the only area which showed normal GFAP immunoreactivity compared to the control tissue (Figure 5-11F).
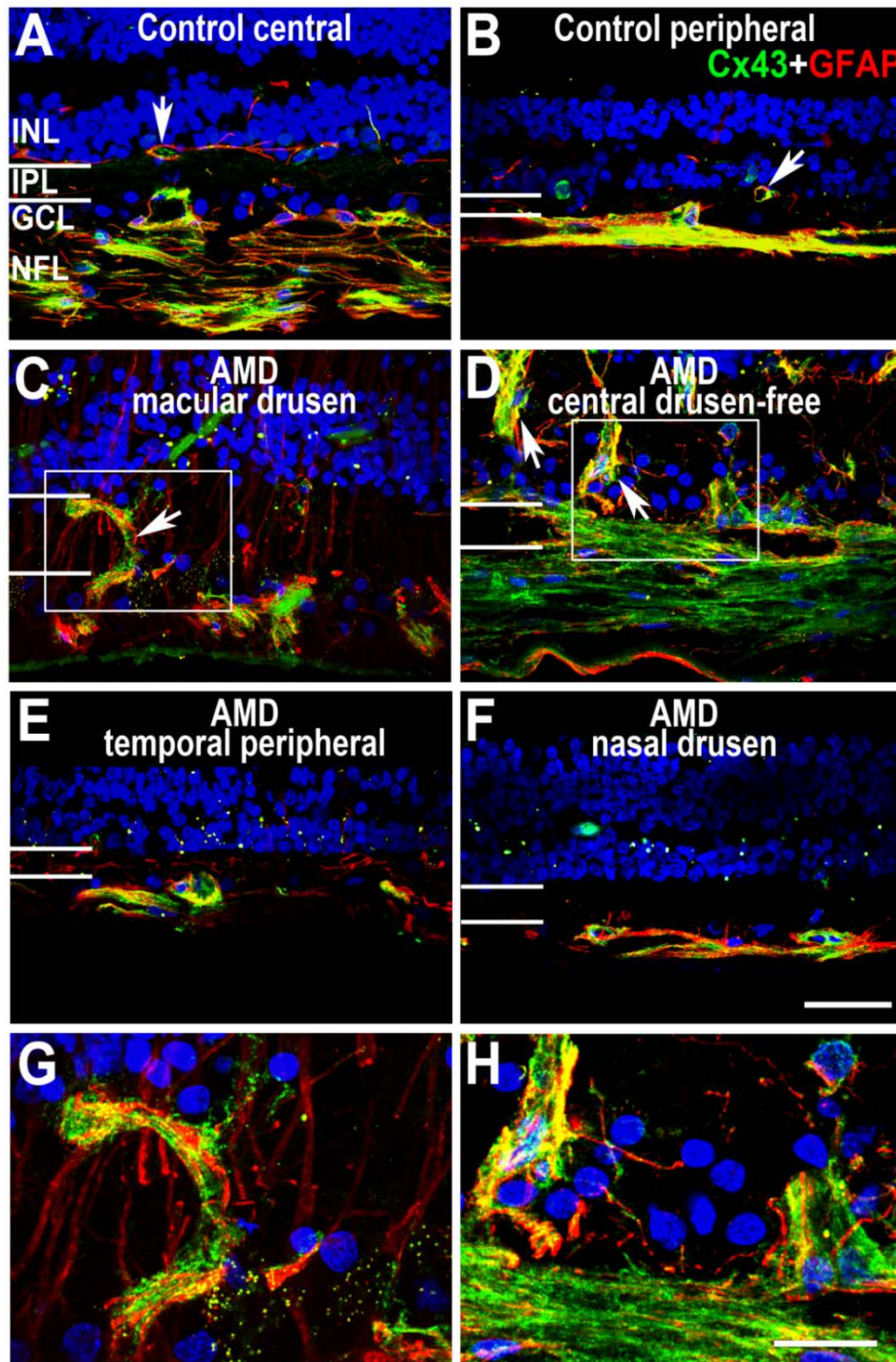
Figure 5-11. Confocal images showing double labelling of GFAP and Cx43 in control and AMD affected retina. A&B: Double labelling of GFAP (red) and Cx43 (green) in the central (**A**) and peripheral (**B**) retina from the control donor tissue. **C-F:** Double labelling of GFAP (red) and Cx43 (green) in the macular drusen (**C**), central drusen-free (**D**), temporal peripheral (**E**) and nasal drusen (**F**) areas in the retina from an AMD affected donor. **G&H:** Enlarged views of areas highlighted in C and D, respectively. DAPI (blue) was used to indicate the retinal layers. Abbreviations: **NFL,** nerve fibre layer; **ONL**, outer nuclear layer; **OPL**, outer plexiform layer; **INL**, inner nuclear layer. **A-F:** Scale bar = 50µm. **G&H:** Scale bar = 25 µm.

Ionised calcium-binding adaptor molecule-1 (Iba-1) is a marker for residential macrophages and microglia (Ahmed *et al.*, 2007). In the present study, it was used to investigate microglial activities in the control and AMD affected retinas. In the aged, normal retina, microglia were located in the ganglion cell layer, inner plexiform layer and the outer plexiform layer in both central and peripheral areas (Figure 5-12A&B). The microglial cells had the morphology of resting phase microglia with a smaller cell body and fewer processes (Damani *et al.*, 2011). In the retina from an AMD affected donor, only the nasal drusen area showed a similar location of Iba-1-labelled microglia to that of control tissue (Figure 5-12F). However, these cells had rounder and larger cell bodies, indicating they were in the activated phase (Figure 5-12F). The central drusen-free area showed the most microglia in the AMD affected retina. These cells were spread throughout all retinal layers and showed various morphologies (Figure 5-12D&G). Interestingly, fewer Iba-1-labelled cells were detected in the macular drusen area than the central drusen-free area in AMD affected retina (Figure 5-12C). The temporal peripheral area also showed activated microglia located in all layers of the AMD affected retina (Figure 5-12E&H).
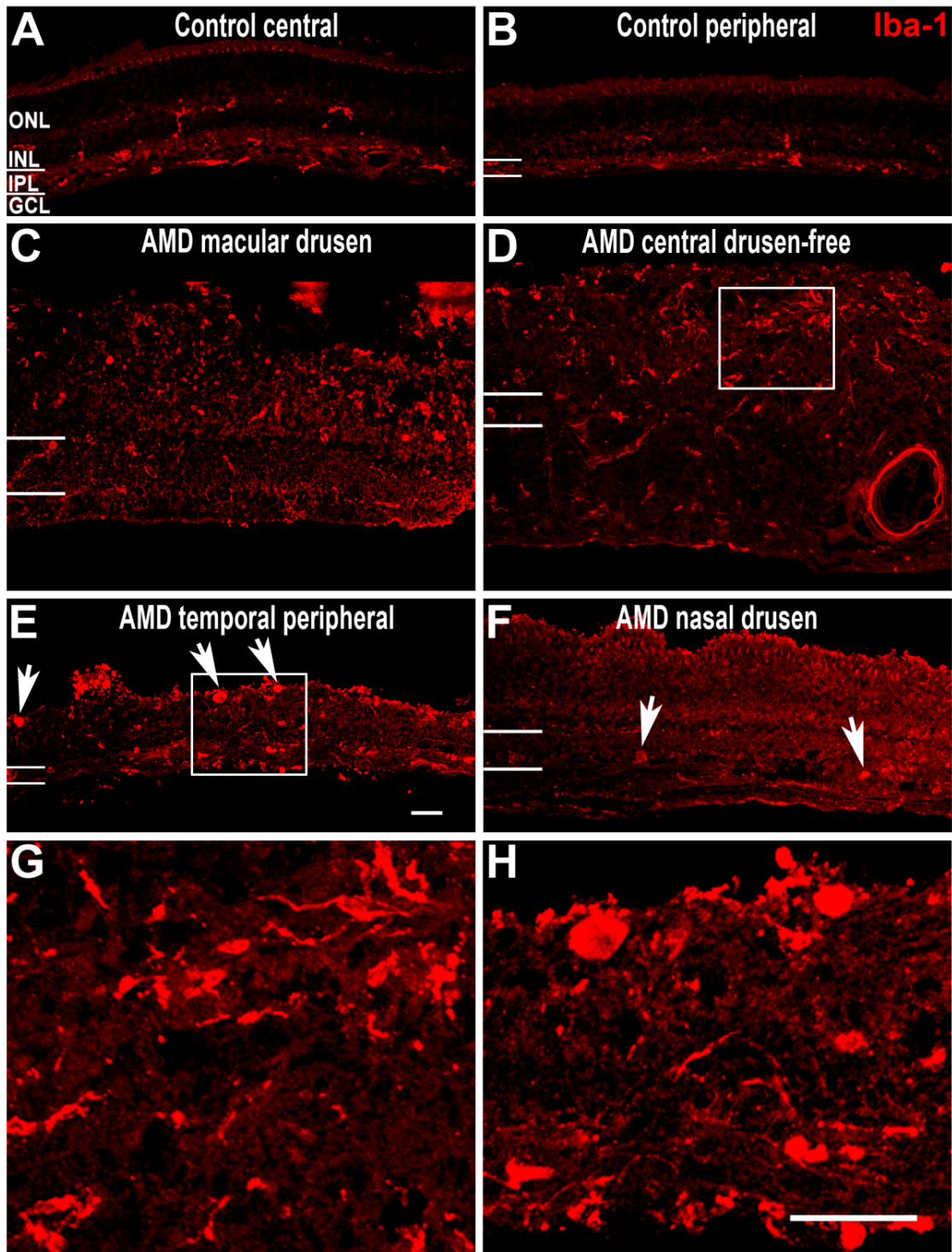
Figure 5-12. Confocal images showing Iba-1-labelled microglia in control and AMD affected retina. A&B: Retinal microglia labelled with Iba-1 in the central (**A**) and peripheral (**B**) retina from control donor tissue. **C-F:** Iba-1 immuno-labelling in the macular drusen (**C**), central drusen-free (**D**), temporal peripheral (**E**) and nasal drusen (**F**) areas in the retina from an AMD affected donor. **G&H:** Enlarged views of highlighted areas in **D** and **E** respectively. Abbreviations: **ONL**, outer nuclear layer; **OPL**, outer plexiform layer; **INL**, inner nuclear layer; **ONL,** outer nuclear layer. **A-F:** Scale bar = 50 µm; **G&H:** Scale bar = 25 µm.

5.4 Discussion

The current study has demonstrated that there were regional changes of increased oxidative stress and inflammation that were closely associated with increased expression of Cx43 in the retina from AMD affected donors. Although the macular area showed the most severe photoreceptor degeneration, this area did not reveal the strongest oxidative stress and inflammatory responses. It was the area surrounding the macula where there were still many surviving neurons that showed the maximum increased Cx43 immunoreactivity and glia-mediated inflammation.

5.4.1 Reactive nitric species are specific to the AMD condition

AMD is recognised as a vascular disease. Blood vessel changes are highly associated with pathogenesis and progress of the disease (Coorey *et al.*, 2012). In early stages of AMD, a greater number of non-functional retinal capillaries have been detected by histological methods and they have thicker vascular walls compared to those in the normal aged retina (Ramírez *et al.*, 2001). Nitric oxide (NO) is an important molecule for vasodilation in blood vessels. It is mainly produced by nitric oxide synthases (NOSs) located in endothelial cells and perivascular nitrergic neurons (Alderton *et al.*, 2001). Low expression of nitric oxide synthases (NOSs) in AMD leads to low production of NO and may contribute to the constriction of blood vessels (Bhutto *et al.*, 2010). Inflammatory mediators, such as bradykinin, induce NO synthesis through various pathways (Komarova & Malik, 2010). The present study has revealed that immunoreactivity to nitrotyrosine, a marker for endogenous nitrosation and nitration, was located on endothelial cells in the nasal drusen area of AMD affected retinal tissue (Figure 5-8) indicating blood vessels were under stress in that area. The stressed endothelial cells may cause dysfunction of the blood vessels and lead to further inflammation contributing to additional tissue damage (Bucci *et al.*, 2000).

194

In addition to nitrotyrosine, two other oxidative markers were used to analyse the oxidative stress in AMD affected donor tissue. One marker was superoxide dismutase 1 (SOD-1), which provides the first line of defence for reactive oxygen species (ROS)-induced damage. SOD-1-deficient (SOD-1$^{-/-}$) mice have drusen, choroidal neovascularisation and RPE damage (Imamura *et al.*, 2006), and they also exhibit progressively decreased amplitudes of a- and b-waveforms from electroretinogram (ERG) recording (Hashizume *et al.*, 2008). Pattern ERG results have shown that the ganglion cell function was significantly reduced in SOD-1$^{-/-}$ mice (Yuki *et al.*, 2011). Studies using SOD-1$^{-/-}$ mice have demonstrated that SOD-1 protects the retinal neurons from hypoxia-induced oxidative stress (Dong *et al.*, 2006). Results from the present study showed that SOD-1 immunoreactivity was mainly located in the retinal ganglion cell layer in both AMD affected donor tissue and the age-matched control tissue (Figure 5-9), suggesting its key role in protecting ganglion cells in human retinal tissue. There was no significant difference on the labelling intensity between AMD and control tissue, indicating no alteration on the expression level of SOD-1 in the human dry AMD condition.

8-oxoguanine (8-oxoG) is frequently generated and highly mutagenic DNA damage from guanine following oxidative stress (Mambo *et al.*, 2002; van Loon *et al.*, 2010). In retinas from aged donors with established maculopathy, mitochondrial DNA (mtDNA) deletion has also been found to be significantly higher in photoreceptors compared to a young healthy donor (Barron *et al.*, 2001). The mtDNA repair enzyme, 8-oxoguanine-DNA glycosylate 1 (OGG1) has been found to be decreased in the RPE in AMD donors compared to age-matched control donors (Lin *et al.*, 2011). 8-oxoguanine immunoreactivity was increased in the photoreceptor synaptic terminals in the albino rat retina following intense light exposure (Cortina *et al.*, 2005). The present study has demonstrated presence of 8-oxoguanine immunoreactivity in the ganglion cell layer and inner plexiform layer in both AMD affected and aged control retinas (Figure 5-10). An increased immunoreactivity was detected in the central drusen-free area in AMD affected retina indicating that oxidative stress promotes mitochondrial or nuclear DNA damage in this area.

5.4.2   AMD retina showed increased glia-mediated inflammatory responses

Residential glial cells of the retina include astrocytes, Müller cells and microglia (Coorey *et al.*, 2012). The activity of astrocytes has been analysed in this study on AMD affected donor tissue compared to the age-matched controls. Glial fibrillary acidic protein (GFAP) is a specific marker of astrocytes (Trivino *et al.*, 1996) and reactive astrocytes are usually associated with increased expression of GFAP (Kaur *et al.*, 2008). In the aged human retina, GFAP immunoreactivity is higher than that in younger age groups (Ramírez *et al.*, 2001). An early report has shown that GFAP immunoreactivity is associated with Müller cells in AMD affected donors, but absent in normal young and aged donor tissues (Madigan *et al.*, 1994). A later study has further clarified that increased GFAP immunoreactivity is associated with AMD, and Müller cells express GFAP in both early and late stages (geographic atrophy) of dry AMD (Wu *et al.*, 2003). The results from this study demonstrated consistent findings in AMD affected retina in the macular drusen area (Figure 5-11C). However, our results further indicated that small individual drusen on the nasal side may not necessarily be associated with enhanced GFAP immunoreactivity (Figure 5-11F). In contrast, the drusen-free areas, including central and temporal peripheral areas, showed moderately increased GFAP labelling (Figure 5-11D&E). These interesting results suggest that the macula-surrounding area, rather than the macula-affected area itself should be targeted as is more likely to react most favourably to inflammation-suppressing treatments. It may be too late to treat the affected areas but attention could be placed on reducing disease progression.

In addition to astrocytes, we also investigated microglial activity. The results from different areas of AMD affected retina were compared with astrocyte activity as shown by GFAP immunoreactivity. It is not surprising that macular drusen areas in AMD affected retina showed enhanced microglial activity, including amoeboid-shaped cell bodies and migration from the inner and outer plexiform layers to the outer nuclear layer and subretinal area. This is consistent with previous findings showing glial activation in the human AMD condition (Gupta *et al.*, 2003; Buschini *et al.*, 2011) and supports the idea that altered microglial

activities may be associated with photoreceptor degeneration and removal of cell debris. The present study demonstrated that nasal drusen area has lower glial activation, similar to levels of astrocyte activity, compared to other areas in AMD retina (Figure 5-12F). In addition, the drusen-free areas, including central and temporal peripheral areas, showed microglial activation and migration (Figure 5-12C-E). Taken together, these findings suggest a progressive aspect to the AMD condition and, as noted above, targeting of these areas may be the direction for investigating potential therapies.

5.4.3 Cx43 is associated with oxidative stress and inflammation and may provide a therapeutic target to rescue or improve the function of remaining neurons

In the present study, a noticeable increase in Cx43 immunoreactivity associated with enhanced astrocyte activity was demonstrated in macular drusen and central drusen-free area in AMD affected donor retina compared to other areas in AMD and control retinas. This result is consistent with a series of findings on central nervous system disorders and ocular conditions. Up-regulated Cx43 protein and/or transcript have been found in many human CNS injuries and diseases, including stroke, epilepsy and Huntington's disease and the increased Cx43 expression in the human brain tissue is mainly limited to the astrocytes (Elisevich *et al.*, 1997; Vis *et al.*, 1998; Nakase *et al.*, 2006). In addition to astrocytes, microglia may be another cell type with changes in Cx43 expression in the CNS following injury. Four days after brain stab wounding, increased Cx43 protein expression has been detected in cell interfaces at the edge around the wound (Eugenín *et al.*, 2001). The immunoreactivity of Cx43 is up-regulated in human retina from glaucomatous eyes compared to normal retinal tissue. Increased Cx43 expression is mainly on the astrocytes in the retinal ganglion cell layer and along the GFAP-labelled Müller cell processes throughout the entire retina (Kerr *et al.*, 2011). In addition, this study demonstrated that Cx43 immunoreactivity is also associated with oxidative stress in endothelial cells. However, no upregulation of Cx43 expression was evident in these cells. This is consistent with the

197

findings in glaucoma, where retinal endothelial cells retain the same expression level of Cx43 as the controls (Kerr *et al.*, 2011).

In summary, results from this study support the hypothesis that the lesion-surrounding and lesion-free areas show stronger oxidative stress and inflammation than the lesion area itself in AMD patients. Cx43 expression is associated with increased nitric oxidation in blood vessels and the glia-mediated inflammatory response in drusen-free areas. Pharmaceutical down-regulation of pathologically increased Cx43 may improve retinal function and rescue the surviving retinal neurons from stress and cell death, thus providing a novel therapeutic approach for human AMD.

Chapter 6: General discussion and conclusions

6.1   Summary of findings

This thesis has used the light-damaged albino rat as an animal model for age-related macular degeneration (AMD). Retinal function has been assessed using electroretinograms at various time points following injury. Characterisation of inflammation, oxidative stress and intercellular communication during the process of tissue injury in the model has been conducted with the use of a range of markers. The effect on retinal function of blocking of connexin43 (Cx43) hemichannels with a Cx43 mimetic peptide has been demonstrated in the light-damaged rat model. Furthermore, Cx43 expression, inflammation and oxidative stress have been also analysed in human AMD affected post-mortem ocular tissues. The principle aims of the thesis listed in the introduction are individually considered in the following summary:

1) *To characterise the light-damaged albino rat eye and determine whether this is a good animal model for studying the early stages of AMD.*

Electroretinogram (ERG) results from the present study demonstrated that retinal function was dramatically low in the light-damaged animal at all tested time-points following intense light exposure (0, 6, 24, 48 hours and 7 days). Further analysis showed that photoreceptoral and post-photoreceptoral functions involving both rod and cone pathways were affected. To determine which tissue injury processes contribute to the impaired neural functions, the present study has found photoreceptor cell death following light damage, consistent with previous studies showing photoreceptor loss (Noell *et al.*, 1966; Wenzel *et al.*, 2005). Microglia activation and migration from the plexiform layers into the nuclear layers was confirmed. These activated microglia may then secrete neurotoxic factors and initiate or continue neuron cell death processes (Marín-Teva *et al.*, 2012).

Gap junction proteins, connexins, have been reported to play important roles in phototransduction pathways (Söhl *et al.*, 2005; Goodenough & Paul, 2009). Cx36 and Cx45 were expressed in the inner plexiform layer from non-light-exposed control rats, which was comparable with previous findings on connexin protein expressions in rats (Veruki &

Hartveit, 2009). Following light damage, Cx36 immunoreactivity was markedly increased and in contrast Cx45 immunoreactivity was markedly decreased at 24 hours compared to the non-light-damaged control. The alterations in connexin expression in the inner plexiform layer may contribute to the reduction of post-photoreceptoral function detected by ERG b-waveforms.

Up-regulation of connexin43 (Cx43), the most ubiquitous gap junction protein, has been shown to be involved in tissue injury (De Maio *et al.*, 2002; Danesh-Meyer & Green, 2008; O'Carroll *et al.*, 2008; Chew *et al.*, 2010). A significant increase in Cx43 expression was detected in the choroid following light damage as assessed using the Western blot technique. This increased expression was associated with significantly increased levels of the oxidative stress marker, nitrotyrosine. Double immunohistochemical labelling showed that macrophages started to express Cx43 and nitrotyrosine in the choroid following light damage, indicating a close relationship between oxidative stress, inflammation and Cx43.

2) *To characterise the functional and molecular effect of Cx43 modulation.*

It was hypothesised that the inflammatory response might be suppressed and rescue the tissue from secondary injury arising from inflammation by regulating Cx43 channel function. Intravitreal injection of a Cx43 mimetic peptide, peptide5, was used to modulate the function of Cx43 hemichannels locally. The peptide was shown to penetrate readily through the retina into the choroid and sclera, through an intravitreal injection of fluorescein isothiocyanate (FITC)-conjugated peptide. Light-damaged (LD) animals receiving a single injection of peptide5 post-LD showed a trend toward improvement in function of both rod and cone pathways when compared to the sham-injected rats. Four different treatment strategies were also assessed with double injections. All of these groups showed some significant improvement or a trend to improvement of retinal function. The major observation was that the rats that were given one injection during-LD and another post-LD, with their ERG tested 24 hours post-LD (strategy B) showed the most significant functional improvement on both rod and cone pathways. Cellular analysis of harvested tissues has

201

demonstrated that the glia-mediated inflammatory response was down-regulated compared to the sham-treated animals, including decreased expression of the glial fibrillary acidic protein (GFAP) and fewer macrophages in the choroid. This suppressed glia-mediated inflammatory response may diminish the level of neurotoxic factors released, and, therefore, lead to an increased neuronal survival rate (Boje & Arora, 1992; Chao *et al.*, 1992).

Interestingly, one group of rats that were given injections at 0 and 6 hours post-LD and had ERG tested at 24 hours post-LD (strategy C) showed significantly decreased cone post-photoreceptoral function (PII response). This is possibly caused by non-specific binding of peptide5 to the conserved sequence of other connexin proteins in the retina, such as Cx36 and Cx45 (Goodenough *et al.*, 1996; Kumar & Gilula, 1996; Yeager & Nicholson, 1996). This non-specific binding may block the hemichannels on the cone horizontal cell dendrites (Malchow *et al.*, 1993), abolishing the inhibition feedback from the ON horizontal cell to the cones (Kamermans *et al.*, 2001), and so leading to a decreased cone response. This non-specific binding was thought to be transient as the group with two injections, 6 hours apart, but ERG tested 7 days post-LD (strategy D) did not show this effect on cone PII response. In addition, the non-specific binding could be concentration-dependent, with addition of the second injection to remaining peptide from the first injection. The group with two injections, 22 hours apart, did not show any reduced cone PII response, but did show a significantly increased cone PII amplitude.

3) *To verify the significant findings from the animal model in human eyes.*

In terms of translational research from the animal model to the human eyes, there were three significant findings in human age-related retinal degeneration. First, Cx43 immunoreactivity was increased in the inner plexiform layer, inner nuclear layer and outer plexiform layer in the central drusen-free area. Second, nitrotyrosine immunoreactivity indicating oxidative damage from reactive nitrogen species (RNS) was specifically detected associated with blood vessels in the nasal drusen area, but not in other areas from the AMD sample or the

control sample. The other tested markers, superoxide dismutase 1 (SOD-1) and 8-oxoguanine (8-oxoG), were found not to be specifically different in AMD samples compared to the control. Third, up-regulated Cx43 immunoreactivity was associated with increased GFAP expression in the inner retina in the drusen-free area. Activated microglia were discovered in the nuclear layers in drusen-free areas too. These findings extend the focus from the lesion (drusen-affected) area to the lesion-surrounding (drusen-free) and peripheral areas in the AMD retina. The evidence for raised Cx43 immunoreactivity and amplified inflammatory responses in these areas may indicate their close association with lesion spread in the human AMD condition.

6.2 A grand synthesis of peptide5 functioning mechanism

Results from this thesis have demonstrated that peptide5 is able to preserve retinal function in the light-damaged animal model for AMD, possibly through inhibiting immune responses in the retina and choroid.

Under physiological condition, resting microglia enhance neuronal survival, possibly by releasing trophic factors, such as transforming growth factor-β (TGF-β), nerve growth factor (NGF) (Orellana *et al.*, 2009). Astrocytes are highly coupled to each other through gap junctions, forming extensive intercellular networks (Karpuk *et al.*, 2011). When tissue is under stress and/or primary inflammatory response, ATP released via hemichannels from microglia promotes microglial migration from less affected regions. Activated microglia can also release glutamate through hemichannels and oxygen- and nitrogen-derived free radicals that are neurotoxic (Orellana *et al.*, 2009; Orellana *et al.*, 2011a). Microglia mediated neurotoxicity is known to be progressive over time, and therefore, immunosuppression reduces delayed cell death. In contrast to increased opening of hemichannels, astrocyte gap junction communication is reduced, impairing glutamate and K^+ spatial buffering, which enhanced neuronal susceptibility (Karpuk *et al.*, 2011). Similar mechanisms also work on the macrophages in the choroid, possibly with more involvement of blood vessels.

Hemichannels on endothelial cells are activated and opening through Ca^{2+} wave propagation, which may lead to dysfunction of endothelial cells and then, blood vessel leakage and leucocyte diapedesis across the endothelium (Orellana *et al.*, 2009). Cx43-formed hemichannels have been found to be the main component in the series of inflammatory responses (Karpuk *et al.*, 2011; Orellana *et al.*, 2011a; Orellana *et al.*, 2011b).

In this study, local delivery of peptide5 through intravitreal injections may block the opening of Cx43-based hemichannels on microglia, astrocytes, macrophages and endothelial cells in the retina and the choroid, which result in suppression of inflammatory response and inflammation-mediated neurotoxicity. Many studies have demonstrated that inflammation is prolonged and progressive in AMD condition (Madigan *et al.*, 1994; Gupta *et al.*, 2003; Sullivan *et al.*, 2003; Wu *et al.*, 2003; Ding *et al.*, 2009). Therefore, targeting Cx43, peptide5 could be a potential novel treatment for AMD.

6.3   Clinical highlights, limitations of the current study and future directions

Current treatment options for AMD are limited to the late stage of this condition (neovascularisation) which include laser photocoagulation, verteporfin with photodynamic therapy (vPDT) and anti-vascular endothelial growth factor (VEGF) agents (Fernández-Robredo *et al.*, 2014). Until recently, there is no therapy available for early stage of AMD (Rickman *et al.*, 2013). This study has demonstrated the light-damaged animal model showed comparable inflammatory responses in human donor's tissue with early stage of AMD. Peptide5 directly reduces microglia/macrophage-mediated inflammation and secondary damage through Cx43-formed hemichannels in the animal model. The valuable aspect of peptide5 is its specificity on stressed/damaged cells. Hemichannels only open on the activated inflammatory cells (microglia/macrophages) and stressed endothelial cells under pathological condition. Peptide5 provides its potential safety via specifically targeting these opening hemichannels without affecting physiological functions of intercellular gap

204

junction channels. In addition, peptide5 can be applied through intravitreal injections, which is a common clinical approach for many ocular treatments. Therefore, peptide5 is a novel potential therapeutic drug for early stage of AMD.

As common as any other research, this study also has some limitations. The first two specific aims of the current study were conducted by using the light-damaged albino rat as an animal model for the human AMD condition. Limitations include the anatomical difference between the rat retina and human macula. The human macula is a cone-dominant region consistent with its role in high-acuity stereoscopic vision (Bron *et al.*, 1997), while the rat retina is rod-dominant and does not possess a macula (Huber *et al.*, 2010). In addition, the pathogenesis of AMD in human is a long-term process, taking several years (Lim *et al.*, 2012). In the light-damaged animal model, we have investigated the injury up to only seven days after light damage. It is a short-term acute wound model compared to the chronic pathogenesis of human AMD. Human AMD may have more complex processes of tissue injury and repair, including fibrous scarring (Lim *et al.*, 2012).

In terms of characterising the animal model as presented in Chapter 3, further analysis of protein expression levels for the oxidative stress marker, nitrotyrosine, inflammatory markers, and Cx43 in the choroid and retina over longer recovery periods would be of interest. These would be from 24 hours up to one month. Such data might provide a better understanding of tissue injury and repair mechanisms over the longer term in this light-damaged albino rat model.

AMD has been recognised as being a vascular condition (Coorey *et al.*, 2012). Studies of human post-mortem tissue affected by AMD has shown the loss of choriocapillaris during the early stages of the disease and in adjacent areas to neovascularisation in wet AMD (McLeod *et al.*, 2002; McLeod *et al.*, 2009). In the present study, it has been shown that up-regulated expression of Cx43 and nitrotyrosine, and increased numbers of CD45-positive macrophages are present in the choroid following the light damage. Future investigations of

205

the choriocapillaris are warranted in order to better understand vascular conditions in the light-damaged animal model.

The disrupted retinal pigment epithelium (RPE) and discontinuous Bruch's membrane in the light-damaged albino rat has been reported in previous studies (Noell *et al.*, 1966; van Best *et al.*, 1997; Marc *et al.*, 2008; Rutar *et al.*, 2010). The current study showed disrupted actin filaments stained with phalloidin in some patches of the RPE in the central retina at 24 hours following the light damage (Figure 3-18, Chapter 3). Actin is a key component of cytoskeletal architecture in the RPE, regulating the cellular apical polarisation (Davis *et al.*, 1995). Destabilisation of actin leads to reduction in plasma-membrane integrity and blebbing along with an increase in cellular apoptosis (Franklin-Tong & Gourlay, 2008). Actin is susceptible to oxidative damage, for example, 4-hydroxynonenal (4-HNE) modification (Kokubo *et al.*, 2008). 4-HNE treatment causes destabilisation of actin and an increase in soluble actin (Yu *et al.*, 2012). Further investigation into the phalloidin-stained patches of RPE, by applying a range of stress markers, would provide further information on the mechanisms involved in RPE damage following intense light exposure.

With specific reference to the study of Cx43 mimetic peptide intervention in the light-damaged animal model presented in Chapter 4, future investigation is required to clarify whether the decreased cone response in the animals treated with a double dose immediately after light damage and recovered for 24 hours post-LD (Strategy A) (Figure 4-1, Chapter 4) was actually caused by non-specific binding of the mimetic peptide to other connexin hemichannels located on the cone photo-transduction pathway. This could be achieved by using a non-specific hemichannel blocker, such as carbenoxolone to treat the animals following Strategy A and comparing that with Cx36 specific blockers should these become available. Alternatively, an antisense or RNAi approach could be used to specifically target Cx36 and Cx45 to see if the same result is achieved. ERG would be analysed following the same protocol and compared to the data collected from peptide5-treated animals. Additionally, further insight might be obtained with a range of dosages of peptide5. It is also of note that there is as yet little information on peptide5 stability in the

eye or its pharmacodynamics and modified (more stable) peptides would also be worth trying.

Cellular analysis of the collected tissue from animals treated under Strategy A demonstrated that down-regulation of the glia-mediated inflammatory response without affecting connexin expression may be a trigger for improvement of retinal function. Further investigation of inflammatory responses in the tissue treated under other strategies may be particularly useful in order to obtain the best time point to initiate treatment and to determine optimum time intervals between doses.

With respect to the study of human AMD affected post-mortem tissue presented in Chapter 5, it was shown that there was a regional increase in Cx43, oxidative stress and glia-mediated inflammation in the retina. Due to the poor histological condition of the tissue, little data was collected from the choroid. This created difficulties in identifying tissue-injury events happening in the choroid in the human AMD condition and to make comparison to the light-damaged animal model. Further inspection of the choroid in AMD post-mortem tissues would be valuable, especially employing human-specific antibodies for detecting oxidative stress and inflammation. This might provide valuable evidence for the role of the choroid in the pathogenesis of AMD.

6.4   Conclusions

Cx43 has a close association with early stages of tissue damage and the glia-mediated inflammatory responses in both the light-damaged animal model and the human AMD condition. Local administration of a Cx43 mimetic peptide, peptide5 demonstrated significant improvement in retinal function is possible by blocking Cx43 hemichannels. This protective effect on retinal neurons may be achieved through moderating inflammatory

responses. These data suggest a pharmaceutical potential for peptide5 in the treatment of AMD.

References

Abbott, N.J., Rönnbäck, L. & Hansson, E. (2006) Astrocyte–endothelial interactions at the blood–brain barrier. *Nature Reviews Neuroscience*, **7**, 41-53.

Ablonczy, Z., Knapp, D., Darrow, R., Organisciak, D. & Crouch, R.K. (2000) Mass spectrometric analysis of rhodopsin from light damaged rats. *Mol Vis*, **6**, 109-115.

Acosta, M.L., Fletcher, E.L., Azizoglu, S., Foster, L.E., Farber, D.B. & Kalloniatis, M. (2005a) Early markers of retinal degeneration in rd/rd mice. *Mol Vis*, **11**, 717-728.

Acosta, M.L., Kalloniatis, M. & Christie, D.L. (2005b) Creatine transporter localization in developing and adult retina: importance of creatine to retinal function. *American Journal of Physiology-Cell Physiology*, **289**, C1015-C1023.

Adamis, A.P., Ishida, S., Yamashiro, K., Usui, T., Kaji, Y., Ogura, Y., Hida, T., Honda, Y. & Oguchi, Y. (2003) Leukocytes mediate retinal vascular remodeling during development and vaso-obliteration in disease. *Nat Med*, **9**, 781-788.

Ahmed, Z., Shaw, G., Sharma, V.P., Yang, C., McGowan, E. & Dickson, D.W. (2007) Actin-binding proteins coronin-1a and IBA-1 are effective microglial markers for immunohistochemistry. *J Histochem Cytochem*, **55**, 687-700.

Albarracin, R., Eells, J. & Valter, K. (2011) Photobiomodulation protects the retina from light-induced photoreceptor degeneration. *Invest Ophthalmol Vis Sci*, **52**, 3582-3592.

Albarracin, R. & Valter, K. (2012) 670 nm Red light preconditioning supports müller cell function: evidence from the white light induced damage model in the rat retina. *Photochemistry and Photobiology*, **88**, 1418-1427.

Alderton, W.K., Cooper, C.E. & Knowles, R.G. (2001) Nitric oxide synthases: structure, function and inhibition. *Biochemical Journal*, **357**, 593-615.

Algvere, P.V. & Seregard, S. (2002) Age-related maculopathy: pathogenetic features and new treatment modalities. *Acta Ophthalmologica Scandinavica*, **80**, 136-143.

Alm, A. & Bill, A. (1973) Ocular and optic nerve blood flow at normal and increased intraocular pressures in monkeys (Macaca irus): a study with radioactively labelled microspheres including flow determinations in brain and some other tissues. *Exp Eye Res*, **15**, 15-29.

Amin, R.H., Frank, R.N., Kennedy, A., Eliott, D., Puklin, J.E. & Abrams, G.W. (1997) Vascular endothelial growth factor is present in glial cells of the retina and optic nerve of human subjects with nonproliferative diabetic retinopathy. *Invest Ophthalmol Vis Sci*, **38**, 36-47.

Anand, R.J., Dai, S., Gribar, S.C., Richardson, W., Kohler, J.W., Hoffman, R.A., Branca, M.F., Li, J., Shi, X.-H. & Sodhi, C.P. (2008) A role for connexin43 in macrophage phagocytosis and host survival after bacterial peritoneal infection. *The Journal of Immunology*, **181**, 8534-8543.

Anderson, A.J. & Vingrys, A.J. (2001) Small samples: does size matter? *Invest Ophthalmol Vis Sci*, **42**, 1411-1413.

Anderson, D.H., Mullins, R.F., Hageman, G.S. & Johnson, L.V. (2002a) A role for local inflammation in the formation of drusen in the aging eye. *Am J Ophthalmol*, **134**, 411-431.

Anderson, R.E., Maude, M.B. & Bok, D. (2001) Low docosahexaenoic acid levels in rod outer segment membranes of mice with rds/peripherin and P216L peripherin mutations. *Invest Ophthalmol Vis Sci*, **42**, 1715-1720.

Anderson, R.E., Maude, M.B., McClellan, M., Matthes, M.T., Yasumura, D. & LaVail, M.M. (2002b) Low docosahexaenoic acid levels in rod outer segments of rats with P23H and S334ter rhodopsin mutations. *Mol Vis*, **8**, 351-358.

Ashwell, K., Hollander, H., Streit, W. & Stone, J. (1989) The appearance and distribution of microglia in the developing retina of the rat. *Vis Neurosci*, **2**, 437-448.

Babior, B.M. (2000) Phagocytes and oxidative stress. *The American Journal of Medicine*, **109**, 33-44.

Balboa, R.M. & Grzywacz, N.M. (2000) The role of early retinal lateral inhibition: more than maximizing luminance information. *Vis Neurosci*, **17**, 77-89.

Banks, E.A., Toloue, M.M., Shi, Q., Zhou, Z.J., Liu, J., Nicholson, B.J. & Jiang, J.X. (2009) Connexin mutation that causes dominant congenital cataracts inhibits gap junctions, but not hemichannels, in a dominant negative manner. *J Cell Sci*, **122**, 378-388.

Barnes, S., Merchant, V. & Mahmud, F. (1993) Modulation of transmission gain by protons at the photoreceptor output synapse. *Proceedings of the National Academy of Sciences*, **90**, 10081-10085.

Barron, M.J., Johnson, M.A., Andrews, R.M., Clarke, M.P., Griffiths, P.G., Bristow, E., He, L.P., Durham, S. & Turnbull, D.M. (2001) Mitochondrial abnormalities in ageing macular photoreceptors. *Invest Ophthalmol Vis Sci*, **42**, 3016-3022.

Battelle, B.A. & LaVail, M.M. (1978) Rhodopsin content and rod outer segment length in albino rat eyes: modification by dark adaptation. *Exp Eye Res*, **26**, 487-497.

Baudouin, C., Peyman, G., Fredj-Reygrobellet, D., Gordon, W., Lapalus, P., Gastaud, P. & Bazan, N. (1992) Immunohistological study of subretinal membranes in age-related macular degeneration. *Japanese Journal of Ophthalmology*, **36**, 443-451.

Bazarbachi, A., Merhi, R.A., Gessain, A., Talhouk, R., El-Khoury, H., Nasr, R., Gout, O., Sulahian, R., Homaidan, F. & Hermine, O. (2004) Human T-cell lymphotropic virus type I-infected cells extravasate through the endothelial barrier by a local angiogenesis-like mechanism. *Cancer Res*, **64**, 2039-2046.

Beardslee, M.A., Laing, J.G., Beyer, E.C. & Saffitz, J.E. (1998) Rapid turnover of connexin43 in the adult rat heart. *Circ Res*, **83**, 629-635.

Beatty, S., Koh, H., Phil, M., Henson, D. & Boulton, M. (2000) The role of oxidative stress in the pathogenesis of age-related macular degeneration. *Surv Ophthalmol*, **45**, 115-134.

Becker, D.L., McGonnell, I., Makarenkova, H.P., Patel, K., Tickle, C., Lorimer, J. & Green, C.R. (1999) Roles for α1 connexin in morphogenesis of chick embryos revealed using a novel antisense approach. *Developmental Genetics*, **24**, 33-42.

Bergoffen, J., Scherer, S., Wang, S., Scott, M.O., Bone, L., Paul, D., Chen, K., Lensch, M., Chance, P. & Fischbeck, K. (1993) Connexin mutations in X-linked Charcot-Marie-Tooth disease. *Science*, **262**, 2039-2042.

Berry, V., Mackay, D., Khaliq, S., Francis, P.J., Hameed, A., Anwar, K., Mehdi, S.Q., Newbold, R.J., Ionides, A. & Shiels, A. (1999) Connexin 50 mutation in a family with congenital" zonular nuclear" pulverulent cataract of Pakistani origin. *Human genetics*, **105**, 168-170.

Berthoud, V.M., Beyer, E.C. & Seul, K.H. (2000) Peptide inhibitors of intercellular communication. *American Journal of Physiology*, **279**, L619-L622.

Bhutto, I. & Lutty, G. (2012) Understanding age-related macular degeneration (AMD): Relationships between the photoreceptor/retinal pigment epithelium/bruch's membrane/choriocapillaris complex. *Molecular Aspects of Medicine*, **33**, 295-317.

Bhutto, I.A., Baba, T., Merges, C., McLeod, D.S. & Lutty, G.A. (2010) Low nitric oxide synthases (NOS) in eyes with age-related macular degeneration (AMD). *Exp Eye Res*, **90**, 155.

Biarnés, M., Monés, J., Alonso, J. & Arias, L. (2011) Update on geographic atrophy in age-related macular degeneration. *Optometry & Vision Science*, **88**, 881-889.

Bidwell III, G.L. & Raucher, D. (2010) Cell penetrating elastin-like polypeptides for therapeutic peptide delivery. *Advanced Drug Delivery Reviews*, **62**, 1486-1496.

Bill, A. (1975) Blood circulation and fluid dynamics in the eye. *Physiological Reviews*, **55**, 383-417.

Bill, A. & Sperber, G. (1990) Control of retinal and choroidal blood flow. *Eye (Lond)*, **4**, 319-325.

Birch, D.G., Hood, D.C., Nusinowitz, S. & Pepperberg, D.R. (1995) Abnormal activation and inactivation mechanisms of rod transduction in patients with autosomal dominant retinitis pigmentosa and the pro-23-his mutation. *Invest Ophthalmol Vis Sci*, **36**, 1603-1614.

Bird, A.C. (2010) Therapeutic targets in age-related macular disease. *J Clin Invest*, **120**, 3033-3041.

Blaauwgeers, H.G.T., Holtkamp, G.M., Rutten, H., Witmer, A.N., Koolwijk, P., Partanen, T.A., Alitalo, K., Kroon, M.E., Kijlstra, A. & van Hinsbergh, V.W.M. (1999) Polarized vascular endothelial growth factor secretion by human retinal pigment epithelium and localization of vascular endothelial growth factor receptors on the inner choriocapillaris: evidence for a trophic paracrine relation. *The American Journal of Pathology*, **155**, 421-428.

Bloomfield, S.A. & Dacheux, R.F. (2001) Rod vision: pathways and processing in the mammalian retina. *Prog Retin Eye Res*, **20**, 351-384.

Bloomfield, S.A. & Volgyi, B. (2009) The diverse functional roles and regulation of neuronal gap junctions in the retina. *Nat Rev Neurosci*, **10**, 495-506.

Bloomfield, S.A. & Völgyi, B. (2004) Function and plasticity of homologous coupling between AII amacrine cells. *Vision Res*, **44**, 3297-3306.

Bobbie, M.W., Roy, S., Trudeau, K., Munger, S.J. & Simon, A.M. (2010) Reduced connexin 43 expression and its effect on the development of vascular lesions in retinas of diabetic mice. *Invest Ophthalmol Vis Sci*, **51**, 3758-3763.

Boitano, S., Dirksen, E.R. & Sanderson, M.J. (1992) Intercellular propagation of calcium waves mediated by inositol trisphosphate. *Science*, **258**, 292-295.

Boje, K.M. & Arora, P.K. (1992) Microglial-produced nitric oxide and reactive nitrogen oxides mediate neuronal cell death. *Brain Research*, **587**, 250-256.

Boretsky, A., Motamedi, M., Bell, B. & van Kuijk, F. (2011) Quantitative evaluation of retinal response to laser photocoagulation using dual-wavelength fundus autofluorescence imaging in a small animal model. *Invest Ophthalmol Vis Sci*, **52**, 6300-6307.

Boycott, B. & Wässle, H. (1991) Morphological classification of bipolar cells of the primate retina. *European Journal of Neuroscience*, **3**, 1069-1088.

Bressler, S.B. (2009) Introduction: Understanding the role of angiogenesis and antiangiogenic agents in age-related macular degeneration. *Ophthalmology*, **116**, S1.

Bron, A.J., Tripathi, R.C. & Tripathi, B.J. (eds) (1997) *Wolff's anatomy of the eye and orbit*. Chapman & Hall Medical, London, UK.

Bruzzone, S., Guida, L., Zocchi, E., Franco, L. & De Flora, A. (2001) Connexin 43 hemi channels mediate Ca^{2+}-regulated transmembrane NAD^{+} fluxes in intact cells. *The FASEB Journal*, **15**, 10-12.

Bucci, M., Gratton, J.-P., Rudic, R.D., Acevedo, L., Roviezzo, F., Cirino, G. & Sessa, W.C. (2000) In vivo delivery of the caveolin-1 scaffolding domain inhibits nitric oxide synthesis and reduces inflammation. *Nat Med*, **6**, 1362-1367.

Buschini, E., Piras, A., Nuzzi, R. & Vercelli, A. (2011) Age related macular degeneration and drusen: neuroinflammation in the retina. *Prog Neurobiol*, **95**, 14-25.

Caicedo, A., Espinosa-Heidmann, D.G., Pina, Y., Hernandez, E.P. & Cousins, S.W. (2005) Blood-derived macrophages infiltrate the retina and activate Muller glial cells under experimental choroidal neovascularization. *Exp Eye Res*, **81**, 38-47.

Camelliti, P., Green, C.R., LeGrice, I. & Kohl, P. (2004) Fibroblast Network in Rabbit Sinoatrial Node Structural and Functional Identification of Homogeneous and Heterogeneous Cell Coupling. *Circ Res*, **94**, 828-835.

Cao, X., Shen, D., Patel, M.M., Tuo, J., Johnson, T.M., Olsen, T.W. & Chan, C.C. (2011) Macrophage polarization in the maculae of age-related macular degeneration: A pilot study. *Pathology international*, **61**, 528-535.

Carresi, C., Cruciani, F., Paolucci, F., Curto, T., Mazzeo, L., Cuozzo, G., Moramarco, A. & Gharbiya, M. (2009) Montelparo study: risk factors for age-related macular degeneration in a little rural community in Italy. *Clin Ter*, **160**, e43-e51.

Chan-Ling, T., Hughes, S., Baxter, L., Rosinova, E., McGregor, I., Morcos, Y., van Nieuwenhuyzen, P. & Hu, P. (2007) Inflammation and breakdown of the blood–retinal barrier during "physiological aging" in the rat retina: a model for CNS aging. *Microcirculation*, **14**, 63-76.

Chao, C., Hu, S., Molitor, T., Shaskan, E. & Peterson, P. (1992) Activated microglia mediate neuronal cell injury via a nitric oxide mechanism. *The Journal of Immunology*, **149**, 2736-2741.

Chaytor, A., Evans, W. & Griffith, T. (1998) Central role of heterocellular gap junctional communication in endothelium-dependent relaxations of rabbit arteries. *The Journal of Physiology*, **508**, 561-573.

Chaytor, A., Evans, W., Griffith, T. & Thornbury, K. (1997) Peptides homologous to extracellular loop motifs of connexin 43 reversibly abolish rhythmic contractile activity in rabbit arteries. *The Journal of Physiology*, **503**, 99-110.

Chen, L., Yang, P. & Kijlstra, A. (2002) Distribution, markers, and functions of retinal microglia. *Ocul Immunol Inflamm*, **10**, 27-39.

Cherepanoff, S., McMenamin, P., Gillies, M.C., Kettle, E. & Sarks, S.H. (2010) Bruch's membrane and choroidal macrophages in early and advanced age-related macular degeneration. *Brit J Ophthalmol*, **94**, 918-925.

Chew, S.S.L., Johnson, C.S., Green, C.R. & Danesh-Meyer, H.V. (2010) Role of connexin43 in central nervous system injury. *Exp Neurol*, **225**, 250-261.

Chew, S.S.L., Johnson, C.S., Green, C.R. & Danesh-Meyer, H.V. (2011) Response of retinal Connexin43 to optic nerve injury. *Invest Ophthalmol Vis Sci*, **52**, 3620-3629.

Choi, Y.K. & Kim, K.W. (2008) Blood-neural barrier: its diversity and coordinated cell-to-cell communication. *BMB Reports*, **41**, 345-352.

Combadière, C., Feumi, C., Raoul, W., Keller, N., Rodéro, M., Pézard, A., Lavalette, S., Houssier, M., Jonet, L. & Picard, E. (2007) CX3CR1-dependent subretinal microglia cell accumulation is associated with cardinal features of age-related macular degeneration. *J Clin Invest*, **117**, 2920-2928.

Conlon, K.A., Zharkov, D.O. & Berrios, M. (2003) Immunofluorescent localization of the murine 8-oxoguanine DNA glycosylase (mOGG1) in cells growing under normal and nutrient deprivation conditions. *DNA Repair (Amst)*, **2**, 1337-1352.

Contreras, J.E., Sánchez, H.A., Eugenín, E.A., Speidel, D., Theis, M., Willecke, K., Bukauskas, F.F., Bennett, M.V.L. & Sáez, J.C. (2002) Metabolic inhibition induces opening of unapposed connexin 43 gap junction hemichannels and reduces gap junctional communication in cortical astrocytes in culture. *Proceedings of the National Academy of Sciences*, **99**, 495-500.

Cook, J.E. & Becker, D.L. (1995) Gap junctions in the vertebrate retina. *Microscopy Research and Technique*, **31**, 408-419.

Cooper, C.D. & Lampe, P.D. (2002) Casein kinase 1 regulates connexin-43 gap junction assembly. *Journal of Biological Chemistry*, **277**, 44962-44968.

Coorey, N.J., Shen, W., Chung, S.H., Zhu, L. & Gillies, M.C. (2012) The role of glia in retinal vascular disease. *Clinical and Experimental Optometry*, **95**, 266-281.

Cortina, M.S., Gordon, W.C., Lukiw, W.J. & Bazan, N.G. (2005) Oxidative stress-induced retinal damage up-regulates DNA polymerase gamma and 8-oxoguanine-DNA-glycosylase in photoreceptor synaptic mitochondria. *Exp Eye Res*, **81**, 742-750.

Cotrina, M.L., Kang, J., Lin, J.H.C., Bueno, E., Hansen, T.W., He, L., Liu, Y. & Nedergaard, M. (1998) Astrocytic gap junctions remain open during ischemic conditions. *The Journal of Neuroscience*, **18**, 2520-2537.

Cotrina, M.L., Lin, J.H.-C., López-García, J.C., Naus, C.C. & Nedergaard, M. (2000) ATP-mediated glia signaling. *The Journal of Neuroscience*, **20**, 2835-2844.

Coutinho, P., Qiu, C., Frank, S., Tamber, K. & Becker, D. (2003) Dynamic changes in connexin expression correlate with key events in the wound healing process. *Cell Biology International*, **27**, 525-541.

Coutinho, P., Qiu, C., Frank, S., Wang, C., Brown, T., Green, C. & Becker, D. (2005) Limiting burn extension by transient inhibition of Connexin43 expression at the site of injury. *Br J Plast Surg*, **58**, 658-667.

Criswell, M.H., Ciulla, T.A., Hill, T.E., Small, W., Danis, R.P., Snyder, W.J., Lowseth, L.A. & Carson, D.L. (2004) The squirrel monkey: characterization of a new-world primate model of experimental choroidal neovascularization and comparison with the macaque. *Invest Ophthalmol Vis Sci*, **45**, 625-634.

Cronin, M., Anderson, P.N., Cook, J.E., Green, C.R. & Becker, D.L. (2008) Blocking connexin43 expression reduces inflammation and improves functional recovery after spinal cord injury. *Mol Cell Neurosci*, **39**, 152-160.

Crooks, J. & Kolb, H. (1992) Localization of GABA, glycine, glutamate and tyrosine hydroxylase in the human retina. *The Journal of Comparative Neurology*, **315**, 287-302.

Cuadros, M.A. & Navascués, J. (1998) The origin and differentiation of microglial cells during development. *Prog Neurobiol*, **56**, 173-189.

Cuenca, N., Fernández, E., García, M. & De Juan, J. (1993) Dendrites of rod dominant ON-bipolar cells are coupled by gap junctions in carp retina. *Neurosci Lett*, **162**, 34-38.

Curcio, C.A., Medeiros, N.E. & Millican, C.L. (1996) Photoreceptor loss in age-related macular degeneration. *Invest Ophthalmol Vis Sci*, **37**, 1236-1249.

Curcio, C.A. & Millican, C.L. (1999) Basal linear deposit and large drusen are specific for early age-related maculopathy. *Arch Ophthalmol-Chic*, **117**, 329-339.

Curcio, C.A., Owsley, C. & Jackson, G.R. (2000) Spare the rods, save the cones in aging and age-related maculopathy. *Invest Ophthalmol Vis Sci*, **41**, 2015-2018.

Curcio, C.A., Sloan, K.R., Kalina, R.E. & Hendrickson, A.E. (1990) Human photoreceptor topography. *The Journal of Comparative Neurology*, **292**, 497-523.

Cuthbertson, R. & Mandel, T. (1986) Anatomy of the mouse retina. Endothelial cell-pericyte ratio and capillary distribution. *Invest Ophthalmol Vis Sci*, **27**, 1659-1664.

Dacey, D.M. & Lee, B.B. (1994) The'blue-on'opponent pathway in primate retina originates from a distinct bistratified ganglion cell type. *Nature*, **367**, 731-735.

Dacey, D.M. & Packer, O.S. (2003) Colour coding in the primate retina: diverse cell types and cone-specific circuitry. *Current Opinion in Neurobiology*, **13**, 421-427.

Dahl, D. (1979) The radial glia of Müller in the rat retina and their response to injury. An immunofluorescence study with antibodies to the glial fibrillary acidic (GFA) protein. *Exp Eye Res*, **28**, 63-69.

Damani, M.R., Zhao, L., Fontainhas, A.M., Amaral, J., Fariss, R.N. & Wong, W.T. (2011) Age-related alterations in the dynamic behavior of microglia. *Aging Cell*, **10**, 263-276.

Danesh-Meyer, H.V. & Green, C.R. (2008) Focus on molecules: connexin 43--mind the gap. *Exp Eye Res*, **87**, 494-495.

Danesh-Meyer, H.V., Huang, R., Nicholson, L.F. & Green, C.R. (2008) Connexin43 antisense oligodeoxynucleotide treatment down-regulates the inflammatory response in an in vitro interphase organotypic culture model of optic nerve ischaemia. *J Clin Neurosci*, **15**, 1253-1263.

Danesh-Meyer, H.V., Kerr, N.M., Zhang, J., Eady, E.K., O'Carroll, S.J., Nicholson, L.F.B., Johnson, C.S. & Green, C.R. (2012) Connexin43 mimetic peptide reduces vascular leak and retinal ganglion cell death following retinal ischaemia. *Brain*, **135**, 506-520.

Davidson, J.O., Green, C.R., B Nicholson, L.F., O'Carroll, S.J., Fraser, M., Bennet, L. & Jan Gunn, A. (2012a) Connexin hemichannel blockade improves outcomes in a model of fetal ischemia. *Ann Neurol*, **71**, 121-132.

Davidson, J.O., Green, C.R., Nicholson, L.F.B., Bennet, L. & Gunn, A.J. (2012b) Deleterious effects of high dose connexin 43 mimetic peptide infusion after cerebral ischaemia in near-term fetal sheep. *International Journal of Molecular Sciences*, **13**, 6303-6319.

Davis, A.A., Bernstein, P.S., Bok, D., Turner, J., Nachtigal, M. & Hunt, R.C. (1995) A human retinal pigment epithelial cell line that retains epithelial characteristics after prolonged culture. *Invest Ophthalmol Vis Sci*, **36**, 955-964.

de Jong, P.T.V.M. (2006) Age-related macular degeneration. *New England Journal of Medicine*, **355**, 1474-1485.

De Maio, A., Vega, V.L. & Contreras, J.E. (2002) Gap junctions, homeostasis, and injury. *J Cell Physiol*, **191**, 269-282.

de Souza, C.F., Kalloniatis, M., Polkinghorne, P.J., McGhee, C.N. & Acosta, M.L. (2012) Functional activation of glutamate ionotropic receptors in the human peripheral retina. *Exp Eye Res*, **94**, 71-84.

Deans, M.R., Volgyi, B., Goodenough, D.A., Bloomfield, S.A. & Paul, D.L. (2002) Connexin36 is essential for transmission of rod-mediated visual signals in the mammalian retina. *Neuron*, **36**, 703-712.

Dedek, K., Schultz, K., Pieper, M., Dirks, P., Maxeiner, S., Willecke, K., Weiler, R. & Janssen-Bienhold, U. (2006) Localization of heterotypic gap junctions composed of connexin45 and connexin36 in the rod pathway of the mouse retina. *European Journal of Neuroscience*, **24**, 1675-1686.

Delmelle, M. (1977) Retinal damage by light: possible implication of singlet oxygen. *European Biophysics Journal*, **3**, 195-198.

Deniz, S., Wersinger, E., Schwab, Y., Mura, C., Erdelyi, F., Szabó, G., Rendon, A., Sahel, J.A., Picaud, S. & Roux, M.J. (2011) Mammalian retinal horizontal cells are unconventional GABAergic neurons. *J Neurochem*, **116**, 350-362.

DeVries, S. & Schwartz, E. (1992) Hemi-gap-junction channels in solitary horizontal cells of the catfish retina. *The Journal of Physiology*, **445**, 201-230.

DeVries, S.H. (2001) Exocytosed protons feedback to suppress the Ca^{2+} current in mammalian cone photoreceptors. *Neuron*, **32**, 1107-1117.

Dick, A.D., Robertson, M.J., Erwig, L.P., Liversidge, J., Forrester, J.V. & Rees, A.J. (2002) Retinal microenvironment controls resident and infiltrating macrophage function during uveoretinitis. *Invest Ophthalmol Vis Sci*, **43**, 2250-2257.

Ding, X., Patel, M. & Chan, C.C. (2009) Molecular pathology of age-related macular degeneration. *Prog Retin Eye Res*, **28**, 1-18.

Dong, A., Shen, J., Krause, M., Akiyama, H., Hackett, S.F., Lai, H. & Campochiaro, P.A. (2006) Superoxide dismutase 1 protects retinal cells from oxidative damage. *J Cell Physiol*, **208**, 516-526.

Dong, C.J. & Werblin, F.S. (1998) Temporal contrast enhancement via GABAC feedback at bipolar terminals in the tiger salamander retina. *Journal of Neurophysiology*, **79**, 2171-2180.

Dong, Y., Roos, M., Gruijters, T., Donaldson, P., Bullivant, S., Beyer, E. & Kistler, J. (1994) Differential expression of two gap junction proteins in corneal epithelium. *European Journal of Cell Biology*, **64**, 95-100.

Dong, Z., Kase, S., Ando, R., Fukuhara, J., Saito, W., Kanda, A., Murata, M., Noda, K. & Ishida, S. (2012) Alphab-crystallin expression in epiretinal membrane of human proliferative diabetic retinopathy. *Retina*, **32**, 1190-1196.

Dora, K.A., Martin, P.E.M., Chaytor, A.T., Evans, W.H., Garland, C.J. & Griffith, T.M. (1999) Role of heterocellular gap junctional communication in endothelium-dependent smooth muscle hyperpolarization: inhibition by a connexin-mimetic peptide. *Biochem Biophys Res Commun*, **254**, 27-31.

Dorey, C.K., Wu, G., Ebenstein, D., Garsd, A. & Weiter, J.J. (1989) Cell loss in the aging retina. Relationship to lipofuscin accumulation and macular degeneration. *Invest Ophthalmol Vis Sci*, **30**, 1691-1699.

Eastman, S.D., Chen, T.H., Falk, M.M., Mendelson, T.C. & Iovine, M.K. (2006) Phylogenetic analysis of three complete gap junction gene families reveals lineage-specific duplications and highly supported gene classes. *Genomics*, **87**, 265-274.

Edwards, A.O., Ritter III, R., Abel, K.J., Manning, A., Panhuysen, C. & Farrer, L.A. (2005) Complement factor H polymorphism and age-related macular degeneration. *Science*, **308**, 421-424.

Eichler, W., Reiche, A., Yafai, Y., Lange, J. & Wiedemann, P. (2008) Growth-related effects of oxidant-induced stress on cultured RPE and choroidal endothelial cells. *Exp Eye Res*, **87**, 342-348.

Elisevich, K., Rempel, S.A., Smith, B.J. & Edvardsen, K. (1997) Hippocampal connexin 43 expression in human complex partial seizure disorder. *Exp Neurol*, **145**, 154-164.

Erickson, K.K., Sundstrom, J.M. & Antonetti, D.A. (2007) Vascular permeability in ocular disease and the role of tight junctions. *Angiogenesis*, **10**, 103-117.

Errede, M., Benagiano, V., Girolamo, F., Flace, P., Bertossi, M., Roncali, L. & Virgintino, D. (2002) Differential expression of connexin43 in foetal, adult and tumour-associated human brain endothelial cells. *The Histochemical Journal*, **34**, 265-271.

Ettaiche, M., Guy, N., Hofman, P., Lazdunski, M. & Waldmann, R. (2004) Acid-sensing ion channel 2 is important for retinal function and protects against light-induced retinal degeneration. *The Journal of Neuroscience*, **24**, 1005-1012.

Eugenín, E.A., Brañes, M.C., Berman, J.W. & Sáez, J.C. (2003) TNF-α plus IFN-γ induce connexin43 expression and formation of gap junctions between human monocytes/macrophages that enhance physiological responses. *The Journal of Immunology*, **170**, 1320-1328.

Eugenín, E.A., Eckardt, D., Theis, M., Willecke, K., Bennett, M.V.L. & Sáez, J.C. (2001) Microglia at brain stab wounds express connexin 43 and in vitro form functional gap

junctions after treatment with interferon-γ and tumor necrosis factor-α. *Proceedings of the National Academy of Sciences*, **98**, 4190-4195.

Euler, T., Detwiler, P.B. & Denk, W. (2002) Directionally selective calcium signals in dendrites of starburst amacrine cells. *Nature*, **418**, 845-852.

Evans, J.R. (2001) Risk factors for age-related macular degeneration. *Prog Retin Eye Res*, **20**, 227-253.

Evans, J.R., Fletcher, A.E. & Wormald, R.P. (2005) 28,000 Cases of age related macular degeneration causing visual loss in people aged 75 years and above in the United Kingdom may be attributable to smoking. *Brit J Ophthalmol*, **89**, 550-553.

Evans, W.H. & Boitano, S. (2001) Connexin mimetic peptides: specific inhibitors of gap-junctional intercellular communication. *Biochem Soc Trans*, **29**, 606-612.

Evans, W.H., De Vuyst, E. & Leybaert, L. (2006) The gap junction cellular internet: connexin hemichannels enter the signalling limelight. *Biochem J*, **397**, 1-14.

Evans, W.H. & Martin, P.E.M. (2002) Gap junctions: structure and function *Molecular Membrane Biology*, **19**, 121-136.

Faigle, M., Seessle, J., Zug, S., El Kasmi, K.C. & Eltzschig, H.K. (2008) ATP release from vascular endothelia occurs across Cx43 hemichannels and is attenuated during hypoxia. *Plos One*, **3**, e2801.

Fain, G.L. & Lisman, J.E. (1993) Photoreceptor degeneration in vitamin A deprivation and retinitis pigmentosa: the equivalent light hypothesis. *Exp Eye Res*, **57**, 335-340.

Falk, M.M., Kumar, N.M. & Gilula, N.B. (1994) Membrane insertion of gap junction connexins: polytopic channel forming membrane proteins. *J Cell Biol*, **127**, 343-355.

Fallon, R.F. & Goodenough, D.A. (1981) Five-hour half-life of mouse liver gap-junction protein. *J Cell Biol*, **90**, 521-526.

Feeney-Burns, L., Berman, E.R. & Rothman, H. (1980) Lipofuscin of human retinal pigment epithelium. *Am J Ophthalmol*, **90**, 783-791.

Feigenspan, A., Janssen-Bienhold, U., Hormuzdi, S., Monyer, H., Degen, J., Söhl, G., Willecke, K., Ammermüller, J. & Weiler, R. (2004) Expression of connexin36 in cone pedicles and OFF-cone bipolar cells of the mouse retina. *The Journal of Neuroscience*, **24**, 3325-3334.

Feigenspan, A., Teubner, B., Willecke, K. & Weiler, R. (2001) Expression of neuronal connexin36 in AII amacrine cells of the mammalian retina. *The Journal of Neuroscience*, **21**, 230-239.

Fernandes, R., Girão, H. & Pereira, P. (2004) High glucose down-regulates intercellular communication in retinal endothelial cells by enhancing degradation of connexin 43 by a proteasome-dependent mechanism. *Journal of Biological Chemistry*, **279**, 27219-27224.

Fernández-Robredo, P., Sancho, A., Johnen, S., Recalde, S., Gama, N., Thumann, G., Groll, J. & García-Layana, A. (2014) Current Treatment Limitations in Age-Related Macular Degeneration and Future Approaches Based on Cell Therapy and Tissue Engineering. *Journal of Ophthalmology*, **2014**.

Field, G.D. & Chichilnisky, E.J. (2007) Information processing in the primate retina: circuitry and coding. *Annu Rev Neurosci*, **30**, 1-30.

Finkel, T. (2011) Signal transduction by reactive oxygen species. *J Cell Biol*, **194**, 7-15.

Fite, K.V., Bengston, L. & Donaghey, B. (1993) Experimental light damage increases lipofuscin in the retinal-pigment epithelium of Japanese-Quail (Coturnix-Coturnix-Japonica). *Exp Eye Res*, **57**, 449-460.

Fletcher, A.E., Bentham, G.C., Agnew, M., Young, I.S., Augood, C., Chakravarthy, U., de Jong, P.T., Rahu, M., Seland, J., Soubrane, G., Tomazzoli, L., Topouzis, F., Vingerling, J.R. & Vioque, J. (2008) Sunlight exposure, antioxidants, and age-related macular degeneration. *Arch Ophthalmol-Chic*, **126**, 1396-1403.

Fliesler, S.J. & Anderson, R.E. (1983) Chemistry and metabolism of lipids in the vertebrate retina. *Progress in Lipid Research*, **22**, 79-131.

Fontainhas, A.M., Wang, M., Liang, K.J., Chen, S., Mettu, P., Damani, M., Fariss, R.N., Li, W. & Wong, W.T. (2011) Microglial morphology and dynamic behavior is regulated by ionotropic glutamatergic and GABAergic neurotransmission. *Plos One*, **6**, e15973.

Francis, R.J.B. & Lo, C.W. (2006) Primordial germ cell deficiency in the connexin 43 knockout mouse arises from apoptosis associated with abnormal p53 activation. *Development*, **133**, 3451-3460.

Frank, R.N., Das, A. & Weber, M.L. (1989) A model of subretinal neovascularization in the pigmented rat. *Curr Eye Res*, **8**, 239-247.

Franklin-Tong, V. & Gourlay, C. (2008) A role for actin in regulating apoptosis/programmed cell death: evidence spanning yeast, plants and animals. *Biochem J*, **413**, 389-404.

Friedburg, C., Allen, C., Mason, P. & Lamb, T. (2004) Contribution of cone photoreceptors and post-receptoral mechanisms to the human photopic electroretinogram. *The Journal of Physiology*, **556**, 819-834.

Friedman, E. (1997) A hemodynamic model of the pathogenesis of age-related macular degeneration. *Am J Ophthalmol*, **124**, 677-682.

Fry, T., Evans, J.H. & Sanderson, M.J. (2001) Propagation of intercellular calcium waves in C6 glioma cells transfected with connexins 43 or 32. *Microscopy Research and Technique*, **52**, 289-300.

Fukumoto, M., Nakaizumi, A., Zhang, T., Lentz, S.I., Shibata, M. & Puro, D.G. (2012) Vulnerability of the retinal microvasculature to oxidative stress: ion channel-dependent mechanisms. *American Journal of Physiology-Cell Physiology*, **302**, C1413-C1420.

Fulton, A.B., Reynaud, X., Hansen, R.M., Lemere, C.A., Parker, C. & Williams, T.P. (1999) Rod photoreceptors in infant rats with a history of oxygen exposure. *Invest Ophthalmol Vis Sci*, **40**, 168-174.

Gaietta, G., Deerinck, T.J., Adams, S.R., Bouwer, J., Tour, O., Laird, D.W., Sosinsky, G.E., Tsien, R.Y. & Ellisman, M.H. (2002) Multicolor and electron microscopic imaging of connexin trafficking. *Science*, **296**, 503-507.

Gandhi, G.K., Ball, K.K., Cruz, N.F. & Dienel, G.A. (2010) Hyperglycaemia and diabetes impair gap junctional communication among astrocytes. *ASN Neuro*, **2**, e00030.

Gehrig, A., Langmann, T., Horling, F., Janssen, A., Bonin, M., Walter, M., Poths, S. & Weber, B.H.F. (2007) Genome-wide expression profiling of the retinoschisin-deficient retina in early postnatal mouse development. *Invest Ophthalmol Vis Sci*, **48**, 891-900.

Giepmans, B.N.G., Hengeveld, T., Postma, F.R. & Moolenaar, W.H. (2001) Interaction of c-Src with gap junction protein connexin-43. *Journal of Biological Chemistry*, **276**, 8544-8549.

Godley, B.F., Shamsi, F.A., Liang, F.Q., Jarrett, S.G., Davies, S. & Boulton, M. (2005) Blue light induces mitochondrial DNA damage and free radical production in epithelial cells. *Journal of Biological Chemistry*, **280**, 21061-21066.

Gold, B., Merriam, J.E., Zernant, J., Hancox, L.S., Taiber, A.J., Gehrs, K., Cramer, K., Neel, J., Bergeron, J. & Barile, G.R. (2006) Variation in factor B (BF) and complement component 2 (C2) genes is associated with age-related macular degeneration. *Nat Genet*, **38**, 458-462.

Goliger, J.A. & Paul, D.L. (1995) Wounding alters epidermal connexin expression and gap junction-mediated intercellular communication. *Molecular Biology of The Cell*, **6**, 1491-1501.

Gonçalves, A., Leal, E., Paiva, A., Teixeira Lemos, E., Teixeira, F., Ribeiro, C., Reis, F., Ambrósio, A. & Fernandes, R. (2012) Protective effects of the dipeptidyl peptidase

IV inhibitor sitagliptin in the blood–retinal barrier in a type 2 diabetes animal model. *Diabetes, Obesity and Metabolism*, **14**, 454-463.

Goodenough, D.A., Goliger, J.A. & Paul, D.L. (1996) Connexins, connexons, and intercellular communication. *Annu Rev Biochem*, **65**, 475-502.

Goodenough, D.A. & Paul, D.L. (2003) Beyond the gap: functions of unpaired connexon channels. *Nature Reviews Molecular Cell Biology*, **4**, 285-295.

Goodenough, D.A. & Paul, D.L. (2009) Gap junctions. *Cold Spring Harb Perspect Biol*, **1**, a002576.

Gottsch, J.D., Pou, S., Bynoe, L.A. & Rosen, G.M. (1990) Hematogenous photosensitization - a mechanism for the development of age-related macular degeneration. *Invest Ophthalmol Vis Sci*, **31**, 1674-1682.

Gourdie, R.G., Wei, Y., Kim, D., Klatt, S.C. & Mikawa, T. (1998) Endothelin-induced conversion of embryonic heart muscle cells into impulse-conducting Purkinje fibers. *Proceedings of the National Academy of Sciences*, **95**, 6815-6818.

Gray, D.A. & Woulfe, J. (2005) Lipofuscin and aging: a matter of toxic waste. *Science of Aging Knowledge Environment*, **2005**, re1.

Green, D.G. & Kapousta-Bruneau, N.V. (1999) A dissection of the electroretinogram from the isolated rat retina with microelectrodes and drugs. *Vis Neurosci*, **16**, 727-741.

Greenberg, M.E., Li, X.M., Gugiu, B.G., Gu, X., Qin, J., Salomon, R.G. & Hazen, S.L. (2008) The lipid whisker model of the structure of oxidized cell membranes. *Journal of biological chemistry*, **283**, 2385-2396.

Gregerson, D.S., Sam, T.N. & McPherson, S.W. (2004) The antigen-presenting activity of fresh, adult parenchymal microglia and perivascular cells from retina. *The Journal of Immunology*, **172**, 6587-6597.

Gregerson, D.S. & Yang, J. (2003) CD45-positive cells of the retina and their responsiveness to in vivo and in vitro treatment with IFN-gamma or anti-CD40. *Invest Ophthalmol Vis Sci*, **44**, 3083-3093.

Grimm, C., Reme, C.E., Rol, P.O. & Williams, T.P. (2000a) Blue light's effects on rhodopsin: photoreversal of bleaching in living rat eyes. *Invest Ophthalmol Vis Sci*, **41**, 3984-3990.

Grimm, C., Wenzel, A., Hafezi, F., Yu, S., Redmond, T.M. & Remé, C.E. (2000b) Protection of Rpe65-deficient mice identifies rhodopsin as a mediator of light-induced retinal degeneration. *Nat Genet*, **25**, 63-66.

Grosche, J., Härtig, W. & Reichenbach, A. (1995) Expression of glial fibrillary acidic protein (GFAP), glutamine synthetase (GS), and Bcl-2 protooncogene protein by Müller (glial) cells in retinal light damage of rats. *Neurosci Lett*, **185**, 119-122.

Grupcheva, C.N., Laux, W.T., Rupenthal, I.D., McGhee, J., McGhee, C.N.J. & Green, C.R. (2012) Improved corneal wound healing through modulation of gap junction communication using Connexin43-specific antisense oligodeoxynucleotides. *Invest Ophthalmol Vis Sci*, **53**, 1130-1138.

Guo, H., Acevedo, P., Parsa, F.D. & Bertram, J.S. (1992) Gap-junctional protein connexin 43 is expressed in dermis and epidermis of human skin: differential modulation by retinoids. *Journal of Investigative Dermatology*, **99**, 460-467.

Gupta, N., Brown, K.E. & Milam, A.H. (2003) Activated microglia in human retinitis pigmentosa, late-onset retinal degeneration, and age-related macular degeneration. *Exp Eye Res*, **76**, 463-471.

Guthrie, P.B., Knappenberger, J., Segal, M., Bennett, M.V.L., Charles, A.C. & Kater, S. (1999) ATP released from astrocytes mediates glial calcium waves. *The Journal of Neuroscience*, **19**, 520-528.

Hageman, G.S., Anderson, D.H., Johnson, L.V., Hancox, L.S., Taiber, A.J., Hardisty, L.I., Hageman, J.L., Stockman, H.A., Borchardt, J.D. & Gehrs, K.M. (2005) A common haplotype in the complement regulatory gene factor H (HF1/CFH) predisposes individuals to age-related macular degeneration. *Proc Natl Acad Sci U S A*, **102**, 7227-7232.

Hagigit, T., Abdulrazik, M., Orucov, F., Valamanesh, F., Lambert, M., Lambert, G., Behar-Cohen, F. & Benita, S. (2010) Topical and intravitreous administration of cationic nanoemulsions to deliver antisense oligonucleotides directed towards VEGF KDR receptors to the eye. *Journal of Controlled Release*, **145**, 297-305.

Hagins, W., Penn, R. & Yoshikami, S. (1970) Dark current and photocurrent in retinal rods. *Biophysical Journal*, **10**, 380-412.

Haigis, M.C. & Yankner, B.A. (2010) The aging stress response. *Mol Cell*, **40**, 333-344.

Haines, J.L., Hauser, M.A., Schmidt, S., Scott, W.K., Olson, L.M., Gallins, P., Spencer, K.L., Kwan, S.Y., Noureddine, M. & Gilbert, J.R. (2005) Complement factor H variant increases the risk of age-related macular degeneration. *Science*, **308**, 419-421.

Halaris, A. & Plietz, J. (2007) Agmatine: metabolic pathway and spectrum of activity in brain. *CNS Drugs*, **21**, 885-900.

Handa, J.T. (2012) How does the macula protect itself from oxidative stress? *Molecular Aspects of Medicine*, **33**, 418-435.

Hanisch, U.K. & Kettenmann, H. (2007) Microglia: active sensor and versatile effector cells in the normal and pathologic brain. *Nature Neuroscience*, **10**, 1387-1394.

Hanitzsch, R., Küppers, L. & Flade, A. (2004) The effect of GABA and the GABA-uptake-blocker NO-711 on the b-wave of the ERG and the responses of horizontal cells to light. *Graefe's Archive for Clinical and Experimental Ophthalmology*, **242**, 784-791.

Harris, A.L. (2001) Emerging issues of connexin channels: biophysics fills the gap. *Q Rev Biophys*, **34**, 325-472.

Hartveit, E. & Lin Veruki, M. (2012) Electrical synapses between AII amacrine cells in the retina: function and modulation. *Brain Research*, **1487**, 160-172.

Hashizume, K., Hirasawa, M., Imamura, Y., Noda, S., Shimizu, T., Shinoda, K., Kurihara, T., Noda, K., Ozawa, Y. & Ishida, S. (2008) Retinal dysfunction and progressive retinal cell death in SOD1-deficient mice. *The American Journal of Pathology*, **172**, 1325-1331.

Haupt, C., Witte, O. & Frahm, C. (2007) Temporal profile of connexin 43 expression after photothrombotic lesion in rat brain. *Neuroscience*, **144**, 562-570.

Haverkamp, S., Grünert, U. & Wässle, H. (2000) The cone pedicle, a complex synapse in the retina. *Neuron*, **27**, 85-95.

Hawat, G., Hélie, P. & Baroudi, G. (2012) Single intravenous low-dose injections of connexin 43 mimetic peptides protect ischemic heart in vivo against myocardial infarction. *J Mol Cell Cardiol*, **53**, 559-566.

Hazen, S.L. (2008) Oxidized phospholipids as endogenous pattern recognition ligands in innate immunity. *Journal of Biological Chemistry*, **283**, 15527-15531.

Hecker, L.A., Edwards, A.O., Ryu, E., Tosakulwong, N., Baratz, K.H., Brown, W.L., Issa, P.C., Scholl, H.P., Pollok-Kopp, B. & Schmid-Kubista, K.E. (2010) Genetic control of the alternative pathway of complement in humans and age-related macular degeneration. *Human Molecular Genetics*, **19**, 209-215.

Hernandez, M., Rodriguez, F.D., Sharma, S. & Vecino, E. (2009) Immunohistochemical changes in rat retinas at various time periods of elevated intraocular pressure. *Mol Vis*, **15**, 2696-2709.

Hevel, J., White, K. & Marletta, M. (1991) Purification of the inducible murine macrophage nitric oxide synthase. Identification as a flavoprotein. *Journal of Biological Chemistry*, **266**, 22789-22791.

Heyworth, P., Curnutte, J., Nauseef, W., Volpp, B., Pearson, D., Rosen, H. & Clark, R. (1991) Neutrophil nicotinamide adenine dinucleotide phosphate oxidase assembly.

Translocation of p47-phox and p67-phox requires interaction between p47-phox and cytochrome b558. *J Clin Invest*, **87**, 352-356.

Hidaka, S., Akahori, Y. & Kurosawa, Y. (2004) Dendrodendritic electrical synapses between mammalian retinal ganglion cells. *The Journal of Neuroscience*, **24**, 10553-10567.

Hirasawa, H. & Kaneko, A. (2003) pH changes in the invaginating synaptic cleft mediate feedback from horizontal cells to cone photoreceptors by modulating Ca^{2+} channels. *The Journal of General Physiology*, **122**, 657-671.

Hofer, A. & Dermietzel, R. (1998) Visualization and functional blocking of gap junction hemichannels (connexons) with antibodies against external loop domains in astrocytes. *Glia*, **24**, 141-154.

Hogg, R.E., Woodside, J.V., Gilchrist, S.E.C.M., Graydon, R., Fletcher, A.E., Chan, W., Knox, A., Cartmill, B. & Chakravarthy, U. (2008) Cardiovascular disease and hypertension are strong risk factors for choroidal neovascularization. *Ophthalmology*, **115**, 1046-1052.

Hollyfield, J.G., Bonilha, V.L., Rayborn, M.E., Yang, X.P., Shadrach, K.G., Lu, L., Ufret, R.L., Salomon, R.G. & Perez, V.L. (2008) Oxidative damage-induced inflammation initiates age-related macular degeneration. *Nat Med*, **14**, 194-198.

Hombach, S., Janssen-Bienhold, U., Söhl, G., Schubert, T., Büssow, H., Ott, T., Weiler, R. & Willecke, K. (2004) Functional expression of connexin57 in horizontal cells of the mouse retina. *European Journal of Neuroscience*, **19**, 2633-2640.

Hood, D.C. & Birch, D.G. (1990) The a-wave of the human electroretinogram and rod receptor function. *Invest Ophthalmol Vis Sci*, **31**, 2070-2081.

Hossain, M., Peeling, J., Sutherland, G., Hertzberg, E. & Nagy, J. (1994) Ischemia-induced cellular redistribution of the astrocytic gap junctional protein connexin43 in rat brain. *Brain Research*, **652**, 311-322.

Hu, E.H., Pan, F., Völgyi, B. & Bloomfield, S.A. (2010) Light increases the gap junctional coupling of retinal ganglion cells. *The Journal of Physiology*, **588**, 4145-4163.

Hua, G., Pennesi, M., Shah, K., Qiao, X., Hariprasad, S.M., Mieler, W.F., Wu, S.M. & Holz, E.R. (2003) Safety of intravitreal voriconazole: electroretinographic and histopathologic studies. *Transactions of the American Ophthalmological Society*, **101**, 183-189.

Huber, G., Heynen, S., Imsand, C., vom Hagen, F., Muehlfriedel, R., Tanimoto, N., Feng, Y., Hammes, H.-P., Grimm, C. & Peichl, L. (2010) Novel rodent models for macular research. *Plos One*, **5**, e13403.

Hübscher, U. & Maga, G. (2011) DNA replication and repair bypass machines. *Current Opinion in Chemical Biology*, **15**, 627-635.

Hunter, A.W., Barker, R.J., Zhu, C. & Gourdie, R.G. (2005) Zonula occludens-1 alters connexin43 gap junction size and organization by influencing channel accretion. *Molecular Biology of The Cell*, **16**, 5686-5698.

Hyman, L., Schachat, A.P., He, Q. & Leske, M.C. (2000) Hypertension, cardiovascular disease, and age-related macular degeneration. *Arch Ophthalmol-Chic*, **118**, 351.

Ibrahim, A.S., El-Remessy, A.B., Matragoon, S., Zhang, W., Patel, Y., Khan, S., Al-Gayyar, M.M., El-Shishtawy, M.M. & Liou, G.I. (2011) Retinal microglial activation and inflammation induced by amadori-glycated albumin in a rat model of diabetes. *Diabetes*, **60**, 1122-1133.

Ikeda, Y., Yonemitsu, Y., Onimaru, M., Nakano, T., Miyazaki, M., Kohno, R., Nakagawa, K., Ueno, A., Sueishi, K. & Ishibashi, T. (2006) The regulation of vascular endothelial growth factors (VEGF-A,-C, and-D) expression in the retinal pigment epithelium. *Exp Eye Res*, **83**, 1031-1040.

Imai, S., Inokuchi, Y., Nakamura, S., Tsuruma, K., Shimazawa, M. & Hara, H. (2010) Systemic administration of a free radical scavenger, edaravone, protects against light-induced photoreceptor degeneration in the mouse retina. *Eur J Pharmacol*, **642**, 77-85.

Imamura, Y., Noda, S., Hashizume, K., Shinoda, K., Yamaguchi, M., Uchiyama, S., Shimizu, T., Mizushima, Y., Shirasawa, T. & Tsubota, K. (2006) Drusen, choroidal neovascularization, and retinal pigment epithelium dysfunction in SOD1-deficient mice: a model of age-related macular degeneration. *Proceedings of the National Academy of Sciences*, **103**, 11282-11287.

Jackson, G.R., McGwin, G., Phillips, J.M., Klein, R. & Owsley, C. (2006) Impact of aging and age-related maculopathy on inactivation of the a-wave of the rod-mediated electroretinogram. *Vision Res*, **46**, 1422-1431.

Jager, R.D., Mieler, W.F. & Miller, J.W. (2008) Age-related macular degeneration. *New England Journal of Medicine*, **358**, 2606-2617.

Janssen-Bienhold, U., Dermietzel, R. & Weiler, R. (1998) Distribution of connexin43 immunoreactivity in the retinas of different vertebrates. *The Journal of Comparative Neurology*, **396**, 310-321.

Janssen-Bienhold, U., Trümpler, J., Hilgen, G., Schultz, K., De Sevilla Müller, L.P., Sonntag, S., Dedek, K., Dirks, P., Willecke, K. & Weiler, R. (2009) Connexin57 is expressed in dendro-dendritic and axo-axonal gap junctions of mouse horizontal cells and its distribution is modulated by light. *The Journal of Comparative Neurology*, **513**, 363-374.

Jara, P.I., Boric, M.P. & Saez, J.C. (1995) Leukocytes express connexin 43 after activation with lipopolysaccharide and appear to form gap junctions with endothelial cells after ischemia-reperfusion. *Proceedings of the National Academy of Sciences*, **92**, 7011-7015.

Jay, P.Y., Harris, B.S., Maguire, C.T., Buerger, A., Wakimoto, H., Tanaka, M., Kupershmidt, S., Roden, D.M., Schultheiss, T.M. & O Brien, T.X. (2004) Nkx2-5 mutation causes anatomic hypoplasia of the cardiac conduction system. *J Clin Invest*, **113**, 1130-1137.

Johansson, K., Bruun, A. & Ehinger, B. (1999) Gap junction protein connexin43 is heterogeneously expressed among glial cells in the adult rabbit retina. *The Journal of Comparative Neurology*, **407**, 395-403.

John, S.A., Kondo, R., Wang, S.Y., Goldhaber, J.I. & Weiss, J.N. (1999) Connexin-43 hemichannels opened by metabolic inhibition. *Journal of Biological Chemistry*, **274**, 236-240.

Johnson, L.V., Leitner, W.P., Staples, M.K. & Anderson, D.H. (2001) Complement activation and inflammatory processes in Drusen formation and age related macular degeneration. *Exp Eye Res*, **73**, 887-896.

Jones, B., Marc, R., Watt, C., Vaughan, D. & Organisciak, D. (2006) Neural plasticity revealed by light-induced photoreceptor lesions. *Adv Exp Med Biol*, **572**, 405-410.

Jones, B.W. & Marc, R.E. (2005) Retinal remodeling during retinal degeneration. *Exp Eye Res*, **81**, 123-137.

Jordan, K., Chodock, R., Hand, A.R. & Laird, D.W. (2001) The origin of annular junctions: a mechanism of gap junction internalization. *J Cell Sci*, **114**, 763-773.

Juneja, S.C., Barr, K.J., Enders, G.C. & Kidder, G.M. (1999) Defects in the germ line and gonads of mice lacking connexin43. *Biology of Reproduction*, **60**, 1263-1270.

Kaitz, M. & Auerbach, E. (1979) Action spectrum for light-induced retinal degeneration in dystrophic rats. *Vision Res*, **19**, 1041-1044.

Kalloniatis, M., Tomisich, G., Wellard, J.W. & Foster, L.E. (2002) Mapping photoreceptor and postreceptoral labelling patterns using a channel permeable probe (agmatine) during development in the normal and RCS rat retina. *Vis Neurosci*, **19**, 61-70.

Kamermans, M., Fahrenfort, I., Schultz, K., Janssen-Bienhold, U., Sjoerdsma, T. & Weiler, R. (2001) Hemichannel-mediated inhibition in the outer retina. *Science Signalling*, **292**, 1178-1180.

Karlstetter, M., Ebert, S. & Langmann, T. (2010) Microglia in the healthy and degenerating retina: Insights from novel mouse models. *Immunobiology*, **215**, 685-691.

Karpuk, N., Burkovetskaya, M., Fritz, T., Angle, A. & Kielian, T. (2011) Neuroinflammation leads to region-dependent alterations in astrocyte gap junction communication and hemichannel activity. *The Journal of neuroscience*, **31**, 414-425.

Kasai, H. & Nishimura, S. (1984) Hydroxylation of deoxyguanosine at the C-8 position by ascorbic acid and other reducing agents. *Nucleic Acids Res*, **12**, 2137-2145.

Kaur, C., Foulds, W. & Ling, E. (2008) Blood–retinal barrier in hypoxic ischaemic conditions: basic concepts, clinical features and management. *Prog Retin Eye Res*, **27**, 622-647.

Kawarai, M. & Koss, M.C. (1998) Sympathetic vasoconstriction in the rat anterior choroid is mediated by α1-adrenoceptors. *Eur J Pharmacol*, **363**, 35-40.

Ke, F.C., Fang, S.H., Lee, M.T., Sheu, S.Y., Lai, S.Y., Chen, Y.J., Huang, F.L., Wang, P.S., Stocco, D.M. & Hwang, J.J. (2005) Lindane, a gap junction blocker, suppresses FSH and transforming growth factor β1-induced connexin43 gap junction formation and steroidogenesis in rat granulosa cells. *Journal of Endocrinology*, **184**, 555-566.

Kelsell, D., Dunlop, J., Stevens, H., Lench, N., Liang, J., Parry, G., Mueller, R. & Leigh, I. (1997) Connexin 26 mutations in hereditary non-syndromic sensorineural deafness. *Nature*, **387**, 80-83.

Kern, T.S., Du, Y.P., Smith, M.A. & Miller, C.M. (2002) Diabetes-induced nitrative stress in the retina, and correction by aminoguanidine. *J Neurochem*, **80**, 771-779.

Kerr, N.M., Johnson, C.S., de Souza, C.F., Chee, K.S., Good, W.R., Green, C.R. & Danesh-Meyer, H.V. (2010) Immunolocalization of gap junction protein connexin43 (GJA1) in the human retina and optic nerve. *Invest Ophthalmol Vis Sci*, **51**, 4028-4034.

Kerr, N.M., Johnson, C.S., Green, C.R. & Danesh-Meyer, H.V. (2011) Gap junction protein connexin43 (GJA1) in the human glaucomatous optic nerve head and retina. *J Clin Neurosci*, **18**, 102-108.

Khan, J., Thurlby, D., Shahid, H., Clayton, D., Yates, J., Bradley, M., Moore, A. & Bird, A. (2006) Smoking and age related macular degeneration: the number of pack years of cigarette smoking is a major determinant of risk for both geographic atrophy and choroidal neovascularisation. *Brit J Ophthalmol*, **90**, 75-80.

Khandhadia, S., Cipriani, V., Yates, J. & Lotery, A.J. (2012) Age-related macular degeneration and the complement system. *Immunobiology*, **217**, 127-146.

Khandhadia, S. & Lotery, A. (2010) Oxidation and age-related macular degeneration: insights from molecular biology. *Expert Rev Mol Med*, **12**, e34.

Kihara, A., Paschon, V., Cardoso, C., Higa, G., Castro, L., Hamassaki, D. & Britto, L. (2009) Connexin36, an essential element in the rod pathway, is highly expressed in the essentially rodless retina of Gallus gallus. *The Journal of Comparative Neurology*, **512**, 651-663.

Kihara, A.H., Mantovani de Castro, L., Moriscot, A.S. & Hamassaki, D.E. (2006) Prolonged dark adaptation changes connexin expression in the mouse retina. *J Neurosci Res*, **83**, 1331-1341.

Kim, E. & Fishman, G.I. (2012) Designer gap junctions that prevent cardiac arrhythmias. *Trends in Cardiovascular Medicine*, **23**, 33-38.

Kinnunen, K., Petrovski, G., Moe, M.C., Berta, A. & Kaarniranta, K. (2011) Molecular mechanisms of retinal pigment epithelium damage and development of age-related macular degeneration. *Acta Ophthalmol*, **90**, 299-309.

Klaassen, L., Fahrenfort, I. & Kamermans, M. (2012) Connexin hemichannel mediated ephaptic inhibition in the retina. *Brain Research*, **1487**, 25-38.

Klaver, C., Kliffen, M., van Duijn, C.M., Hofman, A., Cruts, M., Grobbee, D.E., van Broeckhoven, C. & De Jong, P. (1998a) Genetic association of apolipoprotein E with age-related macular degeneration. *American Journal of Human Genetics*, **63**, 200-206.

Klaver, C.C.W., Wolfs, R.C.W., Vingerling, J.R., Hofman, A. & de Jong, P.T.V.M. (1998b) Age-specific prevalence and causes of blindness and visual impairment in an older population: the Rotterdam Study. *Arch Ophthalmol-Chic*, **116**, 653-658.

Klein, M.L., Mauldin, W.M. & Stoumbos, V.D. (1994) Heredity and age-related macular degeneration. Observations in monozygotic twins. *Arch Ophthalmol-Chic*, **112**, 932-937.

Klein, R.J., Zeiss, C., Chew, E.Y., Tsai, J.Y., Sackler, R.S., Haynes, C., Henning, A.K., SanGiovanni, J.P., Mane, S.M. & Mayne, S.T. (2005) Complement factor H polymorphism in age-related macular degeneration. *Science*, **308**, 385-389.

Kliffen, M., Sharma, H.S., Mooy, C.M., Kerkvliet, S. & de Jong, P.T.V.M. (1997) Increased expression of angiogenic growth factors in age-related maculopathy. *Brit J Ophthalmol*, **81**, 154-162.

Klump, K.E., Zhang, A.-J., Wu, S.M. & Marshak, D.W. (2009) Parvalbumin-immunoreactive amacrine cells of macaque retina. *Vis Neurosci*, **26**, 287-296.

Knaus, U.G., Heyworth, P.G., Evans, T., Curnutte, J.T. & Bokoch, G.M. (1991) Regulation of phagocyte oxygen radical production by the GTP-binding protein Rac 2. *Science*, **254**, 1512-1515.

Kofuji, P., Ceelen, P., Zahs, K.R., Surbeck, L.W., Lester, H.A. & Newman, E.A. (2000) Genetic inactivation of an inwardly rectifying potassium channel (Kir4. 1 subunit) in mice: phenotypic impact in retina. *The Journal of neuroscience*, **20**, 5733-5740.

Kokubo, J., Nagatani, N., Hiroki, K., Kuroiwa, K., Watanabe, N. & Arai, T. (2008) Mechanism of destruction of microtubule structures by 4-hydroxy-2-nonenal. *Cell Structure and Function*, **33**, 51-59.

Kolb, H. (1974) The connections between horizontal cells and photoreceptors in the retina of the cat: electron microscopy of Golgi preparations. *The Journal of Comparative Neurology*, **155**, 1-14.

Kolb, H. & Dekorver, L. (1991) Midget ganglion cells of the parafovea of the human retina: a study by electron microscopy and serial section reconstructions. *The Journal of Comparative Neurology*, **303**, 617-636.

Kolb, H., Fernandez, E., Schouten, J., Ahnelt, P., Linberg, K.A. & Fisher, S.K. (1994) Are there three types of horizontal cell in the human retina? *The Journal of Comparative Neurology*, **343**, 370-386.

Kolb, H., Linberg, K.A. & Fisher, S.K. (1992) Neurons of the human retina: a Golgi study. *The Journal of Comparative Neurology*, **318**, 147-187.

Komarova, Y. & Malik, A.B. (2010) Regulation of endothelial permeability via paracellular and transcellular transport pathways. *Annual Review of Physiology*, **72**, 463-493.

Konerding, M.A. (2004) Ocular angiogenesis: translating preclinical indications to successful clinical development. *Expert Opinion on Therapeutic Targets*, **8**, 255-258.

Kretz, M., Euwens, C., Hombach, S., Eckardt, D., Teubner, B., Traub, O., Willecke, K. & Ott, T. (2003) Altered connexin expression and wound healing in the epidermis of connexin-deficient mice. *J Cell Sci*, **116**, 3443-3452.

Kreutzberg, G.W. (1996) Microglia: a sensor for pathological events in the CNS. *Trends in Neurosciences*, **19**, 312-318.

Kumar, N.M. & Gilula, N.B. (1996) The gap junction communication channel. *Cell*, **84**, 381-388.

Kuo, I.Y., Chan-Ling, T., Wojcikiewicz, R.J. & Hill, C.E. (2008) Limited intravascular coupling in the rodent brainstem and retina supports a role for glia in regional blood flow. *The Journal of Comparative Neurology*, **511**, 773-787.

Kur, J., Newman, E.A. & Chan-Ling, T. (2012) Cellular and physiological mechanisms underlying blood flow regulation in the retina and choroid in health and disease. *Prog Retin Eye Res*, **31**, 377-406.

Kurz-Isler, G. & Wolburg, H. (1986) Gap junctions between horizontal cells in the cyprinid fish alter rapidly their structure during light and dark adaptation. *Neurosci Lett*, **67**, 7-12.

Kwak, B.R. & Jongsma, H.J. (1999) Selective inhibition of gap junction channel activity by synthetic peptides. *The Journal of Physiology*, **516**, 679-685.

Kwak, B.R., Pepper, M.S., Gros, D.B. & Meda, P. (2001) Inhibition of endothelial wound repair by dominant negative connexin inhibitors. *Molecular Biology of The Cell*, **12**, 831-845.

Laird, D.W. (2006) Life cycle of connexins in health and disease. *Biochem J*, **394**, 527-543.

Laird, D.W., Puranam, K.L. & Revel, J.P. (1991) Turnover and phosphorylation dynamics of connexin43 gap junction protein in cultured cardiac myocytes. *Biochem J*, **273**, 67-72.

Lampe, P.D., TenBroek, E.M., Burt, J.M., Kurata, W.E., Johnson, R.G. & Lau, A.F. (2000) Phosphorylation of connexin43 on serine368 by protein kinase C regulates gap junctional communication. *J Cell Biol*, **149**, 1503-1512.

Langmann, T. (2007) Microglia activation in retinal degeneration. *J Leukocyte Biol*, **81**, 1345-1351.

Lauritzen, K.H., Cheng, C., Wiksen, H., Bergersen, L.H. & Klungland, A. (2011) Mitochondrial DNA toxicity compromises mitochondrial dynamics and induces hippocampal antioxidant defenses. *DNA Repair (Amst)*, **10**, 639-653.

Laux-Fenton, W.T., Donaldson, P.J., Kistler, J. & Green, C.R. (2003) Connexin expression patterns in the rat cornea: molecular evidence for communication compartments. *Cornea*, **22**, 457-464.

Lee, H.C., Galione, A. & Walseth, T.F. (1994) Cyclic ADP-ribose: metabolism and calcium mobilizing function. *Vitamins & Hormones*, **48**, 199-257.

Lee, I.H., Lindqvist, E., Kiehn, O., Widenfalk, J. & Olson, L. (2005) Glial and neuronal connexin expression patterns in the rat spinal cord during development and following injury. *The Journal of Comparative Neurology*, **489**, 1-10.

Leeson, T. (1979) Rat retinal blood vessels. *Canadian Journal of Ophthalmology*, **14**, 21-28.

Lens, A., Nemeth, S.C. & Ledford, J.K. (eds) (2008) *Ocular anatomy and physiology*. SLACK Incorporated Thorofare, USA.

Leto, T.L., Lomax, K.J., Volpp, B.D., Nunoi, H., Sechler, J., Nauseef, W.M., Clark, R.A., Gallin, J.I. & Malech, H.L. (1990) Cloning of a 67-kD neutrophil oxidase factor with similarity to a noncatalytic region of p60c-src. *Science*, **248**, 727-730.

Levin, L.A., Nilsson, S.F.E., Ver Hoeve, J., Wu, S.M., Kaufman, P.L. & Alm, A. (eds) (2011) *Adler's physiology of the eye*. Saunders Elsevier, Edinburgh.

Leybaert, L. & Sanderson, M.J. (2012) Intercellular Ca^{2+} waves: mechanisms and function. *Physiological Reviews*, **92**, 1359-1392.

Li, A., Lane, W.S., Johnson, L.V., Chader, G.J. & Tombran-Tink, J. (1995) Neuron-specific enolase: a neuronal survival factor in the retinal extracellular matrix? *The Journal of Neuroscience*, **15**, 385-393.

Li, A.F., Sato, T., Haimovici, R., Okamoto, T. & Roy, S. (2003) High glucose alters connexin 43 expression and gap junction intercellular communication activity in retinal pericytes. *Invest Ophthalmol Vis Sci*, **44**, 5376.

Li, L., Cheng, C., Xia, C., White, T.W., Fletcher, D.A. & Gong, X. (2010) Connexin mediated cataract prevention in mice. *Plos One*, **5**, e12624.

Li, W. & DeVries, S.H. (2004) Separate blue and green cone networks in the mammalian retina. *Nature Neuroscience*, **7**, 751-756.

Li, Z., Liu, B., Maminishkis, A., Mahesh, S.P., Yeh, S., Lew, J., Lim, W.K., Sen, H., Clarke, G. & Buggage, R. (2008) Gene expression profiling in autoimmune noninfectious uveitis disease. *The Journal of Immunology*, **181**, 5147-5157.

Libby, R.T. & Gould, D.B. (2010) Endoplasmic reticulum stress as a primary pathogenic mechanism leading to age-related macular degeneration. *Adv Exp Med Biol*, **664**, 403-409.

Lim, L.S., Mitchell, P., Seddon, J.M., Holz, F.G. & Wong, T.Y. (2012) Age-related macular degeneration. *The Lancet*, **379**, 1728-1738.

Lin, H., Xu, H., Liang, F.Q., Liang, H., Gupta, P., Havey, A.N., Boulton, M.E. & Godley, B.F. (2011) Mitochondrial DNA damage and repair in RPE associated with aging and age-related macular degeneration. *Invest Ophthalmol Vis Sci*, **52**, 3521-3529.

Lin, J.H.C., Weigel, H., Cotrina, M.L., Liu, S., Bueno, E., Hansen, A.J., Hansen, T.W., Goldman, S. & Nedergaard, M. (1998) Gap-junction-mediated propagation and amplification of cell injury. *Nature Neuroscience*, **1**, 494-500.

Linsenmeier, R.A. & Braun, R. (1992) Oxygen distribution and consumption in the cat retina during normoxia and hypoxemia. *The Journal of General Physiology*, **99**, 177-197.

Liu, B., Wei, L., Meyerle, C., Tuo, J., Sen, H.N., Li, Z., Chakrabarty, S., Agron, E., Chan, C.C. & Klein, M.L. (2011) Complement component C5a promotes expression of IL-22 and IL-17 from human T cells and its Implication in age-related macular degeneration. *Journal of Translational Medicine*, **9**, 1-12.

Lommatzsch, A., Hermans, P., Müller, K., Bornfeld, N., Bird, A. & Pauleikhoff, D. (2008) Are low inflammatory reactions involved in exudative age-related macular degeneration? *Graefe's Archive for Clinical and Experimental Ophthalmology*, **246**, 803-810.

Lotery, A. & Trump, D. (2007) Progress in defining the molecular biology of age related macular degeneration. *Human Genetics*, **122**, 219-236.

Lukasiewicz, P. (2005) Synaptic mechanisms that shape visual signaling at the inner retina. *Progress in Brain Research*, **147**, 205-218.

Lukasiewicz, P., Maple, B. & Werblin, F. (1994) A novel GABA receptor on bipolar cell terminals in the tiger salamander retina. *The Journal of Neuroscience*, **14**, 1202-1212.

Ly, A., Yee, P., Vessey, K.A., Phipps, J.A., Jobling, A.I. & Fletcher, E.L. (2011) Early inner retinal astrocyte dysfunction during diabetes and development of hypoxia, retinal stress, and neuronal functional loss. *Invest Ophthalmol Vis Sci*, **52**, 9316-9326.

Ma, P., Luo, Y., Zhu, X., Ma, H., Hu, J. & Tang, S. (2009a) Phosphomannopentaose sulfate (PI-88) inhibits retinal leukostasis in diabetic rat. *Biochem Biophys Res Commun*, **380**, 402-406.

Ma, W., Zhao, L., Fontainhas, A.M., Fariss, R.N. & Wong, W.T. (2009b) Microglia in the mouse retina alter the structure and function of retinal pigmented epithelial cells: a potential cellular interaction relevant to AMD. *Plos One*, **4**, e7945.

Madigan, M.C., Penfold, P.L., Provis, J.M., Balind, T.K. & Billson, F.A. (1994) Intermediate filament expression in human retinal macroglia. Histopathologic changes associated with age-related macular degeneration. *Retina*, **14**, 65-74.

Malchow, R., Qian, H. & Ripps, H. (1993) Evidence for hemi-gap junctional channels in isolated horizontal cells of the skate retina. *J Neurosci Res*, **35**, 237-245.

Maloney, S., Godeiro, K., Odashiro, A. & Burnier, M. (2007) Current and emerging concepts in the management of neovascular age-related macular degeneration. *Cardiovascular & Hematological Agents in Medicinal Chemistry*, **5**, 147-154.

Mambo, E., Nyaga, S.G., Bohr, V.A. & Evans, M.K. (2002) Defective repair of 8-hydroxyguanine in mitochondria of MCF-7 and MDA-MB-468 human breast cancer cell lines. *Cancer Res*, **62**, 1349-1355.

Marc, R.E., Jones, B.W., Watt, C.B., Vazquez-Chona, F., Vaughan, D.K. & Organisciak, D.T. (2008) Extreme retinal remodeling triggered by light damage: implications for age related macular degeneration. *Mol Vis*, **14**, 782-806.

Marín-Teva, J.L., Cuadros, M.A., Martín-Oliva, D. & Navascués, J. (2012) Microglia and neuronal cell death. *Neuron Glia Biology*, **1**, 1-16.

Marneros, A.G., Fan, J., Yokoyama, Y., Gerber, H.P., Ferrara, N., Crouch, R.K. & Olsen, B.R. (2005) Vascular endothelial growth factor expression in the retinal pigment epithelium is essential for choriocapillaris development and visual function. *The American Journal of Pathology*, **167**, 1451-1459.

Martinez, G., Campbell, A., Reinken, J. & Allan, B. (1982) Prevalence of ocular disease in a population study of subjects 65 years old and older. *Am J Ophthalmol*, **94**, 181-189.

Maxeiner, S., Dedek, K., Janssen-Bienhold, U., Ammermüller, J., Brune, H., Kirsch, T., Pieper, M., Degen, J., Krüger, O. & Willecke, K. (2005) Deletion of connexin45 in mouse retinal neurons disrupts the rod/cone signaling pathway between AII amacrine and ON cone bipolar cells and leads to impaired visual transmission. *The Journal of Neuroscience*, **25**, 566-576.

McGeer, E.G., Klegeris, A. & McGeer, P.L. (2005) Inflammation, the complement system and the diseases of aging. *Neurobiol Aging*, **26**, S94-S97.

McLeod, D.S., Grebe, R., Bhutto, I., Merges, C., Baba, T. & Lutty, G.A. (2009) Relationship between RPE and choriocapillaris in age-related macular degeneration. *Invest Ophthalmol Vis Sci*, **50**, 4982-4991.

McLeod, D.S., Taomoto, M., Otsuji, T., Green, W.R., Sunness, J.S. & Lutty, G.A. (2002) Quantifying changes in RPE and choroidal vasculature in eyes with age-related macular degeneration. *Invest Ophthalmol Vis Sci*, **43**, 1986-1993.

McMenamin, P.G. (1999) Subretinal macrophages in the developing eye of eutherian mammals and marsupials. *Anatomy and Embryology*, **200**, 551-558.

Mendoza-Naranjo, A., Saéz, P.J., Johansson, C.C., Ramírez, M., Mandakovic, D., Pereda, C., López, M.N., Kiessling, R., Sáez, J.C. & Salazar-Onfray, F. (2007) Functional gap junctions facilitate melanoma antigen transfer and cross-presentation between human dendritic cells. *The Journal of Immunology*, **178**, 6949-6957.

Mese, G., Richard, G. & White, T.W. (2007) Gap junctions: basic structure and function. *Journal of Investigative Dermatology*, **127**, 2516-2524.

Meyers, S.M. & Zachary, A.A. (1988) Monozygotic twins with age-related macular degeneration. *Arch Ophthalmol-Chic*, **106**, 651-653.

234

Milam, A.H., Gupta, N. & Brown, K.E. (2003) Activated microglia in human retinitis pigmentosa, late-onset retinal degeneration, and age-related macular degeneration. *Exp Eye Res*, **76**, 463-471.

Mills, S.L. & Massey, S.C. (2000) A series of biotinylated tracers distinguishes three types of gap junction in retina. *The Journal of Neuroscience*, **20**, 8629-8636.

Mills, S.L., O'Brien, J.J., Li, W., O'Brien, J. & Massey, S.C. (2001) Rod pathways in the mammalian retina use connexin 36. *J Comp Neurol*, **436**, 336-350.

Mitchell, P., Smith, W. & Wang, J.J. (1998) Iris color, skin sun sensitivity, and age-related maculopathy: the Blue Mountains Eye Study. *Ophthalmology*, **105**, 1359-1363.

Miyagi, M., Sakaguchi, H., Darrow, R.M., Yan, L., West, K.A., Aulak, K.S., Stuehr, D.J., Hollyfield, J.G., Organisciak, D.T. & Crabb, J.W. (2002) Evidence that light modulates protein nitration in rat retina. *Molecular & Cellular Proteomics*, **1**, 293-303.

Mohand-Said, S., Deudon-Combe, A., Hicks, D., Simonutti, M., Forster, V., Fintz, A.-C., Léveillard, T., Dreyfus, H. & Sahel, J.-A. (1998) Normal retina releases a diffusible factor stimulating cone survival in the retinal degeneration mouse. *Proceedings of the National Academy of Sciences*, **95**, 8357-8362.

Morgan, J.I.W., Hunter, J.J., Masella, B., Wolfe, R., Gray, D.C., Merigan, W.H., Delori, F.C. & Williams, D.R. (2008) Light-induced retinal changes observed with high-resolution autofluorescence imaging of the retinal pigment epithelium. *Invest Ophthalmol Vis Sci*, **49**, 3715-3729.

Mori, R., Power, K.T., Wang, C.M., Martin, P. & Becker, D.L. (2006) Acute downregulation of connexin43 at wound sites leads to a reduced inflammatory response, enhanced keratinocyte proliferation and wound fibroblast migration. *J Cell Sci*, **119**, 5193-5203.

Moyer, K., Davis, A., Saggers, G., Mackay, D. & Ehrlich, H. (2002) Wound healing: the role of gap junctional communication in rat granulation tissue maturation. *Experimental and Molecular Pathology*, **72**, 10-16.

Mullins, R.F., Russell, S.R., Anderson, D.O.N.H. & Hageman, G.S. (2000) Drusen associated with aging and age-related macular degeneration contain proteins common to extracellular deposits associated with atherosclerosis, elastosis, amyloidosis, and dense deposit disease. *The FASEB Journal*, **14**, 835-846.

Musil, L.S. & Goodenough, D.A. (1993) Multisubunit assembly of an integral plasma membrane channel protein, gap junction connexin43, occurs after exit from the ER. *Cell*, **74**, 1065-1077.

Nagy, J., Yamamoto, T., Sawchuk, M., Nance, D. & Hertzberg, E. (1992) Quantitative immunohistochemical and biochemical correlates of connexin43 localization in rat brain. *Glia*, **5**, 1-9.

Naka, K.I. & Rushton, W.A.H. (1966) S-potentials from luminosity units in retina of fish (Cyprinidae). *Journal of Physiology*, **185**, 587-599.

Nakamura, Y. (2002) Regulating factors for microglial activation. *Biological and Pharmaceutical Bulletin*, **25**, 945-953.

Nakano, Y., Oyamada, M., Dai, P., Nakagami, T., Kinoshita, S. & Takamatsu, T. (2008) Connexin43 knockdown accelerates wound healing but inhibits mesenchymal transition after corneal endothelial injury in vivo. *Invest Ophthalmol Vis Sci*, **49**, 93-104.

Nakase, T., Fushiki, S. & Naus, C.C.G. (2003) Astrocytic gap junctions composed of connexin 43 reduce apoptotic neuronal damage in cerebral ischemia. *Stroke*, **34**, 1987-1993.

Nakase, T., Yoshida, Y. & Nagata, K. (2006) Enhanced connexin 43 immunoreactivity in penumbral areas in the human brain following ischemia. *Glia*, **54**, 369-375.

Nawy, S. & Jahr, C.E. (1990) Suppression by glutamate of cGMP-activated conductance in retinal bipolar cells. *Nature*, **346**, 269-271.

Nelson, R. (1977) Cat cones have rod input: a comparison of the response properties of cones and horizontal cell bodies in the retina of the cat. *The Journal of Comparative Neurology*, **172**, 109-135.

Ng, K.P., Gugiu, B., Renganathan, K., Davies, M.W., Gu, X., Crabb, J.S., Kim, S.R., Rozanowska, M.B., Bonilha, V.L., Rayborn, M.E., Salomon, R.G., Sparrow, J.R., Boulton, M.E., Hollyfield, J.G. & Crabb, J.W. (2008) Retinal pigment epithelium lipofuscin proteomics. *Molecular & Cellular Proteomics* **7**, 1397-1405.

Ng, T.F. & Streilein, J.W. (2001) Light-induced migration of retinal microglia into the subretinal space. *Invest Ophthalmol Vis Sci*, **42**, 3301-3310.

Ng, T.F., Turpie, B. & Masli, S. (2009) Thrombospondin-1–mediated regulation of microglia activation after retinal injury. *Invest Ophthalmol Vis Sci*, **50**, 5472-5478.

Ni, Y., Xu, G., Hu, W., Shi, L. & Qin, Y. (2008) Neuroprotective effects of naloxone against light-induced photoreceptor degeneration through inhibiting retinal microglial activation. *Invest Ophthalmol Vis Sci*, **49**, 2589-2598.

Nickla, D.L. & Wallman, J. (2010) The multifunctional choroid. *Prog Retin Eye Res*, **29**, 144-168.

Nilsson, S. (1996) Nitric oxide as a mediator of parasympathetic vasodilation in ocular and extraocular tissues in the rabbit. *Invest Ophthalmol Vis Sci*, **37**, 2110-2119.

Nixon, P.J., Bui, B.V., Armitage, J.A. & Vingrys, A.J. (2001) The contribution of cone responses to rat electroretinograms. *Clin Experiment Ophthalmol*, **29**, 193-196.

Noell, W.K., Walker, V.S., Kang, B.S. & Berman, S. (1966) Retinal damage by light in rats. *Invest Ophthalmol*, **5**, 450-473.

Nowak, J.Z. (2006) Age-related macular degeneration (AMD): pathogenesis and therapy. *Pharmacological Reports*, **58**, 353-363.

O'Brien, J., Nguyen, H.B. & Mills, S.L. (2004) Cone photoreceptors in bass retina use two connexins to mediate electrical coupling. *The Journal of Neuroscience*, **24**, 5632-5642.

O'Brien, J.J., Li, W., Pan, F., Keung, J., O'Brien, J. & Massey, S.C. (2006) Coupling between A-type horizontal cells is mediated by connexin 50 gap junctions in the rabbit retina. *The Journal of Neuroscience*, **26**, 11624-11636.

O'Carroll, S.J., Alkadhi, M., Nicholson, L.F. & Green, C.R. (2008) Connexin 43 mimetic peptides reduce swelling, astrogliosis, and neuronal cell death after spinal cord injury. *Cell Commun Adhes*, **15**, 27-42.

O'Quinn, M.P., Palatinus, J.A., Harris, B.S., Hewett, K.W. & Gourdie, R.G. (2011) A peptide mimetic of the connexin43 carboxyl terminus reduces gap junction remodeling and induced arrhythmia following ventricular injury novelty and significance. *Circ Res*, **108**, 704-715.

O'Carroll, S.J., Gorrie, C.A., Velamoor, S., Green, C.R. & Nicholson, L.F. (2013) Connexin43 mimetic peptide is neuroprotective and improves function following spinal cord injury. *Neuroscience Research*, **75**, 256-267.

Ohshima, H., Friesen, M., Brouet, I. & Bartsch, H. (1990) Nitrotyrosine as a new marker for endogenous nitrosation and nitration of proteins. *Food Chem Toxicol*, **28**, 647-652.

Ohsumi, A., Nawashiro, H., Otani, N., Ooigawa, H., Toyooka, T., Yano, A., Nomura, N. & Shima, K. (2006) Alteration of gap junction proteins (connexins) following lateral fluid percussion injury in rats. *Brain Edema XIII*, **96**, 148-150.

Olsen, T.W., Decanini, A., Nordgaard, C.L., Feng, X. & Ferrington, D.A. (2007) Changes in select redox proteins of the retinal pigment epithelium in age-related macular degeneration. *Am J Ophthalmol*, **143**, 607-615.

Olsen, T.W., Edelhauser, H.F., Lim, J.I. & Geroski, D.H. (1995) Human scleral permeability. Effects of age, cryotherapy, transscleral diode laser, and surgical thinning. *Invest Ophthalmol Vis Sci*, **36**, 1893-1903.

Orellana, J.A., Froger, N., Ezan, P., Jiang, J.X., Bennett, M.V.L., Naus, C.C., Giaume, C. & Sáez, J.C. (2011a) ATP and glutamate released via astroglial connexin 43 hemichannels mediate neuronal death through activation of pannexin 1 hemichannels. *J Neurochem*, **118**, 826-840.

Orellana, J.A., Sáez, P.J., Shoji, K.F., Schalper, K.A., Palacios–Prado, N., Velarde, V., Giaume, C., Bennett, M.V.L. & Sáez, J.C. (2009) Modulation of brain hemichannels and gap junction channels by pro-inflammatory agents and their possible role in neurodegeneration. *Antioxid Redox Signal*, **11**, 369-399.

Orellana, J.A., Shoji, K.F., Abudara, V., Ezan, P., Amigou, E., Sáez, P.J., Jiang, J.X., Naus, C.C., Sáez, J.C. & Giaume, C. (2011b) Amyloid β-induced death in neurons involves glial and neuronal hemichannels. *The Journal of Neuroscience*, **31**, 4962-4977.

Organisciak, D.T., Darrow, R.M., Barsalou, L., Kutty, R.K. & Wiggert, B. (2000) Circadian-dependent retinal light damage in rats. *Invest Ophthalmol Vis Sci*, **41**, 3694-3701.

Organisciak, D.T. & Vaughan, D.K. (2010) Retinal light damage: mechanisms and protection. *Prog Retin Eye Res*, **29**, 113-134.

Ormonde, S., Chou, C.Y., Goold, L., Petsoglou, C., Al-Taie, R., Sherwin, T., McGhee, C.N.J. & Green, C.R. (2012) Regulation of connexin43 gap junction protein triggers vascular recovery and healing in human ocular persistent epithelial defect wounds. *Journal of Membrane Biology*, **245**, 381-388.

Orrell, R., De Belleroche, J., Marklund, S., Bowe, F. & Hallewell, R. (1995) A novel SOD mutant and ALS. *Nature*, **374**, 504-505.

Osborne, N.N., Zhang, B. & Rusciano, D. (2008) Orally administered epigallocatechin gallate attenuates retinal neuronal death in vivo and light-induced apoptosis in vitro. *Brain Research*, **1198**, 141-152.

Palamalai, V., Darrow, R.M., Organisciak, D.T. & Miyagi, M. (2006) Light-induced changes in protein nitration in photoreceptor rod outer segments. *Mol Vis*, **12**, 1543-1551.

Pang, J.J., Gao, F., Lem, J., Bramblett, D.E., Paul, D.L. & Wu, S.M. (2010) Direct rod input to cone BCs and direct cone input to rod BCs challenge the traditional view of mammalian BC circuitry. *Proceedings of the National Academy of Sciences*, **107**, 395-400.

Paul, D., Ebihara, L., Takemoto, L., Swenson, K. & Goodenough, D. (1991) Connexin46, a novel lens gap junction protein, induces voltage-gated currents in nonjunctional plasma membrane of Xenopus oocytes. *J Cell Biol*, **115**, 1077-1089.

Paula, K.Y., Balaratnasingam, C., Cringle, S.J., McAllister, I.L., Provis, J. & Yu, D.Y. (2010) Microstructure and network organization of the microvasculature in the human macula. *Invest Ophthalmol Vis Sci*, **51**, 6735-6743.

Pearson, R.A., Dale, N., Llaudet, E. & Mobbs, P. (2005) ATP released via gap junction hemichannels from the pigment epithelium regulates neural retinal progenitor proliferation. *Neuron*, **46**, 731-744.

Pekny, M. (2001) Astrocytic intermediate filaments: lessons from GFAP and vimentin knock-out mice. *Progress in Brain Research*, **132**, 23-30.

Penfold, P.L., Liew, S., Madigan, M.C. & Provis, J.M. (1997) Modulation of major histocompatibility complex class II expression in retinas with age-related macular degeneration. *Invest Ophthalmol Vis Sci*, **38**, 2125-2133.

Penfold, P.L., Madigan, M.C., Gillies, M.C. & Provis, J.M. (2001) Immunological and aetiological aspects of macular degeneration. *Prog Retin Eye Res*, **20**, 385-414.

Penn, J.S., Naash, M.I. & Anderson, R.E. (1987) Effect of light history on retinal antioxidants and light damage susceptibility in the rat. *Exp Eye Res*, **44**, 779-788.

Penn, J.S., Thum, L.A. & Naash, M.I. (1989) Photoreceptor physiology in the rat is governed by the light environment. *Exp Eye Res*, **49**, 205-215.

Pepper, M., Montesano, R., El Aoumari, A., Gros, D., Orci, L. & Meda, P. (1992) Coupling and connexin 43 expression in microvascular and large vessel endothelial cells. *American Journal of Physiology-Cell Physiology*, **262**, C1246-C1257.

Pepper, M., Spray, D., Chanson, M., Montesano, R., Orci, L. & Meda, P. (1989) Junctional communication is induced in migrating capillary endothelial cells. *J Cell Biol*, **109**, 3027-3038.

Pepperberg, D.R., Birch, D.G. & Hood, D.C. (1997) Photoresponse of human rods in vivo derived from paired-flash electroretinograms. *Vis Neurosci*, **14**, 73-82.

Pérez-Álvarez, M., Isiegas, C., Santano, C., Salazar, J., Ramírez, A., Triviño, A., Ramírez, J., Albar, J., de la Rosa, E. & Prada, C. (2008) Vimentin isoform expression in the human retina characterized with the monoclonal antibody 3CB2. *J Neurosci Res*, **86**, 1871-1883.

Pfenniger, A., Chanson, M. & Kwak, B.R. (2013) Connexins in atherosclerosis. *Biochimica et Biophysica Acta (BBA)-Biomembranes*, **1828**, 157-166.

Pham, T.Q., Rochtchina, E., Mitchell, P., Smith, W. & Wang, J.J. (2009) Sunlight-related factors and the 10-year incidence of age-related maculopathy. *Ophthalmic Epidemiol*, **16**, 136-141.

Phillips, M.I., Galli, S.M. & Mehta, J.L. (2000) The potential role of antisense oligodeoxynucleotide therapy for cardiovascular disease. *Drugs*, **60**, 239-248.

Pifferi, F., Perret, M., Guesnet, P., Aujard, F. & Alessandri, J.M. (2012) Fatty acid composition of the brain, retina, liver and adipose tissue of the grey mouse Lemur (Microcebus murinus, Primate). *Lipids*, **47**, 793-801.

Plotkin, L.I., Manolagas, S.C. & Bellido, T. (2002) Transduction of cell survival signals by connexin-43 hemichannels. *Journal of Biological Chemistry*, **277**, 8648-8657.

Plotkin, L.I., Weinstein, R.S., Parfitt, A.M., Roberson, P.K., Manolagas, S.C. & Bellido, T. (1999) Prevention of osteocyte and osteoblast apoptosis by bisphosphonates and calcitonin. *J Clin Invest*, **104**, 1363-1374.

Pocrnich, C.E., Shao, Q., Liu, H., Feng, M.M., Harasym, S., Savage, M., Khimdas, S., Laird, D.W. & Hutnik, C.M.L. (2012) The effect of connexin43 on the level of vascular endothelial growth factor in human retinal pigment epithelial cells. *Graefe's Archive for Clinical and Experimental Ophthalmology*, **250**, 515-522.

Poznanski, R. & Umino, O. (1997) Syncytial integration by a network of coupled bipolar cells in the retina. *Prog Neurobiol*, **53**, 273-291.

Provis, J.M., Penfold, P.L., Edwards, A.J. & van Driel, D. (1995) Human retinal microglia: expression of immune markers and relationship to the glia limitans. *Glia*, **14**, 243-256.

Qiu, C., Coutinho, P., Frank, S., Franke, S., Law, L.Y., Martin, P., Green, C.R. & Becker, D.L. (2003) Targeting connexin43 expression accelerates the rate of wound repair. *Current Biology*, **13**, 1697-1703.

Rahman, S., Carlile, G. & Evans, W.H. (1993) Assembly of hepatic gap junctions. Topography and distribution of connexin 32 in intracellular and plasma membranes determined using sequence-specific antibodies. *Journal of Biological Chemistry*, **268**, 1260-1265.

Ramírez, J.M., Ramírez, A.I., Salazar, J.J., de Hoz, R. & Triviño, A. (2001) Changes of astrocytes in retinal ageing and age-related macular degeneration. *Exp Eye Res*, **73**, 601-615.

Rao, A.K., Ziegler, Y.S., McLeod, I.X., Yates, J.R. & Nardulli, A.M. (2008) Effects of Cu/Zn superoxide dismutase on estrogen responsiveness and oxidative stress in human breast cancer cells. *Molecular Endocrinology*, **22**, 1113-1124.

Rao, N.A., Atalla, L.R. & Sevanian, A. (1988) Immunohistochemical localization of glutathione-peroxidase in ocular tissue. *Curr Eye Res*, **7**, 1023-1027.

Raoul, C., Abbas-Terki, T., Bensadoun, J.-C., Guillot, S., Haase, G., Szulc, J., Henderson, C.E. & Aebischer, P. (2005) Lentiviral-mediated silencing of SOD1 through RNA interference retards disease onset and progression in a mouse model of ALS. *Nat Med*, **11**, 423-428.

Rash, J., Olson, C., Davidson, K., Yasumura, T., Kamasawa, N. & Nagy, J. (2007) Identification of connexin36 in gap junctions between neurons in rodent locus coeruleus. *Neuroscience*, **147**, 938-956.

Rash, J.E., Yasumura, T., Dudek, F.E. & Nagy, J.I. (2001) Cell-specific expression of connexins and evidence of restricted gap junctional coupling between glial cells and between neurons. *The Journal of neuroscience*, **21**, 1983-2000.

Reaume, A.G., de Sousa, P.A., Kulkarni, S., Langille, B.L., Zhu, D., Davies, T.C., Juneja, S.C., Kidder, G.M. & Rossant, J. (1995) Cardiac malformation in neonatal mice lacking connexin43. *Science*, **267**, 1831-1834.

Redburn-Johnson, D. (1998) GABA as a developmental neurotransmitter in the outer plexiform layer of the vertebrate retina. *Perspectives on Developmental Neurobiology*, **5**, 261-267.

Reinboth, J.J., Gautschi, K., Munz, K., Eldred, G. & REMÉ, C.H.E. (1997) Lipofuscin in the retina: quantitative assay for an unprecedented autofluorescent compound (pyridinium bis-retinoid, A2-E) of ocular age pigment. *Exp Eye Res*, **65**, 639-643.

Retamal, M.A., Froger, N., Palacios-Prado, N., Ezan, P., Sáez, P.J., Sáez, J.C. & Giaume, C. (2007) Cx43 hemichannels and gap junction channels in astrocytes are regulated oppositely by proinflammatory cytokines released from activated microglia. *The Journal of Neuroscience*, **27**, 13781-13792.

Reynolds, R., Hartnett, M.E., Atkinson, J.P., Giclas, P.C., Rosner, B. & Seddon, J.M. (2009) Plasma complement components and activation fragments: associations with age-related macular degeneration genotypes and phenotypes. *Invest Ophthalmol Vis Sci*, **50**, 5818-5827.

Rickman, C.B., Farsiu, S., Toth, C.A. & Klingeborn, M. (2013) Dry Age-Related Macular Degeneration: Mechanisms, Therapeutic Targets, and Imaging. *Invest Ophthalmol Vis Sci*, **54**, ORSF68-ORSF80.

Riepe, R.E. & Norenburg, M.D. (1977) Müller cell localisation of glutamine synthetase in rat retina. *Nature*, **268**, 654-655.

Risek, B., Guthrie, S., Kumar, N. & Gilula, N.B. (1990) Modulation of gap junction transcript and protein expression during pregnancy in the rat. *J Cell Biol*, **110**, 269-282.

Rizzolo, L.J., Peng, S., Luo, Y. & Xiao, W. (2011) Integration of tight junctions and claudins with the barrier functions of the retinal pigment epithelium. *Prog Retin Eye Res*, **30**, 296-323.

Rohrer, B., Guo, Y., Kunchithapautham, K. & Gilkeson, G.S. (2007) Eliminating complement factor D reduces photoreceptor susceptibility to light-induced damage. *Invest Ophthalmol Vis Sci*, **48**, 5282-5289.

Rózanowska, M., Jarvis-Evans, J., Korytowski, W., Boulton, M.E., Burke, J.M. & Sarna, T. (1995) Blue light-induced reactivity of retinal age pigment in vitro generation of oxygen-reactive species. *Journal of Biological Chemistry*, **270**, 18825-18830.

Rudnicka, A.R., Jarrar, Z., Wormald, R., Cook, D.G., Fletcher, A. & Owen, C.G. (2012) Age and gender variations in age-related macular degeneration prevalence in populations of European ancestry: a meta-analysis. *Ophthalmology*, **119**, 571-580.

Rufer, M., Wirth, S., Hofer, A., Dermietzel, R., Pastor, A., Kettenmann, H. & Unsicker, K. (1998) Regulation of connexin-43, GFAP, and FGF-2 is not accompanied by changes in astroglial coupling in MPTP-lesioned, FGF-2-treated Parkisonian mice. *J Neurosci Res*, **46**, 606-617.

Runkle, E.A. & Antonetti, D.A. (2011) The blood-retinal barrier: structure and functional significance. *Methods in Molecular Biology*, **686**, 133-148.

Ruskell, G.L. (1997) Peripapillary venous drainage from the choroid: a variable feature in human eyes. *Brit J Ophthalmol*, **81**, 76-79.

Rutar, M., Natoli, R., Kozulin, P., Valter, K., Gatenby, P. & Provis, J.M. (2011a) Analysis of complement expression in light-induced retinal degeneration: synthesis and deposition of C3 by microglia/macrophages is associated with focal photoreceptor degeneration. *Invest Ophthalmol Vis Sci*, **52**, 5347-5358.

Rutar, M., Natoli, R., Provis, J. & Valter, K. (2012a) Complement activation in retinal degeneration. *Adv Exp Med Biol*, **723**, 31-36.

Rutar, M., Natoli, R. & Provis, J.M. (2012b) Small interfering RNA-mediated suppression of Ccl2 in Müller cells attenuates microglial recruitment and photoreceptor death following retinal degeneration. *Journal of Neuroinflammation*, **9**, 221.

Rutar, M., Natoli, R., Valter, K. & Provis, J.M. (2011b) Early focal expression of the chemokine Ccl2 by Müller cells during exposure to damage-inducing bright continuous light. *Invest Ophthalmol Vis Sci*, **52**, 2379-2388.

Rutar, M., Provis, J.M. & Valter, K. (2010) Brief exposure to damaging light causes focal recruitment of macrophages, and long-term destabilization of photoreceptors in the albino rat retina. *Curr Eye Res*, **35**, 631-643.

Sáez, J.C., Connor, J.A., Spray, D.C. & Bennett, M. (1989) Hepatocyte gap junctions are permeable to the second messenger, inositol 1, 4, 5-trisphosphate, and to calcium ions. *Proceedings of the National Academy of Sciences*, **86**, 2708-2712.

Saint-Geniez, M., Maharaj, A.S.R., Walshe, T.E., Tucker, B.A., Sekiyama, E., Kurihara, T., Darland, D.C., Young, M.J. & D'Amore, P.A. (2008) Endogenous VEGF is required for visual function: evidence for a survival role on Müller cells and photoreceptors. *Plos One*, **3**, e3554.

Sakai, N., Decatur, J., Nakanishi, K. & Eldred, G.E. (1996) Ocular age pigment A2-E: An unprecedented pyridinium bisretinoid. *Journal of The American Chemical Society*, **118**, 1559-1560.

Salomon, D., Masgrau, E., Vischer, S., Ullrich, S., Dupont, E., Sappino, P., Saurat, J. & Meda, P. (1994) Topography of mammalian connexins in human skin. *Journal of Investigative Dermatology*, **103**, 240-247.

Sánchez-Alvarez, R., Tabernero, A. & Medina, J.M. (2004) Endothelin-1 stimulates the translocation and upregulation of both glucose transporter and hexokinase in astrocytes: relationship with gap junctional communication. *J Neurochem*, **89**, 703-714.

Santos, A.M., Martin-Oliva, D., Ferrer-Martin, R.M., Tassi, M., Calvente, R., Sierra, A., Carrasco, M.C., Marin-Teva, J.L., Navascues, J. & Cuadros, M.A. (2010) Microglial response to light-Induced photoreceptor degeneration in the mouse retina. *The Journal of Comparative Neurology*, **518**, 477-492.

Sappington, R.M. & Calkins, D.J. (2008) Contribution of TRPV1 to microglia-derived IL-6 and NFkappaB translocation with elevated hydrostatic pressure. *Invest Ophthalmol Vis Sci*, **49**, 3004-3017.

Sato, T., Haimovici, R., Kao, R., Li, A.F. & Roy, S. (2002) Downregulation of connexin 43 expression by high glucose reduces gap junction activity in microvascular endothelial cells. *Diabetes*, **51**, 1565-1571.

Schachat, A.P., Hyman, L., Leske, M.C., Connell, A. & Wu, S.Y. (1995) Features of age-related macular degeneration in a black population. *Arch Ophthalmol-Chic*, **113**, 728-735.

Scholl, H.P.N., Issa, P.C., Walier, M., Janzer, S., Pollok-Kopp, B., Börncke, F., Fritsche, L.G., Chong, N.V., Fimmers, R. & Wienker, T. (2008) Systemic complement activation in age-related macular degeneration. *Plos One*, **3**, e2593.

Schubert, T., Degen, J., Willecke, K., Hormuzdi, S.G., Monyer, H. & Weiler, R. (2005a) Connexin36 mediates gap junctional coupling of alpha-ganglion cells in mouse retina. *The Journal of Comparative Neurology*, **485**, 191-201.

Schubert, T., Huckfeldt, R.M., Parker, E., Campbell, J.E. & Wong, R.O.L. (2010) Assembly of the outer retina in the absence of GABA synthesis in horizontal cells. *Neural Development*, **5**, 15.

Schubert, T., Maxeiner, S., Krüger, O., Willecke, K. & Weiler, R. (2005b) Connexin45 mediates gap junctional coupling of bistratified ganglion cells in the mouse retina. *The Journal of Comparative Neurology*, **490**, 29-39.

Schütte, M., Chen, S., Buku, A. & Wolosin, J. (1998) Connexin50, a gap junction protein of macroglia in the mammalian retina and visual pathway. *Exp Eye Res*, **66**, 605-613.

Schwesinger, C., Yee, C., Rohan, R.M., Joussen, A.M., Fernandez, A., Meyer, T.N., Poulaki, V., Ma, J.J.K., Redmond, T.M. & Liu, S. (2001) Intrachoroidal neovascularization in transgenic mice overexpressing vascular endothelial growth factor in the retinal pigment epithelium. *The American Journal of Pathology*, **158**, 1161-1172.

Sharp, D.M., Lai, S. & Markey, C.M. (2007) Photodynamic therapy with verteporfin for choroidal neovascularization due to age-related macular degeneration and other causes: a New Zealand outcomes study. *Clin Experiment Ophthalmol*, **35**, 24-31.

Sharpe, L.T. & Stockman, A. (1999) Rod pathways: the importance of seeing nothing. *Trends in Neurosciences*, **22**, 497-504.

Simons, K. (1993) Artificial light and early-life exposure in age-related macular degeneration and in cataractogenic phototoxicity. *Arch Ophthalmol-Chic*, **111**, 297-298.

Sivaprasad, S., Adewoyin, T., Bailey, T.A., Dandekar, S.S., Jenkins, S., Webster, A.R. & Chong, N.V. (2007) Estimation of systemic complement C3 activity in age-related macular degeneration. *Arch Ophthalmol-Chic*, **125**, 515-519.

Snell, R.S. & Lemp, M.A. (eds) (1998) *Clinical anatomy of the eye*. Blackwell Science, Inc., Oxford, UK.

Soder, B.L., Propst, J.T., Brooks, T.M., Goodwin, R.L., Friedman, H.I., Yost, M.J. & Gourdie, R.G. (2009) The connexin43 carboxyl-terminal peptide ACT1 modulates the biological response to silicone implants. *Plast Reconstr Surg*, **123**, 1440-1451.

Söhl, G., Degen, J., Teubner, B. & Willecke, K. (1998) The murine gap junction gene connexin36 is highly expressed in mouse retina and regulated during brain development. *FEBS Lett*, **428**, 27-31.

Söhl, G., Joussen, A., Kociok, N. & Willecke, K. (2010) Expression of connexin genes in the human retina. *BMC Ophthalmol*, **10**, 27-38.

Söhl, G., Maxeiner, S. & Willecke, K. (2005) Expression and functions of neuronal gap junctions. *Nature Reviews Neuroscience*, **6**, 191-200.

Söhl, G., Nielsen, P.A., Eiberger, J. & Willecke, K. (2003) Expression profiles of the novel human connexin genes hCx30. 2, hCx40. 1, and hCx62 differ from their putative mouse orthologues. *Cell Communication and Adhesion*, **10**, 27-36.

Solan, J.L. & Lampe, P.D. (2005) Connexin phosphorylation as a regulatory event linked to gap junction channel assembly. *Biochim Biophys Acta*, **1711**, 154-163.

Solan, J.L. & Lampe, P.D. (2009) Connexin 43 phosphorylation: structural changes and biological effects. *Biochem J*, **419**, 261-272.

Soucy, E., Wang, Y., Nirenberg, S., Nathans, J. & Meister, M. (1998) A novel signaling pathway from rod photoreceptors to ganglion cells in mammalian retina. *Neuron*, **21**, 481-493.

Souza, C.F., Acosta, M.L., Polkinghorne, P.J., McGhee, C.N. & Kalloniatis, M. (2013) Amino acid immunoreactivity in normal human retina and after brachytherapy. *Clinical and Experimental Optometry*.

Sparrow, J.R., Nakanishi, K. & Parish, C.A. (2000) The lipofuscin fluorophore A2E mediates blue light–induced damage to retinal pigmented epithelial cells. *Invest Ophthalmol Vis Sci*, **41**, 1981-1989.

Sparrow, J.R., Zhou, J., Ben-Shabat, S., Vollmer, H., Itagaki, Y. & Nakanishi, K. (2002) Involvement of oxidative mechanisms in blue-light-induced damage to A2E-laden RPE. *Invest Ophthalmol Vis Sci*, **43**, 1222-1227.

Spilsbury, K., Garrett, K.L., Shen, W.Y., Constable, I.J. & Rakoczy, P.E. (2000) Overexpression of vascular endothelial growth factor (VEGF) in the retinal pigment epithelium leads to the development of choroidal neovascularization. *The American Journal of Pathology*, **157**, 135-144.

Steuer, H., Jaworski, A., Elger, B., Kaussmann, M., Keldenich, J., Schneider, H., Stoll, D. & Schlosshauer, B. (2005) Functional characterization and comparison of the outer blood–retina barrier and the blood–brain barrier. *Invest Ophthalmol Vis Sci*, **46**, 1047-1053.

Stone, J. & Dreher, Z. (1987) Relationship between astrocytes, ganglion cells and vasculature of the retina. *The Journal of Comparative Neurology*, **255**, 35-49.

Strettoi, E. & Masland, R.H. (1996) The number of unidentified amacrine cells in the mammalian retina. *Proceedings of the National Academy of Sciences*, **93**, 14906-14911.

Strettoi, E., Pignatelli, V., Rossi, C., Porciatti, V. & Falsini, B. (2003) Remodeling of second-order neurons in the retina of rd/rd mutant mice. *Vision Res*, **43**, 867-877.

Striedinger, K., Petrasch-Parwez, E., Zoidl, G., Napirei, M., Meier, C., Eysel, U.T. & Dermietzel, R. (2005) Loss of connexin36 increases retinal cell vulnerability to secondary cell loss. *European Journal of Neuroscience*, **22**, 605-616.

Suadicani, S.O., Vink, M.J. & Spray, D.C. (2000) Slow intercellular Ca2+ signaling in wild-type and Cx43-null neonatal mouse cardiac myocytes. *American Journal of Physiology-Heart and Circulatory Physiology*, **279**, H3076-H3088.

Sui, G.Y., Liu, G.C., Liu, G.Y., Gao, Y.Y., Deng, Y., Wang, W.Y., Tong, S.H. & Wang, L. (2012) Is sunlight exposure a risk factor for age-related macular degeneration? A systematic review and meta-analysis. *Brit J Ophthalmol*, **97**, 389-394.

Sullivan, R., Penfold, P. & Pow, D.V. (2003) Neuronal migration and glial remodeling in degenerating retinas of aged rats and in nonneovascular AMD. *Invest Ophthalmol Vis Sci*, **44**, 856-865.

Sun, D., Bui, B.V., Vingrys, A.J. & Kalloniatis, M. (2007) Alterations in photoreceptor-bipolar cell signaling following ischemia/reperfusion in the rat retina. *The Journal of Comparative Neurology*, **505**, 131-146.

Sunness, J.S., Gonzalez-Baron, J., Bressler, N.M., Hawkins, B. & Applegate, C.A. (1999) The development of choroidal neovascularization in eyes with the geographic atrophy form of age-related macular degeneration. *Ophthalmology*, **106**, 910-919.

Suzuki, M., Kamei, M., Itabe, H., Yoneda, K., Bando, H., Kume, N. & Tano, Y. (2007) Oxidized phospholipids in the macula increase with age and in eyes with age-related macular degeneration. *Mol Vis*, **13**, 772-778.

Tabernero, A., Giaume, C. & Medina, J.M. (1996) Endothelin-1 regulates glucose utilization in cultured astrocytes by controlling intercellular communication through gap junctions. *Glia*, **16**, 187-195.

Tan, J., Mitchell, P., Smith, W. & Wang, J.J. (2007) Cardiovascular risk factors and the long-term incidence of age-related macular degeneration: the Blue Mountains Eye Study. *Ophthalmology*, **114**, 1143.

Tanito, M., Kaidzu, S. & Anderson, R.E. (2007) Delayed loss of cone and remaining rod photoreceptor cells due to impairment of choroidal circulation after acute light exposure in rats. *Invest Ophthalmol Vis Sci*, **48**, 1864-1872.

Tatsukawa, T., Hirasawa, H., Kaneko, A. & Kaneda, M. (2005) GABA-mediated component in the feedback response of turtle retinal cones. *Vis Neurosci*, **22**, 317-324.

Taylor, H.R., Munoz, B., West, S., Bressler, N.M., Bressler, S.B. & Rosenthal, F.S. (1990) Visible light and risk of age-related macular degeneration. *Transactions of the American Ophthalmological Society*, **88**, 163.

Taylor, H.R., West, S., Munoz, B., Rosenthal, F.S., Bressler, S.B. & Bressler, N.M. (1992) The long-term effects of visible light on the eye. *Arch Ophthalmol-Chic*, **110**, 99-104.

Taylor, W.R. & Vaney, D.I. (2002) Diverse synaptic mechanisms generate direction selectivity in the rabbit retina. *The Journal of Neuroscience*, **22**, 7712-7720.

Theis, M., de Wit, C., Schlaeger, T.M., Eckardt, D., Krüger, O., Döring, B., Risau, W., Deutsch, U., Pohl, U. & Willecke, K. (2001) Endothelium-specific replacement of the connexin43 coding region by a lacZ reporter gene. *Genesis*, **29**, 1-13.

Thomas, J.L., Nelson, C.M., Luo, X., Hyde, D.R. & Thummel, R. (2012) Characterization of multiple light damage paradigms reveals regional differences in photoreceptor loss. *Exp Eye Res*, **97**, 105-116.

Thornton, J., Edwards, R., Mitchell, P., Harrison, R., Buchan, I. & Kelly, S. (2005) Smoking and age-related macular degeneration: a review of association. *Eye (Lond)*, **19**, 935-944.

Thrimawithana, T.R., Young, S., Bunt, C.R., Green, C. & Alany, R.G. (2011) Drug delivery to the posterior segment of the eye. *Drug Discovery Today*, **16**, 270-277.

Tomany, S.C., Cruickshanks, K.J., Klein, R., Klein, B.E.K. & Knudtson, M.D. (2004) Sunlight and the 10-year incidence of age-related maculopathy: the Beaver Dam Eye Study. *Arch Ophthalmol-Chic*, **122**, 750-757.

Tortora, G.J. & Grabowski, S.R. (2000) The Special Senses *Principles of Anatomy and Physiology*. John Wiley and Sons, New York, pp. Inc: 512-547.

Trivino, A., Ramirez, J.M., Salazar, J.J., Ramirez, A.N.A.I. & Garcia-sanchez, J. (1996) Immunohistochemical study of human optic nerve head astroglia. *Vision Res*, **36**, 2015-2028.

Tuo, J., Smith, B.C., Bojanowski, C.M., Meleth, A.D., Gery, I., Csaky, K.G., Chew, E.Y. & Chan, C.C. (2004) The involvement of sequence variation and expression of CX3CR1 in the pathogenesis of age-related macular degeneration. *The FASEB Journal*, **18**, 1297-1299.

Ugarte, M. & Osborne, N.N. (1999) The localization of free zinc varies in rat photoreceptors during light and dark adaptation. *Exp Eye Res*, **69**, 459-461.

van Best, J.A., Putting, B.J., Oosterhuis, J.A., Zweypfenning, R.C.V.J. & Vrensen, G.F.J.M. (1997) Function and morphology of the retinal pigment epithelium after light induced damage. *Microscopy Research and Technique*, **36**, 77-88.

van Loon, B., Markkanen, E. & Hübscher, U. (2010) Oxygen as a friend and enemy: How to combat the mutational potential of 8-oxo-guanine. *DNA Repair (Amst)*, **9**, 604-616.

Vaney, D.I. (1991) Many diverse types of retinal neurons show tracer coupling when injected with biocytin or Neurobiotin. *Neurosci Lett*, **125**, 187-190.

Vaney, D.I. (2002) Retinal neurons: cell types and coupled networks. *Progress in Brain Research*, **136**, 239-254.

Vaughan, D.K., Coulibaly, S.F., Darrow, R.M. & Organisciak, D.T. (2003) A morphometric study of light-induced damage in transgenic rat models of retinitis pigmentosa. *Invest Ophthalmol Vis Sci*, **44**, 848-855.

Vergara, L., Bao, X., Bello-Reuss, E. & Reuss, L. (2003) Do connexin 43 gap-junctional hemichannels activate and cause cell damage during ATP depletion of renal tubule cells? *Acta Physiol Scand*, **179**, 33-38.

Veruki, M.L. & Hartveit, E. (2002) Electrical synapses mediate signal transmission in the rod pathway of the mammalian retina. *The Journal of Neuroscience*, **22**, 10558-10566.

Veruki, M.L. & Hartveit, E. (2009) Meclofenamic acid blocks electrical synapses of retinal AII amacrine and on-cone bipolar cells. *Journal of Neurophysiology*, **101**, 2339-2347.

Vessey, K.A., Wilkinson-Berka, J.L. & Fletcher, E.L. (2011) Characterization of retinal function and glial cell response in a mouse model of oxygen-induced retinopathy. *The Journal of Comparative Neurology*, **519**, 506-527.

Virgintino, D., Robertson, D., Errede, M., Benagiano, V., Bertossi, M., Ambrosi, G. & Roncali, L. (2001) Expression of the gap junction protein connexin43 in human telencephalon microvessels. *Microvascular Research*, **62**, 435-439.

Vis, J., Nicholson, L., Faull, R., Evans, W., Severs, N. & Green, C. (1998) Connexin expression in Huntington's diseased human brain. *Cell Biology International*, **22**, 837-847.

Völgyi, B., Abrams, J., Paul, D.L. & Bloomfield, S.A. (2005) Morphology and tracer coupling pattern of alpha ganglion cells in the mouse retina. *The Journal of Comparative Neurology*, **492**, 66-77.

Völgyi, B., Kovács-Öller, T., Atlasz, T., Wilhelm, M. & Gábriel, R. (2013) Gap junctional coupling in the vertebrate retina: variations on one theme? *Prog Retin Eye Res*, **34**, 1-18.

Wachtmeister, L. (1998) Oscillatory potentials in the retina: what do they reveal. *Prog Retin Eye Res*, **17**, 485-521.

Walter, P., Widder, R.A., Luke, C., Konigsfeld, P. & Brunner, R. (1999) Electrophysiological abnormalities in age-related macular degeneration. *Graef Arch Clin Exp*, **237**, 962-968.

Wang, C.M., Lincoln, J., Cook, J.E. & Becker, D.L. (2007) Abnormal connexin expression underlies delayed wound healing in diabetic skin. *Diabetes*, **56**, 2809-2817.

Wang, J.J., Jakobsen, K., Smith, W. & Mitchell, P. (2003) Five-year incidence of age-related maculopathyin relation to iris, skin or hair colour, and skin sun sensitivity: the Blue Mountains Eye Study. *Clin Experiment Ophthalmol*, **31**, 317-321.

Warner, A., Clements, D., Parikh, S., Evans, W. & DeHaan, R. (1995) Specific motifs in the external loops of connexin proteins can determine gap junction formation between chick heart myocytes. *The Journal of Physiology*, **488**, 721-728.

Wässle, H. (2004) Parallel processing in the mammalian retina. *Nature Reviews Neuroscience*, **5**, 747-757.

Weinberg, J., Misukonis, M., Shami, P., Mason, S., Sauls, D., Dittman, W., Wood, E., Smith, G., McDonald, B. & Bachus, K. (1995) Human mononuclear phagocyte inducible nitric oxide synthase (iNOS): analysis of iNOS mRNA, iNOS protein, biopterin, and nitric oxide production by blood monocytes and peritoneal macrophages. *Blood*, **86**, 1184-1195.

Weiter, J.J., Delori, F.C., Wing, G.L. & Fitch, K.A. (1986) Retinal-pigment epithelial lipofuscin and melanin and choroidal melanin in human eyes. *Invest Ophthalmol Vis Sci*, **27**, 145-152.

Wenzel, A., Grimm, C., Samardzija, M. & Remé, C.E. (2005) Molecular mechanisms of light-induced photoreceptor apoptosis and neuroprotection for retinal degeneration. *Prog Retin Eye Res*, **24**, 275-306.

Weymouth, A.E. & Vingrys, A.J. (2008) Rodent electroretinography: methods for extraction and interpretation of rod and cone responses. *Prog Retin Eye Res*, **27**, 1-44.

Williams, T.P. & Howell, W.L. (1983) Action spectrum of retinal light-damage in albino rats. *Invest Ophthalmol Vis Sci*, **24**, 285-287.

Wilson, G.A., Field, A.P. & Wilson, N. (2001) Smoke gets in your eyes: smoking and visual impairment in New Zealand. *New Zealand Medical Journal*, **114**, 471-474.

Wong, R.C.B., Pébay, A., Nguyen, L.T.V., Koh, K.L.L. & Pera, M.F. (2004) Presence of functional gap junctions in human embryonic stem cells. *Stem Cells*, **22**, 883-889.

Wong, W.T., Lee, J.E., Liang, K.J. & Fariss, R.N. (2008) Ex vivo dynamic imaging of retinal microglia using time-lapse confocal microscopy. *Invest Ophthalmol Vis Sci*, **49**, 4169-4176.

Wu, K., Madigan, M., Billson, F. & Penfold, P. (2003) Differential expression of GFAP in early v late AMD: a quantitative analysis. *Brit J Ophthalmol*, **87**, 1159-1166.

Wu, T.H., Handa, J.T. & Gottsch, J.D. (2005) Light-induced oxidative stress in choroidal endothelial cells in mice. *Invest Ophthalmol Vis Sci*, **46**, 1117-1123.

Xu, G.Z., Ni, Y.Q., Hu, W.Z., Shi, L., Qin, Y.W. & Da, C.D. (2008a) Neuroprotective effects of naloxone against light-induced photoreceptor degeneration through inhibiting retinal microglial activation. *Invest Ophthalmol Vis Sci*, **49**, 2589-2598.

Xu, H., Chen, M., Manivannan, A., Lois, N. & Forrester, J.V. (2008b) Age-dependent accumulation of lipofuscin in perivascular and subretinal microglia in experimental mice. *Aging Cell*, **7**, 58-68.

Xu, H. & Liversidge, J. (2011) Quantitative *in situ* analysis of claudin expression at the blood–retinal barrier. *Methods in Molecular Biology* **762**, 321-331.

Xu, H.P., Chen, M. & Forrester, J.V. (2009) Para-inflammation in the aging retina. *Prog Retin Eye Res*, **28**, 348-368.

Xu, H.P., Chen, M., Mayer, E.J., Forrester, J.V. & Dick, A.D. (2007) Turnover of resident retinal microglia in the normal adult mouse. *Glia*, **55**, 1189-1198.

Xu, J., Chalimoniuk, M., Shu, Y., Simonyi, A., Sun, A., Gonzalez, F., Weisman, G., Wood, W. & Sun, G. (2003) Prostaglandin E2 production in astrocytes: regulation by cytokines, extracellular ATP, and oxidative agents. *Prostaglandins, Leukotrienes and Essential Fatty Acids*, **69**, 437-448.

Xu, Q., Kopp, R.F., Chen, Y., Yang, J.J., Roe, M.W. & Veenstra, R.D. (2012) Gating of connexin 43 gap junctions by a cytoplasmic loop calmodulin binding domain. *American Journal of Physiology-Cell Physiology*, **302**, C1548-C1556.

Yasojima, K., Kuret, J., DeMaggio, A.J., McGeer, E. & McGeer, P.L. (2000) Casein kinase 1 delta mRNA is upregulated in Alzheimer disease brain. *Brain Research*, **865**, 116-120.

Yates, J.R.W., Sepp, T., Matharu, B.K., Khan, J.C., Thurlby, D.A., Shahid, H., Clayton, D.G., Hayward, C., Morgan, J. & Wright, A.F. (2007) Complement C3 variant and

the risk of age-related macular degeneration. *New England Journal of Medicine*, **357**, 553-561.

Yeager, M. & Nicholson, B.J. (1996) Structure of gap junction intercellular channels. *Curr Opin Struct Biol*, **6**, 183-192.

Yoon, J.J., Green, C.R., O'Carroll, S.J. & Nicholson, L.F.B. (2010) Dose-dependent protective effect of connexin43 mimetic peptide against neurodegeneration in an *ex vivo* model of epileptiform lesion. *Epilepsy Research*, **92**, 153-162.

Yu, C.-C., Nandrot, E.F., Dun, Y. & Finnemann, S.C. (2012) Dietary antioxidants prevent age-related retinal pigment epithelium actin damage and blindness in mice lacking αvβ5 integrin. *Free Radic Biol Med*, **52**, 660-670.

Yu, D.Y., Cringle, S., Valter, K., Walsh, N., Lee, D. & Stone, J. (2004) Photoreceptor death, trophic factor expression, retinal oxygen status, and photoreceptor function in the P23H rat. *Invest Ophthalmol Vis Sci*, **45**, 2013-2019.

Yu, D.Y. & Cringle, S.J. (2001) Oxygen distribution and consumption within the retina in vascularised and avascular retinas and in animal models of retinal disease. *Prog Retin Eye Res*, **20**, 175-208.

Yu, T.Y., Acosta, M.L., Ready, S., Cheong, Y.L. & Kalloniatis, M. (2007) Light exposure causes functional changes in the retina: increased photoreceptor cation channel permeability, photoreceptor apoptosis, and altered retinal metabolic function. *J Neurochem*, **103**, 714-724.

Yuge, K., Nakajima, M., Miki, H., Uyama, M., Uemura, Y. & Tsubura, A. (1995) Immunohistochemical features of the human retina and retinoblastoma. *Virchows Archiv*, **426**, 571-575.

Yuki, K., Ozawa, Y., Yoshida, T., Kurihara, T., Hirasawa, M., Ozeki, N., Shiba, D., Noda, K., Ishida, S. & Tsubota, K. (2011) Retinal ganglion cell loss in superoxide dismutase 1 deficiency. *Invest Ophthalmol Vis Sci*, **52**, 4143-4150.

Zahs, K.R., Kofuji, P., Meier, C. & Dermietzel, R. (2003) Connexin immunoreactivity in glial cells of the rat retina. *The Journal of Comparative Neurology*, **455**, 531-546.

Zeng, H., Green, W.R. & Tso, M.O.M. (2008) Microglial activation in human diabetic retinopathy. *Arch Ophthalmol-Chic*, **126**, 227-232.

Zeng, H.Y., Zhu, X.A., Zhang, C., Yang, L.P., Wu, L.M. & Tso, M.O.M. (2005) Identification of sequential events and factors associated with microglial activation, migration, and cytotoxicity in retinal degeneration in rd mice. *Invest Ophthalmol Vis Sci*, **46**, 2992-2999.

Zhang, C., Lei, B., Lam, T.T., Yang, F., Sinha, D. & Tso, M.O.M. (2004) Neuroprotection of photoreceptors by minocycline in light-induced retinal degeneration. *Invest Ophthalmol Vis Sci*, **45**, 2753-2759.

Zhang, C., Shen, J.K., Lam, T.T., Zeng, H.Y., Chiang, S.K., Yang, F. & Tso, M.O.M. (2005) Activation of microglia and chemokines in light-induced retinal degeneration. *Mol Vis*, **11**, 887-895.